DEVELOPMENT OF A NOVEL HISTONE-BASED REAGENT TO INCREASE RETROVIRAL TRANSDUCTION BASED ON AN ANALYSIS OF CELL LYSATE EFFECTS

by

Pascal Beauchesne

B.A.Sc. University of Ottawa, 2002

B.Sc. University of Ottawa, 2002

A THESIS SUBMITTED IN PARTIAL FULFILLMENT OF
THE REQUIREMENTS FOR THE DEGREE OF
DOCTOR OF PHILOSOPHY

in

The Faculty of Graduate Studies

(Chemical and Biological Engineering)

The University of British Columbia

(Vancouver)

December 2012

Abstract

Recombinant retroviruses are widely used vectors for engineering cells as they facilitate the delivery and long-term integration of transgenes. Retrovirus-mediated gene transfer is nonetheless challenged by low efficiency due to multiple extracellular rate-limiting steps including mass transport limitations due to the low diffusivity and rapid decay of retroviral vectors as well as limited binding due to electrostatic repulsion between the net negative-charge of both target cells and retroviral vectors. Whole cell lysate was determined to contribute to the variability observed in transduction protocols leading to an increase in the retroviral transduction of TF-1 (human) cells by gibbon ape leukemia virus-pseudotyped vectors and of BaF3 (mouse) cells by ecotropic retroviral vectors. Fractionation of the cell lysate revealed that the bulk of the activity was associated with debris aggregates. These aggregate structures enhanced transduction by increasing mass transport through sedimentation as well as by increasing adsorption of the retroviral vectors to the cells and the culture vessel surfaces. In the presence of this aggregate fraction, transductions of TF-1 and BaF3 cells were enhanced respectively by 59- and 213-fold relative to controls without additives. Further analysis revealed that the aggregate structures were derived from nuclear components sensitive to trypsin digestion, suggesting that nuclear proteins rich in arginines and/or lysines were responsible for the observed enhancement. A subsequent investigation of histone proteins revealed that the arginine-rich fraction, at a concentration of 160 μg/mL, yielded a 22-fold increase in the transduction of TF-1 cells. To mimic the aggregate structures observed in the lysate, histone self-aggregation was stimulated by heat treatment resulting in a 34-fold increase in TF-1 cell transduction while the concentration required was reduced to 10 μg/mL. With BaF3 cells, the transduction exceeded that achieved with lysate under similar conditions. This reagent was also successfully applied to the transduction of primary mouse hematopoietic progenitor cells with long-term reconstitution potential. Overall, a novel histone reagent able to enhance the transduction of primary cells and cell lines with negligible toxicity using both gammaretroviral and lentiviral vectors was designed by isolating the active compounds and analyzing the mechanism of action of lysates on retroviral transduction.

Preface

Each of the chapters included in this thesis corresponds to a manuscript that has either been accepted or will be submitted for publication except for chapter 3 from which an abbreviated version will be submitted to a peer-reviewed journal. I was the main contributor to the decisions regarding the direction of this project along with my supervisors James Piret and Bruce Bowen. I trained and participated in the supervision of the 3 undergraduate students whom contributed to the different chapters: Katherine Bruce (Chapters 2, 3 and 4), Andrew Robinson (Chapter 4) and Calvin Chan (Chapter 5). Michelle Miller, a graduate student in the Keith Humphries laboratory at the BC Cancer Research Center, designed and performed most of the work with primary mouse hematopoietic progenitors. James Piret and Bruce Bowen were my supervisors for all chapters. Keith Humphries provided significant input for Chapter 3. The detailed contributions were as follows:

Chapter 2. The manuscript "Effect of Cell Lysates on Retroviral Transduction Efficiency of Cells in Suspension Culture" was accepted for publication in the peer reviewed journal "Biotechnology and Bioengineering" 105 (6), 2010

Pascal Beauchesne:	Prepared all experimental designs. Completed ~70% of experimental work. Performed all data analysis and wrote all the text in the manuscript.
Katherine Bruce:	Executed ~30% of experimental work.
Bruce Bowen:	Supervision of Pascal Beauchesne and manuscript edition.
James Piret:	Supervision of Pascal Beauchesne and manuscript edition.

Chapter 3. The manuscript "Mechanistic analysis and characterization of lysate-enhanced retroviral transduction of hematopoietic cell lines and stem cells" will be submitted as an abbreviated version to a peer-reviewed journal.

Pascal Beauchesne:	Prepared most experimental designs except for primary mouse hematopoietic progenitor work. Completed ~75% of overall experimental work. Performed ~90% of data analysis and wrote all the text in the manuscript.
Michelle Miller:	Designed primary mouse hematopoietic progenitor experiments. Executed ~15% of overall experimental work and contributed ~10% of data analysis (all primary mouse hematopoietic progenitors).
Katherine Bruce:	Executed ~10% of experimental work.
R. Keith Humphries:	Supervision of Michelle Miller
Bruce Bowen:	Supervision of Pascal Beauchesne and manuscript edition.
James Piret:	Supervision of Pascal Beauchesne and manuscript edition.

Chapter 4. The manuscript "Histone H3.1 increases the gammaretroviral vector transduction efficiency of cell lines and of primitive hematopoietic cells with long-term reconstitution potential will be submitted to a peer-reviewed journal.

Pascal Beauchesne:	Prepared most experimental designs except for primary mouse hematopoietic progenitor work. Completed ~50% of overall experimental work. Performed ~80% of data analysis and wrote ~85% of the manuscript.
Michelle Miller:	Designed primary mouse hematopoietic progenitor experiments. Executed ~30% of overall experimental work and contributed ~20% of data analysis (all primary mouse hematopoietic progenitors).
Katherine Bruce:	Executed ~10% of experimental work (recombinant histones)
Andrew Robinson:	Executed ~10% of experimental work (bovine histones)
R. Keith Humphries:	Supervision of Michelle Miller and manuscript edition
Bruce Bowen:	Supervision of Pascal Beauchesne and manuscript edition.
James Piret:	Supervision of Pascal Beauchesne and manuscript edition.

Chapter 5. The manuscript "Exploiting histone aggregation to further enhance the retroviral transduction of cell lines and primary cells" will be submitted to a peer-reviewed journal.

Pascal Beauchesne:	Prepared most experimental designs except for primary mouse hematopoietic progenitor work. Completed ~55% of overall experimental work. Performed ~95% of data analysis and wrote all of the manuscript.
Michelle Miller:	Designed primary mouse hematopoietic progenitor experiments. Executed ~10% of overall experimental work and contributed ~5% of data analysis (all primary mouse hematopoietic progenitors).

Calvin Chan:	Executed ~35% of experimental work.
R. Keith Humphries:	Supervision of Michelle Miller
Bruce Bowen:	Supervision of Pascal Beauchesne and manuscript edition.
James Piret:	Supervision of Pascal Beauchesne and manuscript edition.

Appendix A "Evaluation of acoustic standing wave fields for large-scale retroviral transduction of suspension cells" is a partial manuscript that may be submitted to a peer-reviewed journal.

Pascal Beauchesne:	All experimental designs, data analysis and manuscript preparation.
Bruce Bowen:	Supervision of Pascal Beauchesne and manuscript edition.
James Piret:	Supervision of Pascal Beauchesne and manuscript edition.

Ethical approval

All work performed with biohazard (level 2) in this research thesis was approved by the UBC BioSafety Committee (Biohazard Approval Certificate Protocol # B09-0105).

Table of Contents

List of Tables

List of Figures

Acknowledgements

I would like to acknowledge all current and former Piret group members for their continuous help, support and valuable feedback throughout the years. In particular, thank you to Volker Gorenflo and Hans Drouin for their assistance with the acoustic cell separator; Venkata Tayi, Corrine Hoesli, Mario Jardon, Véronique Lecault, Marta Szabat, Nicolas Caron, Roger Kiang and Clive Glover for their valuable advice; Darek Sikorski for providing me with a place to stay during my visits to Vancouver as well as great scientific discussions. A special thanks to Chris Sherwood for maintaining the laboratory and teaching me basic mammalian cell culture techniques.

I would also like to recognize the great advice and encouragement received from my supervisors Dr. Jamie Piret and Dr. Bruce Bowen throughout my thesis. Thank you to Dr. R. Keith Humphries (Terry Fox Laboratory, BC Cancer Research Center) as well his graduate students Michelle Miller and Sanja Sekulovic. Their collaboration allowed for the testing of the effect of the lysate and histone reagents on primary mouse hematopoietic progenitor cells.

Thank you to all the undergraduate students who have contributed to this project, in particular Calvin Chan, Andrew Robinson, Katie Bruce and Vivian Hsieh. You all made this research more enjoyable.

This research was made possible by scholarships from the Stem Cell Network, the Natural Sciences and Engineering Research Council of Canada (NSERC) and the University of British Columbia. This project was also supported by an NSERC Strategic Project grant as well as a Collaborative Health Research Project grant from NSERC and Canadian Institutes for Health Research.

Dedication

I dedicate this thesis to my family: my parents Roger and Marielle, my brother Marc and my sister Julie, as well as all my aunts, uncles, cousins and grandparents. Your continuous support through the years has made this work possible. I also dedicate this thesis to all the great undergraduate students that I had the opportunity to mentor during my graduate studies.

1. Introduction

1.1. Retroviruses – from pathogen to gene vector

Retroviruses are RNA-based viruses that enter cells and integrate their genome into the host cell DNA as part of their replication process. These features have been exploited to facilitate the delivery and long-term expression of transgenes in mammalian cells by transforming retroviral pathogens into gene vectors (Mann et al. 1983). This was achieved by engineering packaging cell lines to express the necessary subset of viral proteins (matrix, nucleocapsid, capsid, reverse transcriptase, integrase and envelope). These packaging cell lines then assemble replication-incompetent retroviruses in which native viral genomes have been replaced by the transgenes of interest (Fig. 1) (Markowitz et al. 1988; Miller et al. 1991). Gammaretroviral vectors based on the Moloney murine leukemia virus have successfully been used for gene therapy to treat monogenic haematological disorders such as X-linked- (deficiency of the common gamma-chain of interleukin receptors) and adenosine deaminase-severe combined immunodeficiency (SCID) (Hacein-Bey-Abina et al. 2002; Gaspar et al. 2004; Aiuti et al. 2009). Although their clinical use has diminished in part due to safety concerns such as insertional oncogenesis (Kohn and Candotti 2009), retroviruses remain a valuable tool for genetic research. Examples of recent high impact applications include the development of mouse and human induced pluripotent stem cell technologies (Takahashi et al. 2006; Takahashi et al. 2007) as well as to study the effect of fusion genes on the *ex vivo* expansion of hematopoietic stem cells (Ohta et al. 2007). Alternatively, retroviral vectors provide a simple and inexpensive method to achieve selective and stable gene down-regulation

through the delivery of short hairpin RNA (shRNA) expression cassettes used for mRNA degradation and gene silencing. Retroviral vector-based shRNA libraries targeting over a third of all human genes have been generated (Sliva and Schnierle 2010). The effectiveness of all these applications depends to a substantial degree on achieving high retroviral transduction efficiencies. Although techniques have been derived to enhance retroviral transduction, as will be discussed below, many of these methods are complex, toxic to the target cells and difficult to scale up.

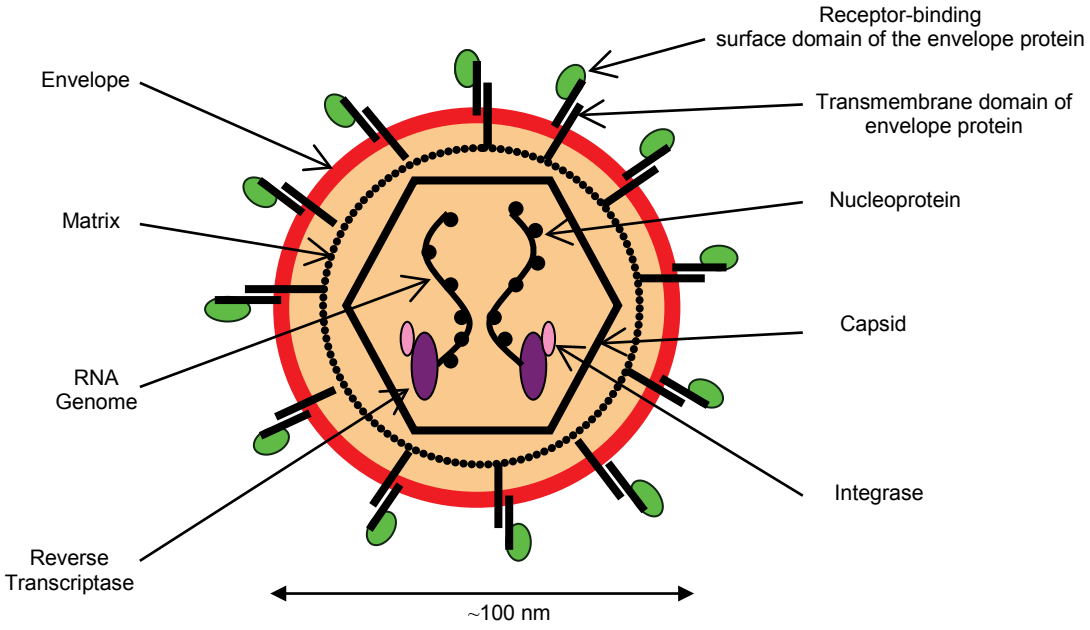

Figure 1.1 Schematic representation of a gammaretrovirus with 2 RNA genome copies.
In a gammaretroviral vector, the viral genome is substituted for the transgene of interest. (Adapted from (Levy 1992).)

1.2. Important steps of the retroviral transduction process

The retroviral transduction of mammalian cells is a multi-step process, where the net transduction efficiency is the product of the efficiencies of multiple individual steps (Fig. 2). In the simplest case (static system), the retroviral vectors are added to a cell

culture where adherent cells are attached to the bottom surface of the culture flask or, with suspension cultures, the cells sediment to the bottom.

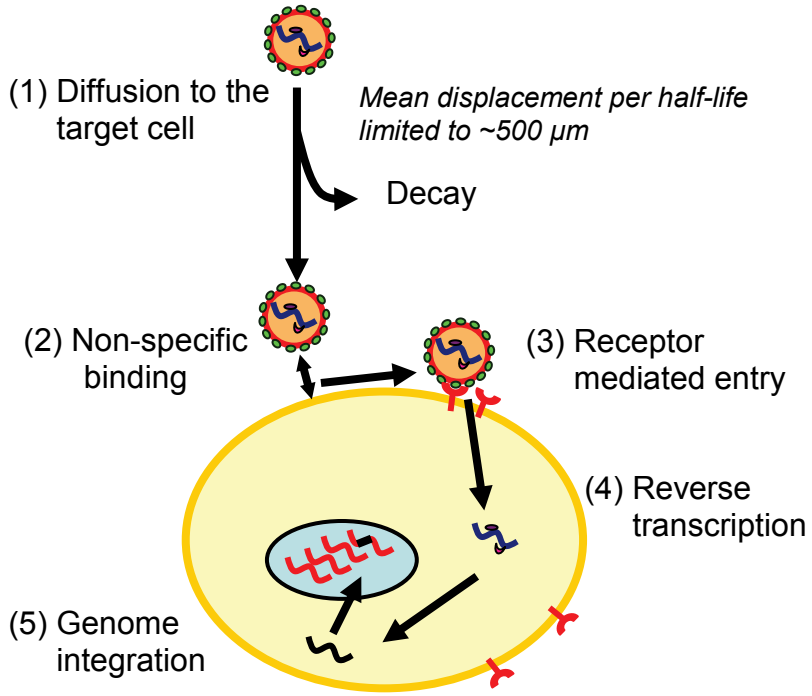

Figure 1.2 Retroviral transduction is a multi-step process which includes (1) diffusion of the retroviral vector to the target cell, (2) non-specific binding to the cell, (3) receptor-mediated entry, (4) reverse transcription and (5) integration of the transgene in the genomic DNA of the cell.

1.2.1. Mass transport to the target cell

The initial step of the transduction process involves the mass transport of the retroviral vectors to the proximity of the target cells (Palsson and Andreadis 1997). Viruses are colloidal particles whose mass transport in a static system relies on Brownian motion (Valentine et al. 1959; Chuck et al. 1996). Assuming that retroviral vectors have a diameter of 100 nm, their diffusivity (D) in a culture medium at 37^{o}C is estimated to be 6.5×10^{-8} cm^2/s using the Stokes-Einstein equation:

$$D = \frac{k_B T}{6\pi\eta r} \qquad \textbf{Eq. 1.1}$$

where k_B is the Boltzmann constant, T the temperature, η the viscosity of the surrounding medium and r the radius of the vector (Chuck et al. 1996). While the diffusive transport of retroviral vectors is slow, it is not by itself a limiting factor. In addition, retroviral vectors based on the widely used murine leukemia virus (MLV) have relatively short extracellular half-lives of 3.5 – 6.5 h at 37^{o}C, and these do not seem to be influenced by the vector pseudotype (ecotropic, amphotropic or VSV-G) (Burns et al. 1993; Paul et al. 1993; Andreadis et al. 2000; Bajaj et al. 2001; Higashikawa et al. 2001; Kwon et al. 2002). Marginal gains in stability have been achieved by reducing the production temperature and through careful selection of the packaging cell line as well as the cholesterol content of the viral membrane (Beer et al. 2003; Carmo et al. 2006). The high decay rate of MLV-derived vectors has been attributed in part to the RNase H* (RNA-RNA duplex nuclease) activity of the reverse transcriptase resulting in the premature degradation of the viral genome (Casali et al. 2008). As reverse transcriptase is an essential component of retroviral vectors, their poor stability at typical cell culture temperatures may be difficult to overcome. As a result of their combined low diffusivity and short half-life, the root-mean-square displacement of the vectors per half-life is limited to 480 ~ 610 μm (Chuck et al. 1996).

1.2.2. Non-specific binding

Once in close proximity to the target cell, the retroviral vector can bind to the cell surface. This initial attachment step is non-specific as it occurs independently of receptor and envelope interactions (Pizzato et al. 1999; Sharma et al. 2000). Binding was found to

be dependent on the viral vector concentration, saturable and to follow a bimolecular noncooperative model for the virus-cell interaction (Yu et al. 1995). Several fundamental physico-chemical interactions that take place between the cell and retroviral vector can influence adsorption. Firstly, attractive van der Waals forces arise from dipole-dipole type interactions. Secondly, electrostatic repulsive forces result from the net negative charges on the lipid bilayers of both the cells and the vectors. Thirdly, hydration or solvation forces result from the need for water expulsion from between the two surfaces. Finally, repulsive steric forces, resulting from proteins on both surfaces that can form spikes up to 10 nm long, can prevent the binding of the retroviral vector to its initial ligand (Palsson and Andreadis 1997).

Retroviral vector binding was reported to be highly dependent on the target cell line. In particular, high binding was reported for adherent cell lines, while poor binding was observed for suspension cells such as hematopoietic cell lines (Pizzato et al. 1999). This may explain at least in part the 100- to 1000-fold greater transduction efficiencies obtained with adherent cells relative to suspension cells. Furthermore, with adherent cells such as NIH 3T3, the amphotropic-murine leukemia virus was found to bind to the fibronectin matrix. For Jurkat suspension cells that express low levels of fibronectin compared with NIH 3T3, less than $1/10^{th}$ the binding was observed after 1 h (Beer and Pedersen 2007). The larger cell surface area available to vector binding on adherent cells may also contribute to the difference observed as transduction was predicted to increase with surface area (Andreadis et al. 2000). The surface properties of viruses were also found to influence initial cell binding. Virus-associated heparan sulfate proteoglycans on the surface of the viral envelope are inherited from the packaging cell membrane during

the budding process and mediate binding onto a specific heparan sulfate binding domain of the fibronectin protein (Kureishy et al. 2006). Therefore, there is a significant opportunity to increase retroviral adsorption and transduction, especially for suspension cells lacking the ability to efficiently adsorb viral vectors (e.g. due to lack of fibronectin expression) or for viral vectors lacking heparan sulfate proteoglycans.

1.2.3. Entry

Entry pathways differ widely between retroviruses. For example, the lentivirus HIV-1 is thought to enter through direct fusion with the cell membrane (Katen et al. 2001), while the wild-type vesicular stomatitis virus entered through clathrin-coated-pit endocytosis followed by fusion with the endosomal membrane (Coll 1995). The entry of ecotropic and amphotropic murine leukemia vectors (E-MLV and A-MLV) has primarily been studied using NIH 3T3 cells. In the case of the E-MLV, endocytosis was found to occur independently of the clathrin-coated-pit-mediated pathway (Lee et al. 1999) and required intact microtubules and an actin network (Kizhatil and Albritton 1997). Both E-MLV and A-MLV were found to enter the cell through caveola-dependent endocytosis. For E-MLV, the receptor mCAT-1 was associated with cholesterol-rich membrane rafts together with caveolin. Cholesterol depletion by methyl-β-cyclodextrin reduced E-MLV infection by 14-fold while the receptors (mCAT-1) remained intact suggesting that although receptors are required, entry was not mediated by the receptors alone (Lu and Silver 2000). A-MLV receptors (Pit-2) were similarly found to be associated together with caveolin-1 in cholesterol-rich microdomains. Interestingly, entry of fusion defective A-MLV containing unprocessed envelope proteins still occurred (Beer et al. 2005). It is therefore possible that receptors are constitutively endocytosed and that ligand induction

is not required to trigger endocytosis (Lee et al. 1999). Receptors are still required for successful infection (Grabarczyk et al. 2002; Relander et al. 2002) and may act as fusion triggers (Coll 1995).

Viral entry was reported to occur rapidly as internalized vectors were detected within 5 minutes following their exposure to the cells (Lee et al. 1999). The kinetics of infection varies depending on the vector pseudotype. With a VSV-G envelope, the uptake rate of MLV-based vectors was faster than with E-MLV, with half-maximal transduction reached after 1.5 h and 5 h, respectively (Beer et al. 2005; Kwon et al. 2003). Thus, the entry pathway could potentially affect the retroviral transduction kinetics. Internalization of the virus was also found to be temperature dependent with no internalization reported at 4^{o}C (Kizhatil and Albritton 1997) or 15^{o}C (Yu et al. 1995). Results obtained with NIH 3T3 should not be generalized to all cell types. For example, hematopoietic cell lines do not express caveolin-1, suggesting they have an alternative entry pathway to caveola-dependent endocytosis (Beer et al. 2005).

1.2.4. Reverse transcription

Following entry into cells, a poorly characterized uncoating step takes place where most capsid proteins are lost. The reverse transcription process eventually yields the reverse transcription complex (RTC) containing the viral genome, capsid, integrase and reverse transcriptase proteins. The size of the competent RTC was reported to change with time suggesting discrete steps of uncoating and the existence of an organized dissociation during the reverse transcriptase step (Fassati and Goff 1999). During proviral DNA synthesis, the RNA of the RNA-DNA hybrid is digested by the RNase-H activity of the reverse transcriptase (Suzuki and Craigie 2007). Premature termination of

reverse transcription was reported under restrictive conditions such as serum depletion leading to arrested cell growth due to limitations in the availability of deoxyribonucleotides (Goulaouic et al. 1994). It is unclear if this limitation would be significant under normal growth conditions.

1.2.5. Integration

The pre-integration complex (PIC) contains the fully reverse-transcribed proviral DNA as well as the integrase and some residual capsid proteins (Bowerman et al. 1989). The PIC has a much larger diameter than that of a nuclear pore, excluding passive diffusion as a means of nuclear entry (Suzuki and Craigie 2007), and the PIC lacks a competent nuclear localization signal (Seamon et al. 2002). As a result, integration is dependent on cell division and occurs post-metaphase by taking advantage of the dissolution of the nuclear envelope (Lewis and Emerman 1994; Miller et al. 1990; Roe et al. 1993). However, when cells were stimulated to divide 6 h to 10 days after infection, integration did not occur suggesting that the PIC has a short half-life in the cytoplasm (Miller et al. 1990). The intracellular half-life of viral vectors in NIH 3T3 cells was estimated to be 5.5 – 7.5 h (Andreadis et al. 1997), although it is unclear whether this accurately represents the stability of the PIC or another intracellular intermediate such as the RTC. Before integration, the PIC forms a stable association with the chromosomal DNA (Suzuki and Craigie 2007). The integration begins with an end processing step to remove the dinucleotide adjacent to a highly conserved "CA" dinucleotide from the 3' end of the U3 and U5 viral DNA LTRs. This is followed by a joining reaction where DNA is inserted into the cellular DNA resulting in a gapped DNA with a 5' 2-base overhang. Overhang removal followed by gap and nick repair complete the integration

reaction (Hindmarsh and Leis 1999). Host cell factors, such as the "barrier to self-integration" that prevents autointegration of the proviral DNA, also play a role in the integration process (Lee and Craigie 1998).

1.3. Retroviral transduction models

Several models have been developed to characterize the retroviral transduction process. An initial model by Valentine and Allison (1959) assumed that mass transport of the virus relied on Brownian motion in a static system and was based on an ideal situation where viral decay was absent and binding to the cell was instantaneous and irreversible. Under these assumptions, only 63% of the viruses within a 1 mm liquid layer above the closely-packed cells was predicted to adsorb onto the cells within 20 h. This model was later extended by Andreadis et al. (2000) to include viral vector decay kinetics. In equation form, the time- and position-dependent concentration of active retroviral vectors, V, in the cell culture medium is given by

$$\frac{\partial V}{\partial t} = D\frac{\partial^2 V}{\partial z^2} - k_d\, V \qquad \textbf{Eq. 1.2}$$

where D is the Stokes-Einstein diffusivity (Eq. 1.1) of the retroviruses in the medium, z is the distance from the target cells (assumed to reside as a monolayer at the bottom of the vessel) and k_d is the decay rate constant. Andreadis et al. also assumed that any vector diffusing to the vicinity of a cell immediately attached to its surface, i.e., the boundary condition

$$V = 0 \text{ at } z = 0 \qquad \textbf{Eq. 1.3}$$

was employed. For similar conditions as those used by Valentine and Allison, Eq. 1.2 predicted that less than 20% of the initial active retroviral vectors would be successfully

adsorbed onto the cells' surfaces and that, above a critical liquid depth of ~0.5 mm, additional volumes of virus-containing media (VCM) would not lead to increases in transduction.

Finally, this model was further extended (Kwon and Peng 2002a) to include viral uptake rate as a boundary condition, i.e.,

$$D\frac{\partial V}{\partial z} = k_a V \text{ at } z = 0 \qquad \textbf{Eq. 1.4}$$

where k_a is the retroviral uptake rate constant which includes both adsorption and internalization. When compared to viral titer assays, this model predicted that only 1 out of every 143 – 179 initially active Moloney murine leukemia virus particles would lead to a successful transduction event on NIH 3T3 cells (Kwon et al. 2003). The evolution of these models clearly demonstrates that slow mass transport, a short half-life and poor binding severely limit retroviral transduction. Overall, altering conditions to improve mass transport while minimizing extracellular decay and maximizing binding of the retroviral vectors to the cells has the potential to increase transduction efficiency by over 2 orders of magnitude.

Efforts have been made to extend retroviral transduction models beyond extracellular events to include intracellular limitations. These have incorporated, among other factors, estimates of intracellular retroviral decay and integration rates (Andreadis et al. 2000; Tayi et al. 2010). However, these parameters can vary widely for different target cell – retroviral vector systems. For example, while the intracellular half-life of amphotropic retroviral vectors from the psi CRIP packaging cell line was estimated at 5.5 – 7.5 h in NIH 3T3 cells (Andreadis et al. 2000), the intracellular decay was found to be negligible in K-562 cells using a vector with a gibbon ape leukemia virus envelope from

the PG-13 packaging cell (Tayi et al. 2010). Given these significant differences, it is difficult to make a generalization on intracellular limitations that would apply to most target cell – retroviral vector systems.

1.4. Methods to improve retroviral transduction

1.4.1. Concentration of viral vectors

In order to achieve greater transduction efficiency, retroviral vector preparations can be concentrated prior to their addition to the target cells. Concentration was performed based on the size of E-MLV and A-MLV vectors by tangential flow filtration using plates (Kotani et al. 1994) or hollow fibre bundles (Makino et al. 1994; Paul et al. 1993). Vectors were concentrated by 10- to 30-fold while recovery ranged from 50 to 94%. An increase in the operating pressure resulted in up to a 90% loss in activity, presumably due to the shear sensitivity of the vectors. Retroviral vectors were also concentrated by centrifugation on the basis of their greater density of 1.16 – 1.18 g/cm^3 (Prachar et al. 1988; Fassati et al. 1999). However, with shear-sensitive vectors such as E-MLV, this approach is limited to relatively low centrifugal forces as ultracentrifugation at 50,000×g resulted in a 99% loss of activity. VSV-G pseudotyped MLV vectors do not exhibit as much shear sensitivity and were successfully concentrated 220-fold with a 96% recovery (Burns et al. 1993). To improve concentration under low centrifugation conditions (<3000×g), vectors can be adsorbed onto a larger carrier substrate. The addition of calcium phosphate allowed vectors to be concentrated by 13- to 32-fold at only 2060×g with a recovery rate of 50%. However, the toxicity of the calcium phosphate precipitate requires an additional dialysis step before the vectors can be added

to the cells (Pham et al. 2001). Alternatively, the heat-killed, formalin-fixed bacterium *Staphylococcus aureus* (Pansorbin) has also been used as a dense substrate to enhance sedimentation resulting in concentration increases of 5- to 16-fold under gravity alone or up to 200-fold when combined with centrifugation at 2600×g. Adsorption of the vectors on Pansorbin is thought to be mediated via fibronectin binding proteins (fnbA and fnbB) present on the surface of the Pansorbin (Darling et al. 2000). Therefore, the efficiency of this approach relies on the presence of fibronectin secreted by the packaging cell line as well as the affinity of the vectors for fibronectin. This may explain why the high concentrations achieved with PG-13-derived vectors were not reproduced with other packaging lines such as the human sarcoma FLYRD18. Finally, streptavidin-coated paramagnetic particles (PMP) were used to concentrate vectors by up to 113-fold using a magnetic particle concentrator (Hughes et al. 2001). However, adsorption of the vectors to the particles required the use of complex ligand systems, e.g. protein A conjugated with biotin to mediate the attachment of polyclonal rabbit immunoglobulin conjugated with mouse antibody against fibronectin. Similarly to Pansorbin, this approach relies on the presence of fibronectin secreted by the packaging cells. Another system used an affinity capture based on lectins to target the galactosyl(α1-3) groups present on the viral envelope. However, this approach is limited to vectors derived from mouse packaging cell lines as human lines have minimal α-galactosyl groups present. The modification of viral vectors by placing a biotin on the viral envelope has also been explored, but the effect of this treatment on viral stability and productivity remains unclear (Hughes et al. 2001). Interestingly, most increases in titer were well below the potential increase of over 2 orders of magnitudes predicted by the models discussed in section 1.3, i.e., the

maximum that could be achieved by addressing mass transport and binding limitations. Thus, this extra processing step might also contribute additional losses in vector activity. The vectors also remain attached to the carrier leading to the exposure of the target cells to the carrier during the transduction process.

1.4.2. Inhibitor removal – vector purification

The retroviral vector-containing medium has been shown to contain inhibitors secreted by the packaging cell line (Le Doux et al. 1996). The saturation in transduction observed at high vector concentration was partly attributed to the increased concentration of such inhibitors (Morgan et al. 1995). These included proteoglycans as well as glycoaminoglycans that inhibit transduction by up to 90% (Table 1.1) (Kureishy et al. 2006; Le Doux et al. 1999; Toyoshima and Vogt 1969). Purification of vectors using sucrose gradients (Kwon et al. 2003; Prachar et al. 1988) or affinity chromatography (Segura et al. 2007) can remove many of these inhibitors, but the recovery of active viral vectors will be reduced by this additional processing. Alternatively, inhibitors can be digested by treating the viral vector preparation with chondroitinase ABC resulting in a 2-fold increase in transduction (Le Doux et al. 1996). Certain methods, like vector concentration, may co-concentrate inhibitors together with the viral vectors thereby partially negating the benefits of such techniques. Thus, the design of methods that are insensitive to inhibitors secreted by the packaging cell lines could substantially reduce the need for purification. This would be most beneficial if it could significantly reduce the effect of inhibitors by reducing the vector concentration required or even allow the virus-containing medium to be diluted.

Table 1.1 Effect of glycoaminoglycans on retroviral transduction efficiency

Glycoaminoglycans	Cells	Virus or Vector	Transduction relative to Control	Glycoaminoglycan Concentration (μg/mL)	Reference
Heparin	CEF	RSV	0.2	1-32	(1)
	TE671	A-MLV	0.5	40	(2)
	NIH 3T3	A-MLV	0.5	0.002	(3)
Heparan sulfate	TE671	A-MLV	0.2	40	(2)
	NIH 3T3	A-MLV	0.5	20	(3)
Chondroitin 4 sulfate	TE671	A-MLV	0.4	40	(2)
(Chondroitin sulfate A)	NIH 3T3	A-MLV	0.5	2	(3)
Chondroitin 6 sulfate	TE671	A-MLV	0.3	40	(2)
(Chondroitin sulfate C)	NIH 3T3	A-MLV	No effect		(3)
Dermatan sulfate	TE671	A-MLV	0.1	40	(2)
(Chondroitin sulfate B)	NIH 3T3	A-MLV	0.5	2	(3)
Hyaluronic acid	TE671	A-MLV	0.65	40	(2)
	NIH 3T3	A-MLV	0.5	100	(3)

CEF: chicken embryo fibroblast, RSV: Rous sarcoma virus

(1) (Toyoshima and Vogt 1969)

(2) (Kureishy et al. 2006)

(3) (Le Doux et al. 1999)

1.4.3. Co-culture systems

Co-culture systems overlay target cells directly on the packaging cells. To avoid the proliferation of the packaging line, these cells are usually treated with mitomycin C (Moritz et al. 1993) or irradiated (Dick et al. 1991) prior to the addition of the target cells. The advantages of this approach include a sustained vector production to compensate for vector depletion over time due to decay or cellular uptake, a reduction in the distance vectors must travel due to the proximity of the packaging line to the target cells and the benefit of cell-cell contact for some cells such as hematopoietic stem cells. Also, the assembly of the murine leukemia virus was reportedly polarized and initiated within sites of cell-cell contact that facilitated direct cell-to-cell transmission of the retroviral vector between the packaging cell line and the target cell (Jin et al. 2009). However, this technique risks cross-contamination between the packaging and target cells. Furthermore, it can be difficult to optimize culture conditions to maximize both target cell proliferation and viral vector productivity. Finally, other effects of the packaging line on the target cells can be confounded with the transgene effects, and this has been reported for HSCs to complicate the interpretation of transduction experiments (Deneault et al. 2009). Overall, while it remains in use, the complexity and replication difficulty encountered would make it worthwhile to develop alternative approaches that could match or improve the transduction yields while removing the need for co-culture.

1.4.4. Improved mass transport

To overcome the limitations associated with the low diffusivity and short half-life of retroviral vectors, several approaches to more rapidly transport them to the vicinity of

the target cells have been developed. In the "flow-through" design, convective flow was used to direct the motion of the retroviral vectors toward the target cells placed on a porous membrane (Chuck and Palsson 1996a). The enhancement in transduction efficiency obtained with this technique was dependent on the type of membrane used. For example, there was significant enhancement with a collagen-coated Teflon depth membrane while no effect was obtained with a tissue-culture-treated polyester screen (Chuck and Palsson 1996b). The enhancement was therefore the result of retroviral vector adsorption or entrapment by the membrane rather than direct binding to the target cells.

The greater density of the viral vectors relative to that of the medium has also been exploited by centrifuging the vectors together with the target cells. The transduction efficiency was a function of centrifugation time and relative centrifugal forces of up to 10,000×g (Bahnson et al. 1995). However, due to limitations associated with the use of cell culture plates, this protocol, referred to as "spinocculation", typically uses lower relative centrifugal forces of 1,100 – 2,400×g (Kotani et al. 1994; Bahnson et al. 1995). With suspension cells such as the TF-1 line, issues of crowding arose as the transduction efficiency declined with increasing cell numbers and converged toward the transduction levels obtained with untreated controls. This may be the result of a lower number of vectors available per cell and/or mass transport limitations due to the layering of cells. Increases in transduction efficiency were in the range of 3- to 20-fold with the higher increases obtained using low-titer viral stocks. The modest increases obtained with high-titer stocks may be the result of saturation or the co-sedimentation of viral transduction inhibitors such as proteoglycans in the virus-containing medium (Le Doux et al. 1996).

With spinocculation, it can be difficult to control environmental conditions such as the temperature, the humidity or the CO_2 levels that influence pH when using bicarbonate-based buffer media. Furthermore, unless a binding agent is present, upon completion of the centrifugation cycle, retroviral vectors may desorb and diffuse away from the cells.

Alternatively, retroviral vectors can be adsorbed onto the cell culture vessel surface prior to the addition of target cells. Fibronectin, an extracellular matrix molecule involved in cell adhesion, has a cell binding domain containing the tetrapeptide RGDS that mediates adhesion via the integrin VLA-5, a heparin binding domain that interacts via cell surface proteoglycan molecules and a CS1 sequence that mediates adhesion via the integrin VLA-4 (Hanenberg et al. 1996; Moritz et al. 1994). Non-tissue-culture-treated surfaces are first coated with fibronectin (Hanenberg et al. 1997). This step is followed by pre-loading the viral vectors that bind to the heparin binding domain. Sequential additions of the viral vectors and the cells are necessary as both can compete for the heparin binding domain leading to a lower transduction efficiency. During the loading step, viral vectors diffuse from the bulk solution to the fibronectin-coated surface. Loading efficiency is a function of temperature, loading time and virus concentration. Insufficient loading time will result in incomplete loading but extending the time results in significant losses due to vector decay (Bajaj et al. 2001). Alternatively, centrifugation can be used to accelerate and improve retroviral attachment to the fibronectin-coated surface (Kuhlcke et al. 2002). This method is subject to conditioning of the virus-containing medium as it is inhibited by chondroitin sulfate and heparan sulfate. The addition of polycations such as polybrene can also inhibit fibronectin-assisted transduction (Lei et al. 2002). The specificity of the ligand can contribute to the

variability of this method especially for cell lines that exhibit variable expression levels of VL4 and VL5 (Hanenberg et al. 1996). A fragment of human fibronectin (CH296) containing all 3 binding domains was successfully expressed in *E. coli* (Hanenberg et al. 1996). This fully-defined recombinant product has been the enhancer of choice in several clinical trials (Gaspar et al. 2004; Hacein-Bey-Abina et al. 2002).

Positively-charged surfaces can be used as a less specific alternative to fibronectin-coated surfaces (Hennemann et al. 2000a; Valentine and Allison 1959). Retroviral vectors were shown to bind to poly-L-lysine-coated surfaces, likely through electrostatic attraction. There have also been reports that the retroviral vectors could be simply loaded onto untreated and tissue-culture-treated surfaces by centrifugation at 1000×g prior to the addition of the target cells (Kuhlcke et al. 2002). However, other groups were not able to reproduce these results (Fehse and Kuhlcke 2008), thus indicating that the underlying mechanism may be poorly understood. It is likely that this approach relies on the fibronectin secreted by the packaging cell lines present within the virus-containing medium rather than the physical properties of the culture vessel surface. Thus, this technique can exhibit variability based on the choice of packaging cell line as well as vector production conditions.

Adsorption of vectors onto larger and denser substrates can increase sedimentation to overcome diffusion-based limitations and concentrate the retroviral vectors at the bottom of the cell culture vessel, in proximity to the target cells. A calcium phosphate precipitate has been used to increase E-MLV and A-MLV based transduction by 5- to 50-fold. However, the toxicity of the precipitate limited the concentrations as well as the exposure times used (Morling and Russell 1995). The combination of

polybrene (polycation) and chondroitin sulfate C (polyanion) together with the retroviral vectors formed a high-molecular-weight retrovirus-polymer complex leading to an increase of 3- to 20-fold in transduction (Le Doux et al. 2001). While the complex itself was not toxic to the cells, uncomplexed polybrene was reported to be toxic and chondroitin sulfate C can also inhibit transduction (Kureishy et al. 2006). Furthermore, variable concentrations of endogenous proteoglycans and glycoaminoglycans in the virus-containing medium (Le Doux et al. 1996) may lower the effectiveness of the complexation process. Paramagnetic particles were also used to adsorb retroviral vectors and, by means of a magnetic field, to displace them towards the target cells (Hughes et al. 2001). However, following the transduction process, it is unknown what long-term effect the residual, non-biodegradable paramagnetic particles will have on the cells. Finally, high-molecular-weight poly-L-lysine molecules (>15 kDa) were reported to induce the aggregation of the retroviral vectors through electrostatic interactions leading to increased sedimentation (Davis et al. 2004). Since this aggregation process relies on the viral vectors, variations in vector concentrations are likely to affect this approach. Furthermore, it is unknown if the retroviral vectors entrapped within the aggregates remain available to the target cells or if entry will be limited only to those adsorbed on the surface of the aggregate structure, possibly resulting in significant vector losses.

1.4.5. Increasing vector adsorption to cells

Polycations, such as polybrene, were found to enhance the receptor/envelope independent adsorption of viral vectors on NIH 3T3 cells by up to 10-fold (Davis et al. 2002). Since NIH 3T3 cells were previously reported to already have high adsorption levels, suspension cells with lower adsorption levels (Pizzato et al. 1999) may benefit

even more from the use of polycations. It was also shown that poly-L-lysine was adsorbed onto the surface of cells and viral vectors as a function of concentration. As a result, the ζ-potentials of both cells and vectors were reduced by 30% to 60%, indicating that part of their respective negative charge was shielded thereby reducing the electrostatic repulsion (Davis et al. 2002). While most polycations are simply mixed with the viral vectors and cells, cationic liposomes require an additional step where the viral vectors must first associate with the liposomes before the mixture is added to the target cells (Hodgson and Solaiman 1996; Porter et al. 1998). As summarized in Table 1.2, many cationic compounds were reported to increase transduction, including synthetic polymers, cationic liposomes and peptides. With the exception of a few outliers, increases in transduction efficiency were generally comparable within a range of 5- to 20-fold with A- or E-MLV-based vectors. Optimum concentrations have been reported with most cationic polymers. Even a small deviation can result in a sharp decrease in transduction, especially with cationic liposomes (Hodgson and Solaiman 1996), possibly due to toxicity as well as insufficient or excessive charge modulation. Anionic polymers such as chondroitin sulfate were shown to reduce adsorption by the sequestration of the cationic polymers (Davis et al. 2004). This may account for the reported sensitivity to serum lots with either protamine sulfate and polybrene (Jensen et al. 2003). The toxicity of these cationic compounds differs widely (Table 1.2). For example, protamine sulfate was reported to be less toxic than polybrene while providing similar increases in transduction (Cornetta and Anderson 1989). Toxicity often varies between cell lines. In particular, while NIH 3T3 has been the preferred model cell line for many studies, it may be a poor predictor of primary cell toxicity.

Table 1.2 Summary of polycations used to enhance retroviral transduction

Cationic compound	Target cell	Virus or Vector	Enhancement (fold)	Optimal concentration (μg/mL)	Toxicity (μg/mL)	Reference
Synthetic compounds						
DEAE-dextran	CEF	RSV	29	2	>20	(1)
(MW: $2x10^6$)	NIH 3T3	A/E-MLV	10 – 13	0.1 - 1.75	>5	(3)
	NIH 3T3	E-MLV	17	40	n/a	(4)
	mouse myoblasts	E-MLV	30	40	n/a	(4)
Poly-L-ornithine HBr (MW: $2.1x10^4$)	CEF	RSV	32	2	>20	(1)
Poly-L-lysine HBr (MW:$1x10^5$)	CEF	RSV	50	2	>20	(1)
Polybrene	CEF	RSV	79	2	>20	(1)
(hexadimetrine bromide)	NIH 3T3	E-MLV	8	8	n/a	(2)
(MW: 3600)	NIH 3T3	A/E MLV	5	5	n/a	(3)
	NIH 3T3	E-MLV	6	10	n/a	(4)
	NIH 3T3	E-MLV	n/a	5-20	>32	(5)
	mouse myoblasts	E-MLV	9	10	n/a	(4)
	human T lymphocytes	A-MLV	12	8	n/a	(2)
	human keratocytes (p)	A-MLV	6	8	≥8	(6)
	NIH 3T3	A-MLV	~10	13	≥ 13	(8)
	NIH 3T3	VSG-G MLV	10	8	≥8	(7)
Polyethylenimine	NIH 3T3	A/E-MLV	17 - 19	0.25 - 1.25	>0.5	(3)
Liposomes						
LipofectAmine	NIH 3T3	A/E-MLV	11 – 20	0.5 – 0.7	1	(3)
(DOSPA – DOPE)	NIH 3T3	E-MLV	10	15 μL/mL	n/a	(4)
	mouse myoblast	E-MLV	16	10 μL/mL	n/a	(4)
	HT1080	A-MLV	60	0.8 μM	n/a	(9)

Cationic compound	Target cell	Virus or Vector	Enhancement	Optimal concentration	Toxicity	Reference
			(fold)	(μg/mL)	(μg/mL)	
		Liposomes				
Lipofectin (DOTMA-DOPE)	HT1080	A-MLV	37	1.1 μM	n/a	(9)
DOTAP	HT1080	A-MLV	5	1.8 μM	n/a	(9)
DOSPA-DOPE	NIH 3T3	A-MLV	20	7.1	n/a	(10)
		Lipopolyamine				
DOGS	NIH 3T3	A/E-MLV	24 - 36	1.75 - 5	>30	(3)
		Peptides				
Protamine Sulfate	CEF	RSV	22	32	n/a	(1)
(salmon)	NIH 3T3	E-MLV	5-10	7	n/a	(2)
	NIH 3T3	A/E-MLV	7-11	1-5	>5	(3)
	human T lymphocytes	A-MLV	5-10	10	>10	(2)
	human keratocytes (p)	A-MLV	4	8	≥8	(6)
Mixed histone						
(calf thymus, type II)	CEF	RSV	9	ND	n/a	(1)
(calf thymus, type IIA)	NHI 3T3	E-MLV	6-8	5	>100	(4)
	mouse myoblast	E-MLV	12-15	5	>100	(4)
Polymixin B	CEF	RSV	27	128	>128	(1)

n/a: not available p: primary cells

CEF: chicken embryon fibroblast, RSV: Rous sarcoma virus, DOGS: dioctadecylamidoglycylspermine

LipofectAmine: combination of 2,3-dioleyloxy-N-[2-(sperminecarboxamido)-ethyl]-N,N-dimethyl-1 propanaminium trifluoroacetate (DOSPA) and dioleoyl L-α-phosphatidylethanolamine (DOPE) (3:1 w/w)

(1) (Toyoshima and Vogt 1969) (2) (Cornetta and Anderson 1989) (3) (Themis et al. 1998) (4) (Singh and Rigby 1996) (5) (Davis et al. 2004) (6) (Seitz et al. 1998) (7) (Kwon and Peng 2002b) (8) (Chuck and Palsson 1996a) (9) (Hodgson and Solaiman 1996) (10) (Porter et al. 1998)

Interestingly, mixed histones have also been reported to provide similar increases to those obtained using protamine sulfate and polybrene, but with no toxicity reported up to 100 μg/mL (Singh and Rigby 1996). However their use has been limited to mixed tissue-derived preparations, thereby confounding the effect of each of the 5 histone classes. Histones are a family of cationic proteins rich in positively-charged lysine and arginine residues (Table 1.3) composed of the core histones H2A, H2B, H3.1 and H4 that assemble into an octamer structure around which 146-147 bp of DNA is wrapped to form the nucleosome (Luger et al. 1997). The lysine-rich "linker" histone H1, binds to the DNA entering and exiting the nucleosomes and contributes to the maintenance of higher chromatin structures (Izzo et al. 2008). As opposed to synthetic lysine or arginine homopolymers, basic amino acid residues are not uniformly distributed in histones but instead occur in clusters, primarily near the ends of the protein. In addition to their positive charge, the core histones have cell-penetrating properties as they have been shown to translocate across the cell membrane independently of transporters or specific receptors. The cell penetration potential differs between histone types with H2A and H4 demonstrating the greatest ability to penetrate cells (Hariton-Gazal et al. 2003). Furthermore, multiple nuclear localization signals (NLS) have been identified on all histone proteins, and are essential to mediate their active transport into the nucleus (Baake et al. 2001; Breeuwer and Goldfarb 1990; Schwamborn et al. 1998). NLS were located within the N-terminal domain of the core histones and in their globular region, respectively, for classic NLS and non-classic NLS-types, which depend on the secondary protein structure. These histone features have been used to mediate the nuclear import of proteins and nucleic acids (Balicki and Beutler 1997; Wagstaff et al. 2007). For these

applications, certain histone types, such as histone H2A, were shown to outperform other histones (Balicki and Beutler 1997). Based on these reports, there is a high probability that certain histones types could also mediate greater increases in retroviral transduction. Furthermore, histones present within nucleosomes can bind to cell membranes through an interaction with cell surface proteoglycans. Following their adsorption to the cell surface, they were found to mediate the adsorption of sulfated polysaccharides onto the cell surface (Watson et al. 1999). As retroviral vectors have envelope heparan sulfate proteoglycans inherited from the packaging cell line (Kureishy et al. 2006), histones are excellent candidates to enhance vector adsorption onto target cells. In addition to providing enhanced retroviral adsorption, they have the potential to influence the intracellular trafficking of viral vectors and could facilitate their import into the nucleus.

Table 1.3 Properties of canonical bovine histone proteins

Histone	Molecular Weight (kDa)	Amino acid residues		
		Lysine	Arginine	Cysteine
Lysine-rich				
H1	21 – 22	55 - 63	3 - 4	0
Slightly arginine-rich				
H2A	14.1	14	12	0
H2B	13.9	20	8	0
Arginine-rich				
H3.1	15.4	13	18	2
H4	11.4	11	14	0

(vanHolde 1989) except for H1 where H1.2, H1.3 and H1.4 were obtained from Uniprot (accession # A3KN02, A7MAZ5 and A5PK20)

1.4.6. Minimizing extracellular viral decay

The viral vector decay rate has been found to be exponentially dependent on temperature and was reported to follow a bi-phasic Arrhenius type function in temperature ranges above and below 37^{o}C (Higashikawa and Chang 2001). Increases in

transduction were achieved by transiently lowering the cell culture temperature from 37°C to 32°C in order to reduce the decay rate of the retroviral vectors (Kotani et al. 1994). Lower temperatures may also reduce target cell growth rate (Drouin et al. 2007) and, hence, transduction rates. Thus, this approach may not be suitable for all cell types.

1.4.7. Increased entry and post-entry rates

In order to improve the entry rate of viral vectors, the envelope protein of a different virus can be substituted (pseudotyped) in order to target an alternate receptor expressed at higher levels (Table 1.4). This approach has widened the host range of ecotropic murine leukemia virus-based vectors. In particular, vectors pseudotyped with the vesicular stomatitis virus G (VSV-G) protein offer a wide tropism. However, the constitutive expression of VSV-G is toxic to packaging cells, requiring the use of inducible systems or transient transfection (Ory et al. 1996), and thus significantly complicating retroviral vector production. Furthermore VSV-G pseudotyped vectors cannot be used in co-cultivation systems as the VSV-G protein can induce fusion between the packaging and target cells (Ory et al. 1996).

Table 1.4 Several retroviral pseudotypes and their cellular receptors

Pseudotype / Envelope Protein	Receptor
Murine ecotropic	Cationic amino acid transporter (mCAT-1) [1,2]
Murine amphotropic	Inorganic phosphate transporter (Pit-2) [3]
Gibbon ape leukemia virus	Inorganic phosphate transporter (Pit-1) [4]
Vesicular stomatitis virus G protein	Unknown (not phosphatidylserine) [5]

[1] (Wang et al. 1991), [2](Kim et al. 1991), [3](Chien et al. 1997), [4] (Olah et al. 1994), [5](Coil and Miller 2004)

Alternatively, the cell culture medium changes can increase receptor expression leading to higher transduction. For Pit-1 and Pit-2 receptors, this can be achieved through phosphate depletion of the medium (Chien et al. 1997).

Treatment of the target cells with phosphatidylserine has been shown to enhance transduction by 2- to 20-fold (Coil and Miller 2005a). This effect was not shared by other negatively-charged phospholipids such as phosphatidylcholine, phosphatidylglycerol or phosphatidylethanolamine, and was limited to enveloped viruses. It was therefore hypothesised that phosphatidylserine acted by enhancing membrane fusion without by-passing the receptor requirement. However, in cases where retroviral infection is blocked due to the expression of non-functional N-glycosylated receptors (Tavoloni and Rudenholz 1997), pretreatment of the target cells with phosphatidylserine up to 24 h prior to transduction reversed this blockage (Coil and Miller 2005b).

1.4.8. Lentiviral vectors

Given the requirement for the nuclear envelope to dissolve in order for integration to proceed for gammaretroviral vectors, transduction increases can be achieved by increasing the growth rate of the target cells. Prestimulation of CD34+ cells with cytokines prior to the addition of the retroviral vectors is commonly used to increase transduction (Hanenberg et al. 1997), although this may compromise the maintenance of the hematopoietic stem cell (HSC) population. To alleviate this need to induce the *ex vivo* proliferation of such non-dividing target cell populations, retroviral vectors based on lentiviruses have been designed, which can transduce non-dividing cells (Kafri et al. 1999; Naldini et al. 1996). Lentiviral vectors have similar diameters and stabilities ($t_{1/2}$ ~ 4.5 h) to those reported for gammaretroviral vectors (Higashikawa and Chang 2001), and are therefore subject to similar mass transport limitations. As was the case with gammaretroviral vectors, lentiviral vectors can be pseudotyped with various envelop proteins (Kim et al. 2010).

1.4.9. Acoustic treatments

Recently, increases in retroviral transduction have been reported by exposing the target cells in the presence of retroviral vectors to either running (Naka et al. 2007) or standing acoustic wave fields (Lee and Peng 2005; Lee et al. 2005). With running waves, transduction was apparently increased by 2.3- to 6.6-fold following a 5 s exposure at 1 W/cm^2. Particles of greater density but lower compressibility than the surrounding medium are displaced to the pressure node planes within acoustic standing wave fields where they will accumulate within the local maxima of acoustic energy density (Woodside et al. 1998). These properties have successfully been applied to the development of acoustic filters for the retention of mammalian cells (Gorenflo et al. 2003; Pui et al. 1995; Trampler et al. 1994). The displacement velocity towards the pressure nodes varies as a function of the square of the particle diameter. In the case of mammalian cells, a velocity on the order of 1 mm/s was estimated (Woodside et al. 1997). For a viral vector of 100 nm, the velocity would be <0.0001 mm/s, thus making it unlikely that they would be effectively displaced together with the cells. Based on this analysis, it was surprising that retroviral transduction was reported to be increased by 2- to 4-fold following a 5 minute exposure to a 1 MHz acoustic standing wave field. Lee et al. (2005) hypothesized that the increase was due to the drag on the retroviral vectors induced by acoustic microstreaming, allowing them to circulate between the nodal and antinodal planes, thereby causing increased attachment of the viruses to the target cells. It is unlikely that convective flow alone could generate this increase given that, in the flow-through design, flow alone did not increase transduction (in the absence of significant adsorption of the retroviral vectors to the membrane) (Chuck and Palsson

1996b). Given that cell viability measured by Trypan blue decreased from 99% to 95% within 20 minutes, cell damage may have occurred as a result of the acoustic treatment. This could be due to cavitation or, at high power input, resonance within the field can fail, leading to running waves of high intensity whose resulting shear forces can damage cells (Pui et al. 1995). Furthermore, the increase in transduction peaked at 5 minutes and decreased following prolonged exposure, thus also suggesting the occurrence of cellular damage. An investigation of the potential effect of cell lysate on viral transduction could provide an explanation for these results.

1.5. Thesis objectives

1.5.1. Lysate as a source of variability in transduction protocols

The development of robust protocols requires a more fundamental understanding of the many factors that can influence retroviral transduction. In recent years, cell lysate has been shown to impact multiple bioprocesses including antibody production (Trexler-Schmidt et al. 2010) and cell differentiation (Freberg et al. 2007). An early report also showed that infection by wild-type retroviruses was increased in the presence of a lysate supernatant (Toyoshima and Vogt 1969). Surprisingly, especially since the development of retroviral vectors, this observation has not been followed up to determine its implications for vector transduction. Yet, several lysate components (e.g., proteoglycans, phosphatidylserine and histones) were independently shown to modulate retroviral transduction. In order to improve the robustness of retroviral transduction protocols, the potential magnitude of the lysate effect as well as its mechanism need to be properly investigated. In chapter 2, the impact of cell lysate on the transduction of suspension

cells will be evaluated alone and in combination with two transduction enhancers: protamine sulfate and fibronectin. The impact of cell lysates on acoustic standing wave field-enhanced retroviral transduction will also be described in Appendix A.

1.5.2. Analysis of cell lysate to identify novel transduction-enhancing candidates

Most protocols developed to date only address a single limitation of the retroviral transduction process such as mass transport or binding. As a result, multiple protocols often need to be combined (e.g., centrifugation with addition of Polybrene) in order to maximize the retroviral transduction efficiency (Szyda et al. 2006). The development of methods and reagents that simultaneously address both of these limitations would simplify the overall transduction process while achieving greater transduction efficiencies and likely contribute to an increase in process robustness. Given the net transduction increase observed in chapter 2 with whole cell lysates, chapter 3 will focus on characterizing the active components present in the lysate and analyzing their mechanism(s) of action. This approach will identify novel transduction-enhancing candidates and, by determining the mechanism of action, will provide a foundation towards the development of more effective transduction reagents.

1.5.3. Screening of histone proteins

Characterization of the transduction-enhancing component within cell lysates suggested the involvement of arginine- and/or lysine-rich peptides of nuclear-origin such as histones. To date, the application of histones to enhance transduction has been limited to mixed histone preparations (section 1.4.5). Thus, the effect of individual histone types,

each with a varying content of positively-charged arginines and lysines (Table 1.3), on retroviral transduction has yet to be resolved. In chapter 4, bovine histone fractions will be screened based on their lysine and arginine content. The use of human recombinant histones to increase transduction will also be evaluated.

1.5.4. Development of a transduction reagent based on histone aggregates

The fractionation of the whole cell lysate demonstrated that greater increases in transduction were achieved using aggregates, thus enabling sedimentation of the vector and thereby overcoming mass transport limitations (Chapter 3). In chapter 4, the arginine-rich histone fraction provided greater transduction increases with negligible toxicity. Based on both of these previous observations, it was hypothesized that protein aggregation could be leveraged to further improve the transduction-enhancing potential of histones. In chapter 5, the effect of histone aggregation will be explored as means to develop a histone-based reagent effective on cell lines and primary hematopoietic stem cells using both gamma- and lentiviral vectors.

2. Effect of Cell Lysate on Retroviral Transduction Efficiency of Cells in Suspension Culture [1]

2.1. Introduction

Despite efforts to consistently use the same transduction protocol, significant variability in transduction efficiency often occurs. This occurrence has been attributed in part to variations in factors associated with viral vector production including packaging cell concentrations, harvest duration and pH (Kotani et al. 1994; McTaggart and Al-Rubeai 2000; Reeves et al. 2000). Packaging cell lines have also been shown to secrete proteoglycans that inhibit transduction (Le Doux et al. 1996). Production temperature variations may alter the viral membrane's composition and retroviral vector decay kinetics (Beer et al. 2003; Carmo et al. 2006). Some of the variability observed can also be attributed to the state of the target cells, including their viral receptor expression level and division rate (Grabarczyk et al. 2002; Hennemann et al. 2000b; Miller et al. 1990; Relander et al. 2002; Roe et al. 1993).

Another variable factor in cultures is the presence of cellular debris, such as from the exposure of cells to excessive shear that can lead to membrane disruption and cell lysis (Kim et al. 2007). Some retroviral vector production strategies or transduction protocols currently under development have the potential to generate cell lysates as a by-product. An early study reported that the infection of cells by wild-type retroviruses was increased by the addition of soluble factors present within cell extracts (Toyoshima and Vogt 1969). The transduction by other viral vectors such as adeno-associated viruses was

[1] A version of Chapter 2 was published: Beauchesne PR, Bruce KJ, Bowen BD and Piret JM. 2010. "Effect of cell lysates on retroviral transduction of cells in suspension culture. Biotechnology and Bioengineering. 105 (6), p. 1168-1176.

also increased by cell extracts, although this effect was dependent on the cell line from which the extracts were derived (Tenenbaum et al. 1999).

The impact of whole cell lysates on the transduction of suspension cells by gammaretroviral vectors was therefore investigated. This effect was quantified by measuring the transduction, in the presence of cellular lysates, of human and mouse cell lines by a gibbon ape leukemia virus-pseudotyped retroviral vector (GaLV) carrying the eGFP gene. The hematopoietic human TF-1 and K-562 cell lines were selected to assess the effect of cell lysates as both were previously used as models in studies to evaluate protocols to enhance retroviral transduction (Bahnson et al. 1995; Lee and Peng 2005). The B cell progenitor mouse line BaF3 was also selected to evaluate the effect of cell lysates on the tropism of the GaLV vector as well as to measure the effect of lysate on the mouse system using a Moloney murine leukemia virus-pseudotyped retroviral vector. The effect of lysate derived from NIH 3T3 cells, from which many packaging cell lines were engineered, was evaluated on these cell lines as lysate originating from the packaging cells during vector production could potentially influence retroviral transduction. Given the magnitude of the response obtained with a TF-1 lysate, the effects of lysate and target cell concentrations were further studied. In order to better predict the overall influence of lysate on the transduction of suspension cells, an empirical model was proposed based on the lysed-to-target cell ratio. The stability of the lysate was evaluated to determine whether its activity would outlast that of the viral vectors during culture or long-term storage. Finally, the interaction of lysate with fibronectin and protamine sulfate, two additives commonly used to enhance retroviral transduction, was investigated. Overall, the presence of lysates was shown to

significantly impact retroviral transduction protocols and have the potential to add to the effect of protamine sulfate or completely mask the influence of fibronectin.

2.2. Materials and methods

2.2.1. Cell lines and retroviral vector production

Human erythroleukemia TF-1 cells (CRL-2003, American Type Culture Collection (ATCC), Manassas, VA) were cultured in Dulbecco's modified Eagle's medium (DMEM) (Invitrogen, Burlington, ON, Canada) supplemented with 10% FBS (Invitrogen) and 5 ng/mL human recombinant GM-CSF (Terry Fox Laboratory (TFL), Vancouver, BC, Canada). Human leukemia K-562 cells (CCL-243, ATCC) and mouse fibroblast NIH 3T3 cells (CRL-1648, ATCC) were cultured in DMEM with 10% FBS. Mouse BaF3 pro-B cells were maintained in RPMI 1640 (Invitrogen) supplemented with 10% FBS, 4 mM L-glutamine (Invitrogen), 1:100,000 v/v monothioglycerol (Sigma-Aldrich, St. Louis, MO), and 5 ng/mL murine IL-3 (TFL).

Retroviral vectors with a humanized red-shifted green fluorescent protein (GFP) reporter gene under the control of MSCV long terminal repeats were produced from a PG-13 packaging cell line (GaLV) (TFL) (Hennemann et al. 1999; Miller et al. 1991) or a GP+E-86 packaging cell line (ecotropic) (TFL) (Buske et al. 2001; Markowitz et al. 1988). Both cell lines were cultured in DMEM with 10% FBS in 1700 cm^2 expanded surface roller bottles (Corning, Lowell, MA) at 37^oC and 10% CO_2. Virus-containing medium (VCM) was harvested over 24 h when the cultures reached 90% confluence (Reeves et al. 2000). For each vector, VCMs from 4 roller bottles were pooled, filtered

with a 0.45 μm pore size Durapore PVDF membrane (Millipore, Billerica, MA) and stored at -70^{o}C.

2.2.2. Cell lysates

Cell lysates were obtained through a rapid freeze-thaw process. This approach allowed aseptic processing and cell lysis without chemical additives. Briefly, cells taken from cultures in the exponential growth phase were centrifuged at 200×g for 5 min, separated from the supernatant and resuspended in DMEM at 4×10^{6} cells/mL. 5 mL aliquots were then transferred to 15 mL polypropylene tubes (Sarstedt, Nümbrecht, Germany), put in a -70^{o}C freezer for at least 1 h and thawed at 37^{o}C for 0.5 h. An additional freeze-thaw cycle ensured that no viable cells remained and did not reduce the activity of the whole cell lysate (data not shown). Debris aggregates were resuspended before the lysate preparation was added to the cell culture.

2.2.3. Viable cell count

All cell counts were performed with a Cedex automated cell counter (Innovatis, Bielefeld, Germany) using the trypan blue exclusion method. An average of 20 images analyzed with the Std. Cell (v 5.00) algorithm was taken for each sample. With lysate alone, less than 0.8±0.2% of the lysed cells were counted as viable and 6.5±1.8% as nonviable, leaving over 92±2% of the lysed cells fragmented to debris and therefore uncountable. Incubation of the lysate alone in growth medium over 14 days did not yield any viable cells, demonstrating that the cell counts were not influenced by carry-over of intact cells with the lysate. Thus, the Cedex automated counts of “viable” cells in the lysate were actually not viable cell counts.

2.2.4. Transduction assay

Target cells were resuspended in fresh growth medium before the start of the transduction assay. Unless otherwise stated, the same batch of GaLV retroviral vectors was used for all experiments. VCM was thawed at 37°C for 20 min and diluted with growth medium to obtain a final dilution of 1 in 8. In T-25 untreated flasks (Sarstedt), target cells were mixed with cell lysate (concentration adjusted using DMEM) and VCM at a liquid depth of 3 mm. Target cells were incubated in the presence of viral vectors for 24 h at 37°C and 5% CO_2 in air. A cell count was performed after 24 h. Cells were then transferred into 6-well untreated plates (Sarstedt), diluted 1:5 in growth medium and expanded for an additional 48 h before analysis for GFP expression (Klein et al. 1997). GFP expression was assayed by fluorescence activated cell scanning with a FACSCalibur system (BD Biosciences, San Jose, CA). Flow cytometry controls performed in the absence of target cells showed that the lysate addition did not bias the analysis for GFP expression. Forward and side scatter gating readily excluded the cell debris present within the lysate preparation. Transduction efficiency was expressed as the ratio of viable GFP^+ cells over total viable cells that exclude propidium iodide at 5 µg/mL (Sigma-Aldrich).

2.2.5. Surface coating and loading

Prior to the transduction assay, 24-well non-treated plates (Sarstedt) were coated with 150 µL bovine fibronectin (Sigma-Aldrich) at 67 µg/mL (effectively providing a 5 µg/cm^2 coating), 150 µL lysate at 4×10^6 cells/mL (3×10^5 lysed cells/cm^2) and 400 µL PBS (Invitrogen) as a control for 4 h at 23°C. Excess liquid was removed and the surface

washed with 200 µL PBS. Virus was pre-loaded by adding 300 µL of VCM for 1 h at 37°C while the remaining VCM was stored at 37°C and used for the non-preloaded controls. Target cells were then added and the transduction assay was performed as described above.

2.2.6. Protamine sulfate

Before the transduction assay, protamine sulfate (Sigma-Aldrich) was mixed with the target cells in T-25 tissue-culture-treated flasks (Sarstedt) at a liquid depth of 3 mm with or without the addition of TF-1 cell lysate at 1×10^6 lysed cells/mL.

2.2.7. Statistical analysis

Treatment effects were compared to those of the control without lysate addition using Dunnett's procedure (Dunnett 1964). Model adequacy was assessed by a lack of fit test where residuals were compared to the data variance using an F-test for $p<0.05$. The main effects and interactions were analyzed by an ANOVA for $p<0.05$.

2.3. Results

2.3.1. Effect of target and lysate cell lines

The effect of whole cell lysates derived from the human leukemia suspension cell lines TF-1 and K-562, the mouse pro-B suspension cell line BaF3 and the anchorage-dependent mouse fibroblast line NIH 3T3 on retroviral transduction was determined for TF-1, K-562 and BaF3 target cells. With the exception of NIH 3T3 lysates with K-562 target cells, all lysates significantly enhanced the transduction efficiencies of TF-1 and K-562 but not of BaF3 cells by a GaLV pseudotyped vector (Figure 2.1A). TF-1 and K-562

express Pit-1, the receptor for GaLV, while mouse cells do not express Pit-1 and were therefore not susceptible to transduction by this retroviral vector (Farrell et al. 2002; O'Hara et al. 1990). Thus, the addition of lysates apparently did not alter the viral tropism. When an ecotropic Moloney murine leukemia virus vector was used on BaF3 cells, transduction was significantly enhanced by the addition of lysate (Figure 2.1B), thus demonstrating that the effect of lysate was not limited to retroviral vectors of the GaLV pseudotype.

The magnitude of the enhancement resulting from lysate addition was dependent on the target cell line. Although greater transduction efficiencies were obtained with K-562 target cells, lysate additions had a more pronounced effect on TF-1 cells relative to controls (no lysate), as transduction was increased by 2.7- to 4.5-fold in contrast to the 1.4- to 2.7-fold increases observed with K-562 cells. The increase in transduction efficiency was also a dependent on the cell line used to generate the lysate. Lysates from the adherent cell line NIH 3T3 had the least effect on the transduction of TF-1 and K-562 target cells, while human TF-1 and mouse BaF3 lysates had the greatest effect for both target cell lines. Lysate activity exhibited no species or GaLV receptor expression dependence.

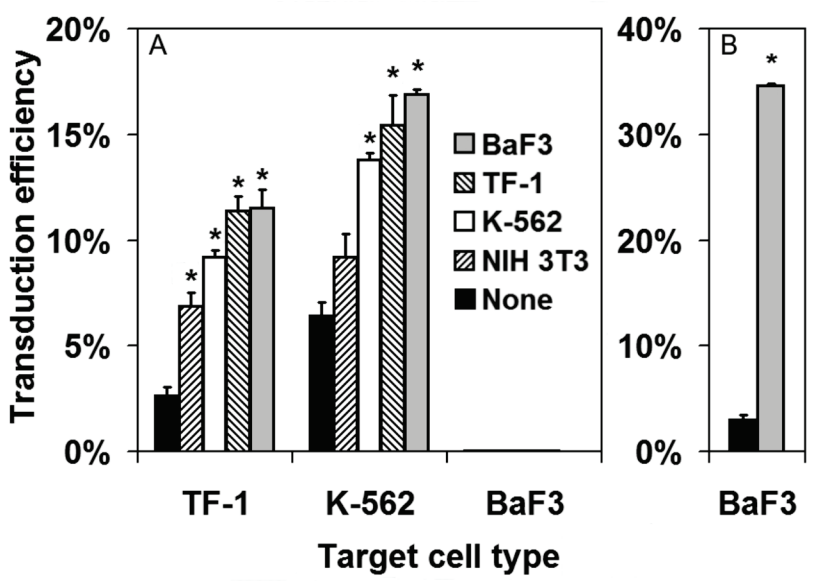

Figure 2.1 Effect of lysate source on the transduction efficiency of TF-1, K-562 and BaF3 target cells by (A) GaLV and (B) ecotropic retroviral vectors.
Lysate types were screened at 5×10^5 lysed cells/mL and 5×10^5 target cells/mL. Conditions with lysate were compared to a control without lysate addition (DMEM only) (* $p<0.01$) (n=3, error bars: SEM). With BaF3 target cells, no significant transduction events were detected using the GaLV vector.

2.3.2. Effect of lysate concentration

Given the magnitude of the enhancement of transduction efficiency previously obtained using GaLV vectors with the TF-1 lysate, this combination was selected to further investigate the effect of lysate concentration. The transduction efficiency of both K-562 and TF-1 target cells increased with increasing concentrations of TF-1 lysates (Figure 2.2). The transduction of TF-1 cells increased by over 7.5-fold and enhancement plateaued with the addition of 15 - 20×10^5 lysed TF-1 cells/mL while the transduction of K-562 increased by 2.7-fold and the effect plateaued at 5×10^5 lysed TF-1 cells/mL. These lysate concentrations did not affect the growth rates of TF-1 (Figure 2.3) and K-562 (data not shown). The parallel cell cultures all essentially doubled after 24 h in the presence of TF-1 lysate (up to ~2×10^6 lysed TF-1 cells/mL). Even over 6 days, the addition of 2×10^6 lysed BaF3 or TF-1 cells/mL to TF-1 or BaF3 cultures had no

observable effect on the maximum cell growth rate (Table 2.1). However, the maximal cell concentration was increased by up to 28% at this lysate level, presumably because the medium was enriched by compounds within the lysate.

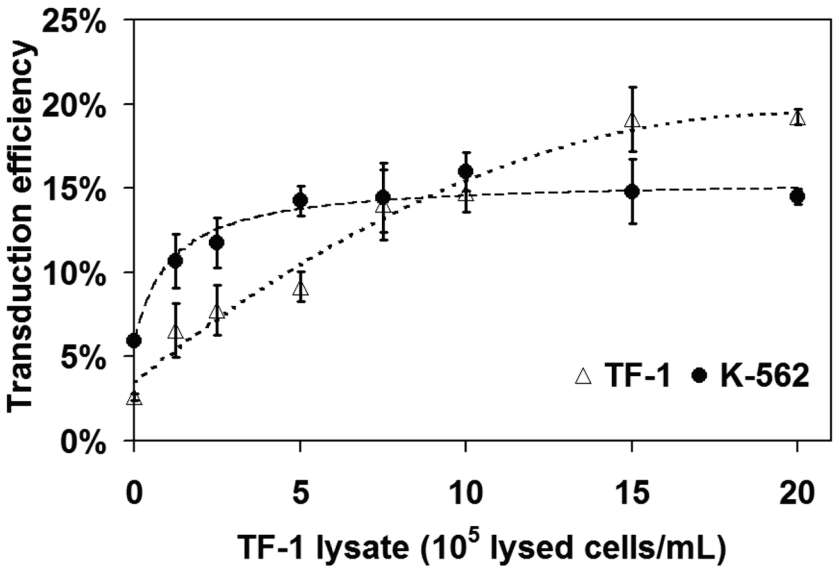

Figure 2.2 Transduction efficiency as a function of lysate concentration.
TF-1 lysate in DMEM was added to K-562 (5.5×10^5 cells/mL) or TF-1 (5.1×10^5 cells/mL) target cells. Transduction enhancement with lysate relative to control was significant ($p<0.05$) for both target cell lines at lysate concentrations greater or equal to 2.5×10^5 lysed cells/mL (n=3, error bars: SEM).

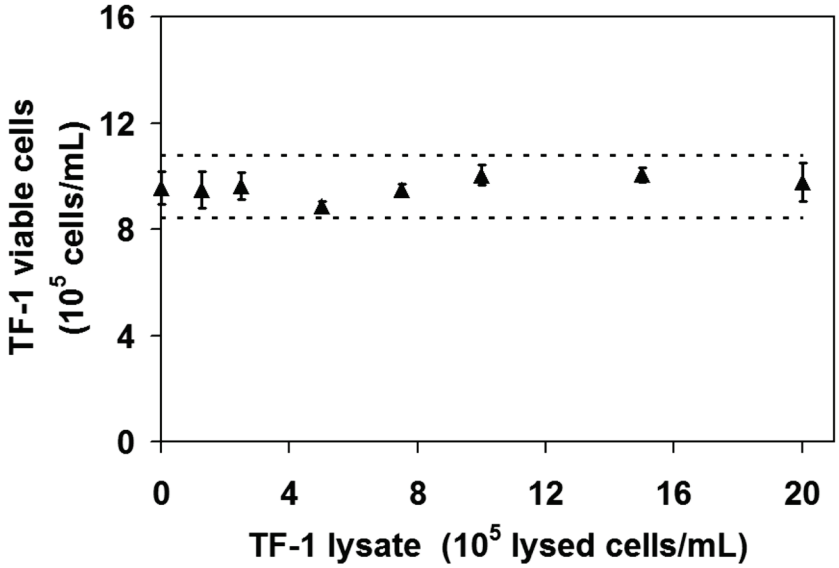

Figure 2.3 TF-1 cell lysate addition of up to 2×10^6 lysed cells/mL to TF-1 cell cultures did not affect growth.
TF-1 target cells were seeded at 5.1×10^5 cells/mL with increasing concentrations of TF-1 cell lysate in DMEM and compared to a control with DMEM only. Cells were cultured for 24 h and counted by a CEDEX automated cell counter using a trypan blue exclusion assay. Dotted lines: 95% confidence interval (n=3, error bars: SEM).

Table 2.1 The maximum growth rates of TF-1 and BaF3 cells were not altered by the addition of TF-1 or BaF3 lysate relative to a control with no lysate.
With BaF3 cells, the average maximum viable cell concentrations were increased by 1.21 to 1.28-fold. With TF-1 cells, only the TF-1 lysate increased the average maximum viable cell concentration by 1.13-fold while the BaF3 lysate had no effect. Cells were seeded at 1×10^5 cells/mL with 2×10^6 lysed cells/mL and cultured over 6 days. Viable cell concentrations were measured at 24 h intervals. The maximum growth rate was evaluated between 0 and 72 h by linear regression. (n =3)

Cell line	Lysate	Control	BaF3	TF-1
TF-1	Average (h^{-1})	**0.0353**	**0.0336**	**0.0356**
	SEM (h^{-1})	0.0007	0.0015	0.0020
	p-value		0.39	0.91
	Maximum viable cell concentration relative to control	-	0.98	1.13
BaF3	Average (h^{-1})	**0.0443**	**0.0448**	**0.0459**
	SEM (h^{-1})	0.0005	0.0011	0.0013
	p-value		0.74	0.18
	Maximum viable cell concentration relative to control	-	1.21	1.28

2.3.3. Effect of target cell concentration

The effect on the transduction efficiency of varying the target cell concentration (1.0×10^5 to 2.0×10^6 TF-1 cells/mL) in the presence of a constant cell lysate concentration (1×10^6 lysed TF-1 cells/mL) was also measured (Figure 2.4). The total number of transduced cells increased in the presence of lysate, but the transduction efficiency decreased as a quadratic function of the target cell concentration. This decrease suggested that the lysate effect was diluted at higher target cell concentrations. It is not expected that the viral vectors became limiting under these conditions since transduction efficiency was further increased by 2-fold when lysate was supplemented with protamine sulfate (see interaction with protamine sulfate section below). Also, in the absence of cell lysate, the number of transduced cells increased with target cell concentration, whereas the transduction efficiency remained constant except at the lowest concentration of target cells (1.0×10^5 cells/mL). Decreased transduction efficiency at low target cell concentration has previously been reported but this phenomenon remains unexplained (Hanenberg et al. 1997; Morgan et al. 1995). To probe whether this was possibly an artifact of the low cell concentration or potentially delayed expression, the cells were expanded for an additional 2 days and transduction efficiency was measured a second time. At 1.0×10^5 target cells/mL, the transduction efficiency increased to a level similar to those obtained with higher cell concentrations in the absence of lysate. The transduction efficiencies of all other controls and all lysate conditions did not change significantly after the initial FACS measurement.

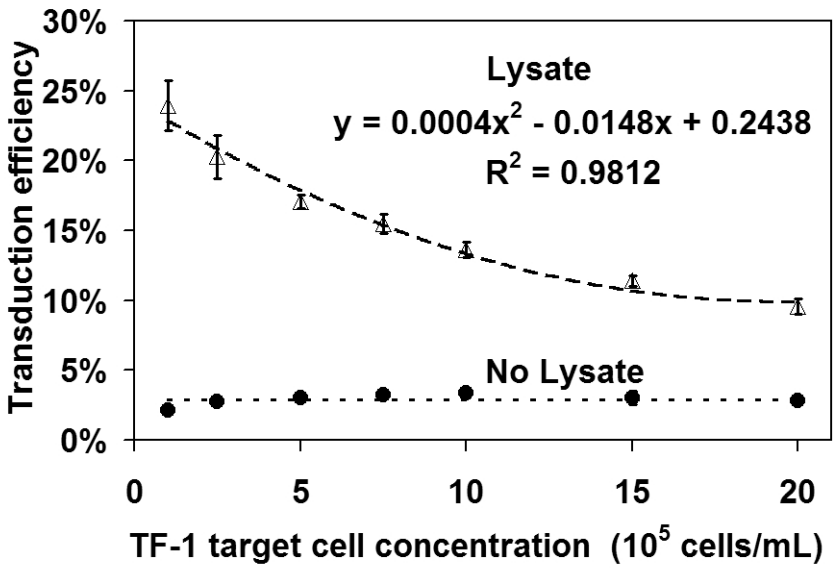

Figure 2.4 At constant TF-1 cell lysate concentration, transduction efficiency decreased as a function of the TF-1 target cell concentration.
TF-1 cell lysate (1×10^6 cells/mL) in DMEM was added to TF-1 target cells whose concentrations ranged from 1.0×10^5 to 2.0×10^6 cells/mL in VCM. A control was also performed using DMEM only. The increase due to lysate addition was significant ($p<0.05$) over all concentrations tested compared to the matching conditions without lysate. In the absence of lysate, except at 1.0×10^5 cells/mL, transduction efficiency did not differ significantly over the range of target cell concentrations. (n=3, error bars: SEM)

2.3.4. Predicting the effect of lysate addition

Although the transduction efficiency can vary between experiments, the fold increase in transduction efficiency for a given lysate and target cell concentration relative to a control without lysate was constant over the range of viral vector concentrations tested. For example, lysate concentrations of 1.0×10^6 lysed TF-1 cells/mL combined with TF-1 target cell concentrations of 5×10^5 cells/mL had transduction efficiencies of 14.7% in Figure 2.2 and 17.1% in Figure 2.4, but the relative increases (5.7- and 5.6-fold, respectively) remained similar. Transduction results, expressed as fold increases, better predict the outcomes of lysate additions over a range of VCM concentrations by normalizing for batch-to-batch titer variations. This allowed the pooling of data from Figure 2.2 and 2.4 for further analysis. The average transduction efficiency of target cells

in the absence of lysate (with the exception of the 1×10^5 cells/mL outlier to not overestimate the lysate effect) was used to calculate fold increases for the variable target cell concentration data set (Figure 2.4).

A dimensionless number, *R*, was defined as the ratio of lysed cells to viable cells. At constant *R*, the relative increases in transduction were similar, even with wide differences in lysate or target cell concentrations. For example, combinations of 2.5×10^5 lysed cells/mL and 5×10^5 target cells/mL or 1×10^6 lysed cells/mL and 2×10^6 target cells/mL both yield *R* values of 0.5 and similar ($p>0.3$) fold increases in transduction efficiency of 2.9 and 3.2, respectively. Increases in transduction efficiency as a function of *R* exhibited a saturation-type behavior (Figure 2.5). The combined effects of the target cell and lysate concentrations could therefore be predicted by the following equation:

$$Fold\ Increase = 1 + Fold_{Max} * \left(\frac{R}{K_L + R} \right) \qquad \textbf{Eq. 2.1}$$

From the data in Figure 2.5, the coefficients $Fold_{Max}$ and K_L were estimated to be 7.57 and 1.19, respectively, using the Hanes-Woolf method (Hanes 1932). Equation 2.1 fit both the variable lysate concentration and variable target cell concentration data sets for TF-1 cells. Based on this model, 77% of the potential increase in the transduction of TF-1 cells by GaLV-pseudotyped retroviral vectors with TF-1 lysate was realized at $R = 4$ and 89% at $R = 10$.

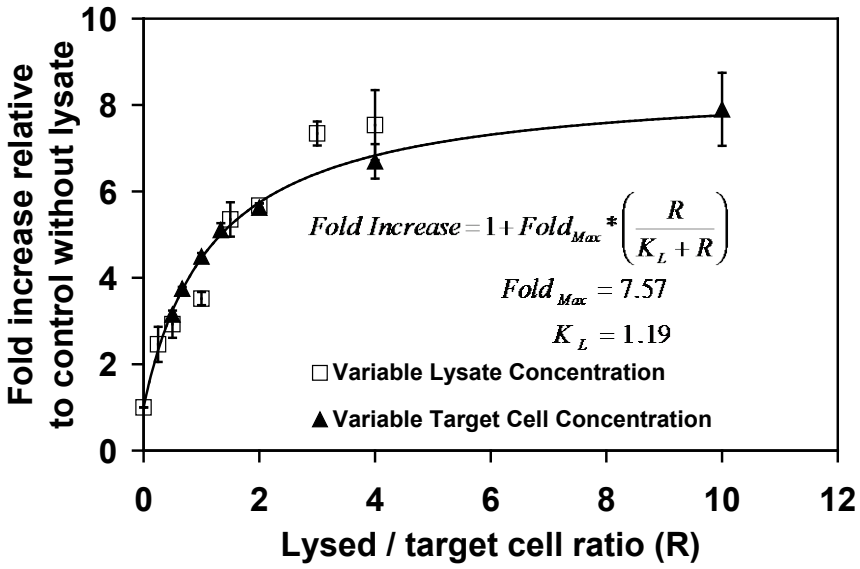

Figure 2.5 The increase in transduction efficiency of TF-1 cells relative to a control without lysate can be predicted using the lysed-to-target cell ratio.
Data sets obtained at variable lysate concentrations (Figure 2.2) (squares) and variable target cell concentrations (Figure 2.5) (triangles) were expressed as dimensionless numbers by taking the ratio of transduction efficiencies with and without lysate addition, and the ratio of the lysed and target cell concentrations. (*n*=3, error bars: SEM)

2.3.5. Lysate stability

Lysate stability was evaluated to determine the expected magnitude of the lysate effect on retroviral transduction over time following a cell lysis event, which could potentially occur prior to the transduction process such as during culture of the target cells, typically at 37°C, of the packaging cell line at 37°C or lower as well as during long term storage of the VCM at -70°C. In order to determine how the activity of TF-1 cell lysates compares with that of the viral vectors, the stability of lysates stored at -70, 4, 23 and 37°C was assessed over 49 days. The decay of the VCM used in the transduction assay and stored at -70°C was negligible as shown by the control without lysate that did not change over time (2.9±0.2%) (Figure 2.6). No significant decay in lysate activity was observed for storage at 4°C or at -70°C (frozen). However, at the two higher

temperatures, lysate activity exhibited first-order decay kinetics, with half-lives of 10.4±2.0 days at 37°C and 24.6±2.8 days at 23°C. Lysates stored for 49 days at 37°C had a transduction efficiency of 0.9%, a 69% reduction relative to that of the control without lysate. A 43% reduction in transduction efficiency relative to the control without lysate was also observed at 23°C after 95 days suggesting a net inhibitory effect. Thus, these results suggest that the lysate may be composed of a mixture of transduction enhancers and inhibitors.

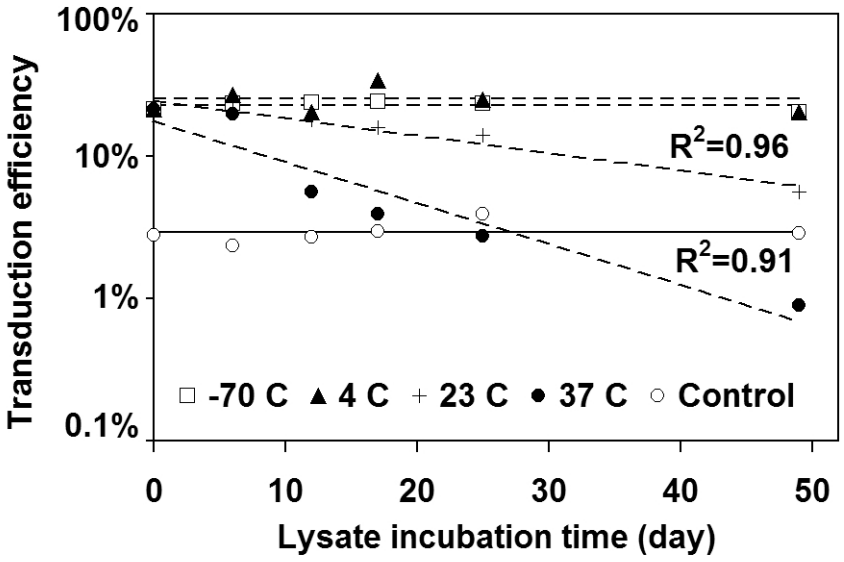

Figure 2.6 Lysate decay exhibited first-order decay kinetics.
Whole cell lysate was pre-incubated at temperatures of -70°C, 4°C, 23°C and 37°C for 0, 6, 12, 17, 25 and 49 days prior to the transduction assay using 5×10^5 TF-1 target cells/mL and 8×10^5 lysed TF-1 cells/mL. A control without lysate was also performed using DMEM only. Significant decay was observed at 23°C and 37°C ($p<0.01$). There was no significant decay at -70°C or 4°C ($p>0.3$).

2.3.6. Interaction with fibronectin

The efficacy of TF-1 cell lysate was compared with that of fibronectin, an extracellular matrix molecule known to mediate both virus and cell adhesion onto coated surfaces and widely used to enhance transduction rates (Moritz et al. 1994). Unlike for the lysate and as expected, the addition of fibronectin in solution did not yield any

increase in transduction efficiency relative to a control without lysate or fibronectin (Figure 2.7). When coated onto the surface prior to the addition of the VCM and target cells, fibronectin increased the transduction efficiency of TF-1 cells by 2.2-fold. Pre-loading the fibronectin-coated surface with viral vectors further increased transduction to 3.0-fold relative to the control without fibronectin. When TF-1 lysate was simply added in solution, the transduction efficiency increased by 7.2-fold, a significant improvement over fibronectin-coated surfaces even when they were pre-loaded with viral vectors. Coating the surface with lysate further increased the transduction efficiency to 10.4-fold as some of the active compounds apparently adhered to the hydrophobic polystyrene surface of the culture plates. Pre-loading of the viral vectors marginally increased transduction by an additional 2%, which was not significant. When lysate was combined with fibronectin either in solution, coated or with pre-loaded vectors, there was no significant difference compared with lysate alone in solution. This demonstrated that the presence of lysed cells has the potential to mask completely the effect of fibronectin and its requirements for surface coating and vector loading.

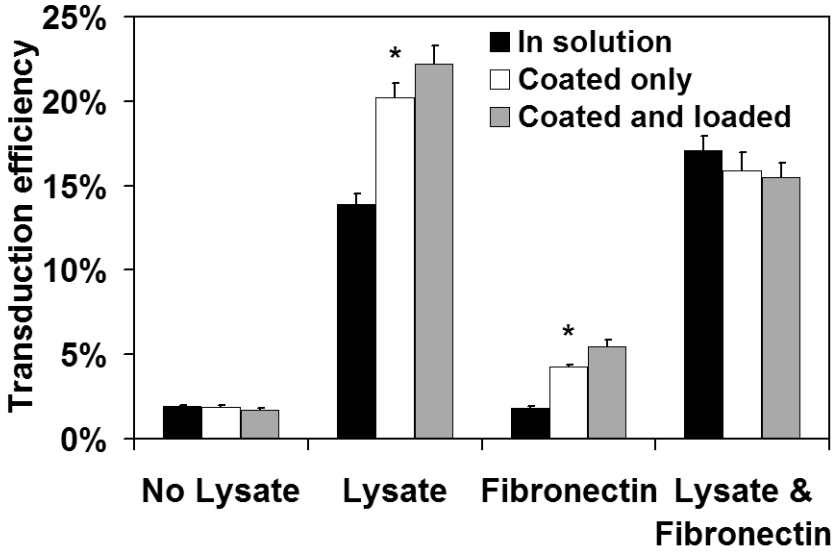

Figure 2.7 Effect of surface coating and viral vector pre-loading with lysate and fibronectin on the transduction efficiency of TF-1 cells (5×10^5 target cells/mL).
In solution, DMEM in the control, TF-1 lysate (1×10^6 lysed cell/mL), fibronectin (16.7 μg/mL equivalent to 5 μg/cm^2) or both were added to the target cells and viral vectors. Surfaces were also coated with PBS in the control, TF-1 cell lysate (3×10^5 lysed cells/cm^2 equivalent to 1×10^6 lysed cells/mL), and fibronectin (5 μg/cm^2) for 4 h at 23°C. On the coated surfaces, viral vectors were loaded for 1 h at 37°C prior to the addition of the target cells. Lysate in solution (1×10^6 lysed cells/mL) was subsequently added to each of the fibronectin conditions. Significance of coating and loading was tested: * $p<0.05$. (*n*=3, error bars: SEM)

2.3.7. Interaction with protamine sulfate

In the absence of lysate, the peak transduction efficiency was obtained at concentrations between 5 and 40 μg/mL of protamine sulfate (Figure 2.8A), in agreement with previous reports (Cornetta and Anderson 1989; Themis et al. 1998; Toyoshima and Vogt 1969). Lysate alone increased the transduction of TF-1 cells to 26.7%, which was significantly higher than the maximum 20.0% obtained with protamine sulfate alone. When lysate (1×10^6 lysed TF-1 cells/mL) was combined with protamine sulfate, the transduction efficiency was further increased up to 57.7% and the peak protamine sulfate concentration shifted to 160 μg/mL. Viable cell concentrations decreased significantly at

protamine sulfate concentrations exceeding 80 µg/mL, independently of the lysate additions (Figure 2.8B). While cell counts were marginally lower in the absence of lysate with protamine sulfate concentrations above 20 µg/mL, the difference was not statistically significant. Together these results suggest that the presence of lysate did not significantly reduce the toxicity of protamine sulfate. With other cell lines, protamine sulfate toxicity has been reported at concentrations as low as 10 µg/mL and may limit the increase in transduction when combined with lysate (Cornetta and Anderson 1989; Yang and Hsieh 2001).

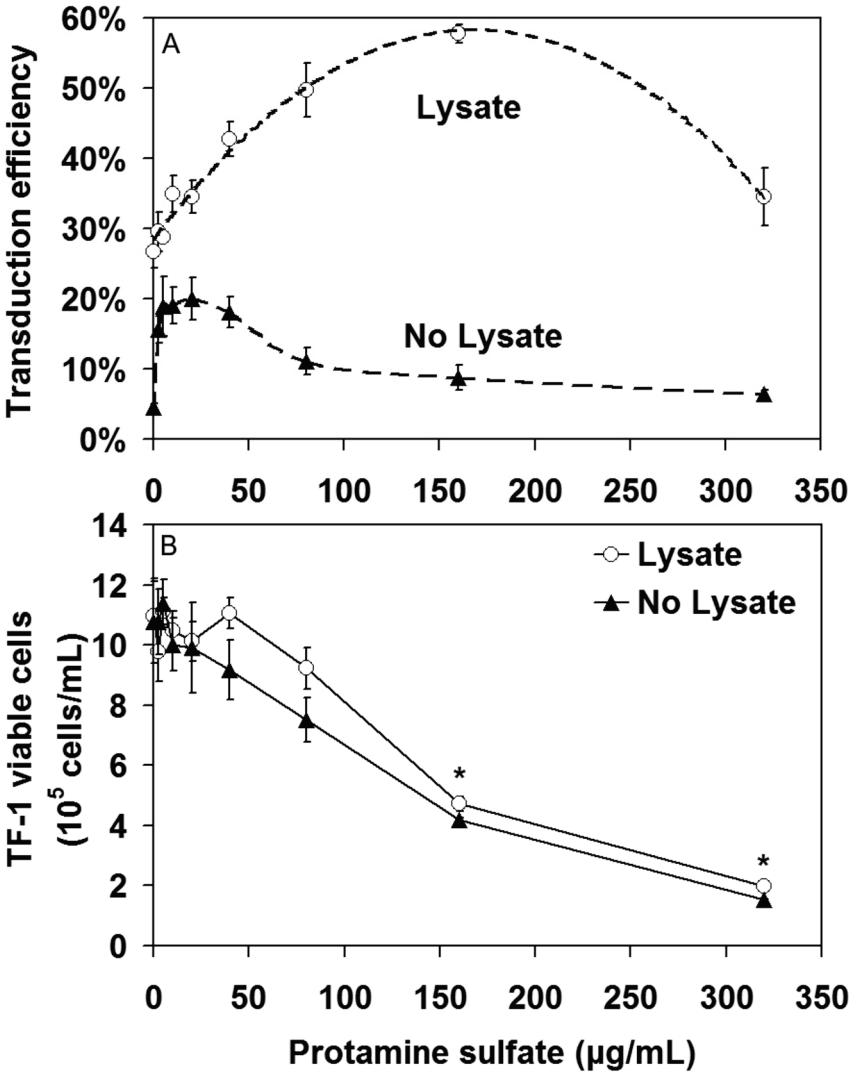

Figure 2.8 The addition of TF-1 cell lysate altered the dose-response obtained with protamine sulfate (A) but did not significantly alter toxicity (B).
Protamine sulfate was added to the target cells (5×10^5 cells/mL) with TF-1 lysate (1×10^6 lysed cells/mL) or without lysate as a control. Transduction was performed in tissue-culture-treated flasks. Cells were counted after 24 h by a Cedex automated cell counter using a trypan blue exclusion assay. Viable cell concentrations were compared to a control without protamine sulfate and lysate (* $p<0.05$). (n=3 except for 160 and 320 µg/mL where n=2, error bars: SEM)

2.4. Discussion

Many manipulations involving cells have the potential to generate lysate. In the case of retroviral transduction, this may take place during the production of the viral

vectors from a packaging cell line, the culture of the target cells prior to transduction, or the transduction protocol itself. Several packaging cell lines including PG-13 (GaLV-pseudotype), GP+E-86 (murine ecotropic) and PA317 (murine amphotropic) were derived from NIH 3T3 cells (Markowitz et al. 1988; Miller and Buttimore 1986; Miller et al. 1991), whose lysate was found to enhance transduction by 1.4- to 2.7-fold. The VCM is often stored frozen prior to the transduction process. Over the storage temperature range of -70 to 37°C tested, the decay rates of the enhancers present within the lysate were found to be far lower than those of the viral vectors. For example, at 37^{o}C where the decay rate was maximal, the lysate half-life was 10.4 days, much greater than the 5 - 10 h half-lives reported for retroviral vectors (Higashikawa and Chang 2001; Kwon and Peng 2002a). As a result, the enhancing ability of cell lysate remains long after most of the vectors have decayed. The presence of lysate in the VCM could also impact the downstream processing of retroviral vectors. Purification strategies often result in a partial loss of vector activity (for a review see Segura et al. 2006). The removal of transduction-enhancing lysate compounds could be responsible for part of this loss of activity.

For low target cell concentrations, such as for stem cell targeted experiments, even a low level of lysate from vector producer cultures could have a major effect on transduction rates. These lysate effects on transduction rates could be highly variable depending on the producer culture lysate content at the time of harvest. In the case where cell lysis occurs during the transduction process, both an increase in the lysate concentration and a decrease in the target cell concentration take place simultaneously. This would result in an increase in the ratio of lysed to target cells and therefore,

according to Equation 1, an increase in the transduction efficiency. Although most transduction protocols are not expected to disrupt the target cells, the exposure of target cells and retroviral vectors to ultrasound in either standing or continuous wave fields has recently been reported to increase retroviral transduction efficiency (Lee and Peng 2005; Lee et al. 2005; Naka et al. 2007). The exact mechanism of action is not yet fully understood. Additional work to characterize the interaction between lysate and acoustic standing wave fields is presented in Appendix A. In all cases tested, cell viability, measured using the trypan blue exclusion assay, decreased as a function of exposure time and power input or wave amplitude of the acoustic field. With acoustic methods, there is a risk of cavitation, which readily induces shear-stress-related lysis. Following freeze-thaw lysis, less than 8% of the cells were detected as being intact, indicating that cell lysis would remain mostly undetected by the trypan blue assay, and that cell viability may not accurately measure the extent of cell lysis. In order to rule out the generation of lysate as the mechanism of action, the lysing impact of new transduction methods on target cells should be measured with an alternative assay that does not rely on the cells remaining intact. Measuring the release of an intracellular enzyme, such as lactate dehydrogenase, may help quantify the degree of cell lysis (Crane et al. 1999; Wagner et al. 1992).

The improvement in transduction efficiency of TF-1 target cells by TF-1 cell lysate was predicted using a saturation equation whose form is similar to that of a Langmuir isotherm. All conditions used to generate this model yielded transduction efficiencies of less than 25%; therefore, the average copy number per transduced cell was expected to be approximately 1 (Kustikova et al. 2003). At higher vector concentrations,

a correction for mean copy number per cell will likely need to be included in the model. The form of the equation suggests that a sorbent-sorbate interaction may be involved in which the viral vectors initially complex with compounds present within the lysate and then these complexes adsorb onto the cells. It is also possible that the lysates first interact with the target cells and then mediate increased vector adsorption. In either case, the saturation observed could have occurred due to cell surface area or receptor limitations (Grabarczyk et al. 2002; Relander et al. 2002). Variations in Pit-1 expression levels between cell lines may be responsible for the earlier saturation and lower enhancement observed with K-562 compared with TF-1 target cells using the same TF-1 lysate. The parameters K_L and $Fold_{Max}$ are therefore expected to vary between different target cell lines. Furthermore, the parameters will likely also be a function of the lysate composition and, therefore, the cell line used to prepare the lysate.

Cell lysates are complex mixtures containing various proteins, lipids, DNA and RNA in soluble or aggregate form. Although GaLV-pseudotyped viruses were reported to bind to the receptor Pit-1 (Farrell et al. 2002), receptor presence did not influence the activity of the lysate as both BaF3 and TF-1 lysates had similar effects. Therefore, it is assumed that the free or membrane fragment-bound receptors did not contribute to the observed increase in transduction. Debris aggregates, such as membrane fragments, could also improve sedimentation of the vectors or binding to other cells, as murine leukemia viruses have been shown to bind non-specifically to cell surfaces (Pizzato et al. 1999).

Several cellular products are known to enhance retroviral transduction and may contribute to the effects of the lysates tested. Fibronectin has been reported to colocalize

retroviral vectors, via adherence to heparin binding domains, and cells, which may bind to the VLA-4 binding site CS1 or the VLA-5 adhesion site CBD (Hanenberg et al. 1996; Moritz et al. 1994). However, the presence of fibronectin, even when surfaces were coated and vector pre-loaded, did not explain the magnitude of the increase in transduction efficiency observed with lysate alone. Although lysate far outperformed fibronectin in solution, the transduction efficiency did increase upon surface coating. While vector pre-loading with lysate did not significantly further increase transduction, extending the pre-loading time could lead to increased transduction efficiencies as reported for fibronectin (Bajaj et al. 2001). Given the inhibitory effects of decayed lysate, surface coating may provide a purification strategy wherein the active compounds of the lysate exhibit a higher affinity for hydrophobic surfaces than do the inhibitors that may be preferentially washed away. The effects of lysate and fibronectin were not additive, suggesting that the lysate competed with fibronectin. This may indicate that compounds within the lysate exhibit a higher affinity than fibronectin for the viral vectors. Alternatively, the lysate may interfere with the adsorption of the vectors to fibronectin by interacting with either the fibronectin heparin binding domain or the heparan sulfate present on the surface of the retroviruses (Lei et al. 2002). Protamine sulfate, an arginine-rich peptide, has also been reported to enhance transduction due to its cationic charge (Cornetta and Anderson 1989; Toyoshima and Vogt 1969). However, protamines replace histones during spermatogenesis and are not expected to be present in somatic cells. Mixed histones have also been reported to increase transduction efficiency, but the exact mechanism of action on retroviral transduction has yet to be fully explained (Singh and Rigby 1996; Toyoshima and Vogt 1969). The phospholipid phosphatidylserine, in a

liposome structure, has been shown to increase transduction, possibly through enhanced fusion (Coil and Miller 2005a).

Cell lysates likely also contain transduction inhibitors, such as proteoglycans and glycoaminoglycans (Le Doux et al. 1996; Le Doux et al. 1999). The relative concentrations of enhancers and inhibitors are likely cell line dependent and could therefore modulate the overall transduction response to lysate. Furthermore, decayed lysate inhibited the transduction of TF-1 cells suggesting that, upon degradation of the enhancers, inhibitory effects dominate. However, it remains unclear whether the decay products of the enhancing compounds inhibit transduction or simply lose their activity. The combined effect of enhancers and inhibitors on retroviral transduction would likely depend on the relative concentration of each species, which could change over time as a function of their respective decay kinetics. Anionic polymers such as chondroitin sulfate C can also interact with cationic polymers through the formation of complexes which increase viral vector sedimentation and can decrease the toxicity of Polybrene (Le Doux et al. 2001). Protamine sulfate added with the lysate may have interacted in a similar fashion, leading to the increase in transduction observed. However, the presence of lysate did not reduce the toxicity of protamine sulfate.

In the absence of fibronectin or protamine sulfate, lysate was shown to significantly increase the transduction efficiency of suspension cells. When combined with protamine sulfate or fibronectin, it has the potential to alter the mechanism of action. In the case of fibronectin, the requirement for surface coating and vector loading was masked by the presence of lysate. With protamine sulfate, the addition of lysate resulted in a shift of the concentration of the former required to obtain the maximum transduction

efficiency. With lysate alone, transduction efficiencies were greater than with protamine sulfate- or fibronectin-based protocols. This was achieved even without surface coating, which was found to further increase transduction. Finally, over the concentration range tested, lysate addition did not alter the growth of TF-1 or K-562 cells. Given these advantages, the mechanism of action of lysate on transduction as a means to facilitate and accelerate genetic research relying on retrovirus-based gene delivery systems will be further investigated in Chapter 3.

3. Mechanistic Analysis and Characterization of Lysate-Enhanced Retroviral Transduction of Hematopoietic Cell Lines and Stem Cells

3.1. Introduction

The presence of cell lysate can significantly alter the outcome of many bioprocesses. For example, during antibody harvesting operations, the presence of cell lysate has been linked to decreased yields due to a reduction of antibody interchain disulfide bonds (Trexler-Schmidt et al. 2010). Cell extracts, with the cell debris removed, increased DNA methylation as well as histone modifications that resulted in cell reprogramming (Freberg et al. 2007). Infection by wild-type retroviruses was enhanced in the presence of cell extracts (Toyoshima and Vogt 1969). In the previous chapter, whole cell lysate was shown to significantly increase the retroviral transduction of suspension cell cultures (Beauchesne et al. 2010). A positive interaction on transduction was also observed between cell lysate and acoustic standing wave treatment (Appendix A). The present chapter investigates both the identity of the active components and their mechanism of action in an effort to specify novel candidates and strategies to further enhance retroviral transduction. The knowledge acquired through this exercise should also improve the ability to predict the impact of cell lysates in other contexts, such as on the production and downstream processing of retroviral vectors. For example, vector yields could decrease should lysate components mediate the adsorption, and loss, of vectors to the surface of the cell culture vessel surface during production of the VCM. Also, losses could occur during clarification of the VCM should vectors adsorb onto debris aggregates that will be removed during filtration.

Upon cell lysis, multiple intracellular compounds are released both in soluble form and as part of the debris aggregates. A limited number of these components have previously been reported to modulate retroviral transduction. Peptides such as histones and fibronectin, and phospholipids such as phosphatidylserine have been identified as enhancers (Coil and Miller 2005a; Hanenberg et al. 1996; Singh and Rigby 1996). In contrast, glycoaminoglycans and proteoglycans were shown to inhibit retroviral transduction (Le Doux et al. 1996). The number of potential components involved presents a significant challenge to the characterization of lysate-enhanced retroviral transduction.

Models have identified diffusion-limited mass transport and cell surface adsorption of retroviral vectors as two significant limiting steps in retrovirus-mediated gene delivery (Andreadis et al. 2000; Kwon and Peng 2002a; Tayi et al. 2010; Valentine and Allison 1959). Enhanced mass transport through sedimentation using centrifugation has been shown to improve retroviral transduction (Bahnson et al. 1995). Also, the addition of cationic species to boost non-specific retroviral vector adsorption to the target cell surface has led to increased transduction (Davis et al. 2002). Preconditioning culture vessel surfaces using additives such as protamine sulfate and fibronectin enhances the co-adsorption of target cells and retroviral vectors leading to greater transduction efficiencies (Hanenberg et al. 1996; Hennemann et al. 2000a).

In order to characterize the active component(s) in the cell lysate, the first step was to design the fractionation scheme shown in Figure 3.1. To determine whether the activity could be attributed to soluble factors or to components residing within the debris aggregates, microfiltration and centrifugation were used to separate the soluble and

insoluble fractions. The aggregates were subsequently disrupted by DNase I digestion to establish if DNA was an active component or if active compounds might be trapped within these large structures. Supplemental targeted enzymatic digestion of selected debris fractions was then used to further characterize the active components. Phospholipase A_2 was used to target phospholipids including phosphatidylserine while trypsin was employed to digest proteins and especially cationic peptides such as histones that are rich in arginine and lysine residues. A comparison between nucleated and anucleated cell lysates demonstrated that there were active components of nuclear origin. The transduction performance of nuclei-derived and whole cell lysates were compared to determine whether the active components were located within the intra- or extra-nuclear space of the cell.

Following the characterization of the active lysate components, the mechanisms of action of the main fractions were analysed. First, the impact of lysate on mass transport was evaluated. In particular, retroviral vector binding to debris aggregates and subsequent co-sedimentation was investigated. The impact of cell lysate on cell surface adsorption was also determined. Finally, the interaction of lysate components with the culture vessel surfaces was measured.

The residual transduction-enhancing potential of each lysate fraction was investigated using 2 cell-vector pairs: a cytokine-independent mouse sub-line derived from the BaF3 B progenitor cell line transduced by an ecotropic retroviral vector based on the Moloney murine leukemia virus, and a human TF-1 erythroleukemic cell line transduced by a retroviral vector pseudotyped with the gibbon ape leukemia virus. Finally, as a proof of concept for gene therapy applications, the lysate fraction exhibiting

the greatest transduction-enhancing potential was applied to increase gene delivery to mouse hematopoietic stem cells. Overall, this work should contribute to a greater understanding of the characteristics and mechanisms of lysate influences on retroviral transduction and provide a substantial foundation for the development of new and improved transduction protocols.

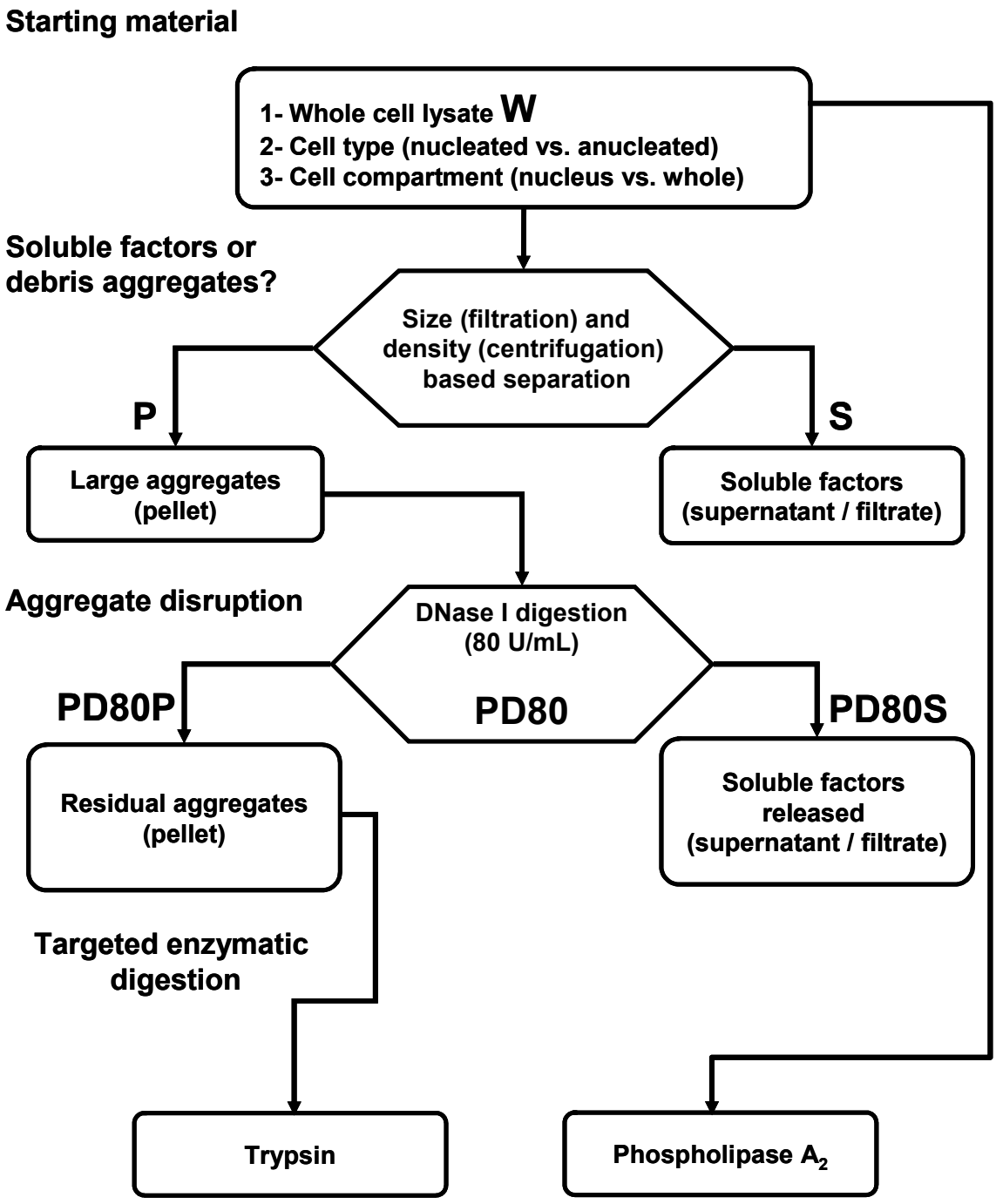

Figure 3.1 Lysate fractionation scheme summary.
Abbreviations of key fractions (W, P, S, PD80, PD80P and PD80S) are provided in larger font as a reference.

3.2. Material and methods

3.2.1. Cell cultures

Human erythroleukemia TF-1 cells (CRL-2003, American Type Culture Collection (ATCC), Manassas, VA, USA) were cultured in Dulbecco's modified Eagle's medium (DMEM) (Invitrogen, Burlington, ON, Canada) supplemented with 10% FBS (Invitrogen) and 5 ng/mL human recombinant GM-CSF (Terry Fox Laboratory (TFL), Vancouver, BC, Canada). The nBaF3 cells were a sub-line derived from mouse pro-B BaF3 cells (TFL) that were cultured in RPMI 1640 medium supplemented with 10% FBS, 4 mM L-glutamine (Invitrogen) and 10 ng/mL mouse recombinant IL-3 (TFL). The IL-3 was withdrawn from the BaF3 cultures and an IL-3 independent population was isolated and designated as nBaF3. Rat fibroblast RAT-1 cells (TFL) were cultured in DMEM supplemented with 10% FBS.

3.2.2. Retroviral vectors

Retroviral vectors with an enhanced green fluorescent protein (GFP) reporter gene under the control of MSCV long terminal repeats were pseudotyped with a gibbon ape leukemia virus (GALV-GFP) envelope and with an ecotropic MoMLV (Eco-GFP) envelope. GALV-GFP vectors were produced from PG-13 packaging cells (Hennemann et al. 1999; Miller et al. 1991) cultured in DMEM with 10% FBS in 1700 cm^2 expanded surface roller bottles (Corning, Lowell, MA, USA) at 37^oC and 10% CO_2 in air. Eco-GFP vectors were produced from a GP+E-86 packaging cell line (Buske et al. 2001; Markowitz et al. 1988) cultured in DMEM with 10% FBS in 850 cm^2 flat surface roller

bottles (Corning) at 37°C and 10% CO_2 in air. In each case, harvests were initiated when the cultures reached 90% confluence and performed at 24 h intervals (Reeves et al. 2000). Virus-containing medium (VCM) was filtered with a 0.45 μm pore size Durapore PVDF membrane (Millipore, Billerica, MA, USA), pooled from 4 roller bottles for GALV-GFP and 5 roller bottles for Eco-GFP, and frozen at −80°C. The same batch of VCM was used throughout all of the GALV-GFP experiments. Two different VCM batches (referred to as A & B) of similar titers were used for all of the Eco-GFP experiments.

3.2.3. Cell lysate preparation and fractionation

The nBaF3 cells in exponential growth were resuspended in DMEM at 4×10^6 lysed cells/mL and aliquoted into 6 mL fractions. The cells were frozen at −80°C, thawed at 37°C for 30 min and refrozen at −80°C until use. Density-based fractionation was performed by centrifuging the lysate at 3000×g for 15 min in order to separate debris aggregates from soluble factors. The supernatant was collected and the pellet fraction resuspended in an equivalent volume of DMEM. Size-based fractionation of the resuspended material was performed using a SteriFlip 0.22 μm pore size filter (Millipore).

Phospholipid digestion was carried out using phospholipase A_2 (PL A_2) from porcine pancreas (Sigma-Aldrich, St. Louis, MO, USA) to cleave the 2nd acyl bond. Briefly, the lysate and the control (DMEM) were incubated for 1 h at 37°C with 2800 U/mL PL A_2 and 10 mM $CaCl_2$ (Sigma-Aldrich). To chelate Ca^{2+} in order to inhibit PL A_2, 10 mM EDTA was then added prior to measuring the post-digestion activity of the lysate.

DNA was digested using the endonuclease DNase I (Invitrogen). Lysate fractions (whole, pellet, supernatant and, as a control, DMEM) were incubated for 24 h at 37°C with 80 U/mL DNase I. The DNase concentration was determined based on a dose response curve where concentrations ≥80 U/mL did not alter the outcome. During the incubation period, the lysate was mixed vigorously 3 times in order to further break down the large debris aggregates. The post-digestion activity was then assayed as described in the next section.

Trypsin was used to target the arginine and lysine containing peptides. The PD80P lysate fraction was centrifuged at 3000×g for 15 min and resuspended in trypsin – EDTA·4Na 0.25% (2.5 g/L trypsin, 1 mM EDTA in Hank's balanced salt solution, HBSS) (Invitrogen). Controls were also prepared with HBSS alone (Invitrogen), HBSS supplemented with 1 mM EDTA·4Na (Sigma-Aldrich) with pH adjusted to 7.2, and DMEM to rule out medium and EDTA effects. All samples were incubated at 37°C for 2 h. Trypsin was removed by discarding the supernatant fraction following centrifugation at 3000×g for 15 min. All pellets were resuspended in DMEM and their residual activity was assayed.

Red blood cell (RBC) lysates were obtained from human blood samples collected in Vacutainer® tubes containing acid-citrate-dextrose (BD, Franklin Lakes, NJ, USA) through a venous puncture. The whole blood was fractionated by centrifugation at 1500×g for 15 min. RBCs were collected from the pellet while the plasma and the buffy coat were discarded. The RBCs were diluted 100-fold in DMEM and their concentration was measured by haemocytometer counts. Additional dilutions were made to obtain a final concentration of 4×10^6 RBCs/mL. The RBCs were aliquoted in 6 mL fractions and

lysed by freeze-thaw as previously described. Untreated and DNase I treated RBC lysates were assayed at 1×10^6 lysed RBCs/mL.

Nuclei were extracted from TF-1 and nBaF3 cells in exponential growth phase using an EZ nuclei extraction kit (Sigma-Aldrich). Briefly, $30\text{-}40\times10^6$ cells were washed in ice-cold PBS and incubated twice on ice in a lysis buffer for 5 min. The supernatant was removed and the nuclei were resuspended in 5 mL DMEM. The nuclei concentration was determined using a haemocytometer and diluted to obtain a final concentration of 4×10^6 nuclei/mL. The nuclei were aliquoted in 4 mL fractions and lysed through 2 freeze-thaw cycles as previously described. The activities of whole and PD80P nuclei fractions were compared to those of whole cell and PD80P lysate fractions at both 5×10^5 and 1×10^6 lysed cells/mL or nuclei/mL.

3.2.4. PD80P fraction characterization

The density of the PD80P fraction was estimated by isopycnic centrifugation on sucrose (Sigma-Aldrich) solutions of 10% w/v (1.0381 g/cm^3), 20% (1.0810 g/cm^3), 30% (1.1270 g/cm^3), 40% (1.1765 g/cm^3), 50% (1.2295 g/cm^3) and 60% (1.2864 g/cm^3) layered in 1 mL increments of a 15 mL tube (Vauthier et al. 1999). A 1 mL aliquot of the PD80P lysate fraction concentrated to 20×10^6 lysed cells/mL was added on top and centrifuged at 3000×g for 0.5 h.

The particle size distribution was measured by laser light scattering using a Mastersizer 2000 system (Malvern, Worcestershire, UK). Refractive index values of 1.4 and 1.6 were assumed for the PD80P material. The total nucleic acid (DNA + RNA) content reduction was measured by comparing the CyQuant assay (Invitrogen) result for the PD80P fraction with that of the whole cell lysate. The assay was performed using

12.5 µL of lysate with 187.5 µL CyQuant GR dye/cell lysis buffer mix in duplicate 96-well plates. The plates were incubated for 2 h at room temperature and read using a Pharos FX molecular imager system (Bio-Rad Laboratories, Hercules, CA, USA).

Residual DNA fragment size analysis was performed by phenol-chloroform extraction followed by separation on an agarose gel. Briefly, 7 µL SDS, 3 µL 0.5 M EDTA and 20 µL of 20 mg/mL proteinase K (all Sigma-Aldrich) were added to 100 µL of the PD80P and whole lysate fractions. Samples were incubated for 3 h at 55°C, followed by 95°C for 5 min. Then 90 µL of deionized distilled water, 100 µL of 7.5 M ammonium acetate and 300 µL phenol-chloroform (1:1) were added. DNA was extracted from the top phase to which 600 µL ethanol were added and the contents were microcentrifuged at 10,000×g. The pellet was washed twice with 70% ethanol and dissolved in 50 µL of water. A 2% agarose gel in tris-acetic acid-EDTA was prepared. DNA was stained using SYBR Safe (Invitrogen). A 100 bp ladder (Invitrogen) was used as a reference to determine the approximate size of the DNA fragments. The wells were loaded with 10 µL samples previously mixed with 2 µL of 6× mass loading dye (Fermentas, Burlington, ON).

3.2.5. nBaF3 and TF-1 cell line transduction assays

Whole, pellet and supernatant lysate fractions were assayed in 6-well untreated plates (Sarstedt) at a 3 mm average liquid depth (3 mL/well). TF-1 and nBaF3 target cells were resuspended in their respective fresh growth media prior to the transduction assay. GALV-GFP and Eco-GFP VCMs were thawed at 37°C for 15 min and diluted 1:2 with TF-1 and nBaF3 growth media, respectively, to obtain a final dilution of 1:8 once mixed with the target cells and lysate. Lysate diluted with DMEM to adjust the

concentration was first added to the wells (50% of the final volume). Target cells (25% of the final volume) were then added to obtain a final cell concentration of 5×10^5 cells/mL. Finally, GALV-GFP or Eco-GFP VCMs (25% of the final volume) were added and then incubated for 24 h at 37°C in 5% CO_2 balance air and 90% relative humidity. A cell count was performed using a Cedex automated cell counter (Innovatis, Bielefeld, Germany) with viable cell numbers determined by the trypan blue exclusion method. The average of 20 images analyzed with the Std. Cell (v 5.00) algorithm was taken for each sample. Also, 150 µL of TF-1 cells and 75 µL of nBaF3 were transferred to 24-well untreated plates (Sarstedt), diluted 1:5 and 1:10 respectively with growth media, and expanded for an additional 48 h prior to analysis for GFP expression (Klein et al. 1997). GFP expression was measured by fluorescence activated cell scanning with a FACSCalibur system (BD Biosciences, San Jose, CA, USA). The transduction efficiency was expressed as the ratio of viable cells expressing GFP over the total viable cells based on propidium iodide (Sigma-Aldrich) exclusion at 5 µg/mL. Different batches of cell lysates were used for each experiment.

All DNase I and trypsin-treated lysates as well as nuclei and RBC-derived lysates were assayed in 24-well untreated plates using an average liquid depth of 3 mm (600 µL/well). Transduction was performed as previously described. The remaining culture volumes of 2 wells were pooled and diluted 1:2 in PBS prior to the cell count. Cell counts were only performed at 2.5, 5, 10 and 20×10^5 lysed cells/mL.

3.2.6. Sedimentation analysis

In situ sedimentation analysis was performed at increasing average liquid depths of 1 mm (200 µL), 2 mm (400 µL), 3 mm (600 µL, standard depth), 5 mm (1000 µL), 10

mm (2000 µL) and 15 mm (3000 µL). The number of cells (1.5×10^5 cells/cm^2) as well as the lysate, protamine sulfate (PS) and VCM concentrations were maintained constant. The cells, additives, medium and VCM were added to 24-well untreated plates per Table 3.1. The cells were then incubated and transduction was measured as previously described.

Table 3.1 Volumes of medium, cells, VCM and additives (DMEM, PD80P, supernatant and PS) added to increase the liquid depth while maintaining the concentration of additives and VCM as well as the total number of cells constant.
TF-1 and nBaF3 cells were resuspended in growth medium at 3×10^6 cells/mL. PD80P and filtered lysate supernatant were added at 4×10^6 lysed cells/mL for TF-1 cells and 2×10^6 lysed cells/mL for nBaF3 cells to achieve respective final concentrations of 10×10^5 lysed cells/mL and 5×10^5 lysed cells/mL. Protamine sulfate (Sigma-Aldrich) was prepared at 40 µg/mL in DMEM to achieve a final concentration of 10 µg/mL. GALV-GFP VCM was pre-diluted 1:2 with growth medium for TF-1 cells and Eco-GFP VCM 1:4 for nBaF3 cells.

Liquid Depth	**Growth Medium**	**Target Cells**	**DMEM, PD80P, Supernatant or PS**	**VCM**
(mm)	(µL)	(µL)	(µL)	(µL)
1	0	100	50	50
2	100	100	100	100
3	200	100	150	150
5	400	100	250	250
10	900	100	500	500
15	1400	100	750	750

Ex situ sedimentation was measured by incubating the filtered supernatant and PD80P lysate fractions alone or mixed with VCM for 6 h at room temperature before separately collecting the top and bottom halves. PD80P and filtered lysate supernatant were diluted with DMEM to a concentration of 2×10^6 lysed cells/mL. GALV-GFP and Eco-GFP were pre-diluted 1:2 and 1:4 respectively with TF-1 and nBaF3 growth media. 10 mL of PD80P, filtered supernatant or each VCM were transferred to 30 mL flat

bottom tubes (i.d. 2.62 cm, 185 mm liquid depth) (Sarstedt). 5 mL of PD80P or filtered supernatant were also mixed with 5 mL of each VCM and similarly transferred into tubes. The headspace of each tube was filled with 10% CO_2 balance air. The tubes were sealed and incubated undisturbed for 6 h at room temperature. The top and bottom fractions were separated by skimming the top half. A transduction assay was then performed on each fraction where pre-mixed lysate and VCM were added at 50% of the culture volume. Corresponding fractions (top/bottom) of incubated VCM were mixed with lysate and DMEM as no-additive controls in the wells (each at 25% of the culture volume). Controls using fresh supernatant and PD80P were also performed with each VCM fraction. TF-1 target cells were added to GALV-GFP VCM and nBaF3 cells to Eco-GFP VCM (50% of culture volume) to obtain a final concentration of 5×10^5 target cells/mL. The transduction was assayed as previously described.

3.2.7. Culture vessel surface coating

Untreated and tissue-culture-treated 6-well plates were coated with whole, filtered supernatant, pellet and PD80P lysate fractions along with protamine sulfate and DMEM. Then, 3 mL of each lysate fraction at 5×10^5 lysed cells/mL, protamine sulfate at 10 μg/mL in DMEM and DMEM alone were added to 2 untreated and 2 tissue-culture-treated wells and incubated for 4 h at 37°C in 5% CO_2 balance air. All coated wells were washed with 2 mL DMEM to remove unbound compounds. DMEM (25% of culture volume) was added to the coated wells. These were compared to non-coated wells containing lysate (25% of culture volume, final concentration: 5×10^5 lysed cells/mL), protamine sulfate (10 μg/mL) and DMEM. TF-1 and nBaF3 target cells in growth medium (50% of culture volume) were then added to achieve a final concentration of

5×10^5 target cells/mL. Finally, VCM pre-diluted 1:2 with growth medium (25% of culture volume) was added (GALV-GFP for TF-1 cells and Eco-GFP for nBaF3 cells). The coating and wash solution activities were assayed as previously described.

3.2.8. Cell surface adsorption

RAT-1 cells were seeded at 5×10^4 cells/cm^2 in tissue-culture-treated 24-well plates 24 h prior to initiation of retroviral transduction. Prior to initiation of the transduction assay, spent medium was removed by aspiration from all wells. Eco-GFP VCM (prediluted 1:12 with growth medium to obtain a 1:16 final dilution) mixed with PD80P (5×10^5 lysed cells/mL), protamine sulfate (10 μg/mL) and DMEM were added to the cells at 4 wells per condition in 2 plates. The first plate was centrifuged at 1000×g for 1 h at room temperature while the second plate was kept under static gravity at room temperature. The contents of 2 wells/condition from each plate were removed and the cells were washed with 600 μL DMEM. Then, 600 μL of growth medium were added to the washed wells. Both plates were incubated for 23 h at 37^{o}C in 5% CO_2 balance air and 90% relative humidity. The cells were trypsinized, resuspended in growth medium and transferred to 6-well tissue-culture-treated plates to expand the cells for an additional 48 h. Prior to FACS analysis, the cells were trypsinized and resuspended in growth medium with 5 μg/mL propidium iodide.

3.2.9. Mouse hematopoietic stem cell transduction assay

To enrich for primitive hematopoietic progenitors, 4 days prior to bone marrow harvest, C57Bl6/6Ly-Peb3b (Peb3b) mice were pre-treated with 150 mg/kg 5-fluorouracil. These bone marrow cells were then prestimulated in bulk cultures for 48 h in DMEM

containing 15% FBS and 10 ng/mL rhIL-6, 6 ng/mL rmIL-3 and 100 ng/mL rmSCF (all reagents from StemCell Technologies, Vancouver, B.C., Canada). Following prestimulation, 1×10^6 starting cell equivalents were transduced with Eco-GFP vectors for each condition. Conditions included a negative control without VCM, a VCM positive control (no additives), VCM supplemented with PD80P at 1×10^6 lysed cells/mL and a co-culture with gamma-irradiated GP+E-86 packaging cells (37 600 MU). Following a 48 h transduction period, the cells were harvested and maintained in culture 72 h post-transduction to measure GFP expression and viability. Also, 2×10^5 starting cell equivalents from each condition were transplanted into lethally irradiated syngenetic C57Bl6/6Ly-c2J (c2J) recipient (n=2) along with 10^5 freshly isolated Peb3b helper cells. These were used to assess the transduction efficiency in primitive progenitors capable of contribution to both lymphoid and myeloid compartments. The peripheral blood of recipient mice was monitored at 4, 8 12 and 20 weeks post-transplantation to assess donor cell contributions to myeloid and lymphoid lineages based on the pan-hematopoietic marker CD45 (Pep3b CD45.1, c2J CD45.2) and the lineage markers Gr1, Mac1, CD4, CD8 and B220 (BD Biosciences).

3.2.10. Statistical analysis

All experiments were performed in triplicate with 2 replicates within each experiment unless otherwise stated. ANOVA (α=0.05) was used for all statistical tests for $p<0.05$.

3.2.11. Transgene integration measured by quantitative PCR

The nBaF3 cells were transduced with Eco-GFP vectors as previously described using the PD80P lysate fraction at lysed-to-target cell ratios ranging from 0 to 20. Cells

from each well were divided into 3 fractions for flow cytometry, cell counts (as previously described) as well as qPCR analysis. Genomic DNA from ~1.5×10^6 cells was prepared for qPCR using a GenElute Mammalian Genomic DNA Miniprep kit (Sigma-Aldrich). As controls, PD80P lysates derived from both TF-1 and nBaF3 cells were tested alone to ensure that any residual DNA within the lysate fraction did not bias the results. The Table 3.2 primers for GFP and the endogenous mouse apoliprotein B (ApoB) (Fujiki et al. 2008; Pan et al. 2002) were from Integrated DNA Technologies (Skokie, Illinois, USA). Reactions were performed for each primer set in triplicate. 200 nM of primers diluted with RNase/DNase free water (Invitrogen) was mixed with Sybr GreenER qPCR surpermix (Invitrogen) and approximately 10 ng/µL sample genomic DNA. Reaction efficiency was determined using 1:4, 1:16 and 1:64 serial dilutions of the control without lysate (R=0) and the sample with the highest lysed-to-viable cell ratio (R=4 or 20). The qPCR was performed on an ABI 7500 Fast real-time PCR system (Applied Biosystems, Foster City, CA, USA) with 1 cycle at 50^{o}C for 120 s, 1 cycle at 95^{o}C for 10 min and 45 cycles at 95^{o}C for 15 s and 58^{o}C for 60 s. These were followed by melting curves to verify the product homogeneity. The data were analyzed with ABI 7500 software where the quantification cycle value (C_q) was automatically determined. The average reaction efficiencies were 0.99±0.04 for ApoB and 1.05±0.04 for GFP. As these results did not differ significantly from 1, an efficiency of 100% was used for all calculations. C_q values ranged from 17 to 20 for ApoB and 19 to 27 for GFP.

Table 3.2 Primer sequences used for q-PCR analysis of nBaF3 cell transduction

Gene	Primer sequence
Humanized red-shifted GFP	
Sense	5'-ACTACAACAGCCACAACGTCTATATCA-3'
Anti-sense	5'-GGCGGATCTTGAAGTTCACC-3'
Mouse apolipoprotein B	
Sense	5'-CGTGGGCTCCAGCATTCTA-3'
Anti-sense	5'-TCACCAGTCATTTCTGCCTTTG-3'

3.3. Results

3.3.1. Quantification of transduction events

Quantitative PCR was used to accurately determine the differences in transgene integration resulting from various treatments according to the following equation:

$$Fold\ increase\ in\ Gene\ Integration = \frac{\left(1+\varepsilon_{GFP}\right)^{\Delta Cq_{GFP}}}{\left(1+\varepsilon_{ApoB}\right)^{\Delta Cq_{ApoB}}} \qquad \textbf{Eq. 3.1}$$

where ε is the reaction efficiency, Cq is the quantification cycle value and $\Delta Cq = Cq_{control} - Cq_{sample}$. The integrated GFP transgene increase relative to a control without additives was corrected for variations in genome copy number between samples using the endogenous mouse apolipoprotein B (ApoB) gene (Fujiki et al. 2008; Pan et al. 2002). While offering a high level of accuracy, this approach was very time-consuming and, therefore, qPCR was not feasible for analyzing the high-throughput experiments presented in the following sections.

Other assays such as flow cytometry that rely on gene expression can provide the throughput required for a large number of experiments. The fold-increase in transduction efficiency (TE) determined by flow cytometry and given by the following equation:

$$Fold\ increase\ in\ TE = \frac{TE_{Sample}}{TE_{Control}} \quad \textbf{Eq. 3.2}$$

predicts the increase in gene integration but only over a very narrow range of up to approximately 13-fold when compared with the qPCR results (Figure 3.2). This method only indicates when at least 1 copy of the transgene is successfully integrated and expressed; it does not account for multiple infections. The Poisson distribution

$$P(k) = \frac{(N_T)^k e^{-(N_T)}}{(k)!} \quad \textbf{Eq. 3.3}$$

can been used to predict the proportion of cells transduced by a given number of retroviral vectors (k) for a given average number of transduction events per cells (N_T, also referred to as the multiplicity of infection) (Knipe et al. 2007). When N_T is low, $P(k>1) \rightarrow 0$, and it can be assumed that most cells expressing GFP have been transduced by a single retroviral vector. Thus, one can only rely on transduction efficiency as a measure of gene integration if limiting dilutions are performed on the VCM. However, this can be difficult to achieve and requires the use of different dilution factors for the control and treatment arms, and, hence, is not practical for high-throughput experiments and complicates the interpretation of the results by altering the composition of the conditioned medium of the VCM.

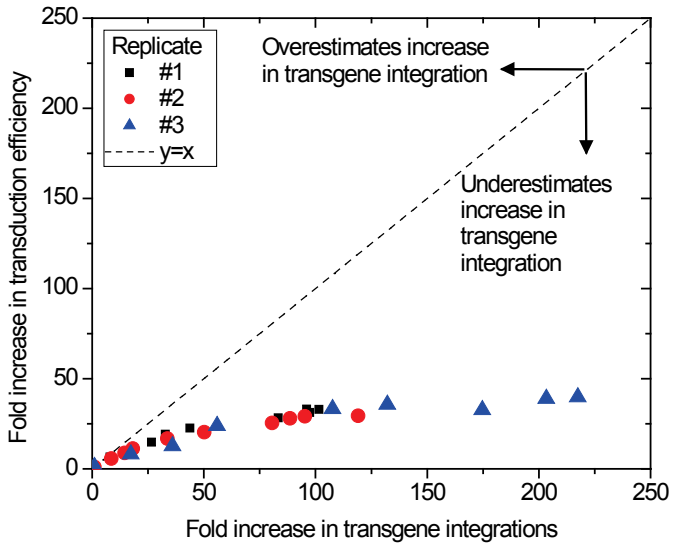

Figure 3.2 Fold-increase in transduction efficiency measured by flow cytometry relative to fold increase in transgene integration measured by qPCR on nBaF3 cells with the Eco-GFP vector for 3 independent trials.
As transduction efficiency increased from 2.6% for the control to 90%, the increase in transduction efficiency significantly underestimates the increase in transgene integrations.

In order to widen the range over which flow cytometry measurements accurately predict the increase in transgene integrations, differences in the fluorescence intensity can be used to distinguish the number of transduction events per cell. Cell lines such as K-562 were reported to exhibit GFP expression, measured as relative fluorescence intensity, that was correlated to the number of transgene integrations (Kustikova et al. 2003). Although significant variability in expression was observed between clones with identical copy numbers (Kustikova et al. 2003), it was hypothesized that, for a large population (e.g., ≥10,000 cells), fluorescence could potentially provide an accurate estimate of the average copy number. Based on this assumption, the increase in copy number would be predicted by

$$Fold\ increase\ in\ average\ copy\ number = \frac{(F_{Sample} - F_{Negative})}{(F_{Control} - F_{Negative})} \qquad \textbf{Eq. 3.4}$$

where F_{Sample} and $F_{Control}$ are the geometric means of the GFP fluorescence of the treated sample and control, respectively, and $F_{Negative}$ corresponds to the geometric mean fluorescence of the non-transduced cells within the negative (i.e., untransduced) control. This value was subtracted from F_{Sample} as well as $F_{Control}$ to account for the autofluorescence of the cells. When the VCM concentration was adjusted such that the transduction efficiency of the untreated control is sufficiently low (2.6±0.1%) and $P(k>1) \rightarrow 0$, the copy number increase should correspond to the average copy number within the transduced cell population. Equations 3.2 and 3.4 were thus combined to give

$$Fold\ increase\ in\ transduction\ events = \frac{TE_{Sample}}{TE_{Control}} \times \frac{(F_{Sample} - F_{Negative})}{(F_{Control} - F_{Negative})} \qquad \textbf{Eq. 3.5}$$

which provides a correction for multiple transgene copies. The fold increase in transduction events measured by flow cytometry was then compared with the results obtained by qPCR (Eq. 3.1) to empirically assess the validity of Eq. 3.5. As shown in Figure 3.3, when the transduction efficiency was used in combination with the geometric mean fluorescence, the fold increase in transduction events measured by flow cytometry provided an accurate estimate of the increase in transgene integrations measured by qPCR. The average bias was 6.7% between qPCR and FACS, with FACS yielding slightly lower results. Equation 3.5 is therefore proven valid for nBaF3 cells transduced with Eco-GFP vectors over transduction efficiencies ranging from 2.6% to 90%, which corresponded to increases of over 220-fold in transduction events and covered all the results presented in the subsequent sections. Over this transduction efficiency range, the average transgene copy number estimated within the transduced cell population increased

up to 5.6. Equation 3.5 was also assumed to be applicable to TF-1 cells transduced with GALV-GFP vectors. While all of the results which follow will be presented in the form of fold increase in transduction events as per Eq. 3.5, the raw transduction efficiency data are also available in Appendix B.1.

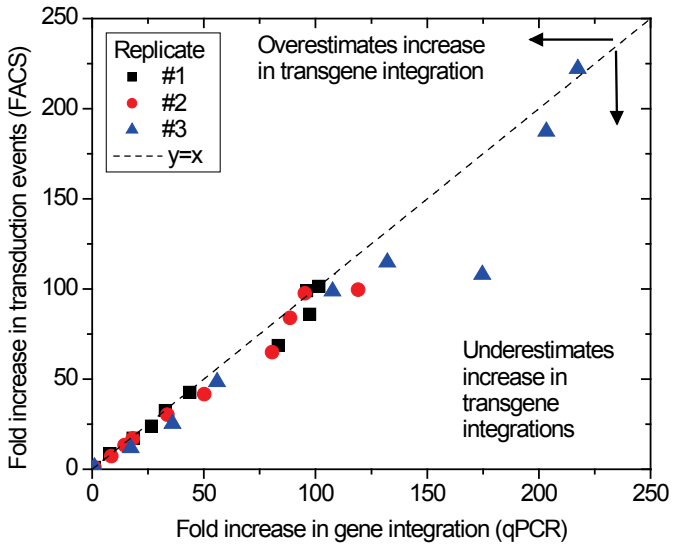

Figure 3.3 Fold increase in transduction events calculated by FACS using the geometric mean fluorescence intensity of GFP to correct for multiple copies relative to the fold-increase in gene integrations measured by qPCR.
FACS results were an accurate predictor of the increase in gene integration for transduction efficiencies ranging from 2.6% for the control up to 90% with the PD80P lysate fraction treatment of nBaF3 cells with Eco-GFP vectors.

3.3.2. Density- and size-based fractionation of cell lysates

Upon cell lysis, soluble compounds are released into the surrounding medium and large debris aggregates are formed as shown in Figure 3.4. In order to determine if the increase in transduction previously observed with whole cell lysate was associated with the soluble compounds or the debris aggregates, a density-based fractionation was performed using centrifugation at 3000×g for 15 minutes to form a pellet. The supernatant fraction was collected and the pellet fraction resuspended in an equal volume

of DMEM. The activity of each fraction on the transduction of nBaF3 and TF-1 cells was compared with that of the whole cell lysate (Figure 3.5). As determined in Chapter 2, the effect of whole cell lysate on transduction was again dose-dependent. For the nBaF3 and TF-1 target cells, the transduction events increased by up to 18- and 10-fold, respectively, relative to a control without lysate. With the pellet fraction, the transduction also increased with increasing lysate concentration and, for the nBaF3 target cells, the improvement in transduction even exceeded that of the whole cell lysate at concentrations above 5×10^5 lysed cells/mL. Greater variability in transduction was observed with both the whole and pellet fractions, likely due to the resuspension process that can influence the size of aggregates. In the case of the supernatant (Figure 3.5), the increase was limited to between 10- to 12-fold for nBaF3 and 3- to 4-fold for TF-1 target cells over the range of lysate concentrations tested. Thus, the increase in transduction was lower than with the whole cell or pellet fractions, and also less dependent on the lysate concentration.

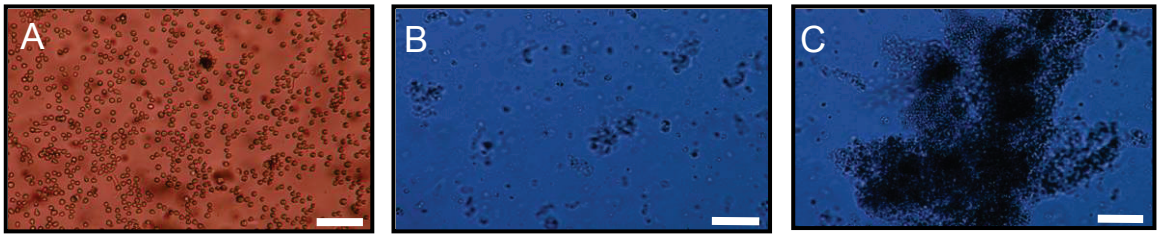

Figure 3.4 Photos taken prior to cell lysis of viable cells in suspension (A) and post-lysis of smaller (B) and larger (C) debris aggregates present within the cell lysates.
Scale bar: 200 µm

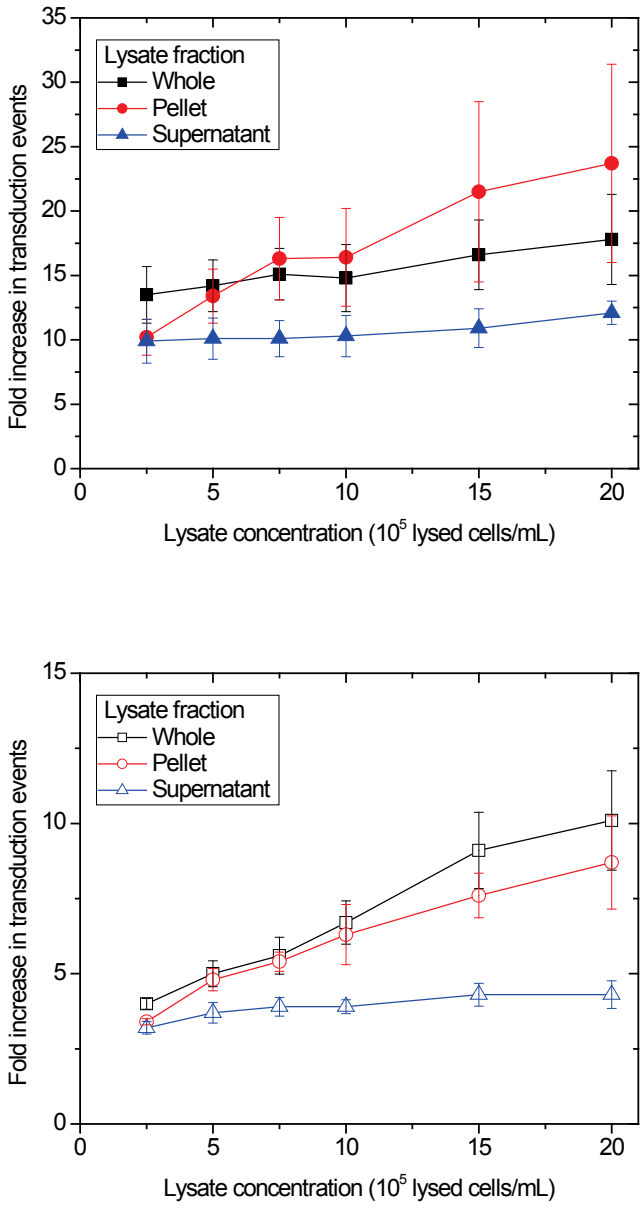

Figure 3.5 Increase in transduction events in the presence of whole (squares), pellet (circles) and supernatant (triangle) lysate fractions.
Increasing doses of each lysate fraction were added to 5×10^5 target cells/mL in 6-well untreated plates using a VCM concentration of 0.125× and a 3 mm average liquid depth.
nBaF3 cells were transduced by Eco-GFP vectors (top, filled symbols) and TF-1 cells by GALV-GFP vectors (bottom, open symbols). (n=3, error bars: SEM)

To confirm that the debris aggregates were responsible for much of the increase in transduction observed and to eliminate the potential of carryover of insoluble factors,

supernatants, resuspended pellets and whole cell lysates were filtered through a 0.2 μm pore size membrane to remove most aggregates prior to the addition of target cells and VCM to the filtrate. As shown in Figure 3.6, filtration significantly reduced the activity of both the whole lysate and the pellet fraction, while the activity of the supernatant did not significantly decrease. The average decrease in activity of the whole cell lysate was 43±3% for nBaF3 cells and 48±1% for TF-1 cells. The decrease was significant over all concentrations tested for TF-1 cells and at 7.5×10^5 and 1.5×10^6 lysed cells/mL for nBaF3 cells. The residual activity of the whole lysate filtrate was similar to that of the supernatant, suggesting that only soluble species or very small solid components remained when the lysate was filtered. Based on these results, roughly half of the activity associated with the whole cell lysate was attributed to debris aggregates removed by the 0.2 μm filter. When filtration was applied to the pellet fraction, presumably enriched in debris aggregates, the average decrease in activity was greater, at 62±2% for nBaF3 cells and 68±2% for TF-1 cells, than with the whole cell lysate. The decrease in activity was significant for all concentrations for TF-1 cells and at 2.5×10^5 and 7.5×10^5 lysed cells/mL for nBaF3 cells. While the relative decrease was comparable at 1.5×10^6 lysed cells/mL, it did not pass a significance test due to the high transduction variability of the pellet fraction. The pellet filtrate activity increased with concentration and converged toward that of the lowest concentration of the supernatant fraction, suggesting that a reduced concentration of soluble compounds were carried over with the pellet. Finally, when filtration was applied to the supernatant fraction, presumably depleted of debris aggregates, the transduction activity was not significantly reduced with lesser decreases of 22±3% for nBaF3 cells and 10±8% for TF-1 cells.

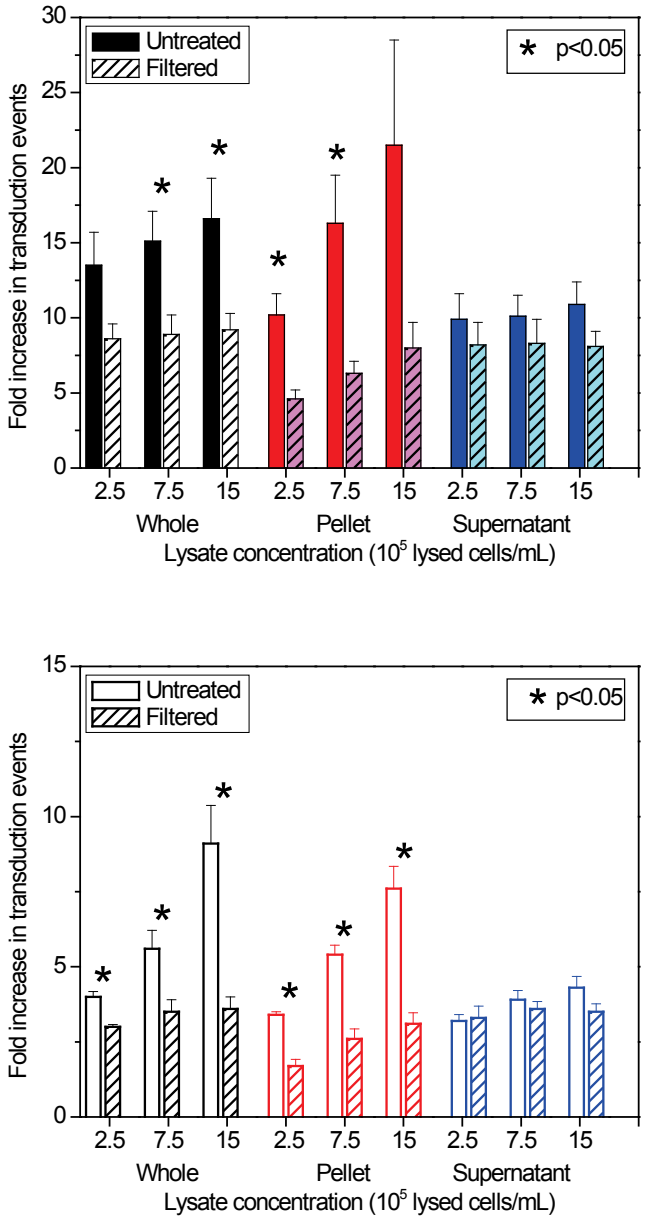

Figure 3.6 Filtration at 0.2 µm of lysate fractions to remove debris aggregates significantly reduced the activity of the whole cell (black) and pellet (red) fractions but not that of the supernatant (blue) fraction as measured using nBaF3 target cells with Eco-GFP vectors (top) and TF-1 target cells with GALV-GFP vectors (bottom). (*n*=3, error bars: SEM)

In Chapter 2, the presence of whole cell lysate did not alter cell proliferation, an important variable given that mitosis is required for the transgene integration of gammaretroviral vectors. With the supernatant and pellet fractions, no significant

decrease in viable cells was observed at any lysate concentration, assessed over a 24 h period (Figure 3.7). For nBaF3, none of the lysate fractions had any significant effect on the concentration of viable cells, based on a 95% confidence interval applied to the control without lysate, as cells were expanded by 2.4-fold over 24 h. For TF-1 cells, only the highest concentration (2×10^6 lysed cells/mL) of whole cell lysate had a viable cell concentration that was outside the 95% confidence interval around the control which expanded by 2.0-fold over 24 h. This last result contrasts with those previously obtained for both short- and long-term growth measurements when lysed TF-1 cells were used rather than nBaF3 lysate (Chapter 2). This suggests that, while TF-1 cell lysates do not impede TF-1 cell growth, other lysed cell types could potentially reduce the target cell growth rates.

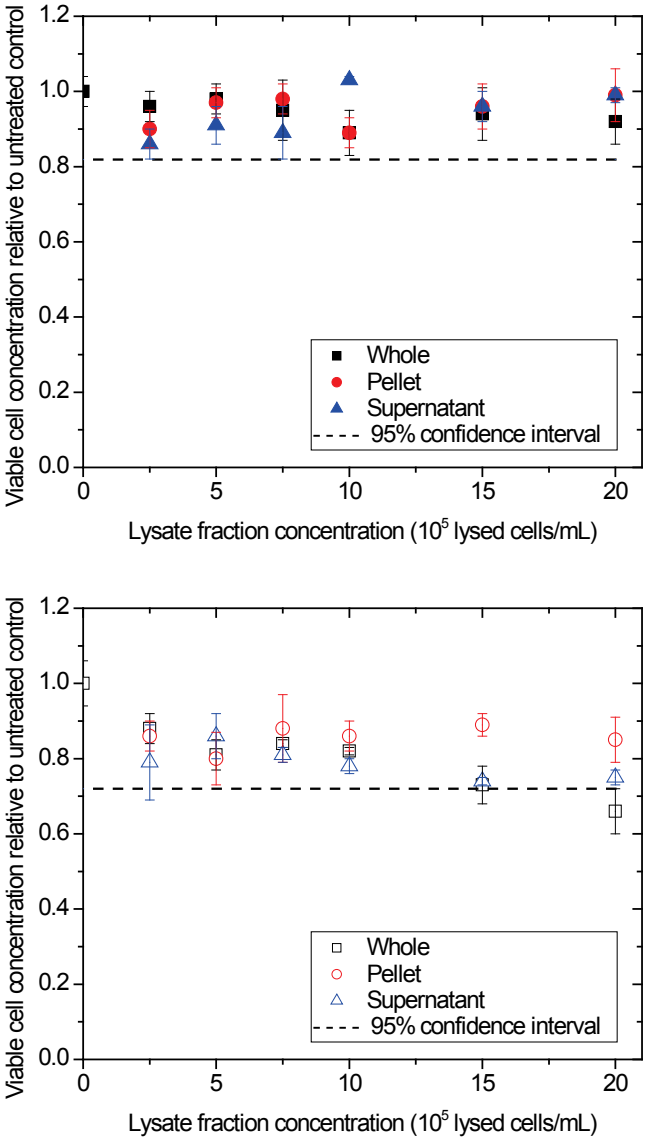

Figure 3.7 Effect of whole (squares), pellet (circles) and supernatant (triangles) lysate fraction concentrations on the viable cell concentration relative to the untreated control measured 24 h after lysate addition for nBaF3 (top) and TF-1 (bottom) cells. (*n*=3, error bars: SEM)

3.3.3. Enzymatic digestion of lysate

To investigate the potential involvement of phospholipids in the observed transduction increase with cell lysate, the whole cell lysate was treated with phospholipase A_2. This treatment (discussed in further detail in Appendix B.1.2) did not

alter the activity of the lysate. It was thus concluded that phospholipids were not a major contributor to the activity of the lysate.

A significant quantity of soluble material could be sequestered within the debris aggregates formed in the cell lysate. In order to disrupt these aggregates (and to evaluate the potential contribution of DNA to the lysate activity), DNase I (80 U/mL) was added to the whole, pellet and, as a no-aggregate control, to the supernatant lysate fractions. The activity of the DNase I-treated fraction was initially compared with that of the untreated lysate (Figure 3.8). With both the whole and pellet lysate fractions, the DNAse treatment significantly increased transduction as the large debris aggregates were observed to be broken down. With the whole lysate, the increase was 2.9±0.6-fold for the nBaF3 cells and 2.3±0.3-fold for the TF-1 cells. With the pellet fraction, the increase observed was dependent on the lysate concentration. At 5×10^5 lysed cells/mL, DNase treatment increased transduction by 4.5±0.4-fold for the nBaF3 cells and 5.0±0.2-fold for the TF-1 cells. Upon doubling the concentration to 1×10^6 lysed cells/mL, the benefit of the DNase treatment increased to 7.5±1.4-fold and 7.3±0.4-fold for the nBaF3 and TF-1 cells, respectively. As expected, the supernatant, free of debris aggregates, was not significantly affected by the DNase treatment when assayed on either nBaF3 or TF-1 cells.

The DNase-treated pellet (PD80) outperformed the whole lysate (WD80) fraction. A dose-response was therefore performed, also including as controls the DNase-treated supernatant (SD80) and DMEM supplemented with DNase. As shown in Figure 3.9, overall, greater increases in transduction events were achieved with the PD80 fraction for both the nBaF3 and TF-1 cells. For the nBaF3 target cells, the maximum transduction

increase was 145-fold with PD80 compared to only 75-fold with WD80. For the TF-1 target cells, the maximum increase was 69-fold with PD80 compared to 42-fold with WD80. These differences were the result of an early saturation observed with the WD80 fraction. At lower concentrations, the transductions obtained with both the WD80 and PD80 fractions were similar. However, at concentrations above 2.5×10^5 lysed cells/mL for nBaF3 cells and 5×10^5 lysed cells/mL for TF-1 cells, a divergence occurred between these fractions as the WD80 transduction appeared to reach a plateau while that of PD80 continued to increase.

Given that PD80 was derived from WD80 (minus the supernatant), similar responses would be expected unless a negative interaction with the supernatant occurred. Based on the near overlap observed with WD80 and PD80 at lower lysate concentrations, it was unlikely that the difference was due to variations in the concentrations of common active compounds shared between these fractions. Thus, the supernatant fraction likely contained inhibitors. Consequently, as the concentration of WD80 was increased, the beneficial effect of additional transduction-enhancing compounds may be limited by the increasing concentration of inhibitors, resulting in the plateau region observed. Even though identical batches of WD80 and PD80 were used for both the TF-1 and nBaF3 target cells, it appeared that higher concentrations with both fractions were required for the TF-1 cell / GALV-GFP vector combination. This may be the result of different affinities between the active compounds of the lysate and the viral vectors, or between the lysate and the target cells, or of variations in the conditioned medium of the VCM. With the SD80 fraction, the maximum increase was limited to 21-fold for nBaF3 cells and 11-fold for TF-1 cells. This represents less than 13% and 14% of the total activity of

PD80 and SD80, respectively. The presence of DNase (D80) did not significantly increase the transduction of nBaF3 and TF-1 cells. None of the DNase-treated fractions had a negative effect on the growth of nBaF3 or TF-1 cells (Figure 3.10).

The PD80 fraction was further fractionated by centrifugation into a pellet and supernatant fraction to determine whether the DNase treatment effect on the pellet fraction was due to the generation of smaller aggregates or due to the release of soluble factors sequestered within the debris aggregates. Residual aggregates collected in the pellet were resuspended in DMEM (PD80P) and the supernatant was collected (PD80S) to perform dose response experiments (Figure 3.9). The bulk of the activity of the PD80 fraction was contained within the PD80P fraction, suggesting that the DNase treatment effect was mainly due to the larger aggregates being broken down into smaller particles that would increase the surface area per unit volume available to bind to the target cells and/or viral vectors. The PD80S fraction also increased transduction albeit to a much lower degree. To assess whether the activity observed within the PD80S fraction was due to the release of soluble factors, it was filtered through a 0.2 μm membrane (Figure 3.11). Filtration reduced the activity of the PD80S fraction by 93±2% for nBaF3 cells and 57±24% for TF-1 cells, suggesting that residual particles accounted for most of the PD80S activity observed. When the PD80 and PD80P fractions were filtered, their activities were reduced by 97.5±0.4% and 98.9±0.1% respectively for nBaF3 cells, and by 94.2±1.0% and 97.9±1.5% for TF-1 cells. In agreement with the density-based fractionation outcome, these results indicate that the bulk of the activity is associated with the residual particles.

The PD80P fraction was further characterized with regards to density, size distribution and residual DNA. When separated on a sucrose gradient, the PD80P settled to the bottom layer of a 60% w/v sucrose solution, indicating aggregate densities of at least 1.29 g/cm^3. The size distribution of the particles was measured by laser light scattering (Figure 3.12) using refractive index values of 1.4 and 1.6, based on reports for whole cells (Curl et al. 2005; Song et al. 2006) and for protein aggregates (Song et al. 2006), respectively. As shown in Figure 3.12, use of either the 1.4 or 1.6 refractive index had a negligible impact on the measured size distribution which had an apparent hydrodynamic diameter range of 0.5 - 74 μm and an apparent volume weighted average diameter of 15 μm. This information is primarily provided to demonstrate the wide distribution in particle size of the PD80P fraction and to confirm that the larger aggregates, some exceeding 1 mm, were successfully broken down into smaller particles by DNase digestion (these particles have a wide range of shapes and should not be assumed to be spherical). Compared to whole untreated lysate, the PD80P DNA + RNA was reduced by 91.9±0.5% as measured by the CyQuant method (Jones et al. 2001) and the DNA was reduced by 99.5±0.2% as measured by qPCR using the endogenous mouse apoliprotein B gene. The residual fragments of DNA had an average size of approximately 200 bp as shown in Figure 3.13.

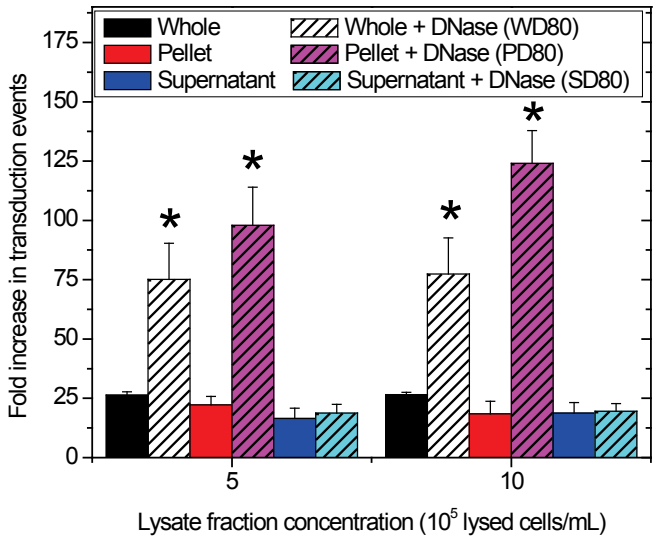

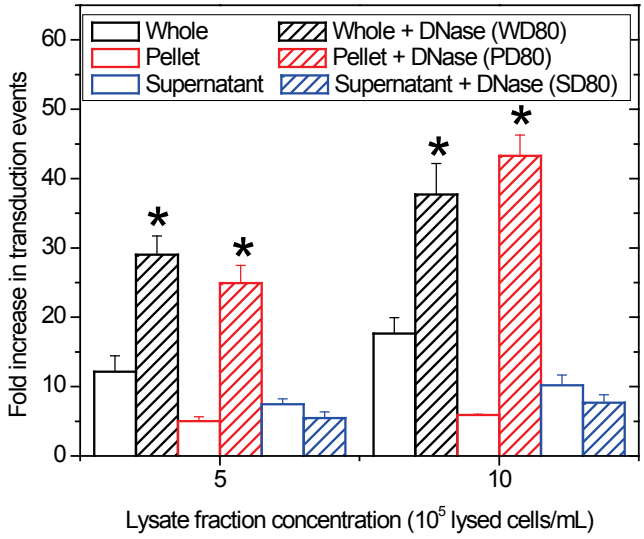

Figure 3.8 The increase in transduction events of DNase I treated whole (black), pellet (red) and supernatant (blue) lysate fractions was compared to that of untreated lysate fractions using nBaF3 target cells with Eco-GFP vectors (top) and TF-1 target cells with GALV-GFP vectors (bottom). The DNase-treated as well as the untreated whole, pellet and supernatant lysate fractions were incubated at 37°C for 24 h prior to the transduction assay. (*n*=3, error bars: SEM)

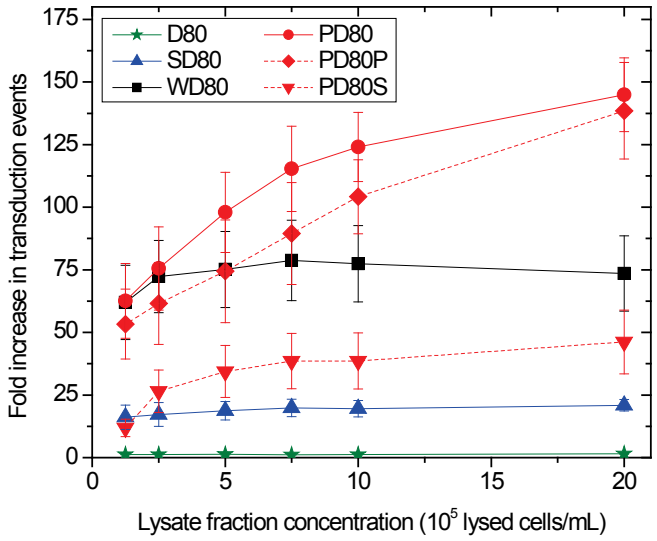

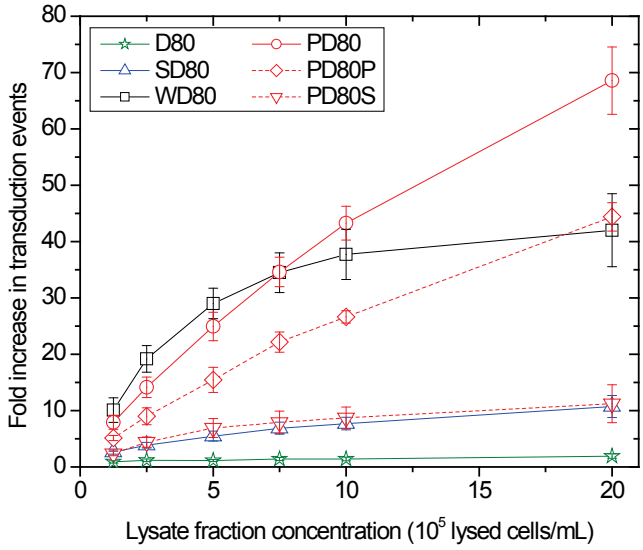

Figure 3.9 Increase in transduction events relative to the concentration of the DNase I treated lysate fractions assayed on nBaF3 target cells with Eco-GFP vectors (top) and on TF-1 target cells with GALV-GFP vectors (bottom).
Lysate fractions included DNase treated whole (WD80, squares), supernatant (SD80, triangles), pellet (PD80, circles), pellet fraction of PD80 (PD80P, diamonds), supernatant fraction of PD80 (PD80S, inverted triangles) and, as a control, DMEM with DNase I (D80, stars). (n=3, error bars: SEM)

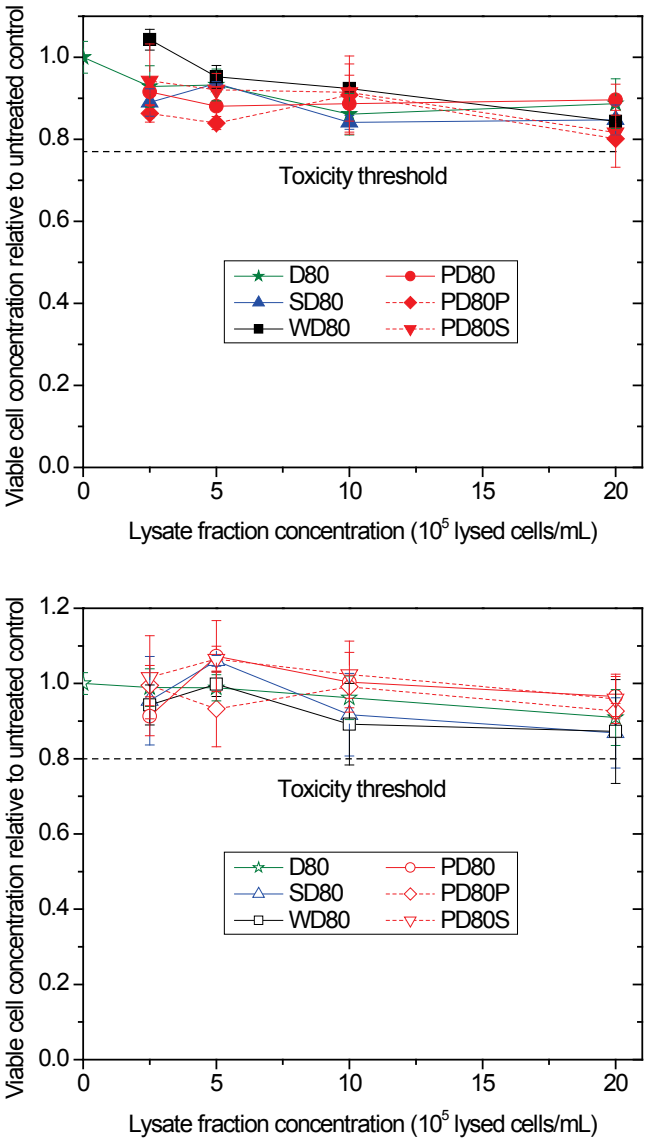

Figure 3.10 Effect of whole (WD80, squares), pellet (PD80, circles) and supernatant (SD80, triangles) treated with DNase I, DMEM with DNase I (D80, stars), and pellet (PD80P, diamonds) and supernatant (PD80S, inverted triangles) fractions of PD80 on the viable cell concentration relative to the untreated control measured 24 h after cell lysate addition to nBaF3 (top) and TF-1 (bottom) cells. (*n*=3, error bars: SEM)

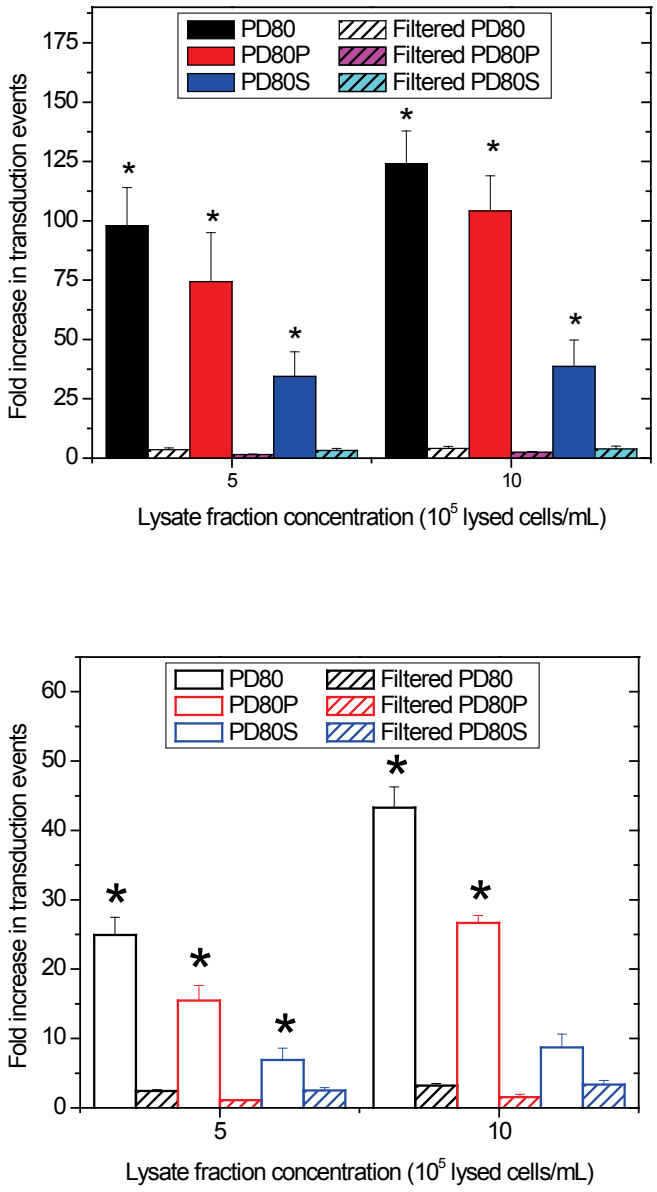

Figure 3.11 Fold-increase in transduction events following filtration at 0.2 µm of the DNase-treated pellet (PD80, black), the pellet of PD80 (PD80P, red) and the supernatant fraction of PD80 (PD80S, blue) assayed on nBaF3 target cells with Eco-GFP vectors (top) and on TF-1 target cells with GALV-GFP (bottom). (*n*=3, error bars: SEM)

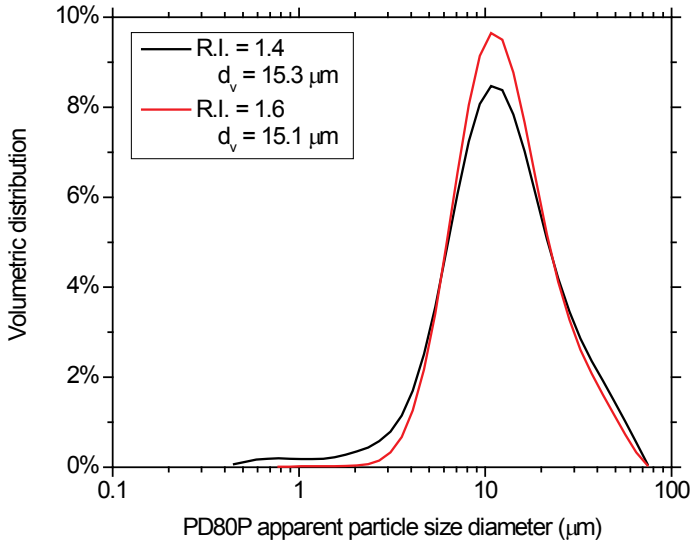

Figure 3.12 Volume weighted apparent size distribution of PD80P lysate fraction measured using a Mastersizer 2000 based on assumed refraction indices (R.I) of 1.4 (black) and 1.6 (red).

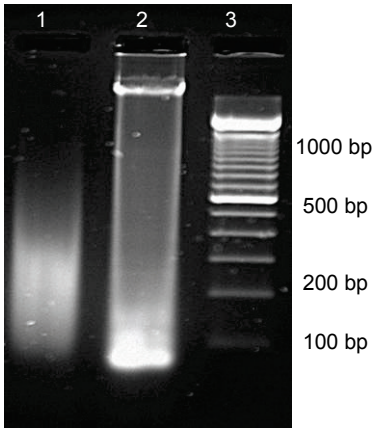

Figure 3.13 Separation of DNA fragments extracted from DNase-treated pellet fraction (PD80P, lane 1) and whole untreated lysate (lane 2) by electrophoresis on a 2% agarose gel.
A 100 bp ladder was added to lane 3.

Cationic peptides rich in arginines and lysines such as protamine sulfate (and histones in one brief report) have been previously reported to enhance retroviral transduction. To explore if a peptide with similar features was responsible for the activity observed, the PD80P fraction was digested by trypsin and, as is shown in Figure 3.14, this eliminated nearly all of the activity. For nBaF3 cells, the increase in

transduction was reduced from 130-fold to 1.4-fold and for the TF-1 cells from 40-fold to 0.7-fold, neither significantly different from the control. A control where a residual volume (200 μL) was kept following trypsin removal by centrifugation was tested and showed minor increases in transduction of 2.7-fold for nBaF3 and 1.4-fold for TF-1 cells. This clearly demonstrated that the reduction in transduction observed was due to the action of trypsin on the PD80P, not because of a trypsin effect on the cells or vectors. Also, the HBSS and EDTA present in the trypsin solution did not negatively influence the activity of the PD80P lysate fraction. Finally, a control using PD80P treated only with DMEM demonstrated that losses of PD80P during incubation and centrifugation to remove the trypsin did not contribute to the reduction in the activity of the lysate. Based on these results, arginine- and/or lysine-rich peptides were hypothesized to be responsible for the bulk of the activity observed with the PD80P fraction.

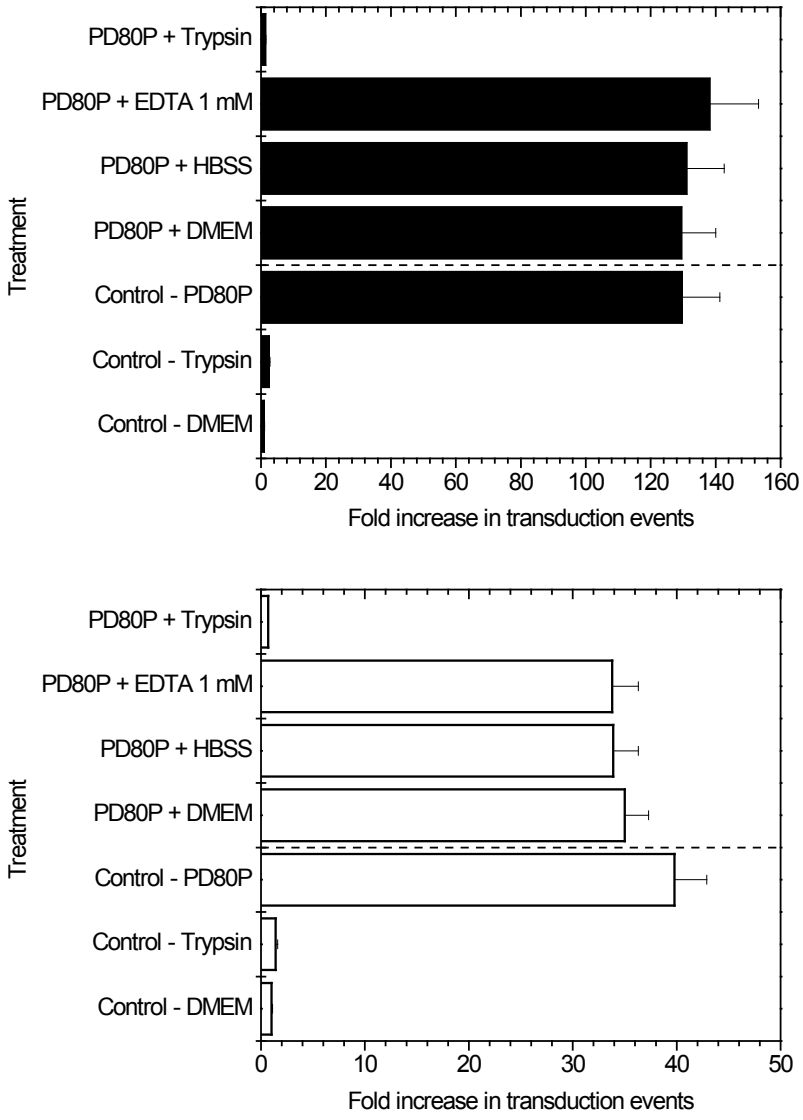

Figure 3.14 Increase in transduction events following treatment of the PD80P lysate fraction with trypsin (containing EDTA in HBSS), HBSS with EDTA, and HBSS measured on nBaF3 target cells with Eco-GFP vectors (top) and on TF-1 target cells with GALV-GFP vectors (bottom).
Controls included residual trypsin in the absence PD80P to evaluate the effect of carried-over trypsin and PD80P in DMEM to evaluate potential loss of PD80P upon trypsin removal. (n=3, error bars: SEM)

3.3.4. Nuclei- and erythrocyte-derived lysates

To define the cellular location of the lysate components primarily responsible for the increase in retroviral transduction, the performance of nuclei-derived lysates was compared to that of whole-cell lysates obtained from nBaF3 cells (Figure 3.15) and TF-1

cells (Figure 3.16). These results were also compared to those acquired using anucleate human erythrocyte (red blood cell) lysates. When assayed on nBaF3 target cells, lysates of both the nBaF3 and TF-1 cell nuclei yielded significantly larger increases in transduction, 3- to 4-fold greater than the whole cell lysates. For the TF-1 target cells, transduction was also increased with nuclei lysates but only by 1.2- to 1.6-fold ($p<0.05$ for both nBaF3 and TF-1 lysates at 5×10^5 lysed cells/mL but not at 10×10^5 lysed cells/mL). Lysates derived from anucleate erythrocytes tested on nBaF3 target cells did not significantly increase transduction relative to the control without lysate. For TF-1 target cells, transduction was only increased by 1.5-fold compared to control, significantly lower than with the nucleated cell lysate. As transduction in the presence of nuclei-derived lysates exceeded that of whole cell lysates in all cases while erythrocyte-derived lysates had little to no effect on transduction, it was apparent that compounds of nuclear origin were responsible for the bulk of the performance increase. Interestingly, the improved performance of the nuclei-derived lysates suggests that inhibitors may be present in the extra-nuclear compartment. This is in agreement with the observation made above where the pellet-derived PD80 fraction outperformed the whole-cell-derived WD80 fraction.

Given the previously observed beneficial effect of the DNase treatment, nuclei- and erythrocyte-derived lysates were subjected to a similar protocol. As previously reported with whole cell lysate, the PD80P fraction significantly increased transduction compared to the untreated lysate (Figures 3.15 and 3.16). With nuclei lysate, however, the increase in transduction for the PD80P compared to the untreated fraction was not significant. With TF-1 lysates, the transduction results obtained using both the whole-

cell and nuclei PD80P fractions appeared to converge, yielding similar increases at 1×10^6 lysed cells/mL for both nBaF3 and TF-1 target cells (Figure 3.16). With nBaF3 lysates, the whole-cell and nuclei PD80P results did not converge as experiments carried out with nuclei PD80P yielded a 40-50% lower increase in transduction (Figure 3.15). As the activity of the nBaF3 nuclei PD80P increased with concentration, it could eventually converge with that of the whole cell PD80P at higher concentrations. To verify whether higher losses of active compounds may have occurred during fractionation, the ratios of the activity of nBaF3 and TF-1 nuclei PD80S to PD80P were compared. Interestingly, nBaF3 had a higher ratio at 0.89±0.03 than that of TF-1 at 0.40±0.05, which was similar to that of the nBaF3 whole-cell lysate at 0.37±0.04. The lower performance of the nBaF3 nuclei PD80P lysate may be attributed to a greater loss of small aggregates and/or soluble factors to the supernatant. This suggests that the extent of DNA digestion of the nBaF3 nuclei may have been greater, thus leading to smaller aggregates. Variations in endogenous DNase I inhibitors such as actin (Lazarides and Lindberg 1974) could influence the size of the residual aggregates. The lower increase with both TF-1 and nBaF3 nuclei PD80P relative to the untreated nuclei lysate, could also be explained by the absence of extra-nuclear inhibitors. These inhibitors may bind to the active component(s) present on the surface of the debris aggregates in the whole-cell lysate. The fracture of these aggregates by DNase I digestion would expose unfouled surfaces. This was also supported by previous results (Figure 3.9) where, with the PD80, from which the inhibitor-containing supernatant was removed, the surfaces of the aggregates would remain unfouled. However, in WD80, from which the supernatant was not removed, the newly-exposed surface area could be fouled by inhibitors present in the

surrounding medium. This may explain both the higher activity of PD80 relative to WD80 (Figure 3.9) as well as the lack of a significant increase due to the untreated nuclei lysate compared to the nuclei PD80 fraction.

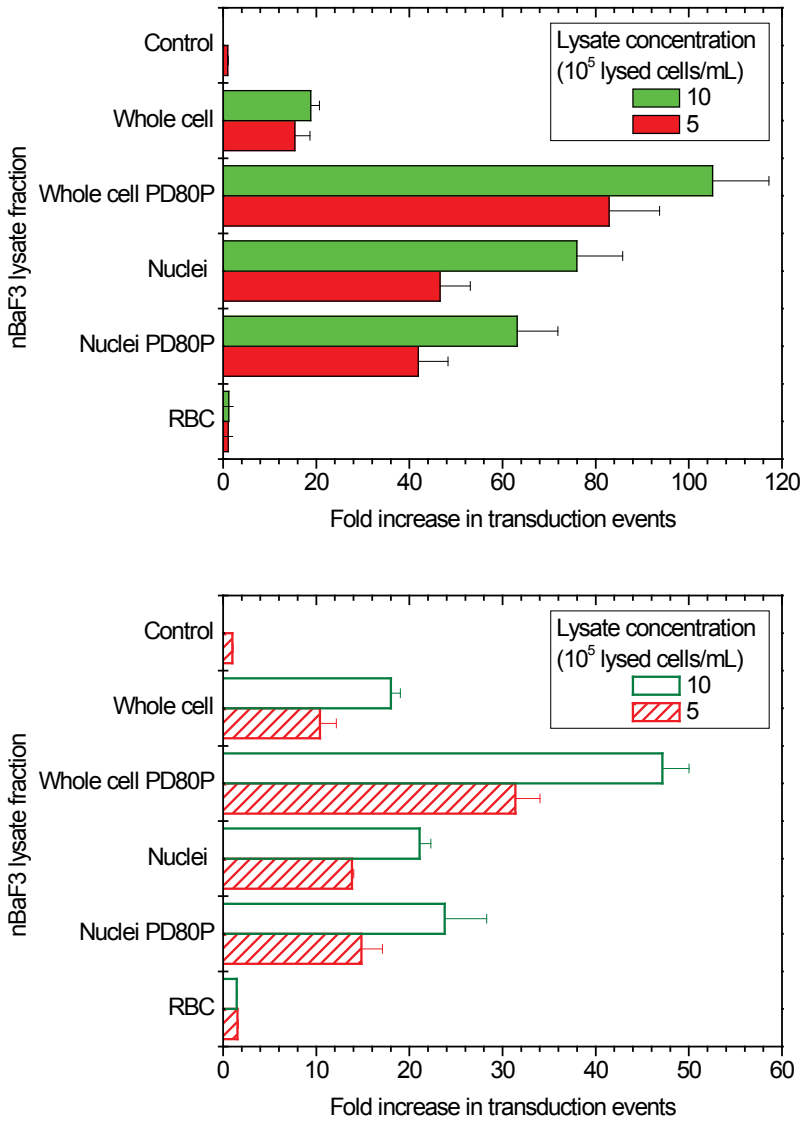

Figure 3.15 Increase in transduction events obtained with nBaF3 whole cell and nuclei lysates, human erythrocytes (RBC) and PD80P fractions derived from nBaF3 whole cells and nuclei assayed on nBaF3 target cells with Eco-GFP vectors (top) and on TF-1 target cells with GALV-GFP vectors (bottom). (*n*=3, error bars: SEM)

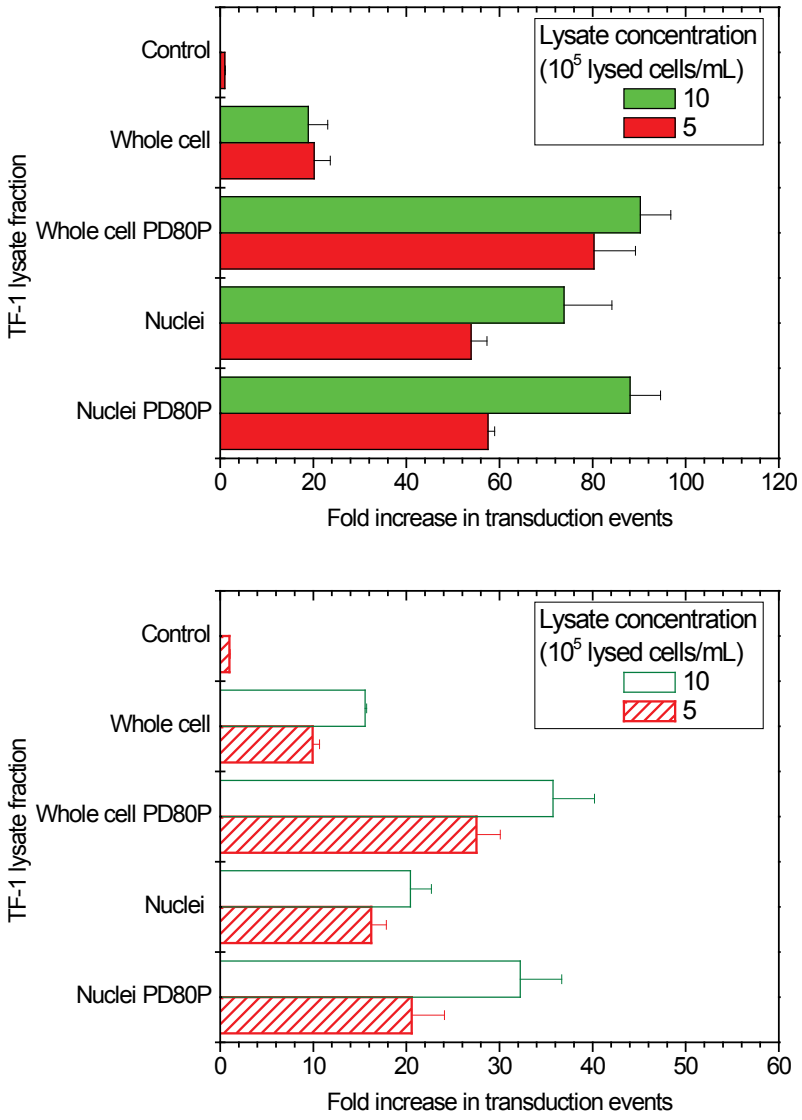

Figure 3.16 Increase in transduction events obtained with TF-1 whole cell and nuclei lysates and PD80P fractions derived from TF-1 whole cells and nuclei assayed on nBaF3 target cells with Eco-GFP vectors (top) and on TF-1 target cells with GALV-GFP vectors (bottom). (*n*=3, error bars: SEM)

3.3.5. Mechanisms

We next investigated the PD80P mechanism of action in an effort to identify novel candidates and strategies to further enhance retroviral transduction. This

knowledge should also improve our ability to predict the impact of cell lysates in other contexts, such as in the production and downstream processing of retroviral vectors.

3.3.6. Sedimentation

The characteristics of the PD80P fraction, which was composed of particles having a higher density than the surrounding medium, suggested that sedimentation may have caused increased mass transfer of retroviral vectors to the target cells. In the absence of additives, mass transport of vectors is governed by diffusion (Chuck et al. 1996). Under diffusion control and due to their relative instability, most of the retroviral vectors located above a liquid depth of ~500 μm will decay prior to reaching the target cells. Thus, no increase in transduction will occur if the static liquid depth is increased above this threshold (Andreadis et al. 2000). Therefore, a transition from a diffusion- to a sedimentation-controlled mass transfer regime should remove this depth limitation and result in increased transduction at greater liquid depths. Transduction events were measured at a constant cell number and VCM concentration for liquid depths increasing from 1 to 15 mm in the presence of either PD80P (5×10^5 lysed cells/mL), lysate supernatant (5×10^5 lysed cells/mL), protamine sulfate (10 μg/mL) or for a no-additive control (Figure 3.17). As anticipated, the transduction with no additives did not increase with liquid depth. The supernatant and protamine sulfate yielded a similar trend, suggesting that these additives did not influence viral vector sedimentation. However, with the PD80P fraction, transduction increased with increasing liquid depths for both the nBaF3 and TF-1 target cells. Transduction increased approximately proportionately up to a depth of 5 mm, suggesting that most of the particles were able to sediment to the target cells over this distance. Above 5 mm, transduction continued to increase with liquid

depth but at a diminishing rate. It is likely that, given the variability in particle shape and size, at the higher liquid depths only a fraction of the PD80P particles will sediment at a velocity sufficient to reach the target cells within the 24 h of the experiment and prior to vector decay. While these results support the role of sedimentation, they do not clearly distinguish between sedimentation of the lysate particles alone (i.e. acting only in proximity to the target cells to stimulate transduction rates) vs. co-sedimentation of the retroviral viral vectors adsorbed onto lysate particles. Thus, the sedimentation step must be uncoupled to distinguish between sedimentation of the lysate particles alone and co-sedimentation of vectors and particles.

In order to distinguish between these two mechanisms, the sedimentation step was performed before the transduction assay. The PD80P and supernatant lysate fractions were incubated at room temperature, either separately (independently incubated) or mixed together (co-incubated) with VCM. After 6 h, the content of each tube was separated into top and bottom halves (top and bottom layers). As a control, VCM was similarly incubated independently at room temperature before being mixed with independently incubated PD80P and supernatant lysate top and bottom layers. If sedimentation occurred, the bottom layer should be enriched in vectors, yielding greater transduction levels. In the absence of sedimentation, both the top and bottom layers should yield similar transduction levels. As expected, similar transduction was obtained for both the top and bottom layers of the VCM incubated without additives (Figure 3.18) as well as combined, post-incubation, with supernatant and PD80P fractions that were not incubated. Lysate supernatant incubated independently or together with VCM did not alter the distribution between the top and bottom layers. With PD80P incubated

independently of the VCM, the bottom layer yielded a significantly greater increase in transduction relative to the top layer. The average of the top and bottom layer matched that of the PD80P that was not incubated, thus, supporting the hypothesis that the increase was due to a higher concentration of PD80P in the bottom layer. However, when the PD80P fraction was co-incubated together with VCM, a 1.5- to 2.0-fold greater increase in transduction was observed for the bottom layer compared with the case where the PD80P and VCM were independently incubated. This suggests a mechanism where the viral vectors bind to the particles present in the PD80P fraction and sediment together leading to an increase in the concentrations of both PD80P and viral vectors in the bottom layer. Pre-incubation of the VCM with PD80P, over 6 h, gave time for an increased proportion of lysate particles to be loaded with viral vectors. Also, the 2-times higher VCM and PD80P concentrations during this period (vs. when mixed together with the target cells) would have increased the adsorption rates. The combination of the increased vector adsorption rate, the extra time allowed for loading the PD80P particles, and the co-sedimentation of vectors and lysate particles likely all contributed to the higher transduction observed.

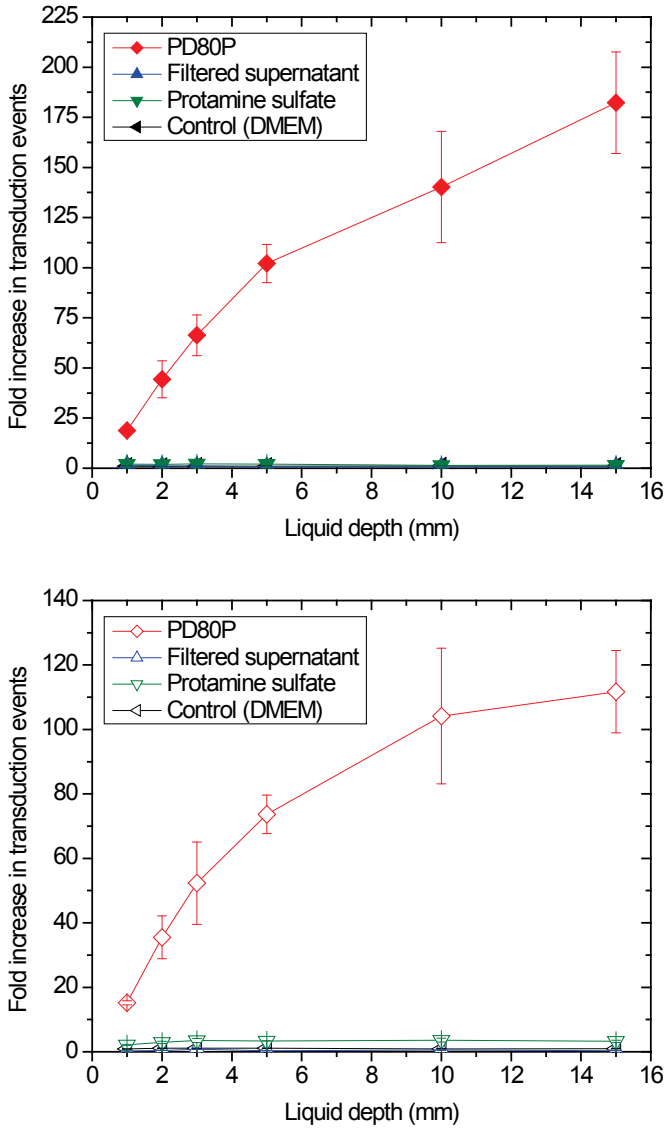

Figure 3.17 Effect of liquid depth on the increase in transduction events relative to the average of the control with no additives (left triangles), with PD80P (diamonds) and supernatant (triangles) lysate fractions (5×10^5 lysed cells/mL), and with protamine sulfate (10 µg/mL) (inverted triangles) assayed on nBaF3 target cells (1.5×10^5 cells/cm^2) with Eco-GFP vectors (0.0625× concentration) (top) and on TF-1 target cells (1.5×10^5 cells/cm^2) with GALV-GFP vectors (0.125× concentration) (bottom). (*n*=3, error bars: SEM)

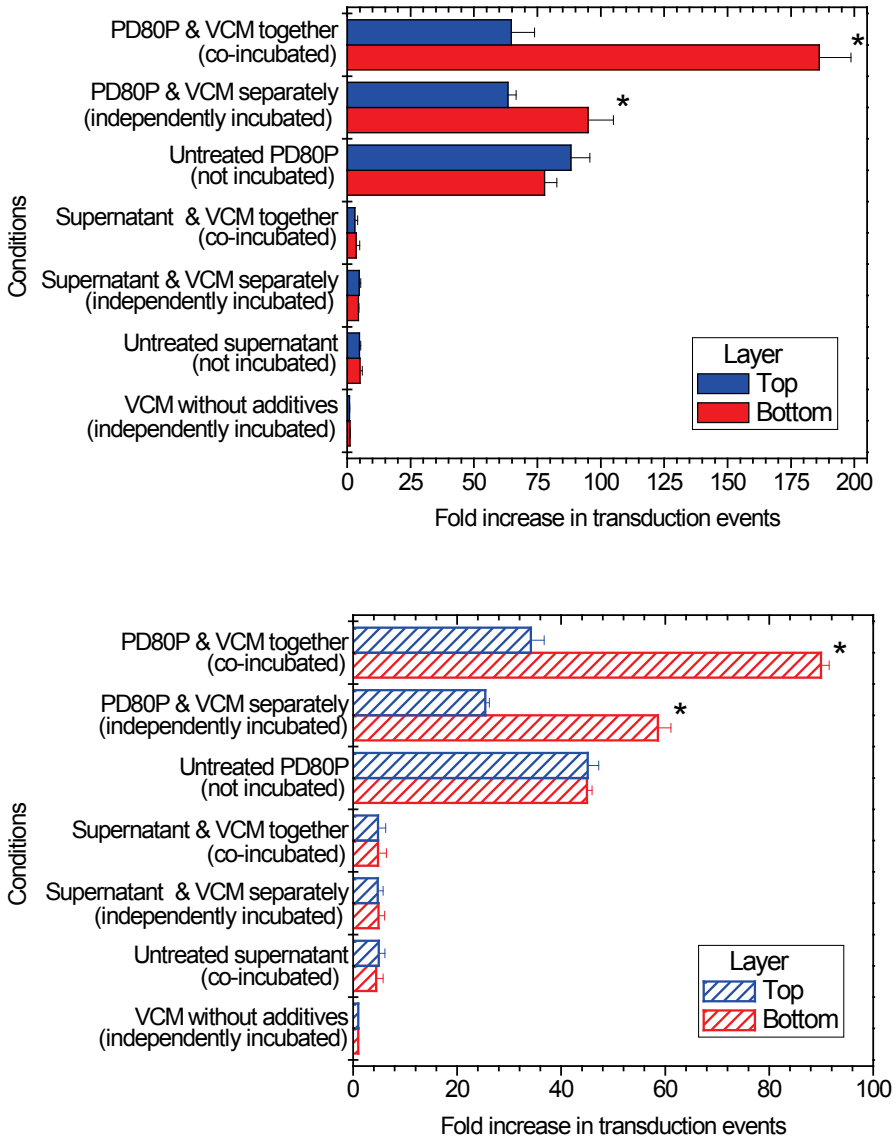

Figure 3.18 Effect of the co-incubation of PD80P and lysate supernatant with VCM prior to the addition of the nBaF3 and TF-1 target cells on transduction.
The VCM was pre-incubated together with PD80P and supernatant lysate fraction (co-incubated) and separately (independently incubated) at 1.8 cm liquid depth for 6 h at room temperature to allow for settling. The contents were then separated into equal volume top and bottom layers prior to their addition to nBaF3 target cells (Eco-GFP vectors) (top) and TF-1 target cells (GALV-vectors) (bottom). The fold increase in transduction events was measured relative to the average (top and bottom layers) of the control without additives (VCM without additives). As additional controls: untreated (not incubated) supernatant and PD80P lysate were added to each layer of the incubated VCM top and bottom layers. (n=3, error bars: SEM)

3.3.7. Cell surface adsorption

Cationic polymers such as protamine sulfate can improve transduction by increasing the non-specific adsorption of viral vectors to target cells. To determine if this mechanism also applies to the PD80P lysate fraction, the adsorption was uncoupled from sedimentation using centrifugation. Centrifugation can rapidly displace the vectors to the target cells thus eliminating the mass transport advantages of the PD80P fraction. Based on the Stokes settling velocity,

$$u = \frac{c\, g\, (\rho_v - \rho_m)\, d_v^2}{18\, \eta} \qquad \textbf{Eq. 3.6}$$

where the retroviral vector has a density (ρ_v) of 1.16 g/cm^3 and a diameter (d_v) of 115 nm, the medium has a density (ρ_m) of 1.01 g/cm^3 (Tayi et al. 2010) and a viscosity (η) of 0.936 g/m·s at 23^{o}C, g is the gravitational acceleration and c is the multiplier due to centrifugation. Thus, vectors centrifuged at 1000 times the gravitational acceleration should reach a terminal settling velocity of ~4 mm/h. For a liquid depth of 3 mm, centrifugation for 1 h should displace all the retroviral vectors to the bottom of the culture vessel, where the target cells reside. Upon the cessation of centrifugation, unbound retroviral vectors will begin to diffuse away from the cells. Alternatively, unbound vectors can be removed by discarding the VCM and washing the cells. To minimize any interaction with the polystyrene surface of the culture vessel, adherent cells (RAT-1 fibroblasts) covering over 90% of the surface were used. The selection of an adherent cell line also facilitated media removal and subsequent washing. Finally, to minimize retroviral vector entry, the centrifugation step was performed at 23^{o}C (Yu et al. 1995).

The PD80P lysate treatment was therefore compared using 3 conditions. First, centrifugation at 1000×*g* in the absence of additives improved mass transport of the viral vectors, but yielded a transduction increase of only 3.6-fold relative to gravity alone (Figure 3.19). Secondly, the addition of protamine sulfate without centrifugation improved viral vector adsorption on the target cells but mass transport remained diffusion-limited resulting in an increase of 7.2-fold relative to the no-additive control. Removal of the VCM after 1 h confirmed that only a small fraction of the vectors reached the cells within this period. Thirdly, centrifugation was combined with protamine sulfate, thus addressing both mass transport and adsorption concerns, and, in a synergistic interaction, yielded an increase of 17.1-fold. In this case, removal of the VCM did not reduce transduction suggesting that most of the vectors leading to successful transduction events were already bound to the surface of the target cells when centrifugation was terminated. When PD80P addition was combined with centrifugation followed by VCM removal, transduction was similar to that of the protamine sulfate combined with centrifugation. This suggests that the PD80P and protamine sulfate shared similar binding properties. However, when the VCM was left in, transduction was further increased to 37.7-fold relative to the untreated control, over 2-fold greater than centrifugation combined with protamine sulfate. In this case, in addition to increasing adsorption, the sedimented PD80P particles with their adsorbed viral vectors maintained these vectors in close proximity to the target cells making them available for subsequent uptake. Interestingly, in the absence of centrifugation, PD80P addition achieved similar transduction to the combined protamine sulfate and centrifugation treatment when the VCM was left in, demonstrating that both methods improved adsorption and mass

transport. However, VCM removal significantly reduced the increase in transduction from 18.6- to 3.6-fold, as the settling velocity of PD80P under normal gravity did not match that achieved for viral vectors with centrifugation.

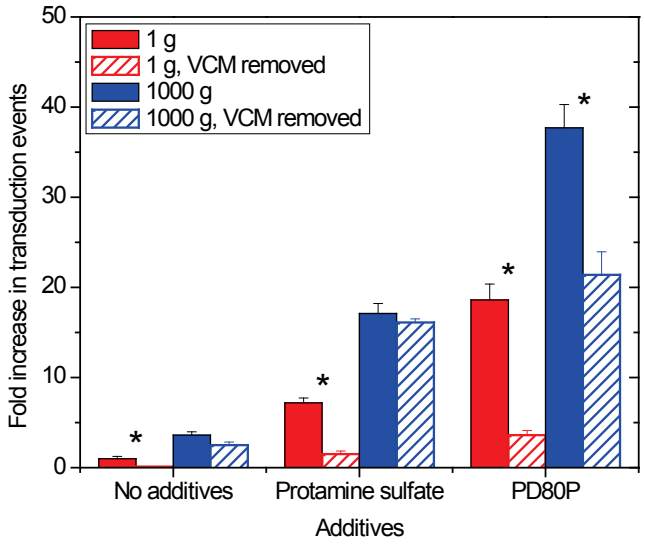

Figure 3.19 Effect of centrifugation alone and in combination with protamine sulfate (10 µg/mL) and PD80P lysate fraction (5×10^5 lysed cells/mL) on the transduction of RAT-1 target cells with Eco-GFP vectors.
Target cells with VCM and additives were transduced under static (1×*g*) (red) and centrifugation at 1000×*g* (blue) for 1 h at 23°C. VCM was left in (filled bars) or removed after 1 h and replaced by growth medium (shaded bars) before transferring the cells to an incubator at 37°C for an additional 23 h. (*n*=3, error bars: SEM)

The addition of PD80P to suspension cell lines also induced cell-cell aggregation as shown in Figure 3.20. This cell-cell aggregation was easily reversed by trituration, i.e., exposing the cells to shear. During the budding process, retroviral vectors inherit part of the packaging cell membrane. Thus, cell-cell aggregation suggests that an increase in retroviral vector-cell adsorption should occur, in agreement with the centrifugation results shown in Figure 3.19.

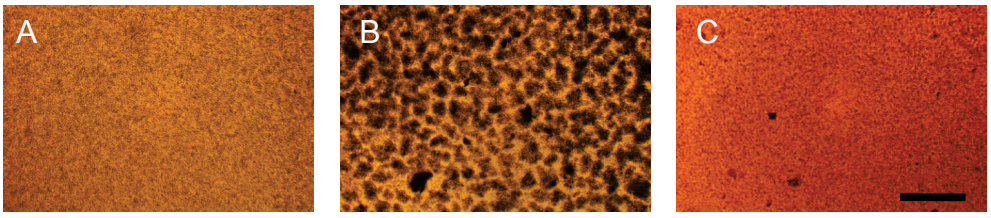

Figure 3.20 (A) Untreated nBaF3 did not aggregate. (B) The addition of PD80P lysate fraction (1×10^6 lysed cells/mL) induced nBaF3 cell-cell aggregation over a 24 h incubation period. (C) Aggregation was reversed by 3 trituration cycles with a 1000 µL pipette. Scale-bar: 500 µm.

3.3.8. Surface coating

Several additives including poly-L-lysine (Hennemann et al. 2000a) and fibronectin (Hanenberg et al. 1996) have been shown to increase transduction by coating culture vessel surfaces, thus modifying their properties to facilitate retroviral vector and target cell co-adsorption. In suspension cell cultures, a large fraction of the culture vessel surface remains exposed to the surrounding medium. Thus, lysate components could interact with these either hydrophobic (e.g., untreated polystyrene) or negatively-charged surfaces (e.g., gas plasma-treated surfaces designed for anchorage-dependent cells). It was previously established in Chapter 2 (Beauchesne et al. 2010) that whole-cell lysates coated untreated surfaces. Based on these preliminary results, the interactions with surfaces of the whole lysate, supernatant, pellet and PD80P fractions were investigated by coating both hydrophobic and negatively-charged tissue culture-treated surfaces prior to the addition of the VCM and target cells (Figure 3.21). Protamine sulfate was also used as a positive control and DMEM as a negative control. All surfaces coated with either whole lysate, pellet, supernatant or PD80P fractions exhibited an increase in transduction, thus confirming that compounds present within the lysate adhere to the culture vessel surface, and presumably enhance transduction by facilitating retroviral vector and target

cell co-adsorption. To rule out post-coating desorption of bound lysate components, the residual activity of the coating and wash solutions was assayed. While significant activity remained in the coating solution suggesting only a partial depletion, no activity was detected in the wash solutions of the whole, pellet and supernatant fractions (data not shown). With the PD80P fraction, less than 10% of the activity measured with the coated surface was present within the wash, suggesting that the bulk of the transduction observed under coated conditions was the result of surface-bound compounds.

When coated, all lysate fractions (whole, pellet, supernatant and PD80P) exhibited significantly greater transduction on untreated surfaces compared with tissue-culture-treated surfaces for both nBaF3 and TF-1 target cells (Figure 3.21). These results suggest that the active compounds found within all lysate fractions possess a higher affinity for hydrophobic surfaces compared to negatively-charged surfaces. Without prior coating (i.e., only adding the VCM and target cells together), surface type effects were no longer significant with all lysate fractions for both the nBaF3 and TF-1 target cells.

Interestingly, when coated surfaces were compared to the uncoated addition of lysate, the trends differed between the nBaF3 and TF-1 target cells. For nBaF3 cells on untreated surfaces, the whole, pellet and supernatant lysate fractions yielded significantly greater transduction when coated relative to the uncoated case. This translated to a 3.8-fold increase for the supernatant, 2.9-fold for the whole-cell and 2.0-fold for the pellet fraction. Given the previously described lower performance of the WD80 fraction compared with the PD80 fraction, the greater transduction obtained with nuclei relative to whole-cell lysate, as well as the presence of inhibitory compounds found in decayed

whole lysate (Chapter 2) (Beauchesne et al. 2010), inhibitors likely at the highest ratio relative to enhancers in the supernatant fraction, would be removed when the coating solution was discarded while enhancers remain surface bound leading to the increase in transduction. There was no significant difference in transduction between the coated and uncoated conditions with the PD80P fraction where the supernatant was removed and residual aggregates were twice resuspended, thus removing the supernatant inhibitors. In contrast to the untreated surfaces, with tissue culture-treated surfaces, the whole lysate, pellet and supernatant fractions exhibited similar transduction levels for both the coated and uncoated conditions. This may be the result of the lower affinity of the lysate for adsorption to tissue culture-treated surfaces. In the case of the PD80P fraction, higher transduction was obtained for the uncoated compared to the coated surface, likely due to combined contributions from improved settling and surface adsorption.

For TF-1 target cells, opposite trends in transduction between the coated and uncoated conditions were observed. On hydrophobic surfaces, no significant differences between the two conditions were measured with the whole lysate, supernatant and pellet fractions, while the PD80P fraction yielded a higher transduction for the uncoated case. On tissue-culture-treated surfaces, all lysate fractions (whole, pellet, supernatant and PD80P) exhibited greater transduction in the absence of precoating. Overall, this may be explained by a higher affinity of the lysate compounds for untreated hydrophobic surfaces as the transduction obtained with coated hydrophobic surfaces was similar to that of both the untreated and tissue-culture-treated surfaces when the whole, pellet and supernatant lysate fractions were added in solution. Finally, with the PD80P fraction, transduction was always greater for the uncoated relative to the coated surface, likely

reflecting the contribution of other mechanisms (cell surface binding and sedimentation). While it is clear that lysate fractions modified the cell culture vessel surfaces, the net contribution of this mechanism to the overall transduction differed between cell lines.

As was the case for lysate, the surface type, the absence or presence of precoating, and the target cell type all influenced the transduction results obtained with protamine sulfate. When added in solution without precoating, protamine sulfate exhibited significant surface-type effects, where the transduction was 14.1-fold and 3.2-fold greater with tissue-culture-treated surfaces compared with untreated surfaces for nBaF3 and TF-1 target cells, respectively (Figure 3.21). For nBaF3 target cells, higher transduction levels were obtained with coated surfaces independent of the surface type. For TF-1 target cells, coating only increased transduction with untreated surfaces while, with tissue-culture-treated surfaces, the coated and uncoated conditions yielded similar increases in transduction. The higher impact of surface coating observed with nBaF3 with protamine sulfate was in line with the lysate results, suggesting that surface coating contributed more to the overall transduction for nBaF3 cells than for TF-1 cells. The lower transductions obtained in solution for both nBaF3 and TF-1 cells represent a significant disadvantage of employing protamine sulfate. Although this can be partly overcome by precoating the surface rather than adding protamine sulfate directly in solution, it exposed certain concerns that should be further explored. Compounds present within the VCM-target cell mixture could potentially interact with the surface thereby preventing the adsorption of protamine sulfate. Alternatively, protamine sulfate may be subject to partial inactivation due to inhibitors present in calf serum (Andreadis and Palsson 1997; Jensen et al. 2003) or secreted by the packaging cell lines (Le Doux et al.

1996). The resulting decrease in concentration combined with a potentially lower affinity for hydrophobic surfaces could drastically reduce the improvement in transduction observed.

The maximum increase in transduction efficiency achieved with protamine sulfate was 45-fold (coated, tissue-culture-treated surface) for nBaF3 target cells and 12-fold (uncoated, tissue-culture-treated surface) for TF-1 target cells. In comparison, with the PD80P lysate fraction, greater increases in transduction of 69- and 25-fold for nBaF3 and TF-1 target cells, respectively, were achieved for the uncoated condition and were independent of the surface type. While protamine sulfate was evaluated near its optimal concentration, the PD80P fraction was at 5×10^5 lysed cells/mL, well below the 2×10^6 lysed cells/mL concentration at which the maximum increase in transduction was previously achieved (Figure 3.9). Based on these results, the use of the PD80P fraction in place of protamine sulfate as a reagent should lead to much greater increases in transduction and a more robust process.

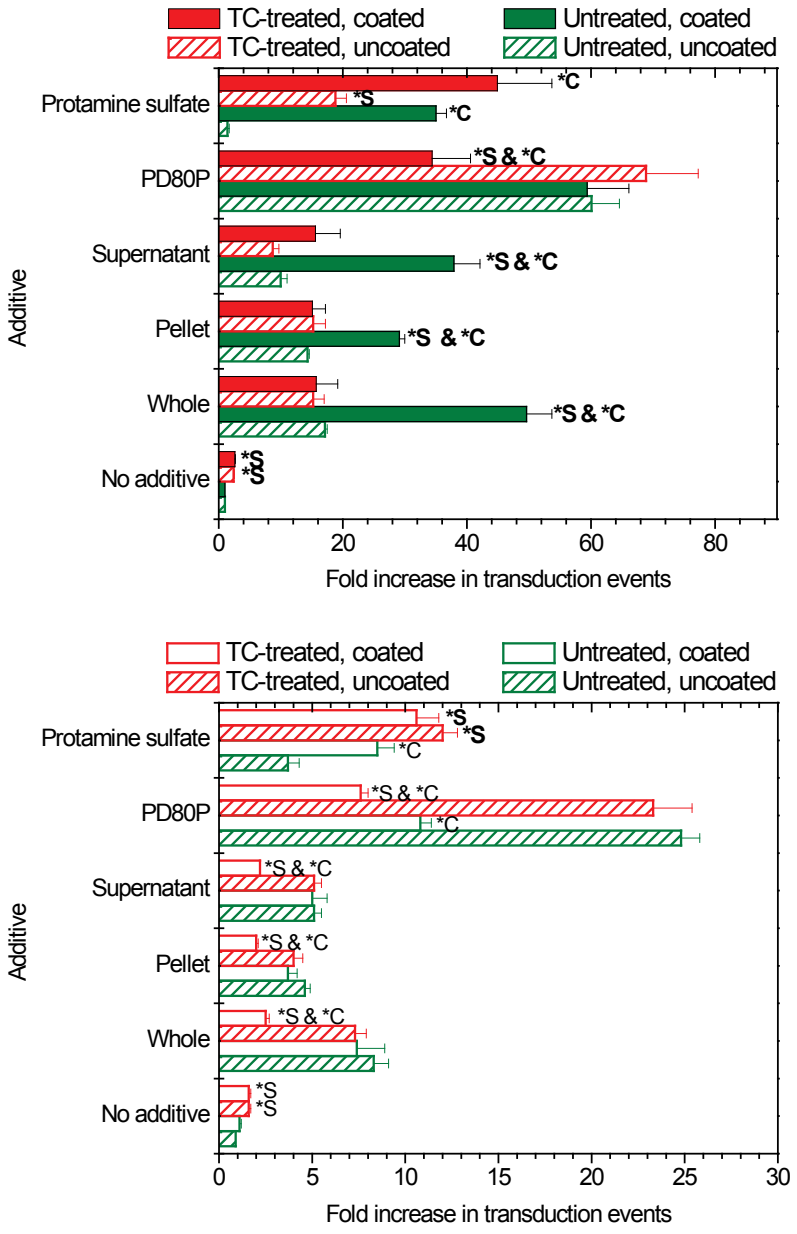

Figure 3.21 Effect of surface type and coating with whole lysate, pellet, supernatant and PD80P fractions as well as protamine sulfate and DMEM controls for nBaF3 target cells with Eco-GFP vectors (top) and TF-1 target cells with GALV-GFP vectors (bottom) on the increase in transduction events relative to a DMEM in solution control on untreated surfaces.
Untreated (green) and tissue-culture-treated surfaces were coated for 4 h with 5×10^5 lysed cells/mL of lysate, 10 µg/mL protamine sulfate in DMEM and DMEM as a control. Coating solutions were subsequently removed and surfaces were washed with DMEM. Target cells and VCM were added to coated wells, which were compared to uncoated wells where lysate, protamine sulfate and DMEM were added in solution. (*S: significant surface type effect, *C: significant coating effect, *n*=3, error bars: SEM)

3.3.9. Increase in transduction with the PD80P fraction predicted by the lysed-to-target cell ratio

The increase in transduction efficiency obtained by using whole-cell lysates was previously shown to be dependent on both the lysed and the target cell concentrations and was adequately predicted by a saturation-based equation (Chapter 2) (Beauchesne et al. 2010). However, it was unclear if this relationship would remain valid for the PD80P lysate fraction. Furthermore, this empirical equation was previously limited to TF-1 cells with GALV-GFP vectors; here it will also be tested for the transduction of nBaF3 cells using Eco-GFP vectors. In addition, in this chapter, the increase in transduction efficiency has been replaced by the increase in transduction events to allow a more accurate quantification of the effect of lysate over an expanded range of its concentration. Thus, the original equation has been replaced by

$$Fold\ increase\ in\ transduction\ events = 1 + Fold_{Max}\ \frac{R}{K_L + R} \qquad \textbf{Eq. 3.7}$$

where, as before, R is the lysed-to-target cell ratio, $Fold_{Max}$ is a parameter corresponding to the maximum increase in transduction events and K_L is a lysate parameter. To establish the parameters, $Fold_{Max}$ and K_L, in Chapter 2, a limited number of data points were available, with only 3 sets of 2 common lysed-to-target cell concentration ratios. To obtain the Eq. 3.7 parameters for the PD80P fraction, the design space was expanded per Table 3.3, where multiple common lysed-to-target cell ratios were selected to assess the robustness of the proposed model.

Table 3.3 Lysed-to-target cell ratios generated by changes in PD80P lysate concentration and nBaF3 or TF-1 target cell concentration.

Initial target cell concentration (10^5 cells/mL)	PD80P lysate fraction concentration (10^5 lysed cells/mL)					
	0	**1.25**	**2.5**	**5.0**	**10.0**	**20.0**
1.25	0	1	2	4	8	16
2.5	0	0.5	1	2	4	8
5.0	0	0.25	0.5	1	2	4
7.5	0	0.17	0.33	0.67	1.33	2.67
10.0	0	0.125	0.25	0.5	1	2

As was the case for the whole lysate in Chapter 2, the increase in transduction with PD80P was dependent on both the lysate and target cell concentrations (Figure 3.22). For all target cell concentrations, transduction was enhanced as the PD80P concentration was increased. At a constant PD80P concentration, transduction decreased with increasing target cell concentrations. Therefore, for both nBaF3 and TF-1 target cells, the maximum increases in transduction of 213- and 59-fold, respectively, were achieved at the lowest target cell concentration (1.25×10^5 cells/mL) and the highest PD80P concentration (20×10^5 lysed cells/mL). In the absence of lysate, the target cell concentration did not influence the transduction efficiency for nBaF3 (2.0±0.2%). As in Chapter 2, for TF-1 cells, the transduction efficiency increased slightly from 1.5% at 1.25×10^5 cells/mL to 2.9% at 20×10^5 cells/mL. However, unlike Chapter 2, the increase in transduction efficiency with increasing target cell concentration was not statistically significant ($p>0.05$). All fold-increases in transduction events were calculated using the no lysate control for the corresponding target cell concentration.

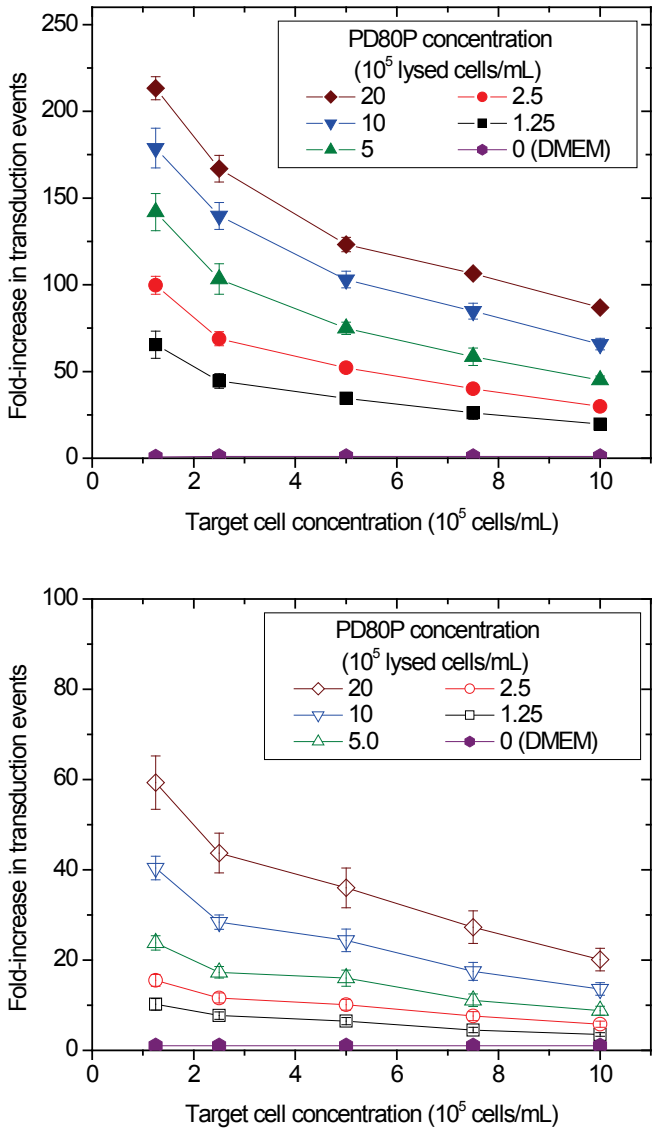

Figure 3.22 Effect of initial target cell and PD80P lysate fraction concentrations (Table 3.3) on the increase in transduction events measured on nBaF3 cells with Eco-GFP vectors (top) and on TF-1 cells with GALV-GFP vectors (bottom). (*n*=3, error bars: SEM)

The validity of the hypothesis that, with PD80P, common lysed-to-target cell ratios will yield similar increases in transduction events, independent of the PD80P and target cell concentrations, was first tested (Figure 3.23). For the nBaF3 target cells, the increase in transduction events was not significantly different ($p \geq 0.09$) for any of the 6 common ratios generated from the multiple different combinations (Table 3.3). This also

held true for the TF-1 cells ($p \geq 0.53$). Having verified this hypothesis, the data were subsequently fitted with the saturation equation (Eq. 3.7) using the Hanes-Woolf method (Hanes 1932) (Figure 3.23 and Table 3.4). The adequacy of the model was tested by a lack-of-fit test. For TF-1 cells, the model adequately predicted the increase in transduction events over the full range of the 25 different combinations of PD80P and target cell concentrations tested (Figure 3.23). However, for the nBaF3 cells, the model failed to adequately predict the increase in transduction over the full range. This appeared to be primarily due to a divergence occurring at the highest PD80P concentration (20×10^5 lysed cell/mL). When the 5 data sets generated at 20×10^5 lysed cells/mL were excluded from the fit, the model adequately predicted the increase in transduction for the remaining 20 data sets. It must be noted that the parameters estimated using all the data points or excluding the highest PD80P concentration (Table 3.4) all provided an adequate fit for the remaining data sets.

In the sedimentation experiments described in section 3.3.6, viral vectors were shown to be adsorbed onto the PD80P particles to form vector-lysate complexes. It was therefore hypothesised that, under conditions where unbound viral vectors are in excess, the increase in transduction would be solely dependent on the PD80P lysate fraction concentration. As the PD80P concentration increases, however, non-complexed viral vectors may become limiting, such that further increases in the lysate concentration will no longer enhance transduction. To test this hypothesis, PD80P was increased to 4×10^6 lysed cells/mL. As expected, this further increase in PD80P concentration yielded no additional increase in transduction for all nBaF3 target cell concentrations tested. For nBaF3 cells, the transition from a lysate-limiting to a vector-limiting state likely occurred

between 1×10^6 and 2×10^6 lysed cells/mL. For TF-1 cells, this transition is expected to occur at a higher lysed cell concentration as transduction continued to increase when the PD80P concentration was raised to 4×10^6 lysed cells/mL. This difference is reflected in the values obtained for the K_L parameter. For TF-1, K_L was 2-fold greater than for nBaF3 cells. Thus, it appears that the GALV-GFP vectors have a lower binding affinity for the particles present in the PD80P compared to the Eco-GFP vectors. However, differences in VCM conditioning and target cell properties impacting cell surface binding could also contribute to the variation observed in K_L values. Finally fractionation of the lysate into PD80P increased $Fold_{Max}$ for TF-1 with GALV-GFP vectors from 7.6 (Chapter 2) (Beauchesne et al. 2010) to 66.7, a gain of nearly 9-fold. This further indicates that whole cell lysate exhibits only a fraction of the transduction-enhancing potential that can be achieved following fractionation.

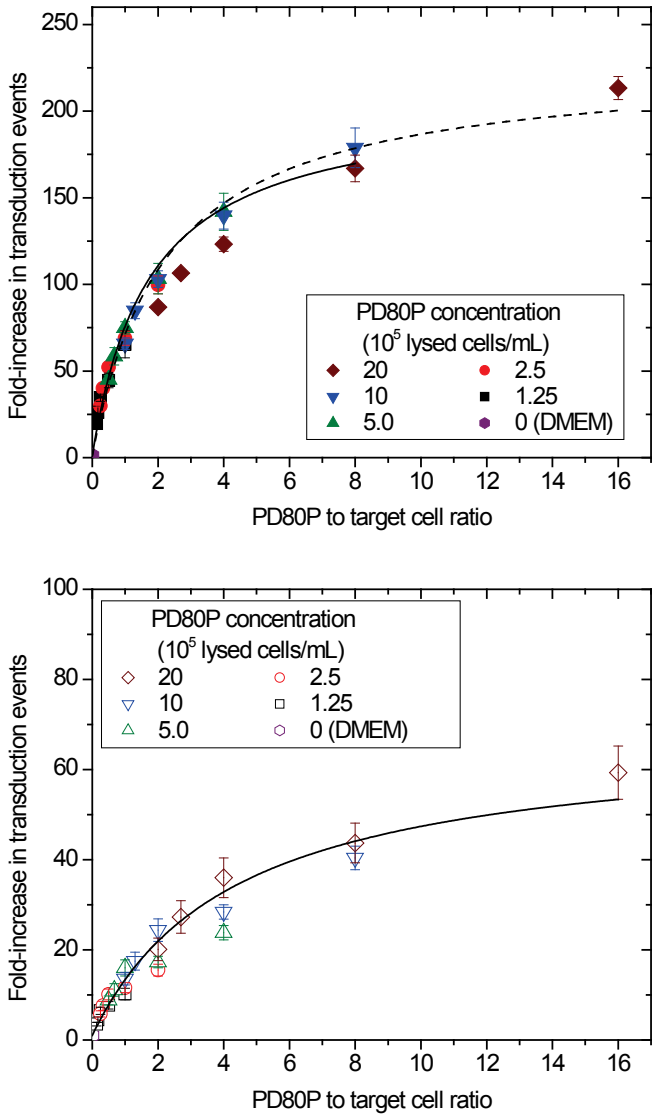

Figure 3.23 Increase in transduction events as a function of the ratio of the PD80P lysate fraction concentration to the initial target cell concentration measured for nBaF3 target cells with Eco-GFP vectors (top) and TF-1 target cells with GALV-GFP vectors (bottom).
All solid-line fits passed a lack-of-fit test. For the nBaF3 cells, the dashed-line fit includes all data while the solid-line fit excludes the data obtained with PD80P at 20×10^5 lysed cells/mL. (Same data set as in Figure 3.22.) (n=3, error bars: SEM)

Table 3.4 Parameters $Fold_{Max}$ and K_L from Eq. 3.7 used to predict the increase in transduction events as a function of the PD80P lysed-to-target cell ratios.
Estimates were obtained using the Hanes-Woolf method.

Target cell / Viral vector	$Fold_{Max}$	K_L
nBaF3 / Eco-GFP		
All data	227	2.22
Excluding 2×10^6 lysed cells/mL	206	1.75
TF-1 / GALV-GFP		
All data	66.7	4.38

3.3.10. Application of the PD80P lysate fraction to enhance the transduction of hematopoietic progenitors with long-term reconstitution potential

The PD80P fraction has shown great promise as a reagent to increase the retroviral transduction of hematopoietic cell lines. In many experimental and clinical settings, primary cells that are more sensitive to the toxicity of additives as well as *ex vivo* culture conditions, are often the gene transfer target. In particular, hematopoietic stem cells have demonstrated great potential for the treatment of monogenic disorders. As such, a model system using mouse bone marrow enriched in hematopoietic stem cells by 5-FU was selected to evaluate the transduction performance of the PD80P lysate fraction using the Eco-GFP vector. Bone marrow transduced with VCM alone (no additives) had a transduction efficiency of 7.1%. The addition of PD80P successfully increased the transduction efficiency of the bulk culture by 8-fold to 57% (experiment performed concurrently with trial #1 of Chapter 4). This result was similar to the 54% transduction efficiency obtained using a co-culture with irradiated producer cells.

To evaluate if the transduction efficiency of the heterogeneous bulk population was reflective of that of the target stem cell population, transduced cells were transplanted in congenic recipients to measure both their long-term transduction and

reconstitution potentials over 20 weeks. As shown in Figure 3.24A, after 20 weeks, the fraction of GFP+ cells within the donor contribution remained high at 31% for the PD80P-treated cells compared with the no-additive control at 6.1%. For the co-culture, the fraction of GFP+ cells within the donor contribution was even higher at 50%. Interestingly, with PD80P addition, the total donor contribution remained greater at both 12 and 20 weeks (Figure 3.24A). At 20 weeks, the PD80P total donor contribution was 26% compared with only 1.6% for the co-culture. These preliminary results suggest increased survival in *ex vivo* cultures without producer cells and/or increased engraftment of progenitors with long-term reconstitution potential and, potentially, of hematopoietic stem cells. Overall, based on transduction efficiency and reconstitution, the PD80P treatment outperformed the co-culture. Finally, the contributions to lympho- and myelopoiesis of the donor cells 20 weeks post-transplant were similar for all treatments (Figure 3.24B). The distribution was also similar between total donor and transduced donor cells. Overall, these results clearly demonstrated that the PD80P lysate fraction successfully transduced primitive hematopoietic cells with long-term reconstitution potential within the culture.

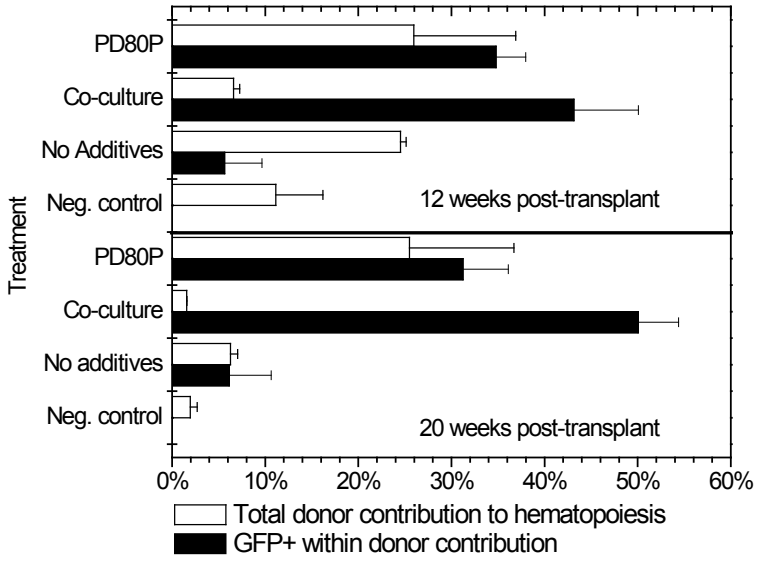

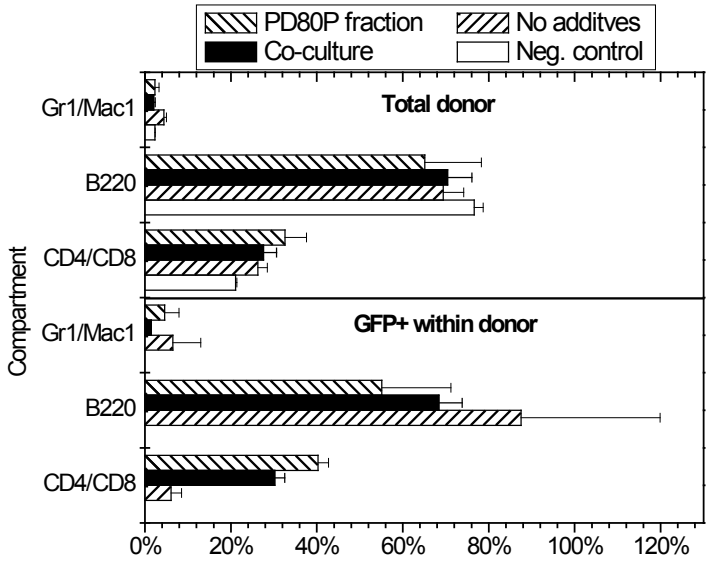

Figure 3.24 (Top) Cells treated with PD80P lysate fraction persisted in the peripheral blood of recipient mice for at least 20 weeks post-transplant at a level similar to cells co-cultured with viral producers. (Bottom) Cells treated with the PD80P lysate fraction contributed to both lymphoid and myeloid lineages 20 weeks post-transplant regardless of GFP expression.
(*n*=2, error bars: SEM)

3.4. Discussion

The analysis of lysate-enhanced retroviral transduction identified several distinct mechanisms of action depending on which lysate fraction was investigated (Figure 3.25). In fractions containing debris aggregates, retroviral vectors were found to bind to these aggregates. The majority of retroviral vector-debris aggregate complexes appeared able to sediment toward the target cells at least 5,000 μm prior to vector decay. This represented a significant-improvement over diffusion-limited mass transport where the root-mean-square displacement within one decay half-life was estimated to be only 480 – 600 μm (Chuck et al. 1996). Once in close proximity to the target cells, the lysate moiety within the complex improved vector adsorption onto the target cell surface. Alternatively, the lysate moiety may facilitate adsorption onto the exposed culture vessel surface, thus immobilizing the retroviral vectors in close proximity to the target cells. Finally, due to the influence of gravity, the complex could remain, unbound, near the target cells. Based on the correlation between transgene integration and expression observed in the presence of the PD80P fraction (Figure 3.3), the presence of lysate did not appear to alter transgene expression. The soluble components found in the supernatant did not improve mass transport. However, they were found to bind to cell culture vessel surfaces, likely enhancing retroviral vector and target cell adsorption, leading to increased transduction. Although not specifically investigated, it seemed probable that the soluble factors also improved adsorption of the retroviral vectors to the target cells.

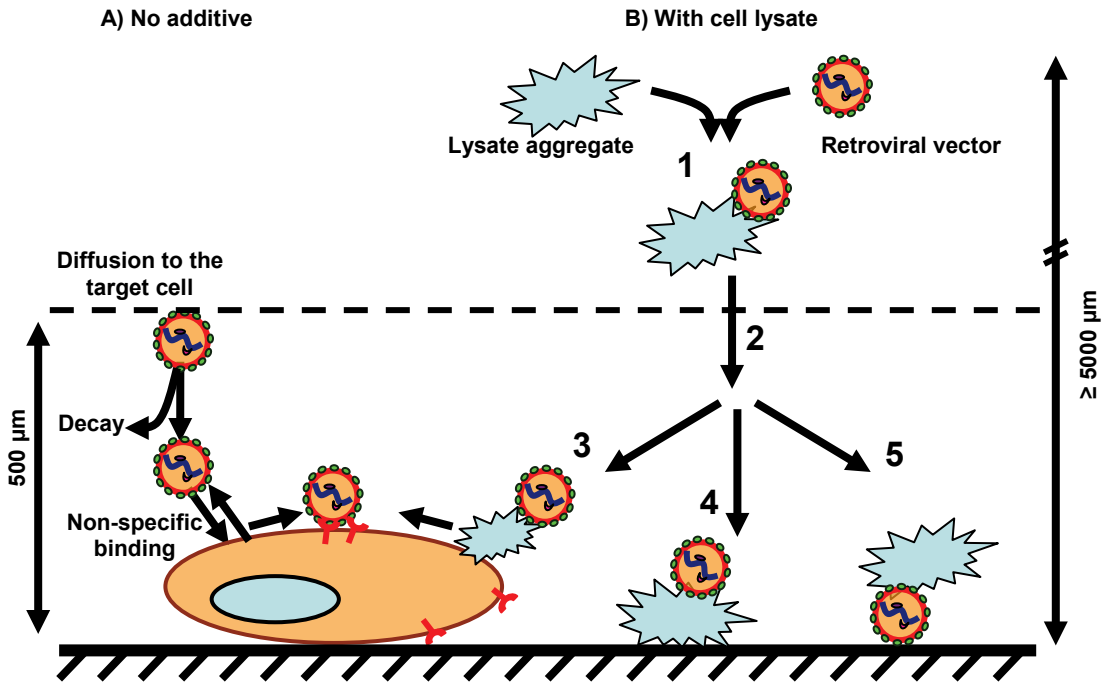

Figure 3.25 Diagram summarizing the effects of lysate on the retroviral transduction process. Without additives, mass transport was diffusion-limited such that, given the short half-life of retroviral vectors, many would decay prior to reaching the cells. In the presence of cell lysate, retroviral vectors adsorbed onto debris aggregates (1) improving mass transport to the target cell through sedimentation over a distance of at least 5000 µm (2). Soluble and aggregate components improved adsorption to the target cells (3) as well as to the culture vessel surface (4). Finally, aggregate-bound retroviruses were maintained at the bottom of the culture vessel in proximity to the target cells by gravitational effects (5).

An earlier assessment of the impact of cell lysates on the infection of mammalian cells by wild-type retroviruses had been limited to soluble compounds (Toyoshima and Vogt 1969). The fractionation scheme of the cell lysate in the present study revealed that most of the activity measured remained associated with the debris aggregates rather than the soluble factors (Figure 3.8). Thus, this earlier report significantly underestimated the potential impact of cell lysates to enhance retroviral transduction. More detailed characterization of the active compounds also showed them to be primarily located within the cell nucleus and that they were absent from anucleated cell erythrocytes (Figure 3.16).

Phosphatidylserine has been reported to enhance viral fusion but failed to increase the adsorption of the retroviral vectors on the target cell surface (Coil and Miller 2005a). In cells where infection was blocked as a result of the glycosylation of the viral receptors,

the culture of these cells in the presence of phosphatidylserine prior to the addition of retroviral vectors improved transduction (Coil and Miller 2005b). Both of these mechanisms were inconsistent with that observed for lysate. When subjected to targeted enzymatic digestion, the active compounds were sensitive to trypsin but not phospholipase A_2 degradation. Thus, it was unlikely that phospholipids (i.e. phosphatidylserine) contributed to the enhancement observed. Rather, these results implicate an arginine- and/or lysine-rich peptide of nuclear origin, potentially histones as free proteins or in a nucleosome conformation. Nucleosomes were reported to facilitate the binding of sulfated polysaccharides to cells through an interaction with cell surface proteoglycans such as heparan sulfate (Watson et al. 1999). Heparan sulfate proteoglycans inherited from packaging cell membranes during the budding process are also present on the surface of retroviral vector envelopes (Kureishy et al. 2006). Thus, histones within a nucleosome structure could facilitate the adsorption of retroviral vectors onto debris aggregates and, subsequently, onto the target cell surfaces. Free histones have also been shown to enhance retroviral transduction (Singh and Rigby 1996). However, this previous work was limited to an undefined histone mixture of types H1, H2A, H2B, H3.1 and H4. As the lysine and arginine contents differ significantly between histone types (vanHolde 1989), there may also be an unequal distribution in retroviral transduction-enhancing potential amongst these species. Additional work to screen individual histone types will therefore be performed in Chapter 4.

This new mechanistic understanding of the effect of cell lysates on retroviral transduction may explain some of the variability reported between transduction protocols. For example, it was initially reported that centrifugation could load retroviral vectors

onto untreated and tissue culture-treated surfaces prior to the addition of target cells (Kuhlcke et al. 2002). However, subsequent work by other groups failed to reproduce these results (Fehse and Kuhlcke 2008). The data presented in this chapter demonstrate that both untreated and tissue-culture-treated surfaces can be conditioned by soluble factors present within cell lysates. It is therefore possible that soluble lysate compounds in the VCM of the earlier report conditioned the surface and enabled increased adsorption. In the subsequent study, if the VCM were free of these lysate components, retroviral vectors would not bind to the culture-vessel surface, thus potentially explaining the discrepancy between the results.

The significance of the results presented in this chapter extends beyond retroviral transduction processes and provides potentially valuable insights applicable to retroviral vector production and purification. Considerable effort has been deployed to engineer packaging cell lines and optimize culture conditions in order to increase retroviral vector titers. The lower productivity observed in systems where cell death and lysis occurred was previously primarily attributed to product degradation due to the release of intracellular components such as proteases (Warnock et al. 2006). In the present study, cell lysate increased retroviral vector adsorption to cells as well as culture vessel surfaces. Thus, during production, retroviral vectors may be sequestered on the surface of the packaging cells as well as on the surrounding culture vessel surfaces, thus resulting in decreased vector recovery and opportunities to increase yields by minimizing cell debris formation.

The first step of retroviral vector purification typically involves clarification of the VCM by low speed centrifugation and/or microfiltration to remove cells and debris

(Ansorge et al. 2010; Segura et al. 2006). In particular, it was previously reported that microfiltration using a 0.45 μm pore size membrane reduced retroviral titers by as much as 74% relative to unfiltered VCM (Reeves and Cornetta 2000). Given that retroviral vectors can be adsorbed onto debris aggregates generated upon cell lysis, filtration could exclude such vectors, while centrifugation could pellet vectors that would otherwise remain in the supernatant. Thus, a significant portion of the retroviral vectors produced could potentially be lost during these debris removal steps. Furthermore, due to the retroviral transduction-enhancing potential of debris aggregates, their removal could exacerbate the reduction in titer observed between filtered and unfiltered VCM.

Packaging cell line and plasmid DNA have both been detected within the VCM (Chen et al. 2001; Sastry et al. 2004). The addition of benzonaze, a genetically engineered endonuclease able to degrade DNA and RNA, can eliminate residual DNA within retroviral preparations. Minimal reductions in titer were reported (Sastry et al. 2004) even when the VCM was incubated at 37^{o}C during this treatment, whereas these conditions should cause significant retroviral decay. Given that the addition of DNase to lysate significantly increased its transduction enhancing potential, the increased potency of DNase-treated lysate could potentially have concealed a decrease in active retroviral concentration leading to similar titer measurements.

Fractionation of the cell lysate significantly increased its retroviral transduction potential. Following DNase digestion of the lysate pellet fraction, transduction was increased by up to 8-fold relative to that of the whole cell lysate (for 20×10^5 lysed cells/mL and 5×10^5 target cells/mL). When the ratio of lysed-to-target cells was increased to 16 by reducing the target cell concentration to 1.25×10^5 cells/mL, retroviral

transduction was increased with the PD80P fraction relative to a control without additives by 213-fold and 59-fold for nBaF3 and TF-1 cells, respectively. Similarly to whole cell lysate, the increase in transduction was adequately predicted using a saturation equation based on the lysed-to-target cell ratio as long as the lysate concentration was limited and the free retroviral vectors were in excess. In the case of TF-1 cells, the $Fold_{Max}$ parameter was increased nearly 9-fold from 7.6 to 66.7 (Beauchesne et al. 2010). These results alone indicate that the PD80P lysate fraction is a highly promising retroviral transduction-enhancing reagent.

Beyond the increase in transduction observed with the PD80P lysate fraction, this approach also showed significant improvements relative to the use of cationic polymers such as protamine sulfate (Cornetta and Anderson 1989) and centrifugation (Bahnson et al. 1995). Cationic polymers increase transduction by enhancing receptor-independent adsorption of the retroviral vectors on the target cells (Davis et al. 2002) and on the culture vessel surfaces (Hennemann et al. 2000a). However, small cationic polymers do not improve mass transport (Davis et al. 2004). In contrast, centrifugation enhances the transport of the retroviral vectors to the target cells but fails to address adsorption limitations (Tayi et al. 2010). Although retroviral vectors were predicted to settle toward the target cells at a velocity of approximately 8 mm/h at a moderate centrifugal force of 1500×*g* (Tayi et al. 2010), retroviral transduction continuously increased over 7 h of centrifugation (Bahnson et al. 1995), much longer than should be required to settle the retroviral vectors. In the absence of additives to enhance adsorption, centrifugation will likely need to be prolonged beyond the time required to settle the vectors in order to prevent their diffusion away from the target cells. This has been observed empirically

when additives enhancing viral adsorption were combined with centrifugation in order to further increase retroviral transduction (Szyda et al. 2006). In this study, such a synergy was observed when protamine sulfate was combined with centrifugation. Interestingly, this combination only matched what was achieved alone with sub-optimal concentrations of the PD80P lysate fraction. This clearly demonstrates the advantage of using a reagent such as the PD80P lysate fraction that can simultaneously address both mass transport and binding limitations. In addition, the PD80P lysate fraction represents a simplified and more robust approach. In particular, the coating of the surface with protamine sulfate was both surface-dependent and needed to be carried out prior to the addition of the target cells and retroviral vectors in order to maximize retroviral transduction. In contrast, the PD80P lysate fraction was surface type-independent and performed best when simply added together with the target cells and retroviral vectors in the absence of prior coating. Also, the transduction efficiencies were higher with the PD80P fraction.

Beyond the promising results obtained using model cell lines, the PD80P lysate fraction was also effective in increasing the retroviral transduction of primary mouse hematopoietic stem cells. While soluble factors within cell lysates were previously reported to reprogram some primitive cells (Freberg et al. 2007), the use of PD80P, from which the soluble factors were removed, did not alter the contribution of hematopoietic progenitors to the myeloid or lymphoid lineages. Furthermore, the presence of PD80P was well tolerated by the primary culture as shown by the increased donor contribution to hematopoiesis measured at 12 and 20 weeks post-transplant relative to the negative control and no-additive conditions.

Overall, the results presented in this chapter provide a better understanding of the impact of cell lysate on retroviral transduction and its contribution to some of the variability observed in previous studies. The transduction-enhancing potential of both the PD80 and PD80P fractions showed significant promise as a retroviral transduction reagent able to address both retroviral binding and mass transport limitations with negligible toxicity to both cell lines and primary cells. Although the active components have yet to be completely defined, this preliminary characterization provides valuable guidance toward the development of a fully-defined reagent. Given the likely involvement of histone proteins, the investigation of lysate fractions in this chapter are followed by a screening study of histone types in Chapter 4.

4. Histone H3.1 Increases the Gammaretroviral Vector Transduction Efficiency of Cell Lines and of Primitive Hematopoietic Cells with Long-Term Reconstitution Potential

4.1. Introduction

The effectiveness of retrovirus-mediated gene transfer can be severely restricted due to several rate-limiting steps including mass transport resulting from their low diffusivity (~6×10^{-8} cm^2/s) and short half-life (~6 h) (Tayi et al. 2010). Furthermore, in close proximity, physico-chemical forces, such as electrostatic repulsion resulting from the negative charge shared by the retrovirus and the target cell, further restrict their encounter frequency (Palsson and Andreadis 1997). These limitations can be partly overcome by co-cultivation of the viral packaging cells together with the target cells (Bodine et al. 1991) to reduce the distance that must be travelled by the vectors to the target cells, though co-culture can complicate the subsequent target cell analysis. Convective mass transport can also overcome diffusion limitations when the retroviral vectors are displaced toward the target cells by centrifugation or fluid flow (Bahnson et al. 1995; Chuck and Palsson 1996a). Alternatively, additives have also been used to increase retroviral transduction. These include biologically-derived peptides such as protamine sulfate, fibronectin and histones as well as chemically synthesized polycations such as polybrene, and cationic liposomes (Cornetta and Anderson 1989; Hanenberg et al. 1996; Hodgson and Solaiman 1996; Singh and Rigby 1996; Themis et al. 1998; Toyoshima and Vogt 1969). These additives can increase non-specific retroviral vector adsorption onto the target cells through charge neutralization, improve cell and vector contact through adsorption on the culture vessel surface and, in the case of higher

molecular weight polycations, enhance sedimentation through vector aggregation (Davis et al. 2002; Davis et al. 2004; Hennemann et al. 2000a). Careful consideration must be given to the toxicity of polycations in order to maximize transduced cell yields, including to not decrease cell growth rates when mitotic nuclear envelope dissolution is required for successful transgene integration (Cornetta and Anderson 1989; Miller et al. 1990; Roe et al. 1993).

The analysis of cell lysates performed in Chapter 3 identified arginine- and/or lysine-rich peptides of nuclear origin (such as histones) as potential candidates that can substantially enhance retroviral transduction. However, to date, the use of histone proteins to improve the transduction efficiency of retroviral vectors has been limited to a few studies that employed mixed preparations derived from calf thymus (Singh and Rigby 1996; Toyoshima and Vogt 1969). These preparations are complex mixtures containing all 5 histones, thus confounding the influence of each histone type. These mixtures include the core histones H2A, H2B, H3 and H4 that assemble into an octamer around which DNA is wrapped to form the nucleosome in cells, and histone H1 which binds to the linker DNA found between the nucleosomes (Luger 2006; Luger et al. 1997). Histones differ widely in their content of the basic amino acids, arginine and lysine, and can be classified as lysine-rich (H1), slightly lysine-rich (H2A and H2B) and arginine-rich (H3 and H4) (Table 1.3). In addition to enhancing retroviral transduction, histones have been applied to the delivery of proteins and nucleic acids to the nucleus (Balicki and Beutler 1997; Wagstaff et al. 2007). In both of these cases, the delivery efficiency was found to be histone-type specific. Based on these reports, it was hypothesized that the

enhancement of retroviral transduction may also exhibit histone-type specificity such that using selected histones could further improve the retroviral transduction efficiency.

The effect of calf thymus histone fractions on the retroviral transduction of human erythroleukemia TF-1 cells was initially screened on the basis of their lysine or arginine residue content using a gibbon ape leukemia virus pseudotyped retroviral vector with an eGFP reporter gene. A lysine-rich fraction (f_1) primarily composed of histone H1 and an arginine-rich fraction (f_3) enriched in histone H3 were compared with unfractionated histones as well as protamine sulfate, poly-L-lysines and poly-L-arginines of similar molecular weights. The performance of each additive was evaluated both for transduction efficiency and cell toxicity. In addition, the effect of untreated hydrophobic surfaces were compared with the effect of negatively-charged tissue-culture-treated surfaces. To refine the analysis to the level of individual histone types, recombinant human (rh) histones ($H1^o$, H2A, H2B, H3.1 and H4) were also tested. The rh histone H3.1 provided a superior enhancement of retroviral transduction relative to all other histone types. Histone H3.1 was then applied to the transduction of mouse bone marrow cells enriched in hematopoietic progenitors to assess if results obtained with the TF-1 hematopoietic model cell line could be translated to primitive primary cells. The histone H3.1 protocol was compared with a co-culture control and its effect on the stem cell population was assessed by a long-term reconstitution assay into irradiated recipients.

4.2. Materials and methods

4.2.1. Histones and other cationic compounds

Lyophilized unfractionated calf thymus histones (type II-A), lyophilized lysine-rich histone fraction (f_1) (type III-S), lyophilized arginine-rich histone fraction (f_3) (type VIII-S) and protamine sulfate (grade X, histone-free) (all Sigma-Aldrich, St. Louis, MO, USA) were reconstituted at 1 mg/mL in phosphate buffered saline (Invitrogen, Burlington, ON, Canada), sterile filtered (0.22 μm) and stored at -80°C. Poly-L-lysine hydrobromide (PLL) (12 – 24 kDa) as well as poly-L-arginine hydrochloride (LMW PLA) (7.5 – 13.3 kDa) and (HMW PLA) (31.7 – 49.5 kDa) (all Sigma-Aldrich) were dissolved in Nanopure water, sterile filtered and stored at -80°C. Recombinant human histones expressed in *E. coli* were obtained in solution at 1 mg/mL (New England Biolabs, Ipswich, MA, USA) and stored at -20°C. Genbank accession numbers were: H1° (X03473), H2A (AY131974), H2B (AY131979), H3.1 (AF531274) and H4 (AF525682).

4.2.2. Cell culture and vector production

Human erythroleukemia TF-1 cells (CRL-2003, American Type Culture Collection, Manassas, VA, USA) were cultured in Dulbecco's modified Eagle's medium (DMEM) (Invitrogen) supplemented with 10% fetal bovine serum (FBS) (Invitrogen) and 5 ng/mL human recombinant GM-CSF (Terry Fox Laboratory (TFL), Vancouver, BC, Canada). Retroviral vectors with a humanized red-shifted green fluorescent protein (GFP) reporter gene under the control of the MSCV long terminal repeats (LTR) of the GALV-pseudotype (GALV-GFP) were produced from a PG-13 packaging cell line (Hennemann

et al. 1999; Miller et al. 1991). The PG-13 cells were cultured in DMEM with 10% FBS in 1700 cm^2 expanded surface roller bottles (Corning, Lowell, MA, USA) at 37°C and 10% CO_2 balance air. Mouse ecotropic retroviral vectors, also with a GFP reporter gene under the control of the MSCV LTR (Eco-GFP), were produced from a GP+E-86 packaging cell line (Buske et al. 2001; Markowitz et al. 1988). GP+E-86 cells were cultured in DMEM with 10% FBS in 850 cm^2 flat surface roller bottles (Corning) at 37°C and 10% CO_2 balance air (batch A), or 75 cm^2 tissue-culture-treated T-flasks (Sarstedt, Nümbrecht, Germany) with 5% CO_2 balance air (batch B). In each case, harvests were initiated at 24 h intervals after the cultures reached 90% confluence (Reeves et al. 2000). Virus-containing medium (VCM) was filtered with a 0.45 μm pore size Durapore PVDF membrane (Millipore, Billerica, MA, USA) and stored at -80°C.

4.2.3. Human hematopoietic (TF-1) cell line transduction assay

TF-1 cells were resuspended in fresh growth medium before the start of the transduction assay. GALV-GFP VCM was thawed at 37°C for 15 min and diluted with TF-1 growth medium to obtain a final dilution of 1 in 8. In untreated and tissue-culture-treated 24-well plates (Sarstedt), target cells (5×10^5 cells/mL) were mixed with VCM at a mean liquid depth of 3 mm containing each additive (concentration adjusted using DMEM), except for recombinant histones. Recombinant human histones were assayed similarly in 96-well untreated plates using a mean liquid depth of 3 mm. Target cells were incubated in the presence of viral vectors for 24 h at 37°C and 5% CO_2 balance air. A cell count was performed using a Cedex automated counter (Innovatis, Bielefeld, Germany) after the initial 24 h for all 24-well cultures. Viable cell numbers were determined by the trypan blue exclusion method. An average of 20 images analyzed with

the Std. Cell (v 5.00) algorithm was taken for each sample. Cells were then transferred into new 24-well untreated plates (Sarstedt), diluted 1:5 in growth medium and expanded for an additional 48 h before analysis of GFP expression (Klein et al. 1997). GFP expression was assayed by fluorescence activated cell scanning with a FACSCalibur system (BD Biosciences, San Jose, CA, USA). Transduction efficiency was expressed as the ratio of viable GFP^+ cells over total viable cells that excluded propidium iodide at 5 μg/mL (Sigma-Aldrich).

4.2.4. Mouse hematopoietic stem cell transduction assay

To enrich for primitive hematopoietic progenitors C57Bl6/6Ly-Peb3b (Peb3b) mice were pre-treated with 150 mg/kg 5-fluorouracil 4 days prior to bone marrow harvest. These bone marrow cells were then pre-stimulated in bulk cultures for 48 h in DMEM containing 15% FBS and a cytokine cocktail of 10 ng/mL rhIL-6, 6 ng/mL rmIL-3 and 100 ng/mL rmSCF (all reagents from StemCell Technologies, Vancouver, B.C., Canada). Following pre-stimulation, 1×10^6 starting cell equivalents were transduced with Eco-GFP vectors for each condition. Conditions included a negative control without VCM, a VCM positive control (no additives), VCM supplemented with 10 μg/mL recombinant human histone H3.1 or co-culture with gamma-irradiated GP+E-86 packaging cells (37 600 MU). Following a 48 h transduction period, the cells were harvested and divided for further analysis. 2×10^5 starting cell equivalents from each condition were transplanted into each lethally irradiated syngenetic C57Bl6/6Ly-c2J (c2J) recipient (n=2 for trial #1, n=4 for trial #2 and n=3 for trial #3) along with 100 000 freshly isolated Peb3b helper cells to assess transduction efficiency into primitive progenitors capable of long-term (20 week) contributions to both lymphoid and myeloid compartments. One fifth of the cells were

maintained in culture to measure GFP expression and viability 72 h post-transduction. The peripheral blood of recipient mice was monitored at 4, 8 12 and 20 weeks post-transplantation to assess donor cell contribution to myeloid and lymphoid lineages based on the pan-hematopoietic marker CD45 (Pep3b CD45.1, c2J CD45.2) and lineage markers (Gr1, Mac1, CD4, CD8 and B220) (BD Biosciences).

4.2.5. Statistical analysis

ANOVA (α=0.05) was used for all significance tests for $p<0.05$.

4.3. Results

4.3.1. Calf-thymus histone fractions

The potential of histone fractions as enhancers of retroviral transduction as well as their toxicity was initially evaluated using TF-1 cells. Unfractionated histones were compared to a lysine-rich fraction (f_1) mainly composed of histone H1, to an arginine-rich fraction (f_3) containing histone H3 (~28% by weight) as well as H2A, H2B and H4, and to protamine sulfate using untreated cell culture plates. For f_3, two distinct local maxima were observed over the 0 to 240 µg/mL concentration range tested (Figure 4.1A). The first local maximum occurred at ~10 µg/mL (see f_3 data in Figure 4.2A), yielding a transduction efficiency of ~14%, a 7-fold increase compared to the control without additives. This result was similar to the maximum transduction efficiencies achieved (Figure 4.1A) with f_1 (40 µg/mL), unfractionated histones (10 – 20 µg/mL) or protamine sulfate (40 µg/mL), all ranging from 12 – 13%. With the exception of f_3, further increases in concentration lead to decreases in transduction efficiency. As the

concentration of f_3 was further increased, a second local maximum occurred at 160 μg/mL where the transduction efficiency increased to 28%, a 17-fold increase relative to the control without additives and a 2.4-fold increase above that of the other histone fractions and protamine sulfate. Under this condition, the presence of large aggregates up to 10 μm in diameter, distinguished the f_3-treated culture.

To investigate if the differences observed between the histone fractions could be explained on the basis of their lysine or arginine content alone, they were compared with synthetic lysine and arginine homopolymers of similar molecular weight (over a narrower range of additive concentrations due to the toxicity of PLL and PLA). Only the transduction efficiency of the recovered viable cells treated with PLL (MW: 12 – 24 kDa) at 10 μg/mL matched the maximum achieved with of f_3 (Figure 4.2A). The two PLAs were selected to include MWs smaller (7.5 – 13.3 kDa) or larger (31.7 – 49.5 kDa) than histones and both yielded lower transduction efficiencies than that of f_3. Thus, the arginine or lysine content alone did not explain the improved transduction obtained with arginine-rich f_3 compared to that of lysine-rich f_1.

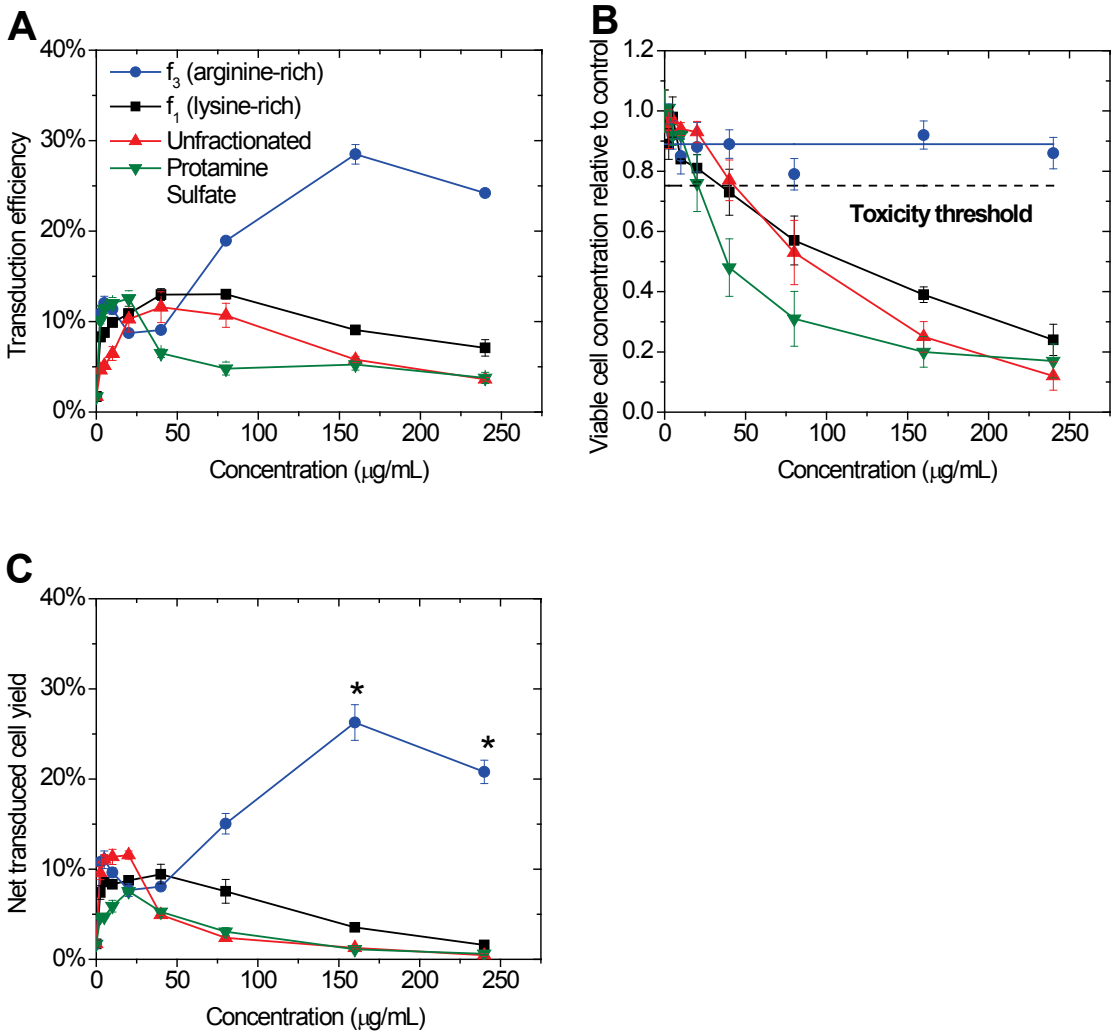

Figure 4.1 Effect of unfractionated, arginine-rich f_3 and lysine-rich f_1 histone fractions as well as protamine sulfate on the transduction and viable cell concentration of TF-1 cells.
The arginine-rich f_3 outperformed unfractionated histones and lysine-rich f_1 as well as protamine sulfate (A-C) with TF-1 cells transduced on untreated tissue culture plates. Transduction efficiency (A) of the recovered viable cells was measured following a 24 h exposure to increasing concentrations of each additive. The viable cell concentration relative to the control without additive was measured by trypan blue exclusion after a 24 h exposure to each condition (B). The toxicity threshold was established using a 95% confidence interval on the untreated control (dashed lines). The net transduced cell yield (C) accounts for cell loss by taking the product of the transduction efficiency and the viable cell concentration relative to the control. (* significantly higher than all other conditions by ANOVA where $p<0.05$ for $\alpha=0.05$) ($n=3$, error bars: SEM)

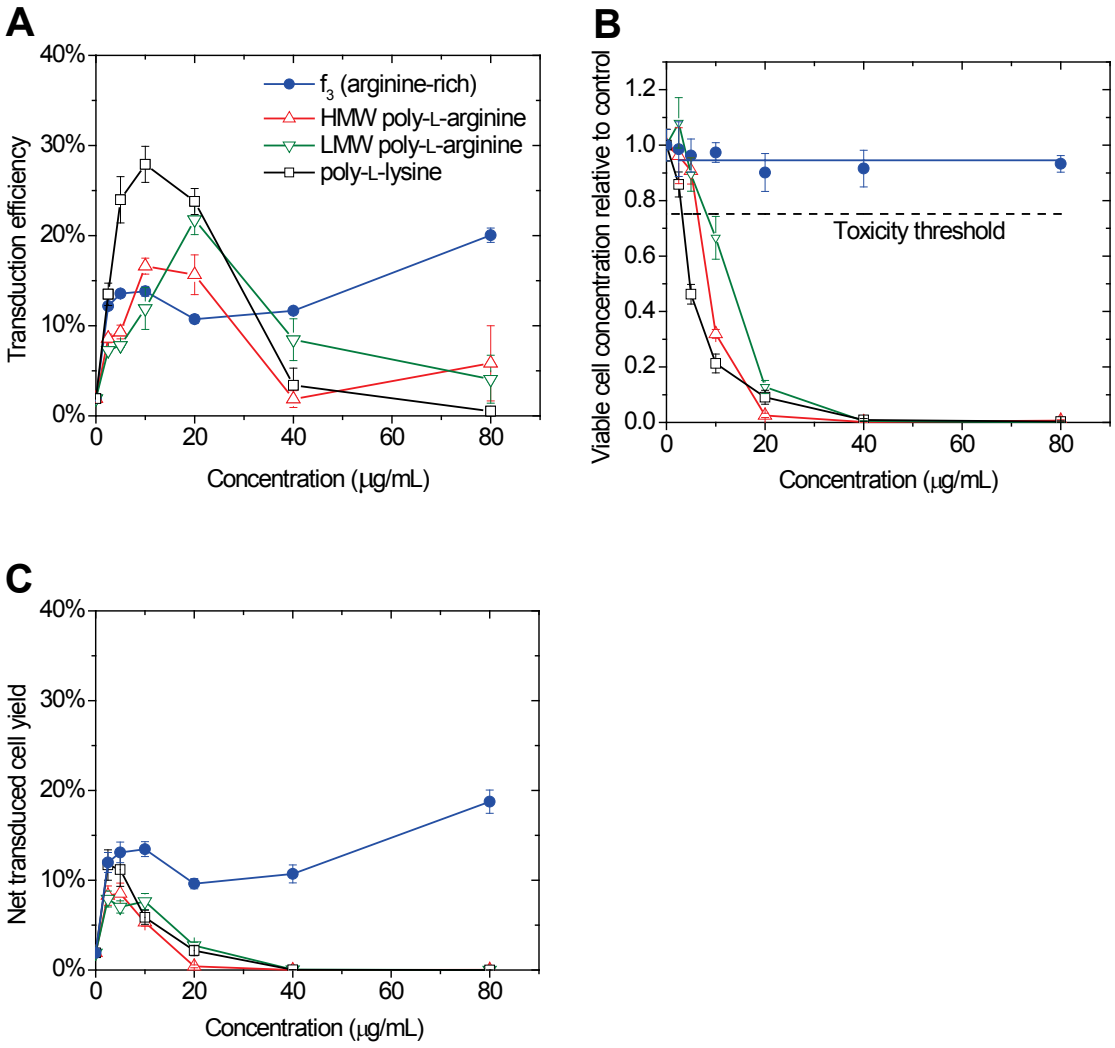

Figure 4.2 Effect arginine-rich f_3 histone fraction as well as poly-L-lysines and poly-L-arginines on the transduction and viable cell concentration of TF-1 cells.
The arginine-rich f_3 outperformed poly-L-lysines and poly-L-arginines (A-C) with TF-1 cells transduced on untreated tissue culture plates. Transduction efficiency (A) of the recovered viable cells was measured following a 24 h exposure to increasing concentrations of each additive. The viable cell concentration relative to the control without additive was measured by trypan blue exclusion after a 24 h exposure to each condition (B). The toxicity threshold was established using a 95% confidence interval on the untreated control (dashed lines). The net transduced cell yield (C) accounts for cell loss by taking the product of the transduction efficiency and the viable cell concentration relative to the control. (* significantly higher than all other conditions by ANOVA where $p<0.05$ for $\alpha=0.05$) (n=3, error bars: SEM)

Toxicity to the target cells must also be considered as part of optimal additive selection. The viable cell concentration was assessed following a 24 h exposure to each condition in the presence of VCM. A toxicity threshold was defined based on a 95% confidence interval for the control without additives. Viable cell concentration measurements falling below the lower limit were considered to reveal significant toxicity to the cells due to either inhibited cell growth and/or cell death. With the exception of f_3, significant toxicity was measured for all additives with increasing concentrations. The unfractionated histones were toxic, falling below the toxicity threshold, at concentrations >40 μg/mL, while f_1 and protamine sulfate were toxic at >20 μg/mL (Figure 4.1B). The PLL and PLA exhibited the greatest toxicity, falling below the toxicity threshold at >2.5 μg/mL and >5 μg/mL (HMW and LMW), respectively (Figure 4.2B). In striking contrast, for f_3, no significant toxicity was detected up to at least 240 μg/mL. On average, between 89% and 95% of the cell concentration measured in the untreated control was recovered following treatment with the f_3 fraction (Figure 4.1B and Figure 4.2B).

An appropriate evaluation of these alternative polycation additives should be made on the combined basis of transduction efficiency and cell toxicity. To facilitate this evaluation, the product of the transduction efficiency and the viable cell concentration relative to the control was calculated and defined at the "net transduced cell yield" (Figures 4.1C and 4.2C). For example, for f_3 where the maximum transduction efficiency was obtained at 160 μg/mL, the transduction efficiency was 28% and the recovered viable cell concentration relative to the control was 92%. This produced a net transduced cell yield of 26% (Figure 4.1C). For PLL at 10 μg/mL, the transduction efficiency was

similar to that of f_3 but the recovered viable cell concentration relative to control was only 21%, resulting in a net transduced cell yield of only 6% (Figure 4.2C). Thus, when the maximum net transduction yields are compared, f_3 clearly outperformed all the polycations tested and provided 3.5-fold improvement over protamine sulfate and 2.2-fold over PLL.

Hematopoietic cell lines, such as TF-1, are cultured in suspension. Under these conditions, a large fraction of the culture plate's surface is exposed to the medium and may therefore interact with the viral vectors and polycations. The effect of surface type was evaluated by comparing the transduction efficiencies measured using untreated hydrophobic surfaces (TE_{UT}), designed for suspension cultures, with those obtained from negatively-charged tissue culture-treated-surfaces (TE_{TC}) designed for adherent cultures. This comparison was limited to the concentration ranges where no cell toxicity was found. Even in the absence of additives, the use of tissue-culture-treated surfaces increased transduction efficiencies by an average of 1.93-fold relative to that measured on an untreated surface (TE_{TC}/TE_{UT}, Table 4.1). Most of the polycations tested also exhibited significant surface-type effects with greater transduction efficiencies achieved on tissue-culture-treated surfaces. Interestingly, protamine sulfate, which has the lowest molecular weight, exhibited the greatest increase on a tissue-culture-treated surface. The lowest increase was measured for HMW PLA such that the surface-type interaction correlated with the molecular weight of the additive. For f_3, the surface-type effects were evaluated separately for each of the 2 local maxima. The first peak (2.5 – 40 μg/mL) also had a significant surface-type effect, whereas the second maximum (40 – 240 μg/mL) had no significant surface-type effect. This suggests that, at lower concentrations, the f_3

mechanism of action may be similar to that of the other polycations tested. However, at increased concentrations, the f_3 mechanism appears to be altered thereby eliminating surface-type dependence and further increasing transduction efficiency. The unfractionated histones and f_1 exhibited no surface-type dependence.

Table 4.1 Effect of tissue culture vessel surface type on the transduction efficiency of TF-1 cells.
The transduction efficiencies (TE) obtained for a tissue-culture-treated surface (TC) and for an untreated (UT) surface were compared using the average ratio of TE_{TC} / TE_{UT} (over the non-toxic concentration range of each additive). For the f_3 fraction, the ratios were calculated for each of the 2 peaks. The significance of the surface type effect was tested by ANOVA for α=0.05, n=3 except for the f_3 fraction at 2.5 – 40 µg/mL, where n=6 using data from both Figures 4.1A and 4.1D.

Additive	Molecular Weight (kDa)	Concentration (µg/mL)	TE_{TC} / TE_{UT}	p-value
Surface type effect				
Protamine sulfate	5.3 [a]	2.5 - 20	2.42	<0.01
No additive	n/a	0	1.93	<0.01
poly-L-arginine	7.5 – 13.3	2.5 - 5	1.70	<0.01
poly-L-lysine	12 – 24	2.5	1.50	<0.05
f_3 (1st peak)	15.3 [b]	2.5 - 40	1.45	<0.01
poly-L-arginine	31.7 – 49.5	2.5 - 5	1.33	<0.01
No surface type effect				
f_3 (2nd peak)	Aggregated	40 - 240	1.01	>0.50
Unfractionated	11 – 22 [b]	2.5 - 40	0.97	>0.50
f_1	21 – 22 [c]	2.5 - 20	0.85	>0.05

[a] (Jensen et al. 2003)
[b] (vanHolde 1989)
[c] UniProt accession #A7MAZ5, A3KN02, A5PK20

4.3.2. Recombinant human histones

The f_3 derived from calf-thymus clearly outperformed all the other additives tested. However, since this fraction was only enriched in histone H3.1 there could be influences from other histone types. Furthermore, many histone post-translational modifications contribute to the heterogeneity of tissue-derived fractions. In order to refine our analysis to specific histone types, recombinant human histones (H2A, H2B, H3.1 and H4) as well as the H1 variant $H1^o$ were assayed. These high purity histones, expressed in *E. coli*, were free of post-translational modifications. A comparison of these rh histones on TF-1 cells, clearly identified the rh histone H3.1 (5 – 10 μg/mL) as the histone type with the greatest enhancing potential, as it significantly outperformed all the other recombinant histones (Figure 4.3). H2A, H2B and H4 yielded similar transduction efficiencies, while $H1^o$ provided the smallest increase. Unlike f_3, a single maximum occurred with the rh H3.1 at 10 μg/mL rather than at 160 μg/mL and the maximum transduction efficiency achieved was 42%, substantially greater than the 28% with f_3. Only limited toxicity was detected at 100 μg/mL with all recombinant histone preparations, a concentration that is well above the optimum value. All recombinant histone preparations contained dithiothreitol (DTT), a reducing agent that may contribute to the cell toxicity observed at higher concentrations.

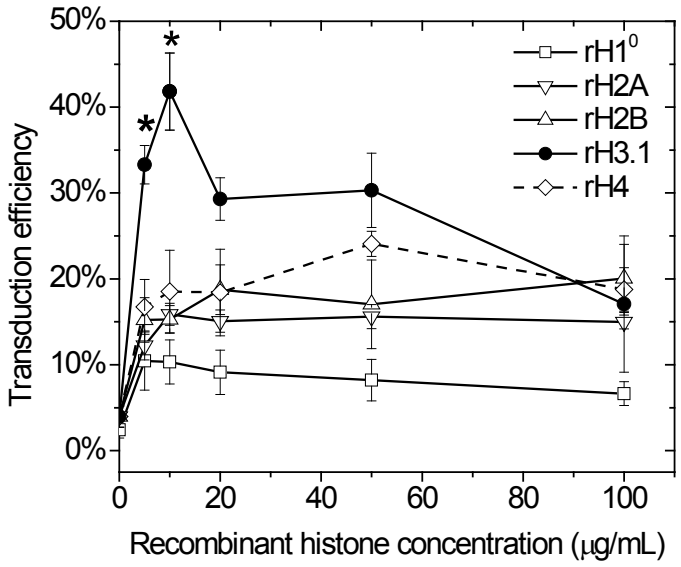

Figure 4.3 Effect of human recombinant histone type and dose on the transduction efficiency of TF-1 cells.
Histones were added to 5×10^5 TF-1 cells/mL in virus-containing medium and incubated for 24 h in 96-well suspension plates. (n=4 for rh H2A, rh H2B, rh H3.1 and rh H4 except for 50 and 100 μg/mL where n=3. For rh H1^o, n=2 for all concentrations, error bars: SEM) (* significantly greater than all other histone types as tested by ANOVA where $p<0.05$ for $\alpha=0.05$).

4.3.3. Primary mouse hematopoietic progenitors

Transduction of primary cells can often be more challenging than that of cell lines adapted to *in vitro* culture, due to the greater sensitivity of primary cells to culture conditions. Hematopoietic stem cells are currently used in multiple clinical settings and are a focus for the development of gene therapy strategies due to their relative ease of access as compared to other tissue stem cells. As such, they were selected as an important model system to evaluate if the positive results using rh histone H3.1 on TF-1 cells would translate to primary hematopoietic stem cells. Mouse bone marrow enriched for primitive hematopoietic cells using 5-FU was isolated, transduced with the Eco-GFP vector, and then transplanted into congenic recipients to evaluate both the long-term transduction and reconstitution potential. VCM supplemented with rh histone H3.1 was

compared to VCM with no additives and to a co-culture with irradiated viral producer cells. GFP expression was evaluated 72 hours after transduction (Table 4.2). The addition of rh histone H3.1 to the VCM increased the average transduction efficiency over 3 separate trials by 8.2±2.1-fold relative to the controls without additives. The enhancement observed with the bulk primary cell population was comparable to that previously determined for the TF-1 model cell line. For the VCM batch A replicates, the transduction efficiency with rh histone H3.1 (52.8±14.8%) matched that of the co-culture (51.3±2.5%). For the VCM batch B, the transduction efficiency with the no-additive control was lower than with batch A, likely due to a lower retroviral vector concentration. Thus, the batch B result did not match that of the co-culture condition. Nonetheless, consistent with the batch A results, the addition of rh histone H3.1 did robustly increase the transduction by 11-fold compared to VCM without additive. The viability and total cell numbers post-transduction were comparable for all conditions and trials (Table B.1). This demonstrates that histone H3.1 effectively enhanced transduction of the bulk primary cell population and, with adequate viral vector concentration (VCM batch A), matched the transduction levels obtained with the co-culture.

Table 4.2 Transduction efficiency of bulk mouse primary cell population.
Cells were transduced for 48 h with the Eco-GFP retroviral vector and transduction efficiency was measured after an additional 72 h of culture. Transduction was performed with VCM supplemented with 10 µg/mL rh histone H3.1, co-culture on irradiated Eco-GFP producing cells, with VCM alone (no additive) and, as a negative control, without VCM. (2 different batches A and B of VCM were used, 2 different lots of histones H3.1 were used in trial 1 and trials 2 & 3)

VCM batch	Trial	Treatment			
		H3.1	Co-culture	No additive	Negative Control
A	**1**	67.5%	53.8%	7.1%	0.0%
	2	38.0%	48.8%	9.3%	0.1%
	Average (1 & 2)	**52.8%**	**51.3%**	**8.2%**	**0.0%**
B	**3**	13.3%	70.3%	1.2%	0.2%

To evaluate the impact of the histone treatment on the transduced primitive hematopoietic cell population, a long-term reconstitution assay was initiated immediately following the transduction process. Cells from each culture were transplanted into congenic recipients cleared of the majority of endogenous hematopoietic stem cells (HSCs) by irradiation. The persistence and output of donor cells to lymphoid and myeloid compartments in the peripheral blood were monitored at 4-week intervals up to 20 weeks post-transplantation. Donor cells were distinguished from recipient cells by the expression of different isoforms of the pan-hematopoietic marker CD45 (CD45.1 vs. CD45.2) that allowed evaluation of the impact of each treatment on both transduced and non-transduced cells in the cultures.

Primitive hematopoietic cells can be distinguished by their greater persistence in recipients (Jones et al. 1990). Those with short-term reconstitution potential generally cannot be detected in the recipient beyond 8 weeks post-transplant, while those with long-term potential persist up to and past 20 weeks. At 20 weeks post-transplant, the GFP^+ fraction of transduced cells in the donor compartment was 6.2-fold greater when histone H3.1 was added (Figure 4.4A) compared with the control (no additives, VCM only) (individual trial data available in Figure B.15). These results were comparable to both the 8.2-fold increase initially measured *in vitro* (described above) and that of the co-culture that was 9.2-fold greater than the control with no additives (Figure 4.4A, $p>0.52$). The donor contribution to hematopoiesis for all treatments was not significantly different from that of the non-transduced negative control ($p>0.1$) (Figure 4.4A). The distribution of the contribution to lympho- and myelopoiesis by donor cells was similar for all treatments 20 weeks post-transplant ($p>0.1$) (Figure 4.4B), regardless of transduction

levels. The distribution was also similar between total donor and transduced (GFP^+) donor cells ($p>0.2$) (Figure B.16). These distributions were consistent with previous transplantation data from the Humphries lab using transduced primitive hematopoietic cells, providing further evidence that histone H3.1 did not significantly alter the differentiation or reconstitution potential of these cells.

Overall, these results demonstrated that histone H3.1 provides an effective method of gene transfer into primitive hematopoietic cells in culture. Similar numbers of GFP^+ cells were observed in the donor compartment in both the myeloid and the lymphoid lineages for both the histone H3.1 and co-culture conditions at levels much greater than were achieved using the VCM alone. The persistence of GFP^+ cells at least 20 weeks post-transplant indicates efficient gene transfer to cells with long-term reconstitution potential. As the donor contribution to hematopoiesis was similar for all conditions including the negative control, these results also suggest that there was no primary cell toxicity associated with the use of histone H3.1.

A.

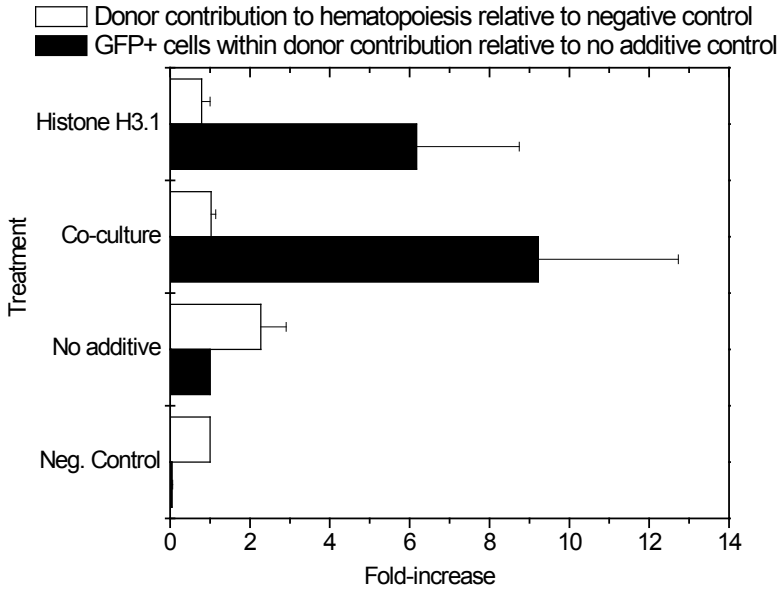

B.

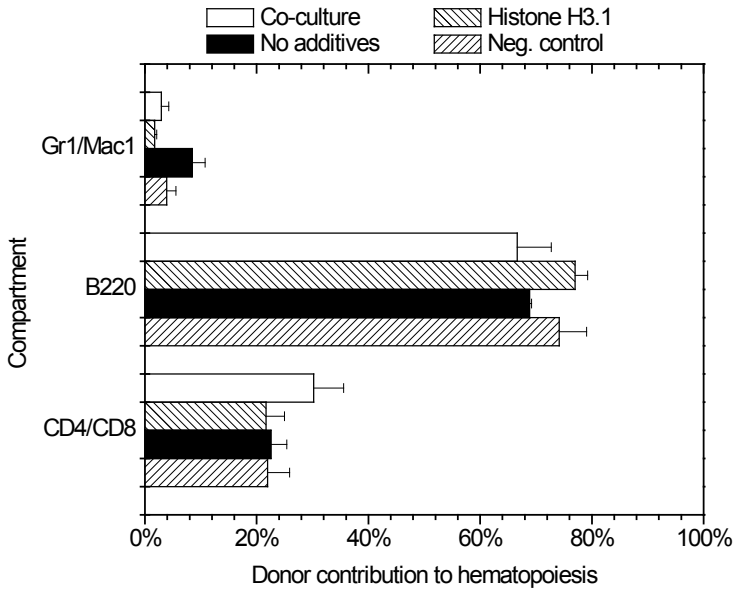

Figure 4.4 Total donor contribution to hematopoiesis as well as myeloid and lymphoid lineages.
A (top). Total donor contribution to hematopoiesis relative to negative control and GFP+ cells within the donor contribution relative to the control without additives measured 20 weeks post-transplant. Histone H3.1 treated GPF^{+} cells persisted in the peripheral blood of recipient mice. Donor contribution to hematopoiesis for all treatment was similar to that of the negative control. B (bottom). Histone H3.1 treated donor cells contributed to both lymphoid and myeloid lineages measured 20 weeks post-transplant. Contribution of histone H3.1 was comparable to that of all other treatments. (n =3, error bars: SEM)

4.4. Discussion

The initial report of mixed histone enhancement of the retroviral transduction of mouse cells hypothesized that histones, given their high content of basic amino acids (Singh and Rigby 1996), may have interacted directly with the mouse ecotropic receptor (mCAT1) that also serves as a basic amino acid transporter (Kim et al. 1991; Wang et al. 1991). In this study, all histones, and especially f_3, were effective in increasing the transduction of TF-1 cells using a gibbon ape leukemia virus pseudotyped retroviral vector whose receptor, Pit-1, acts as an inorganic phosphate transporter (Olah et al. 1994). This therefore suggests a receptor-independent enhancement rather than a specific interaction with the mCAT-1 receptor, as histones were equally able to enhance the transduction of Pit-1 expressing TF-1 cells and of mouse primary cells expressing mCAT1. This would also be consistent with the finding that, in the absence of polycations, the initial binding of retroviral vectors to the target cells occurs independently of envelope and receptor interactions (Pizzato et al. 1999).

The two distinct local maxima in the transduction efficiency due to f_3 additions reveal the presence of two mechanisms of action. Since the first local maximum obtained with f_3 yielded a similar transduction efficiency as that obtained with protamine sulfate, it is likely that both of these polycations share a common mechanism of action. The addition of polycations such as polybrene has previously been shown to increase the receptor-independent adsorption of retroviral vectors on the target cell membrane, thereby increasing the transduction efficiency (Davis et al. 2002). It is therefore probable that, at lower concentrations (<40 μg/mL), the f_3 fraction acted in a similar fashion.

In suspension cell cultures, a large fraction of the tissue culture vessel surface is exposed to the medium and can interact with both polycations and retroviral vectors. Polycations such as poly-L-lysine have been shown to adhere to the tissue culture vessel surface, thereby altering the surface charge to improve the adsorption of viral vectors and, hence, yielding greater transduction efficiencies (Hennemann et al. 2000a). Whereas suspension cells are typically cultured on untreated hydrophobic polystyrene surfaces, tissue-culture-treated (i.e., gas plasma treated) polystyrene is used to provide a negatively-charged hydrophilic surface more suitable for adherent cell cultures (Barker and LaRocca 1994; Ramsey et al. 1984). At lower f_3 concentrations, the surface type had a significant effect, with higher transduction results obtained with tissue-culture-treated surfaces. It is likely that the negative surface charge improved the adsorption of f_3 onto the surface. The greatest surface-type effect was observed with protamine sulfate and this was consistent with results previously reported where greater transduction efficiencies were obtained on tissue-culture-treated dishes compared with untreated surfaces (Hennemann et al. 2000a). Interestingly, the magnitude of the surface-type effect decreased for the higher molecular weight compounds. Protamine sulfate had the smallest molecular weight (5.2 kDa) and the greatest surface-type effect, while the largest PLA (32 – 50 kDa) was less influenced by surface type. While in this case the varying affinity of each compound for each surface type could explain some of the differences observed, with PLAs, the smaller molecular weight compounds (7 – 13 kDa) again had a greater surface effect than the larger ones (32 – 50 kDa). These observations were consistent with the report that, with PLL, polymers with molecular weights exceeding 15 kDa can mediate virus aggregation leading to sedimentation thus providing a different

mechanism to increase the mass transport of the viral vectors to the target cells (Davis et al. 2004). It was previously observed in Chapter 2 that cell lysis products can interact with polycations (Beauchesne et al. 2010) and so the surface-type effect was only evaluated over concentrations where no toxicity was detected. Furthermore, we showed that cell lysates can greatly increase transduction rates and this could explain a substantial portion of the generally greater transduction efficiency obtained with the PLL and PLA over the toxic concentration range.

The occurrence of the second local maximum with the f_3 arginine-rich histone fraction suggests that the mechanism of action was altered at greater concentrations. Consistent with a different mechanism, at the greater f_3 concentrations, the surface-type effect was no longer significant and an increasing amount of aggregates were observed in the cell culture. These results indicate that there was a transition towards sedimentation as the main means of enhanced viral vector transport at higher f_3 concentrations. For PLL, the aggregation process has been reported to be mediated by the interaction between negatively-charged vectors and polycations (Davis et al. 2004). The combination of polybrene with the negatively-charged glycosaminoglycan, chondroitin sulfate C, was also hypothesized to increase transduction through the formation of high-molecular-weight complexes (Le Doux et al. 2001). Studies on homotypic histone interactions have shown that histone H3 and H4 (as well as, to a lesser extent, H2B and H2A) can form high molecular weight aggregates, while H1 tends to only form a weak dimer. Histone aggregation was reported to take place as a function of many variables including ionic strength, temperature as well as concentration (D'Anna and Isenberg 1974; Diggle et al. 1975; Roark et al. 1976; Sperling and Bustin 1975). This may explain the increase in

transduction and lack of a surface-type effect observed at higher concentrations of f_3. As opposed to polybrene or high molecular weight poly-L-lysine where a negatively-charged intermediate (viral vector or glycosaminoglycan) was necessary, the histones may independently form aggregates to which the viral vectors can bind.

The recombinant histone, H3.1 clearly yielded the highest increase in transduction efficiency compared to all other additives. A comparison of the primary protein structures of histones revealed that H3 is the only histone with variants containing cysteine residues. In particular, both bovine and human histone H3.1 contain 2 cysteine residues at positions 96 and 110 (Hake and Allis 2006). The formation of intermolecular disulfide bridges was reported to contribute to the aggregation of histone H3.1 under oxidative conditions (Garrard et al. 1977; Ruiz-Carrillo and Allfrey 1973). Although histone H3 is highly conserved, the cysteine content varies between species (Hake and Allis 2006; vanHolde 1989). Indeed, whereas bovine H3 histones were reported to form high-order aggregates, under similar conditions, Chinese hamster H3, with only one cysteine residue, only formed dimers (Garrard et al. 1977). Thus, if the disulfide bridge contribution to aggregation were significant, the potential of histones to increase transduction would be influenced by the cysteine-content and species dependent. Due to the inability of histone H1 to self-aggregate (Roark et al. 1976), f_1 or rh $H1^o$ were both expected to provide the observed lower transduction increases and their mode of action could be limited to improving adsorption of the retroviral vector to the target cell.

The lower concentration required with the rh H3.1 histone compared to f_3 may reflect the higher purity of the recombinant histone. Another difference may be the presence of post-translational modifications on the animal-origin f_3 histones. For example,

lysine acetylation can reduce the histone positive charge, while phosphorylation introduces additional negative charges, thus altering the net charge of tissue-derived histones (Shechter et al. 2007). Differences in processing could also partially account for the differences observed between f_3 and rh H3.1 histone preparations. For example, partial aggregation of the rh H3.1 histones could occur though this should at least be partially offset by dithiothreitol, a reducing agent, present in the storage buffer.

Although the addition of histones such as the rh H3.1 or the f_3 fraction is likely to have mainly influenced extracellular mass transport and binding of the viral vectors, the possibility of increased intracellular trafficking needs to be considered. Histones were reported to penetrate cells through direct translocation across the cellular membrane and, H2A, H3 and H4 were also shown to pass across lipid bilayers (Hariton-Gazal et al. 2003; Rosenbluh et al. 2005). Furthermore, multiple nuclear localization signals (NLS) were identified on the four human core histones as well as on histone H1 and its variant $H1^o$ (Baake et al. 2001; Breeuwer and Goldfarb 1990; Schwamborn et al. 1998). The lack of an NLS in gammaretroviruses such as the Moloney murine leukemia virus may be responsible for its inability to infect non-dividing cells (Miller et al. 1990; Roe et al. 1993). Intracellular interactions between the preintegration complex and histones could possibly provide an NLS and mediate its import into the nucleus. However, attempts to overcome the inability of gammaretroviruses to transduce non-dividing cells by attaching an NLS to the matrix or integrase proteins have been unsuccessful. It has been proposed that this is due to the larger size of the preintegration complex relative to a lentivirus (Caron and Caruso 2005; Seamon et al. 2002).

Cell line models can be poor predictors of polycation toxicity to primary cells. For example, protamine sulfate was well tolerated by NIH 3T3 cells up to 100 μg/mL but toxic to human T-cell lymphocytes at a 10 times lower concentration (Cornetta and Anderson 1989). It was thus imperative to test the effect of rh histone H3.1 on a relevant primary cell population such as HSC-enriched mouse bone marrow. Our results clearly demonstrated that rh histone H3.1 was well tolerated by this primitive hematopoietic population as determined by cell viability measurements following the initial exposure as well as by a 20-week reconstitution assay, where the donor contribution to hematopoiesis was similar to those of the negative control and co-culture conditions. It was therefore concluded that the rh histone H3.1 was not toxic to either the TF-1 cell line or the primary mouse cells exhibiting long-term reconstitution potential.

In clinical trials, it is preferable to use fully-defined retroviral transduction enhancers, such as the recombinant CH296 fibronectin fragment (Gaspar et al. 2004; Hacein-Bey-Abina et al. 2002). Such reagents are more suitable than animal-derived protamine sulfate or histone preparations that consist of complex mixtures subject to batch-to-batch variability. This variability could influence both transduction efficiency and cell toxicity. Furthermore, the presence of histone variants as well as many different post-translational modifications contribute to the heterogeneity of tissue-derived histone fractions (vanHolde 1989). Recombinant histone H3.1 expressed in *E. coli* offers the advantages of a fully-defined preparation, free of other histone variants and post-translational modifications, and thus it should be much more suitable for use in clinical protocols.

In the comparison performed between histone H3.1 and the co-culture protocol, the experimental design was biased toward the co-culture. In VCM, the half-life of retroviral vectors at 37^{o}C has been reported in the range of 3.5 (Paul et al. 1993) to 6 h (Kwon et al. 2003). As a result, after 24 h, less than ~7% of the initial vectors remain available to transduce the target cells. Thus, from 24 h to 48 h, viral vectors were depleted and additional transduction was likely negligible. However, in the co-culture protocol adapted to maximize transduction, the packaging cell line continuously produced the viral vectors over the full 48 h transduction period. In the co-culture, the close proximity of the target cell to the packaging cell line should also improve transduction, which perhaps may be further augmented by the polarization and initiation of the murine leukemia virus assembly within sites of cell-cell contact (Jin et al. 2009). Therefore, in a co-culture, mass transport occurs over greatly reduced distances and even by direct cell-cell transmission. This contrasts with conventional VCM transduction where mass transport is governed by the diffusion of the viral vector to the target cell (Chuck et al. 1996). Another bias in favour of the co-culture results is that between 17% (Higashikawa and Chang 2001) and 60% (Kwon et al. 2003) of active viral particles have been reported lost during the VCM freeze (-80^{o}C) and thaw process. Despite the sum of all of these disadvantages for the VCM option, the results demonstrated that, with rh histone H3.1, it was possible to match the transduction yields of the co-culture. Thus, the experimental complications of culturing cells with packaging cells can be eliminated by using histone-enhanced cell-free VCM. The availability of single large batches of VCM that can be pre-screened and used consistently over a large number of experiments offers the advantage of reduced experimental variability. To achieve further increases in

transduction, the decayed VCM could be replaced with fresh VCM every 12 or 24 h. Alternatively, the transduction period could be shortened by half from 48 h to 24 h in order to reduce the loss of primitive hematopoietic progenitors during *ex vivo* culture (McNiece et al. 2002).

Overall, bovine fractions enriched in H3.1 or human recombinant H3.1 were shown to provide a greater enhancement of retroviral transduction than other histone types, protamine sulfate and synthetic homopolymers of lysine or arginine. Furthermore, histone H3.1 exhibited no cell toxicity with either TF-1 cells or primary mouse cells with long-term reconstitution potential. Unlike most polycations tested, histone H3.1 yielded greater transduction efficiencies and was not significantly influenced by variations in the tissue-culture surface charge. For scientific research, histone H3.1 (or f_3) provides an alternative that can at least match the high level of transduction obtained by co-culture with packaging cells. H3.1 availability as a recombinant product combined with its low toxicity makes it a promising alternative to recombinant fibronectin in clinical protocols. The mechanism of action of histone H3.1 will be further investigated in Chapter 5 using the f_3 fraction, with particular attention to the correlation between aggregation state and increase in retroviral transduction. Fostering self-aggregation of histone H3.1 prior to its addition to target cells and viral vectors may lead to further improvements in transduction efficiency.

5. Exploiting Histone Aggregation to Further Enhance the Retroviral Transduction of Cell Lines and Primary Cells.

5.1. Introduction

Retroviral vectors improve gene delivery by mediating the transport of the transgene across the cellular membrane and its subsequent integration within the genome. While gammaretroviral vectors only transduce actively dividing cells, lentiviral vectors can overcome this limitation by facilitating the import of the preintegration complex through the nuclear envelope (Lewis and Emerman 1994; Naldini et al. 1996; Roe et al. 1993). However, the retroviral vectors must first be transported to the proximity of the target cells and then undergo non-specific adsorption onto the cell membrane prior to interacting with the specific receptor required for entry (Pizzato et al. 1999; Sharma et al. 2000). Under static conditions, mass transport of the retroviral vectors is diffusion-limited (Chuck et al. 1996) such that, due to their short extracellular half-life, many vectors will decay prior to cell entry (Higashikawa and Chang 2001). The common negative charge shared by both the retroviral vectors and the target cells also limits adsorption (Palsson and Andreadis 1997). While several methods have been developed to increase retroviral transduction, most only address one of these two limiting steps.

Both physical and chemical methods have been investigated to improve the mass transport of retroviral vectors, thereby minimizing the time required to displace and concentrate them near the target cells. Physical methods include convective mass transport by forced flow of the virus-containing medium through a bed of target cells (Chuck and Palsson 1996a) and enhanced sedimentation of the retroviral vectors by centrifugation (Bahnson et al. 1995). Alternatively, chemical methods where retroviral

vectors are adsorbed onto larger and denser substrates such as calcium phosphate precipitates (Morling and Russell 1995), heat-killed formaldehyde-fixed *Staphylococcus aureus* bacteria (Pansorbin) (Darling et al. 2000) and paramagnetic particles (Hughes et al. 2001) have been used under gravity alone and in combination with centrifugation or magnetic fields. As these substrates will be concentrated together with the retroviral vectors near the target cells, their toxicity to the cells can limit their use in culture. For example, the concentration of calcium phosphate is limited in this way (Morling and Russell 1995). To operate at optimal calcium phosphate concentrations, retroviral vectors were precipitated and concentrated *ex situ* and the subsequent removal of excess substrate was required prior to the addition of the concentrated vector preparation to the target cell culture (Pham et al. 2001).

Other approaches focused only on increasing the adsorption of the retroviral vectors onto the membrane surface of the target cells. This was achieved through the addition of cationic polymers such as polybrene, protamine sulfate, poly-L-lysine (MW < 15 kDa), cationic liposomes, and histones (Cornetta and Anderson 1989; Davis et al. 2002; Davis et al. 2004; Hodgson and Solaiman 1996; Singh and Rigby 1996; Toyoshima and Vogt 1969). The effectiveness of many of these additives was highly dependent on the concentration used and their toxicity can limit their use, especially with primary cells (Hunter and Moghimi 2010).

In order to maximize the transduction efficiency, efforts have been made to develop methods able to simultaneously enhance mass transport as well as adsorption. In one approach, the cationic polymer polybrene was complexed with the anionic polymer chondroitin sulfate C and the retroviral vectors to form an aggregate structure prior to its

addition to the cell culture. Formation of these aggregates was sensitive to the ratio of anionic and cationic polymers used. Furthermore, while the resulting complex had negligible cell toxicity, the concentration of polybrene required would be toxic if it remained uncomplexed (Le Doux et al. 2001) or if this complex destabilizes during culture leading to the release of polybrene. Alternatively, long chains (MW > 15 kDa) of poly-L-lysines were also reported to form aggregates with retroviral vectors (Davis et al. 2004). Similarly to polybrene, the use of poly-L-lysine has been associated with cellular toxicity (Hunter and Moghimi 2010). Thus, while these approaches addressing both mass transport and adsorption may yield an improvement in the transduction of cell lines, their suitability for primary cells has yet to be established.

During the previous analysis of the mechanism of cell lysate-enhanced retroviral transduction (Chapter 3), the DNase I digested pellet fraction (PD80P) consisting of aggregates was found to significantly enhance transduction through a combination of improved mass transport via sedimentation and enhanced cell surface adsorption. It was also shown that the PD80P lysate fraction, under gravity alone (Figure 3.19 in Chapter 3), was able to outperform centrifugation, known to only improve mass transport (Tayi et al. 2010), or outperform protamine sulfate, shown to only enhance adsorption (Chapter 3). Addition of the PD80P fraction alone matched the transduction performance of the combination of centrifugation and protamine sulfate, confirming its capacity to address both mass transport and adsorption limitations. Through cellular compartment analysis and targeted enzymatic degradation, the activity found within the PD80P lysate fraction was linked to arginine- and/or lysine-rich proteins of nuclear origin, suggesting the potential involvement of histones.

When the potential of specific histone fractions was later evaluated in Chapter 4, the f_3 arginine-rich fraction at 160 µg/mL was shown to provide the greatest increase in transduction while yielding negligible cell toxicity. As with the PD80P lysate fraction, aggregates were observed within the cell culture with the f_3 fraction. Since histones were directly added to the retroviral vector and cell mixture, it was unclear if the aggregates were formed through interactions between the histones and the retroviral vectors or anionic polymers in the conditioned medium. Alternatively, the core histones (H2A, H2B, H3 and H4) have been reported to self-aggregate through both homotypic (D'Anna and Isenberg 1974; Diggle et al. 1975; Roark et al. 1976; Sperling and Bustin 1975) and heterotypic interactions (Becker 1999). Furthermore, a comparison of histones of recombinant origin showed that H3.1 outperformed the other histones suggesting the potential involvement of disulfide bridges in aggregate formation. Thus, aggregates could potentially be formed without the need for anionic polymers or interaction with the retroviral vectors. As protein aggregates can reach the micrometer size range (Bryant and McClements 1999) and densities of up to 1.45 g/cm^3 (Fischer et al. 2004), a histone-based aggregate could efficiently sediment retroviral vectors. In order to resolve the exact mechanism, in this chapter, aggregate formation will be uncoupled from the presence of retroviral vectors and conditioned medium.

To demonstrate the effect of f_3 histone fraction aggregation on retroviral transduction, aggregation was first induced by heating the protein solution prior to its addition to the target cell and retroviral vector mixture. The correlation between the increase in retroviral transduction of nBaF3 and TF-1 cells lines by gammaretroviral vectors and the aggregation levels of the f_3 fraction was then investigated. The effect of

aggregated f_3 histone fraction concentration on the transduction of TF-1 cells relative to untreated histones was evaluated next. The impact of aggregation on cell toxicity was also measured. To investigate the involvement of disulfide bridge formation between H3.1 histones in the aggregation process, the aggregates where treated with dithiothreitol, a reducing agent. The recruitment of histone H2A, H2B and H4 within the aggregate structure was studied by Western blot. To demonstrate the capacity of the histone aggregates to overcome mass transport limitations by effectively sedimenting retroviral vectors, transduction was measured at increasing liquid depths. The impact of the f_3 aggregated histones method on the transduction and long-term reconstitution potential of primary mouse hematopoietic progenitors was also evaluated. Finally, the performance of aggregated histones was compared with Retronectin, a common but complex approach that requires the coating of surfaces prior to the addition of the retroviral vectors and target cells. Overall, the results presented will demonstrate that pre-aggregation of histone proteins provides a simple approach with negligible toxicity to enhance both the lenti- and gammaretroviral transduction of primary cells as well as cell lines.

5.2. Materials and methods

5.2.1. Cell lines and retroviral vectors

TF-1 (human) and nBaF3 (mouse) cell lines were cultured as previously described in DMEM supplemented with 10% FBS and 5 ng/mL rh GM-CSF, and RPMI 1640 with 10% FBS and 4 mM L-glutamine, respectively. Gammaretroviral vectors pseudotyped with the ecotropic (Eco-GFP) and Gibbon ape Leukemia virus (GALV-GFP) envelopes with an eGFP reporter gene under the control of MSCV LTRs were produced in DMEM

supplemented with 10% FBS from GP+E-86 and PG-13 packaging lines, respectively, as previously described. In addition, gammaretroviral vectors pseudotyped with an amphotropic envelope produced from a Phoenix packaging cell line (Kinsella and Nolan 1996) transiently transfected with pSF91eGFP (Kraunus et al. 2004) were a gift from Dr. Tobias Berg (BC Cancer Research Centre). Lentiviral vectors pseudotyped with the gammaretroviral ecotropic (Lenti-Eco) or amphotropic (Lenti-Ampho) as well as the vesicular stomatitis (Lenti-VSV-g) envelopes were a generous gift from Dr. Derek Persons (St. Judes Children's Research Hospital, Memphis, Tennessee, USA). All lentiviral vectors expressed an eGFP reporter gene under the control of MSCV LTRs (Hanawa et al. 2002; Kim et al. 2010). Titers were estimated on HELA cells at 7×10^6 i.u./mL for Lenti-Eco, 8×10^6 i.u./mL for the Lenti-Ampho and 2×10^7 i.u./mL for the Lenti-VSV-g by the Persons lab. All retroviral vectors were stored at -80^oC.

5.2.2. Histone aggregation

Lyophilized arginine-rich calf thymus histone fraction (f_3) (type VIII-S) (Sigma-Aldrich) was reconstituted in PBS (Invitrogen) at 1 mg/mL, sterile filtered (0.22 μm), aliquoted in 0.5 mL fractions in cryovials and immediately frozen at -80^oC. Prior to use, the f_3 histones were thawed at 37^oC for 2 min. To study the effect of histone aggregation on retroviral transduction, the f_3 fraction was incubated at room temperature ($\sim21^oC$) for 6 and 24 h as well as at 65^oC using a block heater for 2, 6 and 24 h. Unless otherwise specified, the term "aggregated f_3" will refer to f_3 histones incubated at 65^oC for 24 h.

5.2.3. Aggregation measurements

Histone aggregation was evaluated by native polyacrylamide gel electrophoresis (PAGE). Briefly, a 1.5 mm thick 8 cm wide 10% polyacrylamide gel (37.5:1 acrylamide:bis-acrylamide) (Bio-Rad, Hercules, CA, USA) in 50 mM Tris-HCl (EMD Chemicals, Gibbstown, NJ, USA) was cast at pH 7.1. Gels were pre-run at ~175 V for 0.5 h with Tris running buffer. The pre-run buffer was discarded and fresh Tris buffer was added. The loading buffer consisted of 6.25% sucrose (Sigma Aldrich) in Tris buffer. 1.5 μg of f_3 histone were loaded in each well. Cytochrome C (Sigma-Aldrich) was used to mark the front of the gel. The gels were run on the Mini-Protean 3 system (Bio-Rad) with inverted electrodes to reflect the net positive native charge of the histone proteins for 1.5 h at 100 V. The gels were stained overnight with Sypro Ruby (Invitrogen) and imaged with a Pharos FX (Bio-Rad).

The gels were analyzed using Quantity One software (Bio-Rad). First, noise was removed with the filter wizard "salt" option using a 9 × 9 matrix and the background fluorescence was subtracted. The signal was integrated across the width of the lane set at 8 mm along the length of the gel (a representative example is provided in Figure 5.1). In order to facilitate the interpretation of the PAGE results, a dimensionless number referred to as the "aggregation index" was used to quantify the amount of high-order histone aggregates relative to unaggregated histones. High-order aggregates were estimated based on the height of the peak with a negligible relative mobility ($0 \leq R_M \leq 0.05$) within the gel (peak 1 in Figure 5.1) minus the blank. Unaggregated histones were similarly estimated using the height of the peak of high-mobility proteins ($0.7 \leq R_M \leq 1.0$, peak 2 in Figure 5.1). As per the following equation:

$$Aggregation\ index = \frac{High\text{ - }order\ aggregate\ peak\ height}{Unaggregated\ \ peak\ height} \qquad \textbf{Eq. 5.1}$$

the aggregation index is the ratio of peak 1 to peak 2. For example, the untreated f_3 shown in Figure 5.1 has an aggregation index of 0, while the aggregated sample had an aggregation index of 11.

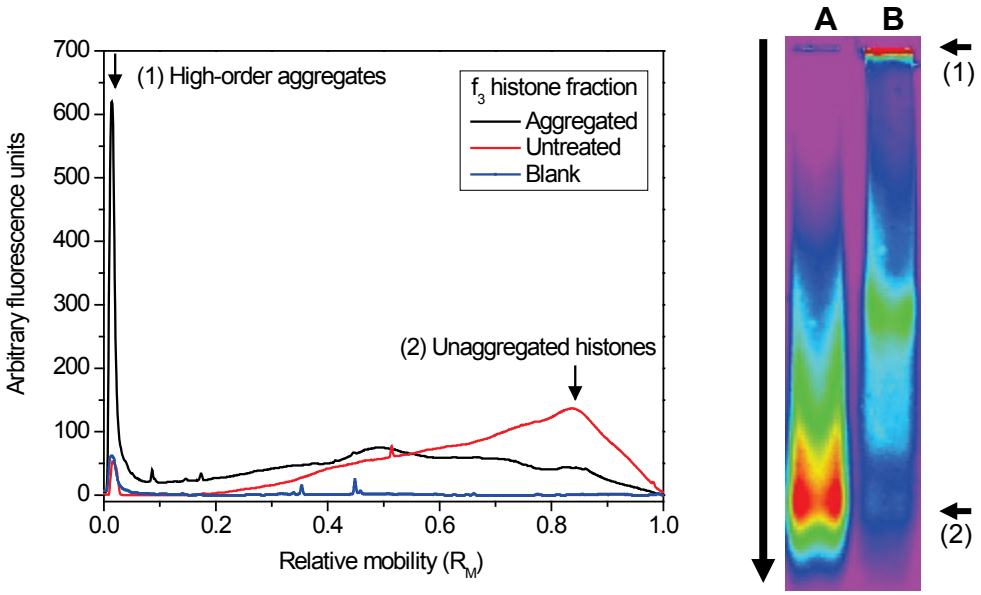

Figure 5.1 Analysis of histone f_3 fraction aggregation.
The aggregation of the histone f_3 fraction was analyzed by native PAGE stained with Sypro Ruby (right). Plots of fluorescent versus relative mobility (left) showed that histones aggregated by heat treatment at 65°C for 24 h (lane B) have an increase in peak (1) located at $R_M \approx 0.03$ likely consisting of high-order aggregates and a decrease in peak (2) located at $R_M \approx 0.85$ likely consisting of unaggregated histones relative to an untreated histone f_3 fraction (lane A). A mass balance performed by integrating along the lane (area under the curve) showed a similar total protein content in both lanes.

The presence of aggregates was also detected by measuring changes in the turbidity of the histone solution (Bryant and McClements 1999). The turbidity of a 1 mg/mL histone solution was measured at 600 nm over a 1 cm path length using a Biochrom Ultrospec 2000 spectrophotometer (Cambridge, UK).

5.2.4. Effect of reducing reagent on aggregation

f_3 histone fractions in PBS (1 mg/mL) were thawed and incubated for 2 h either at 65°C using a block heater or at room temperature. A fresh 1 M solution of dithiothreitol (DTT) (Invitrogen) was prepared in deionized water. Heat-treated and untreated histones were aliquoted into 3 × 400 µL fractions and were incubated with 0, 10 or 100 mM DTT for 4 h at room temperature. The aggregation index was subsequently measured on native PAGE as previously described.

5.2.5. Transduction assay

VCM was thawed at 37°C for 15 min and diluted with growth medium to obtain a final relative concentration of 1:8 for GALV-GFP and 1:16 for Eco-GFP retroviral vectors. Target cells were resuspended in fresh growth medium to obtain a final concentration of 5×10^5 cells/mL unless otherwise specified. In 24-well untreated plates (Sarstedt, Nümbrecht, Germany), 150 µL of histones diluted in PBS were mixed with 150 µL of VCM and 300 µL of target cells (3 mm liquid depth). Transduction was performed at 37°C for a period of 24 h. The cells were then transferred into new wells, diluted 1:5 for TF-1 and 1:10 for nBaF3, and expanded for an additional 48 h. Transduction efficiency and the geometric mean GFP fluorescence were measured using a FACS Calibur (BD Biosciences, San Jose, CA). Results are expressed as the fold-increase in transduction events relative to the control with no additives as previously described in Chapter 3. Transduction efficiency measurements are also provided as supplementary figures in Appendix B.3.

To evaluate the influence of sedimentation, transduction was performed at liquid depths of 1 mm (200 μL), 3 mm (600 μL, standard depth), 5 mm (1000 μL), 10 mm (2000 μL) and 15 mm (3000 μL) while maintaining the number of cells as well as the aggregated f_3 histone fraction and VCM concentrations constant. nBaF3 cells were resuspended in growth medium at 3×10^6 cells/mL and 100 μL of cells were added to each well of 24-well untreated plates effectively providing 1.5×10^5 cells/cm^2. Growth medium was then added to bring the volume to 50% of its final value. 25% of the final volume was comprised of aggregated histones in PBS at a final concentration of 20 μg/mL. Eco-GFP VCM was pre-diluted 1:4 with growth medium and added at 25% of the total volume to obtain a final dilution of 1:16. The cell cultures were then incubated and transduction was measured as previously described.

5.2.6. Transduction of primary mouse hematopoietic progenitors

Transduction of primary mouse hematopoietic progenitors was carried out as described in the previous chapter with the exception that aggregated f_3 histones at a concentration of 20 μg/mL were added to the 2nd and 3rd trials.

5.2.7. Comparison of aggregated f3 histones to RetroNectin

RetroNectin (Clontech Laboratories, Madison, WI, USA) enhanced transduction was performed as per the manufacturer recommended protocol. Briefly, untreated 96-well plates were coated with 90 μL/well of RetroNectin diluted at 20 μg/mL in PBS (5 μg/cm^2) overnight at 4^{o}C. The coating solution was discarded, 90 μL of 2% bovine serum albumin (BSA fraction V) in PBS (Invitrogen) were added and the plates were incubated for 30 min at room temperature. The wells were then washed with 90 μL

Hank's balanced salt solution supplemented with 2.5% (v/v) 1 M HEPES (Invitrogen). Two transduction methods involving RetroNectin with pre-loaded viral vectors or RetroNectin with supernatant were used. In the pre-loading case, the wells were pre-loaded with 30 µL VCM and 30 µL growth medium at 37°C, 5% CO_2 balance air for 5 h. The supernatant was removed and discarded thereby getting rid of any soluble inhibitors present in the VCM. 60 µL of 2 % BSA in PBS were added to prevent the plates from drying. In the supernatant experiments, 30 µL of PBS were added with 30 µL of VCM. 60 µL of target cells resuspended in fresh growth medium were then added to both the pre-loaded and supernatant wells to obtain an initial cell concentration of 5×10^5 target cells/mL.

The effect of RetroNectin was compared to that of the aggregated f_3 histones (50 µg/mL), recombinant human H3.1 histones (New England Biolabs, Ipswich, MA, USA) (10 µg/mL) and a control without additives (PBS only). 30 µL of histones diluted in PBS were added to each well. As per the RetroNectin supernatant protocol, 60 µL of target cells resuspended in fresh growth medium and 30 µL of VCM were added. As previously described, all wells were incubated for 24 h at 37°C. 75 µL were replated in 24-well untreated plates, diluted with growth medium (1:5 for TF-1 and 1:10 for nBaF3) and expanded for an additional 48 h followed by FACS analysis.

5.2.8. Western blots

Untreated and aggregated f_3 histones were first separated by non-reducing Tricine-SDS-PAGE (Schagger 2006). Briefly, a 20% polyacrylamide separating gel (25:1 acrylamide:bis-acrylamide) in 1 M Tris, 0.33 M SDS HCl and 0.3% (wt/v) SDS (pH 8.45) was cast. A 1 cm 4% stacking gel was cast above the separating gel. An anode

buffer consisting of 0.1M Tris, 22.5μM HCl (pH 8.9) and a cathode buffer of 0.1 M Tris, 0.1 M tricine and 1% SDS (wt/v) (pH 8.25) were used (all reagents from Sigma-Aldrich). 5 μg of histones were loaded per well using a loading buffer containing 3% (wt/v) SDS, 7.5% (wt/v) glycerol, 0.05% (wt/v) Coomassie blue G-250 and 37.5 mM Tris/HCl (pH 7.0). The gels were run on the Mini-Protean 3 system (Bio-Rad) at 30 V until samples entered the stacking gel. The voltage was then increased to 90 V and the gels were run for 9 h. Duplicate gels were run simultaneously with one used in the Western blot and the other stained with Sypro Ruby to determine the total protein as previously described.

Electrotransfer to a PVDF membrane (NEN Life Science Products, Boston, MA) was performed using a Bio-Rad Trans-Blot SD semi-dry transfer cell. Briefly, the gel was soaked in Towbin transfer buffer (25 mM Tris, 0.2 M glycine, 20% (v/v) methanol in H_2O) for 15 min. The PVDF membrane was soaked in 95% ethanol for 1 min, rinsed in deionised water for 3 min and soaked in Towbin transfer buffer with a filter paper for 30 min. The transfer was performed at 15 V for 2 h.

For immunoblotting, the membrane was first soaked in blocking buffer consisting of 5% (wt/v) non-fat dried milk (Nestlé, North York, Ontario), 0.1% (v/v) Tween-20 in Tris buffered saline (TBS) (0.02 M Tris base, 0.137 NaCl in Nanopure H_2O at pH 7.6) for 1 h at room temperature. The membrane was then washed 3 times for 15 min with TBS with 0.1% (v/v) Tween-20. Histone H2A and H3 rabbit monoclonal antibodies and histone H2B and H4 mouse monoclonal antibodies (Cell Signaling Technology, Danvers, MA, USA) were diluted 1:1000 with TBS supplemented with 5% (wt/v) BSA and 0.1% (v/v) Tween-20. The membranes were incubated with the primary antibody solutions overnight at 4^oC. The membranes were then washed 3 times using TBS with 0.1% (v/v)

Tween-20. The membranes were incubated with anti-rabbit or anti-mouse IgG secondary antibodies (Cell Signaling Technologies) conjugated to horseradish peroxidase diluted 1:2000 in TBS supplemented with 5% (wt/v) non-fat dried milk and 0.1% (v/v) Tween-20 for 1 h at room temperature. The membrane was washed 3 times using TBS with 0.1% (v/v) Tween-20. Finally, LumiGLO reagent (Cell Signaling Technology) was added and the signal was detected on x-ray film using exposure times of 30 s to 2 min.

5.2.9. Dot blots

PVDF membranes of 2.8 cm × 2.8 cm were incubated for 1 min in 95% ethanol, 3 min in deionized water and soaked for 15 min in Towbin transfer buffer. 5 μg of aggregated f_3 histone fraction and, as controls, 2.5 μg of recombinant human histone H2B, H3 and H4 (New England Biolabs) were loaded using a 10 μL volume. The membranes were incubated at 37°C on filter paper for 1 h. Western blots were subsequently performed as previously described.

5.2.10. Statistical analysis

All errors bars represent the standard error of the mean (SEM). P-values were determined using Student's t-test.

5.3. Results

5.3.1. Aggregation of f_3 histone fraction increased retroviral transduction

In the previous chapter, it was shown that the f_3 histone fraction enhanced retroviral transduction in a dose-dependent manner with a minor peak at 5 μg/mL and a

major peak at 160 μg/mL where aggregation was observed in the target cell/retroviral vector/histone mixture. Based on this observation, it was hypothesized that fostering aggregation of histones prior to their addition to the target cell/retroviral vector mixture could further enhance retroviral transduction. Incubation at higher temperature (65^{o}C) was therefore selected as a means to stimulate the formation of histone protein aggregates through self-aggregation.

The impact of incubation temperature and time on the potential of f_3 histones to enhance retroviral transduction of TF-1 and nBaF3 cells is shown in Figure 5.2. Incubation at room temperature for 6 and 24 h did not appear to increase transduction at the lower doses of 10 and 20 μg/mL relative to freshly thawed f_3 histones. However, at 50 μg/mL, transduction increased slightly with longer incubation times, especially with the nBaF3 target cells and also with TF-1. As the incubation temperature was increased to 65^{o}C, transduction events were increased by up to 139-fold for nBaF3 cells and 53-fold compared with increases of 14- and 11-fold, respectively, when untreated f_3 was used. The enhancement was also dependent on the incubation time as the greatest increase was observed at 24 h. The co-dependence on incubation temperature and time of the performance of the f_3 fraction suggests that the concentration and size of the aggregates may increase over time and at a greater rate when the temperature is increased.

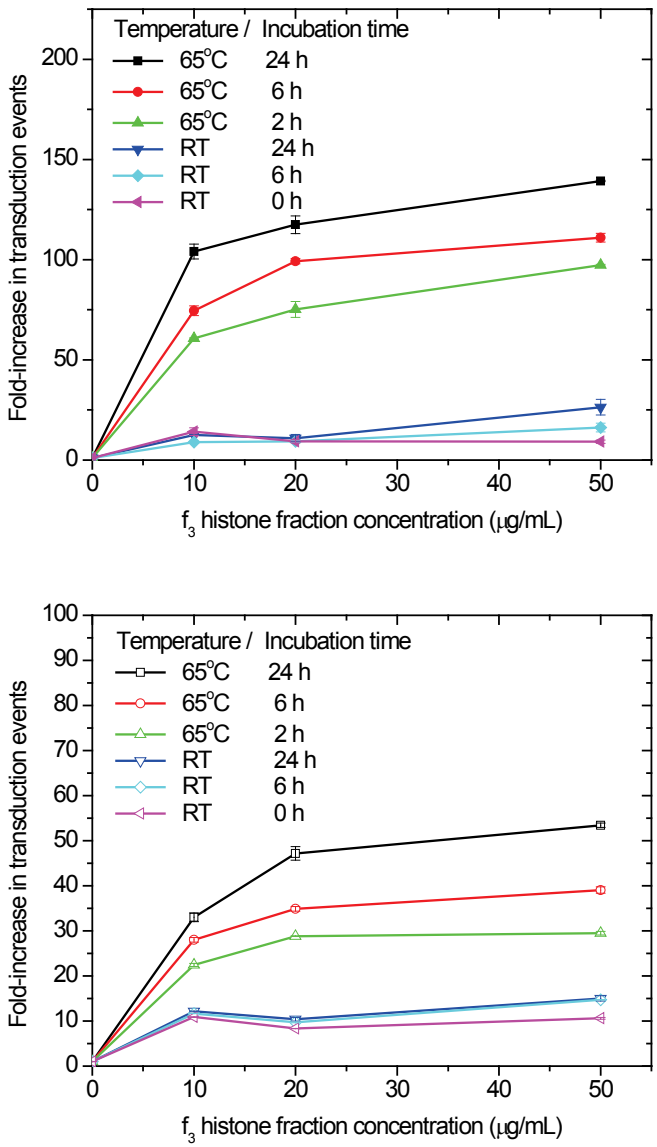

Figure 5.2 Effect of f_3 histone fraction incubation temperature and time on the increase in transduction events.
nBaF3 target cells were transduced with Eco-GFP vectors (top) and TF-1 target cells with GALV-GFP vectors (bottom). Histones were incubated at room temperature (~21°C) or at 65°C for up to 24 h prior to their addition to the target cell and retroviral vector mixture at 10, 20 and 50 μg/mL. (*n*=2 using the same batch of histones.)

To determine if histone aggregation was responsible for the observed enhancement, the aggregation index (see Material and Methods section 5.2.3) of the f_3 fraction was measured following each treatment. The aggregation index was found to increase with both incubation time and incubation temperature. f_3 fractions incubated at

room temperature had aggregation indices ranging from 0.09 to 0.21 suggesting a low concentration of high-order aggregates. At 65°C, the aggregation index further increased from 0.49 following a 2 h incubation to 11.2 after a 24 h incubation. To assess the relationship between histone aggregation and retroviral transduction, the increase in transduction was plotted relative to the aggregation index (Figure 5.3). A sharp increase in transduction was observed as the aggregation index increased from 0 to 0.49 suggesting that aggregate size initially limits the increase in transduction. As the aggregation index further increased from 0.49 to 11.2, transduction was further increased, but at a lower rate. Over this range, sufficiently large aggregates may be present and the increase in transduction may become a function of the concentration of these larger aggregates. Aggregation was also assessed by monitoring the changes in turbidity. As shown in Figure 5.4, the turbidity of untreated f_3 fractions was negligible and similar to that of PBS. However, incubation of the f_3 fraction for 24 h at 65°C significantly increased the turbidity, which is indicative of the presence of particles such as protein aggregates.

The aggregation index of the two untreated lots of recombinant human histone H3.1 used to enhance the transduction of primary mouse hematopoietic cells was also measured. While the first lot had an aggregation index of 4.3, that of the second lot was only 2.2. Interestingly, the first yielded a greater increase in transduction than the second, thereby further supporting the role of aggregation in histone performance.

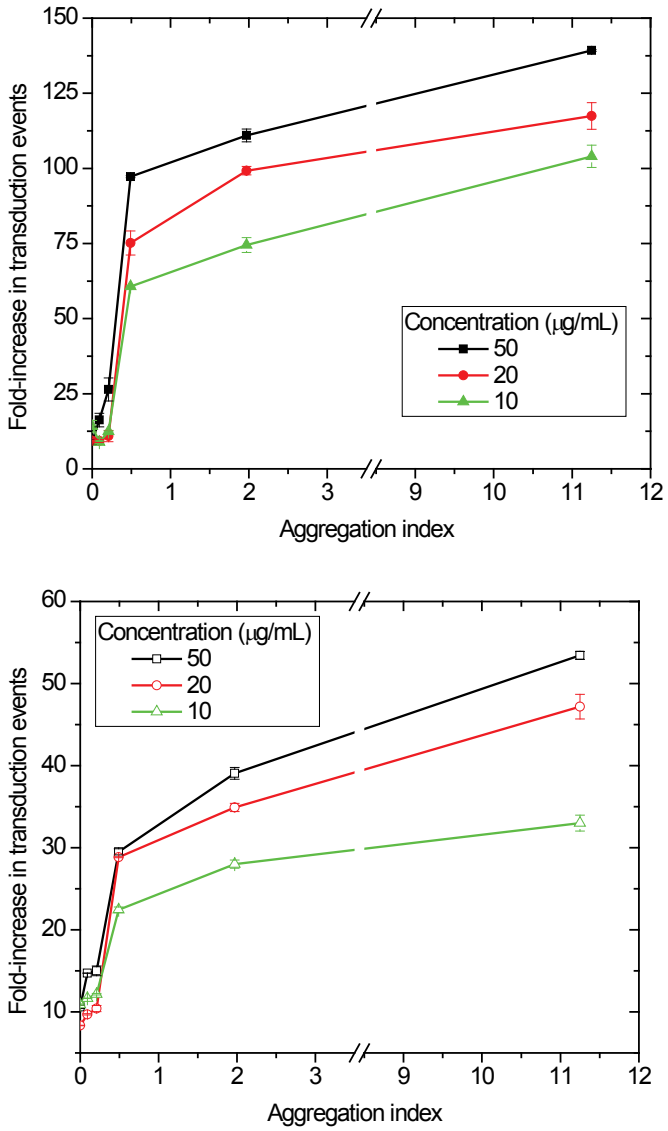

Figure 5.3 Increase in transduction events relative to the aggregation index of the f_3 histone fraction. nBaF3 target cells were transduced with Eco-GFP vectors (top) and TF-1 target cells with GALV-GFP vectors (bottom). Histone aggregates were generated by incubation at 65°C or at room temperature (~21°C) for up to 24 h. (*n*=2 using the same batch of histones.)

Because the f_3 histone fraction aggregated by heating at 65°C for 24 h yielded the greatest increase in transduction together with the highest aggregation index, it was selected for an expanded dose-response experiment whose results are shown in Figure 5.5. For comparison, results obtained with untreated f_3 in Chapter 4 (Figures 4.1 and 4.2) are

also shown and expressed as fold-increases in transduction events relative to a control with no additive. Aggregation of the f_3 fraction significantly altered the dose-response profile relative to the non-aggregated f_3. First, the maximum increase in transduction events was magnified with aggregated f_3 to 34-fold from 22-fold with non-aggregated f_3, representing a 1.5-fold increase in the retroviral enhancing potential of this fraction. Second, while the maximum increase in transduction events with aggregated f_3 occurred at 40 μg/mL, there was no statistically significant difference in the enhancement obtained at concentrations ranging from 5 to 80 μg/mL, whereas the untreated f_3 displayed a minor peak at 5 μg/mL and a major peak at 160 μg/mL. Finally, in its aggregated form, the concentration of f_3 required to achieve maximum transduction was reduced by at least 16-fold to 10 μg/mL from 160 μg/mL.

The results obtained with pre-aggregated f_3 strongly suggest that aggregation was responsible for the second peak observed with untreated f_3. In this case, because non-aggregated histone was added at the start of the experiment, the aggregation occurred during the course of the transduction process. Because these aggregates form slowly subject to the co-dependence on temperature and time (Figure 5.2), it is unlikely that a sufficient quantity of large aggregates would be generated within the 24 h of retroviral transduction, thus explaining the higher concentration required and lower enhancement achieved. Furthermore, as the pre-aggregated f_3 was generated *ex situ*, it does not appear that interaction with the retroviral vectors or other compounds in the VCM is required for aggregation to take place.

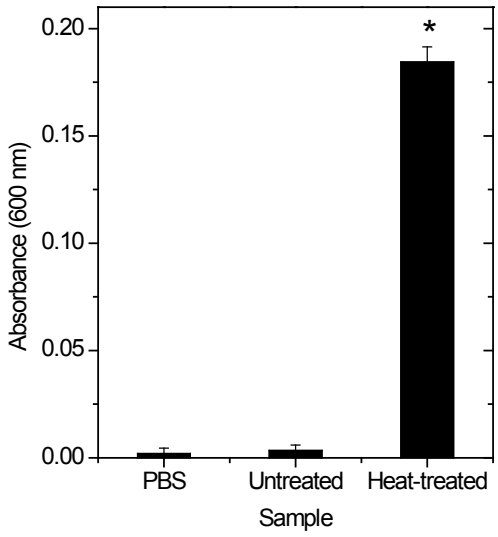

Figure 5.4 Effect of f_3 histone fraction aggregation on turbidity.
Turbidity measurements for the f_3 histone fraction before (untreated) and after heat-treatment at 65°C for 24 h were compared to the phosphate buffered saline (PBS) control. (* $p<0.05$ relative to PBS.) (n=6 for heat-treated histones and n=2 for untreated histones and PBS.)

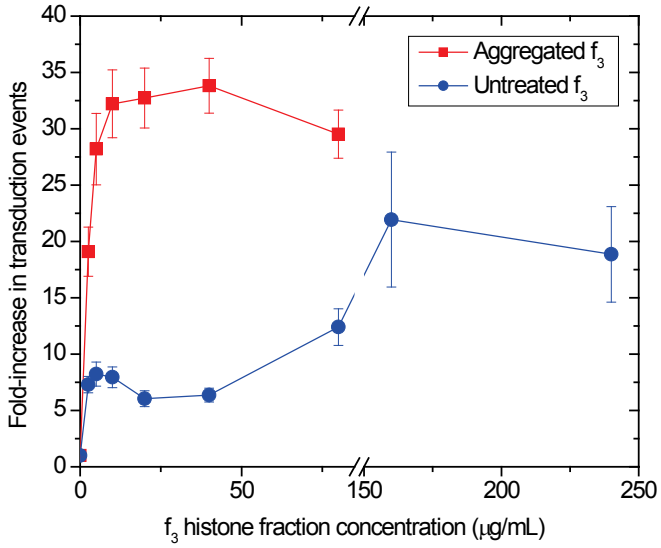

Figure 5.5 Effect of the concentration of untreated and pre-aggregated f_3 histone fractions on the transduction of TF-1 cells with GALV-GFP vectors.
(n=3 for aggregated histones and n=6 for untreated histones except at 160 and 240 µg/mL where n=3)

The untreated f_3 fraction was found in the previous chapter to exhibit no significant cell toxicity up to a concentration of at least 240 µg/mL. The formation of aggregates sufficiently large to sediment may lead to an increase in the local concentration near the target cells and that could alter the toxicity of the f_3. Thus, the toxicity of pre-aggregated f_3 was evaluated in the concentration range of 0 – 80 µg/mL and compared to that of the untreated f_3 as shown in Figure 5.6. Aggregation of the f_3 did not result in significant toxicity. The average cell recovery relative to an untreated control was 97.7% after pre-aggregation compared to 94.5% for the untreated f_3.

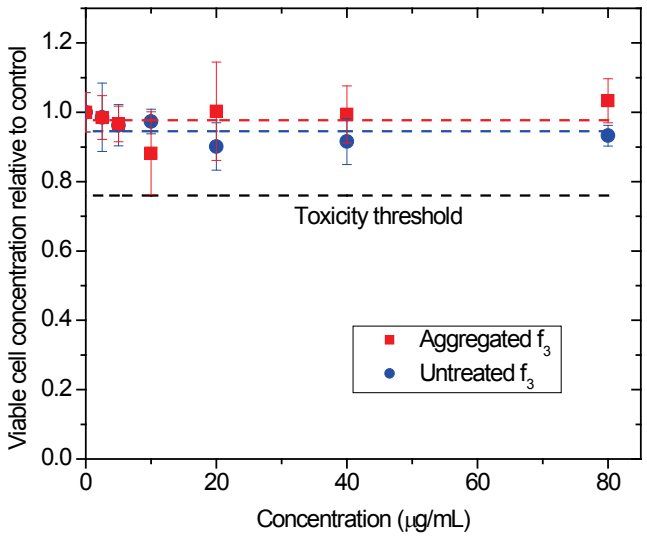

Figure 5.6 Effect of aggregated f_3 histone fraction concentration on viable TF-1 concentration.
The viable TF-1 cell concentration relative to a control without additives was measured by trypan blue exclusion after a 24 h exposure to increasing concentrations of aggregated or untreated f_3 histone fraction. Similarly to the untreated f_3, the aggregated f_3 had negligible toxicity up to at least 80 µg/mL and the average cell recoveries were 94.5% and 97.7%, respectively (dashed lines). The toxicity threshold was estimated based on a 95% confidence interval on the untreated control (black dashed line). (n=3)

5.3.2. Mechanism

In the previous chapter, it was found that the transduction increases obtained by adding recombinant human histone H3.1 were greater than for all other histone types. An aggregation analysis of the rh H3.1 preparations also revealed that they had attained an intermediate state of aggregation. As histone H3.1 is the only histone type and variant with 2 cysteine residues, the role of disulfide bridge formation in the generation of aggregates was explored by exposing the aggregates to reducing conditions. Dithiothreitol (DTT), a reducing agent, was added to f_3 fractions that had been previously aggregated by incubation for 2 h either at 65^{o}C or at room temperature (~21^{o}C). As can be seen in Figure 5.7, the aggregation index was reduced by the addition of 10 mM DTT, but a complete reversal of aggregation was not achieved even when the DTT concentration was raised to 100 mM. Also, the degree of reversal of the aggregates formed at 65^{o}C was less than for those formed at room temperature. Overall, the partial reduction of the aggregation index through the addition of a reducing reagent suggests that, although disulfide bridges between histone H3.1 molecules play a role in the aggregation, they do not entirely explain the amount of aggregation observed. While the f_3 fraction is enriched in histone H3.1, it contains other core histones such as H2A, H2B and H4 that might also participate in the formation of aggregates.

In order to explore which histone types were recruited within the aggregates, Western blots were performed. As previously described, high-order aggregates remain on top of the gel while low-order and unaggregated histones migrate through the gel. As shown in Figure 5.8, in the aggregated f_3, histones H2A, H3 and H4 were detected in both the top and bottom bands corresponding to high-order aggregates and unaggregated

histones, respectively, while several intermediate aggregate structures were also observed with the H3. These intermediate structures were present in both the untreated and aggregated samples. However, in the aggregated sample, fewer intermediate aggregates and more high-order aggregates were observed compared with the untreated sample. While the Western blots were not quantitative, they confirmed that at least these 3 core histones were present in the aggregates.

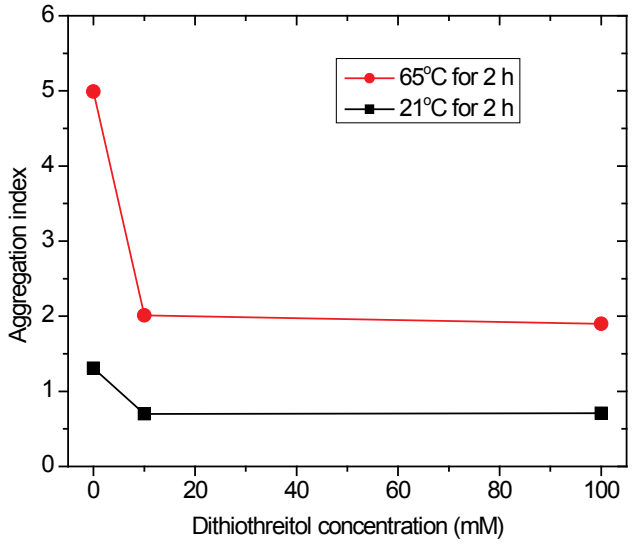

Figure 5.7 Effect of dithiothreitol addition on the aggregation index of the f_3 histone fraction.
Aggregates were formed by incubation of the histone solution at 65°C or 21°C for 2 h.

Western blots were also performed on histone H2B but failed to detect this histone type. To verify whether this was due to a faulty anti-H2B antibody or a lack of H2B within the f_3 fraction, dot blots were performed using rh histone H2B as a control. As shown in Figure 5.9, the antibody against histone H2B successfully detected the rh H2B histone. However, in the aggregated f_3 fraction, only extremely low levels of H2B were detected. This suggests that the f_3 fraction contained only very low levels of H2B and that it was not required for the formation of aggregates.

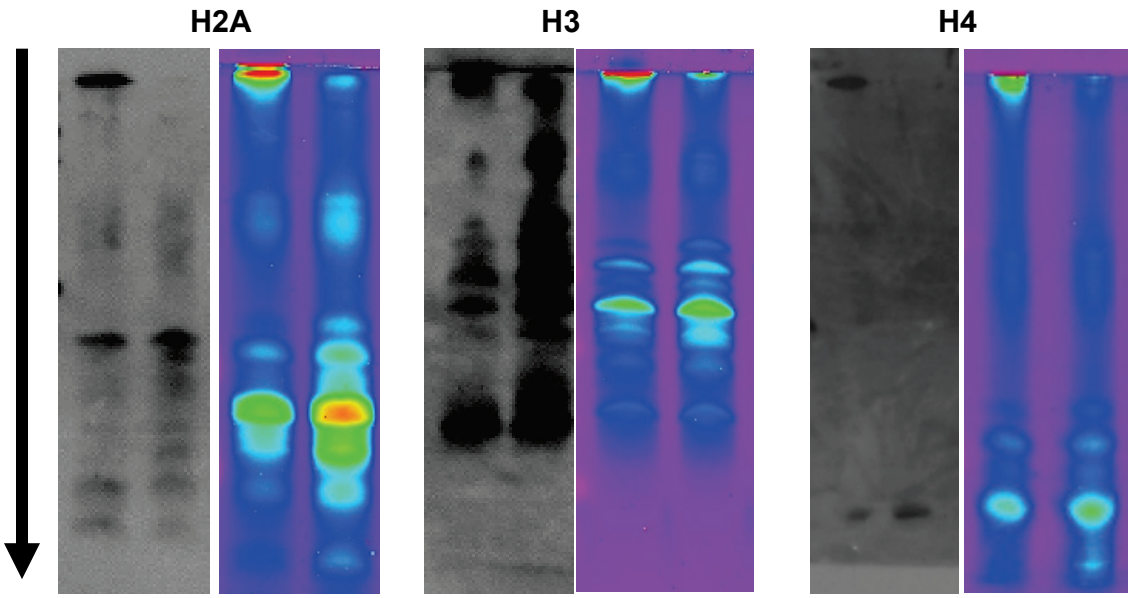

Figure 5.8 Histone H2A, H3 and H4 Western blots of the aggregated f_3 histone fraction.
Western blots (left, grey scale) and total protein (right, pseudocolor) of aggregated (left lane) and untreated (right lane) f_3 histone fractions separated by SDS-PAGE. Histones H2A, H3 and H4 were all recruited into the larger aggregates present on top of the gel.

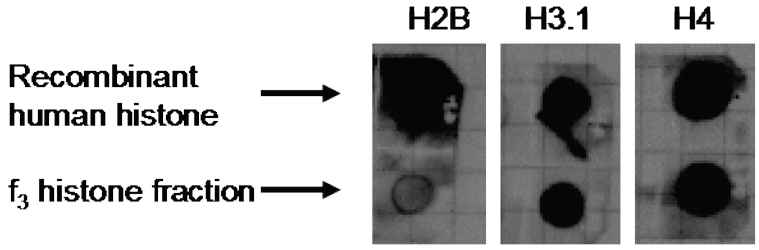

Figure 5.9 Dot blots of the f_3 histone fraction and recombinant human histones H2B, H3 and H4.
The f_3 histone fraction was loaded at 5 µg and the recombinant histones at 2.5 µg.

Because retroviral transduction was found to increase with histone aggregation, it was hypothesized that the presence of aggregates primarily improved the transport of retroviral vectors to the target cells through sedimentation. As shown in Figure 5.10, in the absence of aggregated histones where transport is governed by diffusion, transduction did not increase with increasing liquid depth at a constant cell number and retroviral vector concentration. However, when aggregated f_3 fractions were added, transduction events increased with liquid depth to at least 15 mm. This supports the hypothesis that

aggregates were able to effectively settle retroviral vectors through a distance of at least 15 mm. Settling appeared to be most effective at a depth of ~1 mm and become progressively less effective at depths > 1 mm, which may indicate that some aggregates failed to effectively settle the retroviral vectors through the full distance.

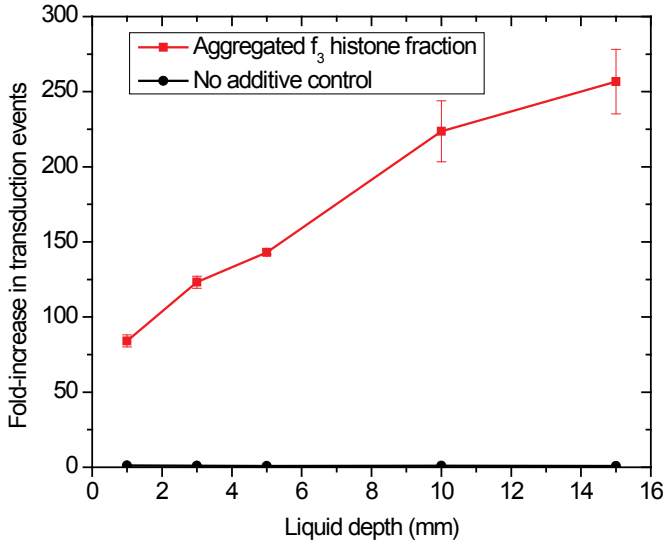

Figure 5.10 Effect of the average liquid depth on the increase in transduction events with the aggregated f_3 histone fraction.
The increase in transduction events with the aggregated f_3 histone fraction at 20 µg/mL of nBaF3 target cells with Eco-GFP vectors relative to the average of the controls with no additives was measured at increasing liquid depths (1 – 15 mm). Vector concentration and target cell number (1.5×10^5 cells/cm^2) remained constant at all liquid depths. (*n*=2 using same batch of aggregated histones)

As was previously observed with the PD80P lysate fraction containing aggregates, in the presence of aggregated f_3 histones, the target cell concentration influenced transduction (Figure 5.11). The fold-increase in transduction decreased as the target cell concentration increased. This was likely the result of a lower quantity of retroviral vectors complexed with histone aggregates available on a per cell basis as the retroviral vector and histone concentrations were held constant while the cell concentration was increased.

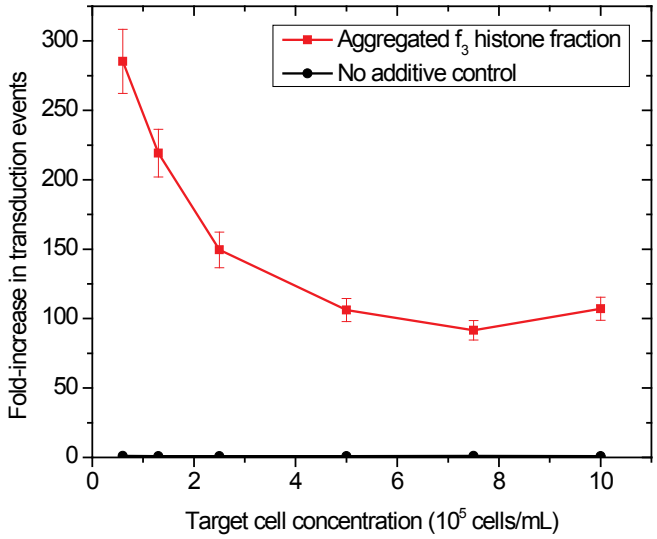

Figure 5.11 Effect of the initial nBaF3 target cell concentration on the fold-increase in transduction events using a 20 µg/mL aggregated f_3 histone fraction relative to the average of the no-additive control (0.6 – 10 ×10^5 cells/mL, 3 mm liquid depth).
Eco-GFP vectors were employed in both experiments. (*n*=2 using the same batch of aggregated histones)
(At a 3 mm liquid depth, 5×10^5 cells/mL is equivalent to 1.5×10^5 cells/cm^2)

5.3.3. Application of aggregated f_3 histones to the transduction of primary mouse hematopoietic progenitors

Given the cell line transduction increases achieved by pre-aggregating the f_3 fraction, its potential to improve the retroviral transduction of primary mouse hematopoietic progenitors was investigated. The aggregated f_3 was incorporated in the 2nd and 3rd trials described in Chapter 4. As predicted from the TF-1 cell results, the aggregated f_3 fraction outperformed the rh H3.1 histones with the transduction efficiency of the mouse cells further increased by 1.9- to 3.0-fold (Table 5.1). This corresponds to an increase of 7.8- (likely underestimated due to the presence of multiple copy numbers at high transduction efficiency) to 33-fold (likely a better estimate as the lower transduction efficiency lowers the probability of multiple copy numbers) relative to a control without additives. The latter result was comparable with that previously obtained

with the TF-1 model cell line (Figure 5.5). Also, the f_3 fraction toxicity was negligible for the mouse primary bone marrow cells (Table B.2, Appendix B).

Table 5.1 Transduction efficiency of the mouse primary bone marrow cells.
Cells were transduced for 48 h with Eco-GFP retroviral vectors and transduction efficiency was measured after an additional 72 h of culture. Transduction was performed with VCM supplemented with 20 μg/mL of aggregated f_3, with 10 μg/mL of rh histone H3.1, with VCM alone (no additives) and, as a negative control, without VCM. (Two different batches A and B of VCM were used; trials 1 and 2 were performed concomitantly with the last 2 trials presented in the previous chapter.)

VCM batch	Trial	Treatment			
		Aggregated f_3	H3.1	No additives	Negative control
A	**1**	72.9%	38.0%	9.3%	0.1%
B	**2**	39.9%	13.3%	1.2%	0.2%

The intended targets within the bone marrow populations were primitive cells with a long-term reconstitution potential such as hematopoietic stem cells. Following a 20-week reconstitution assay of congenic recipients, GFP^+ cells within the donors demonstrated a successful transduction of primitive cells with long-term reconstitution potential (Figure 5.12B). As the donor contribution to hematopoiesis of aggregated f_3-treated cultures was similar to that of the untreated (negative) control, the aggregated f_3 did not appear to be toxic to primitive hematopoietic cells. Consistent with bulk bone marrow cell results (Table 5.1) the GFP^+ transduced cells within the donor contribution were 2.3-fold higher with the aggregated f_3 relative to the rh H3.1 histones. There also was a 10.9-fold improvement over the control without additives. Finally, the distribution of the contribution to lympho- and myelopoiesis by donor cells of the aggregated f_3-treated cells was similar to that of the negative control regardless of transduction levels (Figures 5.12 and B.23). Interestingly, the contribution of the transduced cell population to myelopoiesis was higher for the aggregated f_3-treated culture than for the rh H3.1 histone-treated culture as the latter was significantly lower than that the control without additives. Overall, these results demonstrate that further increases in transduction can be

achieved by using a pre-aggregated f_3 histone fraction. This was achieved without toxicity or alterations to the distribution of the contribution to lympho- and myelopoiesis.

A.

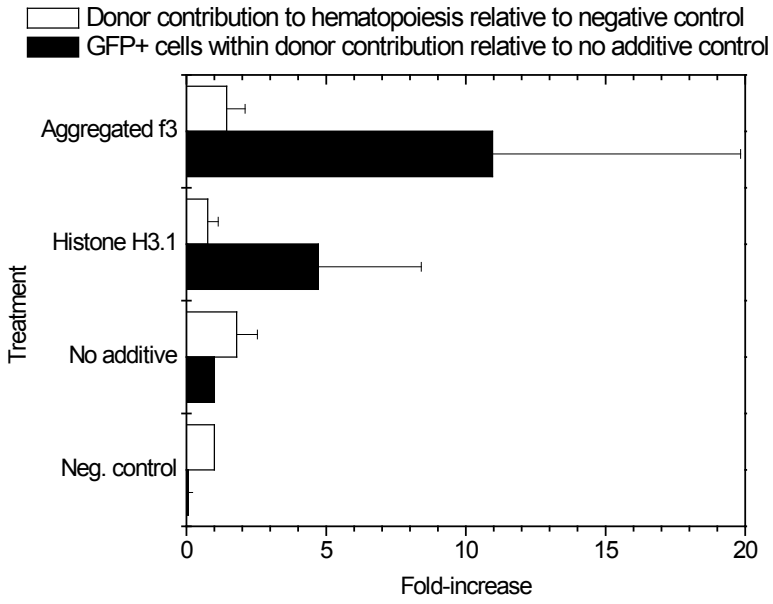

B.

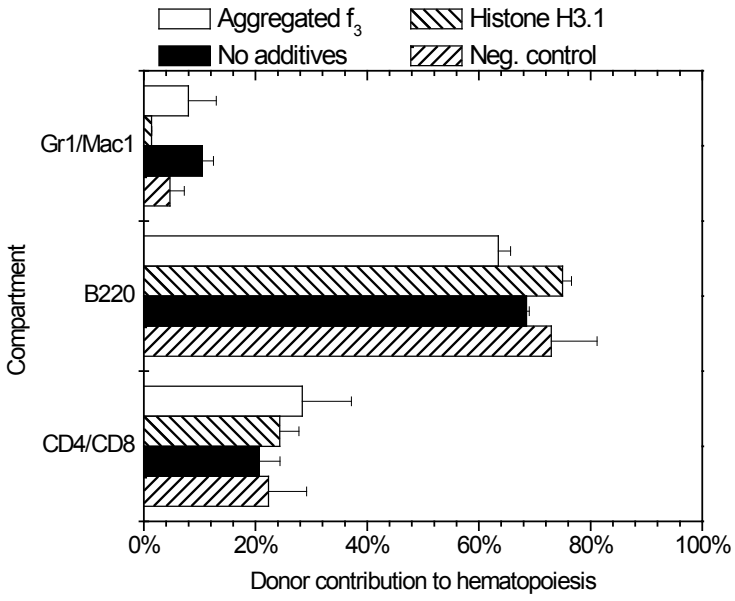

Figure 5.12 Effect of aggregated f_3 histone fraction on total donor contribution to hematopoiesis and lyphoid and myeloid lineages.

A. Effect of treatment on total donor contributions to hematopoiesis relative to negative control, and GFP+ cells within the donor contribution relative to the control without additives measured 20 weeks post-transplant. Total donor contributions did not significantly differ between treatments. Aggregated f_3 treated GFP^+ cells persisted in the peripheral blood of recipient mice at levels exceeding that of histone H3.1. B. Aggregated f_3 treated donor cells contributed to both lymphoid and myeloid lineages measured 20 weeks post-transplant. The aggregated f_3 contribution was comparable to that of the negative control. (n=2)

5.3.4. Lentiviral vectors and RetroNectin

Lentiviral vectors offer the advantage over gammaretroviral vectors of transducing non-dividing cells. RetroNectin is widely used to coat tissue culture surfaces in order to enhance retroviral transduction. Thus, the potential of aggregated f_3 histones to increase transduction relative to RetroNectin was evaluated using lentiviral vectors pseudotyped with either amphotropic or ecotropic murine leukemia virus envelope proteins, or with vesicular stomatitis virus envelope glycoproteins (VSV-g). Also, gammaretroviral vectors pseudotyped with the GALV, amphotropic or ecotropic envelopes were investigated to demonstrate the broader relevance of these results.

The addition of aggregated f_3 successfully increased the retroviral transduction of both TF-1 (Figure 5.13) and nBaF3 (Figure 5.14) target cells by amphotropic lentiviral vectors. The transduction of nBaF3 cells by ecotropic lentiviral vectors was also improved (due to tropism restrictions the latter were not applied to TF-1 cells). However, the transduction of either cell line by the VSV-g pseudotype lentiviruses was not enhanced by the addition of aggregated f_3 (data not shown). This was not limited to the aggregated f_3 as RetroNectin, protamine sulfate and the PD80P lysate fraction also failed to increase transduction for this pseudotype.

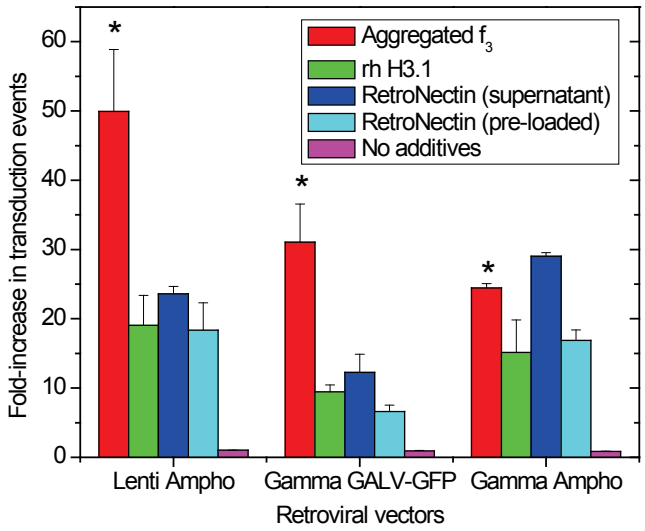

Figure 5.13 Comparison of the effect of aggregated f_3 histone fraction, RetroNectin and rh H3.1 on the transduction of TF-1 cells with lenti- and gammaretroviral vectors.
TF-1 cells were transduced by amphotropic lentiviral vectors as well as GALV-GFP and amphotropic gammaretroviral vectors with 50 µg/mL aggregated f_3 histone fraction, 10 µg/mL rh H3.1 histone, surfaces coated with 5 µg/cm^2 RetroNectin pre-loaded with viral vectors or with viral supernatant, and, as a control, with no additives. The amphotropic lentiviral vectors were diluted 1:20, the GALV-GFP 1:8 and the amphotropic gammaretroviral vectors 1:4. (* $p<0.1$ relative to RetroNectin) (n=2, different batches of aggregated f_3 histones.)

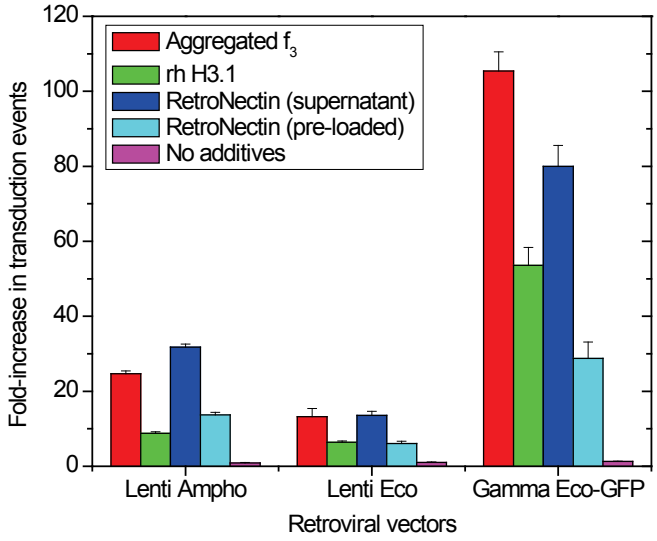

Figure 5.14 Comparison of the effect of aggregated f_3 histone fraction, RetroNectin and rh H3.1 on the transduction of nBaF3 cells with lenti- and gammaretroviral vectors.
nBaF3 cells were transduced by amphotropic and ecotropic lentiviral vectors as well as Eco-GFP gammaretroviral vectors with 50 µg/mL aggregated f_3 histone fraction, 10 µg/mL rh H3.1 histone, surfaces coated with 5 µg/cm^2 RetroNectin pre-loaded with viral vectors or with viral supernatant, and, as a control, with no additives. The amphotropic and ecotropic lentiviral vectors were diluted 1:20 and the Eco-GFP gammaretroviral vectors 1:16. (n=2, within same experiment.)

Aggregated f_3 generally matched or exceeded the enhancement obtained with RetroNectin. With TF-1 target cells (Figure 5.13), the aggregated f_3 improved retroviral transduction by 2.1-fold with amphotropic lentiviral vectors and 2.5-fold with GALV-GFP over that with RetroNectin. The RetroNectin outperformed the aggregated f_3 when amphotropic gammaretroviral vectors were used, albeit by less than 1.2-fold which corresponds to a difference of only 0.5% in transduction efficiency (Figure B.25). With nBaF3 target cells and the Eco-GFP gammaretroviral vectors, transduction using the aggregated f_3 treatment exceeded that of the RetroNectin by 1.3-fold while the transduction levels were matched for ecotropic lentiviral vectors. RetroNectin only outperformed the aggregated f_3 with amphotropic lentiviral vectors, by 1.3-fold. Interestingly, under similar transduction conditions with the amphotropic lentiviral vectors, the transduction of TF-1 cells was further improved with the aggregated f_3 relative to RetroNectin compared to the results obtained using the nBaF3 cells. This suggests that target cell specific factors play a role in determining the increase in transduction. Finally, with all viral vector preparations, the RetroNectin supernatant protocol outperformed the pre-loading procedure. This implies that the diluted retrovirus-containing media did not contain a significant concentration of soluble inhibitors that would have been removed by the pre-loading protocol.

5.4. Discussion

The results demonstrate that retroviral transduction can be further increased through the production of histone aggregates prior to their addition to the target cell and retroviral vector mixture. The use of aggregates reduced the concentration of the f_3 histone fraction required and had negligible toxic effects on TF-1, bone marrow or hematopoietic progenitor cells with a long-term reconstitution potential. While large, dense substrates have previously been applied to concentrate viral vector preparations and to improve their mass transport through sedimentation, histone aggregates provide significant improvements over these technologies. Chemicals such as calcium phosphate have been used as transduction enhancers, but their concentrations and exposure times were limited because of the toxicity of the precipitates formed (Morling and Russell 1995). The use of calcium phosphate has therefore been restricted to the *ex situ* concentration of retroviral vectors followed by a dialysis step to remove the toxic compound (Pham et al. 2001). Bacteria such as heat killed, formalin-fixed *Staphylococuss aureus* (Pansorbin), have successfully been used to enhance the transduction of primary human umbilical cord blood cells (Szyda et al. 2006). However, as retroviral vector adsorption is thought to be mediated by fibronectin binding proteins present on the surface of Pansorbin, the performance of this approach relies on fibronectin secreted by the packaging cell line (Darling et al. 2000). Polybrene has also been combined with the glycoaminoglycan chondroitin sulfate C to form high-molecular-weight complexes between these positively- and negatively-charged compounds to increase transduction (Le Doux et al. 2001). The high concentration of polybrene and chondroitin sulfate C present a significant concern because, while the complex was not

found to be toxic to the target cells, uncomplexed polybrene was harmful (Le Doux et al. 2001) and chondroitin sulfate C alone is an inhibitor of retroviral transduction (Kureishy et al. 2006). Should the complex destabilize, the release of polybrene may result in cell death. Further complicating this approach, endogenous glycoaminoglycans and proteoglycans present within the virus-containing medium (Le Doux et al. 1996) may interfere with the complexation process. Finally, poly-L-lysine molecules with molecular weights greater than 15 kDa have been reported to induce the aggregation of retroviral viral vectors through electrostatic interactions (Davis et al. 2004). As this process relies on interactions between vectors, variations in vector concentration are likely to influence the size of the aggregates as well as the concentration of poly-L-lysine required. Also, it is unclear whether retroviral vectors sequestered within the core of the complexes remain available and active, or if successful transduction will be limited to the vectors present at the surface. In cases where all vectors remain equally active, these aggregates may lead to multiple vector entries resulting in multiple integrations and thereby increasing the risk of genotoxicity. The addition of poly-L-lysines was also reported to induce mitochondrially-mediated apoptosis (Hunter and Moghimi 2010). Thus, relative to these previous methods, aggregated histones are composed of compounds that, on their own, do not exhibit significant toxic or inhibitory effects on retroviral transduction. Furthermore, histone aggregates were formed *ex situ,* and hence do not rely on compounds present within the virus-containing medium or the retroviral vectors themselves. They therefore have the potential to provide a simpler and more robust approach to retroviral transduction.

Interestingly, the aggregated f_3 histone provided a similar response to that previously observed with the PD80P lysate fraction consisting of cellular debris digested with DNase I. Under similar conditions (5×10^5 target cells/mL, 3 mm liquid depth) the transduction of TF-1 cells was enhanced by 34-fold with aggregated f_3 compared with 36-fold for the PD80P (Chapter 3). With nBaF3, the aggregated f_3 provided an enhancement of 156-fold, greater than the 118-fold previously achieved with the PD80P (Chapter 3). Other similarities included a dependence on target cell concentration as well as, due to their ability to sediment adsorbed retroviral vectors, an increase in transduction with increasing liquid depth. Transduction also increased with liquid depth up to at least 15 mm for the aggregated f_3, in line with the trend observed with the PD80P lysate fraction (Figure 3.17). This suggests that aggregates from the purified histone preparation can similarly enhance the setting rate of the retroviral vectors. It also seems likely that histone aggregation, alone, could explain the increase in transduction previously obtained with the PD80P lysate fraction.

Histones assembled in nucleosomes were reported to bind to cell membranes through an interaction with cell surface proteoglycans. Once adsorbed to the cell surface, they can mediate the adsorption of sulfated polysaccharides onto the cell surface (Watson et al. 1999). Histone aggregates may act in a similar fashion with retroviral vectors. Heparan sulfate proteoglycans inherited from the packaging cell membrane during the budding process present on the retroviral vector envelope (Kureishy et al. 2006) may therefore mediate the vector binding to the histone aggregate. RetroNectin, through a heparan sulfate binding domain, also interacts with retroviruses via proteoglycans present on the viral membrane (Hanenberg et al. 1996; Kureishy et al. 2006). It was observed

that, with the amphotropic lentiviral vector, the aggregated histones outperformed RetroNectin with TF-1 cells but only matched it with nBaF3 cells under similar transduction conditions. These differences could be explained by the different ligands used for cell binding by the histone aggregates compared to the RetroNectin. While RetroNectin binding relies on the integrins VLA-4 and VLA-5, histone aggregates may depend instead on cell surface proteoglycans. Thus, in cell lines expressing high levels of cell surface proteoglycans, aggregated histones could yield greater transduction enhancement. Cell types such as B-cell lines lack heparan sulfate expression (Jarousse et al. 2008) and thus for nBaF3 derived from a B-cell progenitor (Palacios and Steinmetz 1985), decreased cell surface heparan sulfate expression may account for the lower performance relative to RetroNectin.

While we have obtained higher transduction efficiencies with increased levels of high-order aggregates, further studies are required to characterize their size distribution through techniques such as laser light scattering (Bryant and McClements 1999). Furthermore, residual unaggregated histones could potentially act as competitive inhibitors by occupying binding sites on the retroviral vectors as well as the target cells, thus limiting interaction with the more potent aggregates. The removal of unaggregated histones from aggregate preparations through methods such as dialysis may further enhance the transduction performance. Buffer selection may also influence histone aggregation. In this study, PBS was used to solubilize the lyophilized histone preparation. As histones bind to DNA through interactions with phosphates (Luger et al. 1997), the phosphate present in the buffer may contribute to non-disulfide bridge-mediated aggregation. While it was demonstrated qualitatively through Western blots that at least

3 of the core histones (H2A, H3 and H4) were recruited within the aggregate structures, quantitative methods such as reverse phase chromatography (Shechter et al. 2007) may resolve the relative contributions of each histone type to the aggregate. This information could be applied to facilitate the transition from a tissue-derived reagent to a fully-defined reagent formulated using recombinant histones. The current source of recombinant histones could be improved by not including DTT given that it was shown to partially reverse histone-based aggregation.

Aggregated f_3 histones were effective for both gammaretroviral and lentiviral vectors pseudotyped with ecotropic, amphotropic and Gibbon ape leukemia virus envelopes produced from either human HEK 293 or mouse NIH 3T3 cells. The only exception was with lentiviral vectors pseudotyped with the VSV-g envelope, a limitation shared by protamine sulfate and RetroNectin. Overall, with target cells such as TF-1, a 2-fold increase in transduction relative to RetroNectin was obtained with amphotropic lentiviral vectors as well as with GALV gammaretroviral vectors. In both cases, this would increase the likelihood of reaching a clinically or scientifically significant level of gene expression in an increasing number of cells. In cases where this threshold has already been achieved, the use of histone aggregates could potentially lower the viral vector concentration required by 2-fold. This may be particularly beneficial for lentiviral vectors which are difficult to produce due to the toxicity of some of the HIV proteins to the producing cells, thus requiring the use of transient transfection (Naldini et al. 1996) or inducible expression systems (Kafri et al. 1999).

Finally, aggregated histones could also be combined with other methods to yield further increases in transduction. For example centrifugation was shown to increase

retroviral transduction but required high centrifugal forces of up to 10,000×g and prolonged treatment times of over 7 h to concentrate the viral vectors in the vicinity of the target cells, and subsequently prevent them from diffusing away (Bahnson et al. 1995). The addition of histone aggregates would likely reduce the relative centrifugal force required to effectively sediment the viral vectors. In proximity to the target cells, the histone aggregates would also facilitate adsorption of vectors to the cell surfaces by preventing their back-diffusion into the bulk medium (Tayi 2010). Furthermore, vectors adsorbed to a denser substrate, able to sediment under gravity alone, would also be maintained near the cell surface upon discontinuation of centrifugation, thus minimizing the centrifugation time.

Overall it was shown that prior aggregation of the f_3 histone fraction containing H3 together with H2A and H4 can lead to a 1.5-fold increase in retroviral transduction relative to untreated histones. This treatment reduced the concentration of f_3 required by an order of magnitude and had no significant cell toxicity. This approach was simpler than the commonly used RetroNectin method as aggregated histones were added directly to the target cell/viral vector mixture, thereby forgoing all surface coating requirements. Furthermore, target cells were easily recovered with 98% recovery achieved relative to an untreated control. Finally, the promising results obtained with cell lines were translated to primary cells including hematopoietic progenitors with long-term reconstitution potential. These features clearly demonstrate the potential of this histone-based reagent and these results provide strong foundations for future improvements.

6. Conclusions and Future Directions

The data presented in this thesis demonstrate that cell lysates potentially generated prior to transduction during the culture of the target cells or the production of the retroviral vectors, or during the transduction protocol, can influence the outcome of the retroviral transduction process. Alone, whole cell lysate enhanced retroviral transduction following a saturation equation based on the lysed-to-target cell ratio. With a fibronectin-based protocol, the presence of lysate completely masked the effect of fibronectin. In the case of protamine sulfate, lysate increased transduction efficiency by 3-fold relative to protamine sulfate alone and also increased the concentration of protamine sulfate required to achieve peak transduction. The additional data presented in Appendix A demonstrated that lysate coupled with an acoustic standing wave field treatment increased transduction efficiency while the acoustic treatment alone did not. Overall, the presence of lysate may explain some of the variability reported despite the use of consistent transduction methods. Furthermore, in the development of new techniques to increase retroviral transduction, the potential impact of lysate should be determined in order to appropriately resolve the mechanism of action.

The mechanistic analysis of cell lysates identified multiple modes of action that contribute to the increase in retroviral transduction:

1. Retroviral vectors adsorb onto debris aggregates improving mass transport to the target cell through sedimentation over a distance of at least 5000 μm.
2. Soluble and aggregate components improve adsorption of the retroviral vectors to the target cells.

3. Soluble and aggregate components also improve adsorption of the retroviral vectors to the culture vessel surface in proximity to the target cells.
4. Aggregate-bound retroviruses are maintained at the bottom of the culture vessel in proximity to the target cells by gravitational effects.

Thus, components within the lysate were able to improve mass transport as well as binding of the retroviral vector to the target cells, two key limitations in the retroviral transduction process and desirable attributes of an effective transduction reagent. A lysate fraction consisting of the remaining aggregates following DNAse treatment of the whole lysate aggregates (PD80P) was found to increase the transduction of mouse (nBaF3) and human (TF-1) cells lines by over 213- and 59-fold respectively when the lysed-to-target cell ratio was increased to 16. It was also effective on sensitive mouse hematopoietic progenitors with long-term reconstitution potential. This lysate-derived reagent outperformed both centrifugation and protamine sulfate transduction protocols with RAT-1 cells.

Characterization of the lysate-derived reagent identified the active component as an arginine- and/or lysine-rich peptide of nuclear origin such as histones. A subsequent screening study of bovine histone fractions found that arginine-rich histones including histone H3 but also containing H2A and H4, increased transduction at concentrations of up to 160 μg/mL with negligible cell toxicity. Similarly, the recombinant human arginine-rich histone H3.1 outperformed other histone proteins.

A histone-based reagent was developed by leveraging the knowledge derived from the fractionation analysis of the cell lysate. Aggregates were generated by heat-induced self-aggregation of the arginine-rich bovine histone fraction. The aggregated

histones increased the transduction of TF-1 cells by 34-fold relative to an untreated control compared with 22-fold for unaggregated histones while reducing the concentration required to less than 10 μg/mL from 160 μg/mL. When compared under similar conditions to the fractionated lysate (5×10^5 target cells/mL, 3 mm liquid depth), the performance of aggregated histones (34-fold increase) closely matched that of the PD80P lysate fraction (36-fold increase). With nBaF3 target cells, aggregated histones outperformed the PD80P lysate fraction with an increase in transduction of 156-fold compared with 118-fold for the PD80P. The aggregated histone reagent was also effective on primary mouse hematopoietic progenitor cells with reconstitution potential. It was applicable to both gammaretroviral and lentiviral vectors. The aggregated f_3 histones generally matched or exceeded the enhancement obtained with RetroNectin but were simpler to use as surface coating is not required. Overall, using the knowledge derived from this study of cell lysate, a histone-based transduction reagent was developed with negligible toxicity to cell lines as well as primary cells.

The scope of this thesis was limited to the impact of lysate and histones on extracellular transduction-limiting steps. In order to fully determine the mechanism of action, an analysis of the effect of these reagents on intracellular events is required. For example, it is unclear if aggregated histones are endocytosed together with the retroviral vectors. In the case where histones would remain associated with the vector post-entry, the ultimate fate of the reagent should be investigated to determine if it undergoes an early degradation or remains associated with the reverse transcription complex and potentially the pre-integration complex.

Histone aggregates were generated as a proof-of-concept and the aggregation process needs to be optimized as both the size of the aggregates and residual unaggregated histones are expected to influence transduction. Although H2A, H3 and H4 histones were all detected within the aggregate structures, it remains to be determined if all are essential to the formation of aggregates or if an optimal stoichiometric ratio exists between these 3 species. The histone domains (i.e. free cysteine residues, arginine/lysine clusters) responsible for the aggregation as well as the interaction with the retroviral vectors have yet to be identified. This knowledge could then be used to generate a recombinant version of the histone reagent, thus eliminating the need to rely on the potential variability of animal-origin histones.

While additional work is required to fully characterized the histone-based reagent, it represent a novel method offering a highly efficient, simple approach to enhanced the retroviral transduction with either gammaretroviral or lentiviral vectors of cell lines as well as primary cells with negligible toxicity. Overall this histone-based reagent could improve the outcome of scientific research as well as clinical trials that rely on retrovirus-mediated gene transfer.

Bibliography

Aiuti A, Cattaneo F, Galimberti S, Benninghoff U, Cassani B, Callegaro L, Scaramuzza S, Andolfi G, Mirolo M, Brigida I and others. 2009. Gene therapy for immunodeficiency due to adenosine deaminase deficiency. New England Journal of Medicine 360(5):447-458.

Andreadis S, Lavery T, Davis HE, Le Doux JM, Yarmush ML, Morgan JR. 2000. Toward a more accurate quantitation of the activity of recombinant retroviruses: Alternatives to titer and multiplicity of infection (vol 74, pg 1258, 2000). Journal of Virology 74(7):3431-3439.

Andreadis S, Palsson BO. 1997. Coupled effects of polybrene and calf serum on the efficiency of retroviral transduction and the stability of retroviral vectors. Human Gene Therapy 8(3):285-291.

Andreadis ST, Brott D, Fuller AO, Palsson BO. 1997. Moloney murine leukemia virus-derived retroviral vectors decay intracellularly with a half-life in the range of 5.5 to 7.5 hours. Journal of Virology 71(10):7541-7548.

Ansorge S, Henry O, Kamen A. 2010. Recent progress in lentiviral vector mass production. Biochemical Engineering Journal 48(3):362-377.

Baake M, Doenecke D, Albig W. 2001. Characterisation of nuclear localisation signals of the four human core histones. Journal of Cellular Biochemistry 81(2):333-346.

Bahnson AB, Dunigan JT, Baysal BE, Mohney T, Atchison RW, Nimgaonkar MT, Ball ED, Barranger JA. 1995. Centrifugal enhancement of retroviral-mediated gene-transfer. Journal of Virological Methods 54(2-3):131-143.

Bajaj B, Lei P, Andreadis ST. 2001. High efficiencies of gene transfer with immobilized recombinant retrovirus: Kinetics and optimization. Biotechnology Progress 17(4):587-596.

Balicki D, Beutler E. 1997. Histone H2A significantly enhances in vitro DNA transfection. Molecular Medicine 3(11):782-787.

Barker SL, LaRocca PJ. 1994. Method of production and control of a commercial tissue culture surface. Methods in Cell Science 16(3-4):151-153.

Beauchesne PR, Bruce KJ, Bowen BD, Piret JM. 2010. Effect of cell lysates on retroviral transduction efficiency of cells in suspension culture. Biotechnology and Bioengineering 105(6):1168-1177.

Becker PB, editor. 1999. Chromatin protocols. Totowa: Humana Press. 528 p.

Beer C, Andersen DS, Rojek A, Pedersen L. 2005. Caveola-dependent endocytic entry of amphotropic murine leukemia virus. Journal of Virology 79(16):10776-10787.

Beer C, Meyer A, Muller K, Wirth M. 2003. The temperature stability of mouse retroviruses depends on the cholesterol levels of viral lipid shell and cellular plasma membrane. Virology 308(1):137-146.

Beer C, Pedersen L. 2007. Matrix fibronectin binds gammaretrovirus and assists in entry: New light on viral infections. Journal of Virology 81(15):8247-8257.

Bodine DM, Mcdonagh KT, Seidel NE, Nienhuis AW. 1991. Survival and retrovirus infection of murine hematopoietic stem-cells invitro - Effects of 5-Fu and method of infection. Experimental Hematology 19(3):206-212.

Bowerman B, Brown PO, Bishop JM, Varmus HE. 1989. A Nucleoprotein Complex Mediates the Integration of Retroviral DNA. Genes & Development 3(4):469-478.

Breeuwer M, Goldfarb DS. 1990. Facilitated nuclear transport of histone H1 and other small nucleophilic proteins. Cell 60(6):999-1008.

Bryant CM, McClements DJ. 1999. Ultrasonic spectrometry study of the influence of temperature on whey protein aggregation. Food Hydrocolloids 13(6):439-444.

Burns JC, Friedmann T, Driever W, Burrascano M, Yee JK. 1993. Vesicular Stomatitis-Virus G Glycoprotein Pseudotyped Retroviral Vectors - Concentration to Very High-Titer and Efficient Gene-Transfer into Mammalian and Nonmammalian Cells. Proceedings of the National Academy of Sciences of the United States of America 90(17):8033-8037.

Buske C, Feuring-Buske M, Antonchuk J, Rosten P, Hogge DE, Eaves CJ, Humphries RK. 2001. Overexpression of HOXA10 perturbs human lymphomyelopoiesis in vitro and in vivo. Blood 97(8):2286-2292.

Carmo M, Faria TQ, Falk H, Coroadinha AS, Teixeira M, Merten OW, Geny-Fiamma C, Alves PM, Danos O, Panet A and others. 2006. Relationship between retroviral vector membrane and vector stability. Journal of General Virology 87:1349-1356.

Casali M, Zambonelli C, Goldwasser J, Vu HN, Yarmush ML. 2008. Moloney murine leukemia virus decay mediated by retroviral reverse transcriptase degradation of genomic RNA. Virology 380(1):91-98.

Chen J, Reeves L, Sanburn N, Croop J, Williams DA, Cornetta K. 2001. Packaging cell line DNA contamination of vector supernatants: Implication for laboratory and clinical research. Virology 282(1):186-197.

Chien ML, Foster JL, Douglas JL, Garcia JV. 1997. The amphotropic murine leukemia virus receptor gene encodes a 71-kilodalton protein that is induced by phosphate depletion. Journal of Virology 71(6):4564-4570.

Chuck AS, Clarke MF, Palsson BO. 1996. Retroviral infection is limited by Brownian motion. Human Gene Therapy 7(13):1527-1534.

Chuck AS, Palsson BO. 1996a. Consistent and high rates of gene transfer can be obtained using flow-through transduction over a wide range of retroviral titers. Human Gene Therapy 7(6):743-750.

Chuck AS, Palsson BO. 1996b. Membrane adsorption characteristics determine the kinetics of flow-through transductions. Biotechnology and Bioengineering 51(3):260-270.

Coil DA, Miller AD. 2004. Phosphatidylserine is not the cell surface receptor for vesicular stomatitis virus. Journal of Virology 78(20):10920-10926.

Coil DA, Miller AD. 2005a. Enhancement of enveloped virus entry by phosphatidylserine. Journal of Virology 79(17):11496-11500.

Coil DA, Miller AD. 2005b. Phosphatidylserine treatment relieves the block to retrovirus infection of cells expressing glycosylated virus receptors. Retrovirology 2:-.

Coll JM. 1995. The Glycoprotein-G of Rhabdoviruses. Archives of Virology 140(5):827-851.

Cornetta K, Anderson WF. 1989. Protamine sulfate as an effective alternative to polybrene in retroviral-mediated gene-transfer - Implications for human-gene therapy. Journal of Virological Methods 23(2):187-194.

Crane JK, Majumdar S, Pickhardt DF. 1999. Host cell death due to enteropathogenic Escherichia coli has features of apoptosis. Infection and Immunity 67(5):2575-2584.

Curl CL, Bellair CJ, Harris T, Allman BE, Harris PJ, Stewart AG, Roberts A, Nugent KA, Delbridge LMD. 2005. Refractive index measurement in viable cells using quantitative phase-amplitude microscopy and confocal microscopy. Cytometry Part A 65A(1):88-92.

D'Anna JA, Isenberg I. 1974. Conformational-changes of histone ARE (F3,III). Biochemistry 13(24):4987-4992.

Darling D, Hughes C, Galea-Lauri J, Gaken J, Trayner ID, Kuiper M, Farzaneh F. 2000. Low-speed centrifugation of retroviral vectors absorbed to a particulate substrate: a highly effective means of enhancing retroviral titre. Gene Therapy 7(11):914-923.

Davis HE, Morgan JR, Yarmush ML. 2002. Polybrene increases retrovirus gene transfer efficiency by enhancing receptor-independent virus adsorption on target cell membranes. Biophysical Chemistry 97(2-3):159-172.

Davis HE, Rosinski M, Morgan JR, Yarmush ML. 2004. Charged polymers modulate retrovirus transduction via membrane charge neutralization and virus aggregation. Biophysical Journal 86(2):1234-1242.

Deneault E, Cellot S, Faubert A, Laverdure JP, Frechette M, Chagraoui J, Mayotte N, Sauvageau M, Ting SB, Sauvageau G. 2009. A Functional Screen to Identify Novel Effectors of Hematopoietic Stem Cell Activity. Cell 137(2):369-379.

Dick JE, Kamelreid S, Murdoch B, Doedens M. 1991. Gene-transfer into normal human hematopoietic-cells using invitro and invivo assays. Blood 78(3):624-634.

Diggle JH, Mcvittie JD, Peacocke AR. 1975. Self-association of chicken erythrocyte histones. European Journal of Biochemistry 56(1):173-182.

Drouin H, Ritter JB, Gorenflo VM, Bowen BD, Piret JM. 2007. Cell separator operation within temperature ranges to minimize effects on Chinese hamster ovary cell perfusion culture. Biotechnology Progress 23(6):1473-1484.

Dunnett CW. 1964. New tables for multiple comparisons with a control. Biometrics 20(3):482-491.

Farrell KB, Russ JL, Murthy RK, Eiden MV. 2002. Reassessing the role of region A in Pit1-mediated viral entry. Journal of Virology 76(15):7683-7693.

Fassati A, Goff SP. 1999. Characterization of intracellular reverse transcription complexes of Moloney murine leukemia virus. Journal of Virology 73(11):8919-8925.

Fehse B, Kuhlcke K. 2008. Clinical application of a retroviral gene transfer protocol based on centrifugation-mediated vector preloading. Human Gene Therapy 19(6):655-656.

Fischer H, Polikarpov I, Craievich AF. 2004. Average protein density is a molecular-weight-dependent function. Protein Science 13(10):2825-2828.

Freberg CT, Dahl JA, Timoskainen S, Collas P. 2007. Epigenetic reprogramming of OCT4 and NANOG regulatory regions by embryonal carcinoma cell extract. Molecular Biology of the Cell 18(5):1543-1553.

Fujiki Y, Tao K, Bianchi DW, Giel-Moloney M, Leiter AB, Johnson KL. 2008. Quantification of green fluorescent protein by in vivo imaging, PCR, and flow cytometry: Comparison of transgenic strains and relevance for fetal cell microchimerism. Cytometry Part A 73A(2):111-118.

Garrard WT, Nobis P, Hancock R. 1977. Histone H-3 disulfide reactions in interphase, mitotic, and native chromatin. Journal of Biological Chemistry 252(14):4962-4967.

Gaspar HB, Parsley KL, Howe S, King D, Gilmour KC, Sinclair J, Brouns G, Schmidt M, Von Kalle C, Barington T and others. 2004. Gene therapy of X-linked severe combined immunodeficiency by use of a pseudotyped gammaretroviral vector. Lancet 364(9452):2181-2187.

Gorenflo VM, Angepat S, Bowen BD, Piret JM. 2003. Optimization of an acoustic cell filter with a novel air-backflush system. Biotechnology Progress 19(1):30-36.

Gorenflo VM, Beauchesne P, Tayi V, Lara O, Drouin H, Ritter JB, Chow V, Sherwood C, Bowen BD, Piret JM. Acoustic cell processing for viral transduction or bioreactor cell retention.; 2005; European Society for Animal Cell Culture Conference, Harrogate, UK.

Gorenflo VM, Smith L, Dedinsky B, Persson B, Piret JM. 2002. Scale-up and optimization of an acoustic filter for 200 L/day perfusion of a CHO cell culture. Biotechnol Bioeng 80(4):438-44.

Goulaouic H, Subra F, Mouscadet JF, Carteau S, Auclair C. 1994. Exogenous nucleosides promote the completion of MoMLV DNA-synthesis in G0-arrested Balb-C/3t3 fibroblasts. Virology 200(1):87-97.

Grabarczyk P, Wysocki PJ, Gryska K, Mackiewicz A. 2002. Expression of PiT1 and PiT2 retroviral receptors and transduction efficiency of tumor cells. Acta Biochimica Polonica 49(2):333-339.

Hacein-Bey-Abina S, Le Deist F, Carlier F, Bouneaud C, Hue C, De Villartay J, Thrasher AJ, Wulffraat N, Sorensen R, Dupuis-Girod S and others. 2002. Sustained correction of X-linked severe combined immunodeficiency by ex vivo gene therapy. New England Journal of Medicine 346(16):1185-1193.

Hake SB, Allis CD. 2006. Histone H3 variants and their potential role in indexing mammalian genomes: The "H3 barcode hypothesis". Proceedings of the National Academy of Sciences of the United States of America 103(17):6428-6435.

Hanawa H, Kelly PF, Nathwani AC, Persons DA, Vandergriff JA, Hargrove P, Vanin EF, Nienhuis AW. 2002. Comparison of various envelope proteins for their ability to pseudotype lentiviral vectors and transduce primitive hematopoietic cells from human blood. Molecular Therapy 5(3):242-251.

Hanenberg H, Hashino K, Konishi H, Hock RA, Kato I, Williams DA. 1997. Optimization of fibronectin-assisted retroviral gene transfer into human CD34(+) hematopoietic cells. Human Gene Therapy 8(18):2193-2206.

Hanenberg H, Xiao XL, Dilloo D, Hashino K, Kato I, Williams DA. 1996. Colocalization of retrovirus and target cells on specific fibronectin fragments increases genetic transduction of mammalian cells. Nature Medicine 2(8):876-882.

Hanes CS. 1932. Studies on plant amylase. I. The effect of starch concentration upon the velocity of hydrolysis by the amylase of germinated barley. Biochemical Journal 26(5):1406-1421.

Hariton-Gazal E, Rosenbluh J, Graessmann A, Gilon C, Loyter A. 2003. Direct translocation of histone molecules across cell membranes. Journal of Cell Science 116(22):4577-4586.

Hennemann B, Chuo JY, Schley PD, Lambie K, Humphries RK, Eaves CJ. 2000a. High-efficiency retroviral transduction of mammalian cells on positively charged surfaces. Human Gene Therapy 11(1):43-51.

Hennemann B, Conneally E, Pawliuk R, Leboulch P, Rose-John S, Reid D, Chuo JY, Humphries RK, Eaves CJ. 1999. Optimization of retroviral-mediated gene transfer to human NOD SCID mouse repopulating cord blood cells through a systematic analysis of protocol variables. Experimental Hematology 27(5):817-825.

Hennemann B, Oh IH, Chuo JY, Kalberer CP, Schley PD, Rose-John S, Humphries RK, Eaves CJ. 2000b. Efficient retrovirus-mediated gene transfer to transplantable human bone marrow cells in the absence of fibronectin. Blood 96(7):2432-2439.

Higashikawa F, Chang LJ. 2001. Kinetic analyses of stability of simple and complex retroviral vectors. Virology 280(1):124-131.

Hindmarsh P, Leis J. 1999. Retroviral DNA integration. Microbiology and Molecular Biology Reviews 63(4):836-+.

Hodgson CP, Solaiman F. 1996. Virosomes: Cationic liposomes enhance retroviral transduction. Nature Biotechnology 14(3):339-342.

Hughes C, Galea-Lauri J, Farzaneh F, Darling D. 2001. Streptavidin paramagnetic particles provide a choice of three affinity-based capture and magnetic concentration strategies for retroviral vectors. Molecular Therapy 3(4):623-630.

Hunter AC, Moghimi SM. 2010. Cationic carriers of genetic material and cell death: A mitochondrial tale. Biochimica Et Biophysica Acta-Bioenergetics 1797(6-7):1203-1209.

Izzo A, Kamieniarz K, Schneider R. 2008. The histone H1 family: specific members, specific functions? Biological Chemistry 389(4):333-343.

Jarousse N, Chandran B, Coscoy L. 2008. Lack of Heparan Sulfate Expression in B-Cell Lines: Implications for Kaposi's Sarcoma-Associated Herpesvirus and Murine Gammaherpesvirus 68 Infections. Journal of Virology 82(24):12591-12597.

Jensen TW, Chen Y, Miller WM. 2003. Small increases in pH enhance retroviral vector transduction efficiency of NIH-3T3 cells. Biotechnology Progress 19(1):216-223.

Jin J, Sherer NM, Heidecker G, Derse D, Mothes W. 2009. Assembly of the murine leukemia virus is directed towards sites of cell-cell contact. Plos Biology 7(7):-.

Jones LJ, Gray M, Yue ST, Haugland RP, Singer VL. 2001. Sensitive determination of cell number using the CyQUANT (R) cell proliferation assay. Journal of Immunological Methods 254(1-2):85-98.

Jones RJ, Wagner JE, Celano P, Zicha MS, Sharkis SJ. 1990. Separation of pluripotent hematopoietic stem-cells from spleen colony-forming cells. Nature 347(6289):188-189.

Kafri T, van Praag H, Ouyang L, Gage FH, Verma IM. 1999. A packaging cell line for lentivirus vectors. Journal of Virology 73(1):576-584.

Katen LJ, Januszeski MM, Anderson WF, Hasenkrug KM, Evans LH. 2001. Infectious entry by amphotropic as well as ecotropic murine leukemia viruses occurs through an endocytic pathway. Journal of Virology 75(11):5018-5026.

Kim JW, Closs EI, Albritton LM, Cunningham JM. 1991. Transport of cationic amino-acids by the mouse ecotropic retrovirus receptor. Nature 352(6337):725-728.

Kim YC, Kang JH, Park SJ, Yoon ES, Park JK. 2007. Microfluidic biomechanical device for compressive cell stimulation and lysis. Sensors and Actuators B-Chemical 128(1):108-116.

Kim YS, Wielgosz MM, Hargrove P, Kepes S, Gray J, Persons DA, Nienhuis AW. 2010. Transduction of human primitive repopulating hematopoietic cells with lentiviral vectors pseudotyped with various envelope proteins. Molecular Therapy 18(7):1310-1317.

Kinsella TM, Nolan GP. 1996. Episomal vectors rapidly and stably produce high-titer recombinant retrovirus. Human Gene Therapy 7(12):1405-1413.

Kizhatil K, Albritton LM. 1997. Requirements for different components of the host cell cytoskeleton distinguish ecotropic murine leukemia virus entry via endocytosis from entry via surface fusion. Journal of Virology 71(10):7145-7156.

Klein D, Indraccolo S, vonRombs K, Amadori A, Salmons B, Gunzburg WH. 1997. Rapid identification of viable retrovirus-transduced cells using the green fluorescent protein as a marker. Gene Therapy 4(11):1256-1260.

Knipe D, Howley P, Griffin D, Lamb R, Martin M, Roizman B, Straus S. 2007. Field's virology. New York: Wolters Luwer / Lippincott Williams & Wilkings. 3177 p.

Kohn DB, Candotti F. 2009. Gene Therapy Fulfilling Its Promise. New England Journal of Medicine 360(5):518-521.

Kotani H, Newton PB, Zhang SY, Chiang YWL, Otto E, Weaver L, Blaese RM, Anderson WF, Mcgarrity GJ. 1994. Improved Methods of Retroviral Vector Transduction and Production for Gene-Therapy. Human Gene Therapy 5(1):19-28.

Kuhlcke K, Fehse B, Schilz A, Loges S, Lindemann C, Ayuk F, Lehmann F, Stute N, Fauser AA, Zander AR and others. 2002. Highly efficient retroviral gene transfer based on centrifugation-mediated vector preloading of tissue culture vessels. Molecular Therapy 5(4):473-478.

Kureishy N, Faruque D, Porter CD. 2006. Primary attachment of murine leukaemia virus vector mediated by particle-associated heparan sulfate proteoglycan. Biochemical Journal 400:421-430.

Kustikova OS, Wahlers A, Kuhicke K, Stahle B, Zander AR, Baum C, Fehse B. 2003. Dose finding with retroviral vectors: correlation of retroviral vector copy numbers in single cells with gene transfer efficiency in a cell population. Blood 102(12):3934-3937.

Kwon YJ, Hung G, Anderson WF, Peng CA, Yu H. 2003. Determination of infectious retrovirus concentration from colony-forming assay with quantitative analysis. Journal of Virology 77(10):5712-5720.

Kwon YJ, Peng CA. 2002a. Engineering analysis of ex vivo retroviral transduction system. Annals of Biomedical Engineering 30(5):731-742.

Kwon YJ, Peng CA. 2002b. Transduction rate constant as more reliable index quantifying efficiency of retroviral gene delivery. Biotechnology and Bioengineering 77(6):668-677.

Lazarides E, Lindberg U. 1974. Actin is the naturally occcurring inhibitor of deoxyribonuclease-I. Proceedings of the National Academy of Sciences of the United States of America 71(12):4742-4746.

Le Doux JM, Landazuri N, Yarmush ML, Morgan JR. 2001. Complexation of retrovirus with cationic and anionic polymers increases the efficiency of gene transfer. Human Gene Therapy 12(13):1611-1621.

Le Doux JM, Morgan JR, Snow RG, Yarmush ML. 1996. Proteoglycans secreted by packaging cell lines inhibit retrovirus infection. Journal of Virology 70(9):6468-6473.

Le Doux JM, Morgan JR, Yarmush ML. 1999. Differential inhibition of retrovirus transduction by proteoglycans and free glycosaminoglycans. Biotechnology Progress 15(3):397-406.

Lee MS, Craigie R. 1998. A previously unidentified host protein protects retroviral DNA from autointegration. Proceedings of the National Academy of Sciences of the United States of America 95(4):1528-1533.

Lee SY, Zho Y, Anderson WF. 1999. Receptor-mediated moloney murine leukemia virus entry can occur independently of the clathrin-coated-pit-mediated endocytic pathway. Journal of Virology 73(7):5994-6005.

Lee YH, Peng CA. 2005. Enhanced retroviral gene delivery in ultrasonic standing wave fields. Gene Therapy 12(7):625-633.

Lee YH, You JO, Peng CA. 2005. Retroviral transduction of adherent cells in resonant acoustic fields. Biotechnology Progress 21(2):372-376.

Lei P, Bajaj B, Andreadis ST. 2002. Retrovirus-associated heparan sulfate mediates immobilization and gene transfer on recombinant fibronectin. Journal of Virology 76(17):8722-8728.

Levy JA, editor. 1992. The Retroviridae. New York: Plenum Press. 489 p.

Lewis PF, Emerman M. 1994. Passage through mitosis is required for oncoretroviruses but not for the human-immunodeficiency-virus. Journal of Virology 68(1):510-516.

Limaye MS, Hawkes JJ, Coakley WT. 1996. Ultrasonic standing wave removal of microorganisms from suspension in small batch systems. Journal of Microbiological Methods 27(2-3):211-220.

Lu XB, Silver J. 2000. Ecotropic murine leukemia virus receptor is physically associated with caveolin and membrane rafts. Virology 276(2):251-258.

Luger K, Mader AW, Richmond RK, Sargent DF, Richmond TJ. 1997. Crystal structure of the nucleosome core particle at 2.8 angstrom resolution. Nature 389(6648):251-260.

Makino M, Ishikawa G, Yamaguchi K, Okada Y, Watanabe K, Sasakiiwaki Y, Manabe S, Honda M, Komuro K. 1994. Concentration of live retrovirus with a regenerated cellulose hollow-fiber, bmm. Archives of Virology 139(1-2):87-96.

Mann R, Mulligan RC, Baltimore D. 1983. Construction of a retrovirus packaging mutant and its use to produce helper-free defective retrovirus. Cell 33(1):153-159.

Markowitz D, Goff S, Bank A. 1988. A safe packaging line for gene-transfer - Separating viral genes on 2 different plasmids. Journal of Virology 62(4):1120-1124.

McNiece IK, Almeida-Porada G, Shpall EJ, Zanjani E. 2002. Ex vivo expanded cord blood cells provide rapid engraftment in fetal sheep but lack long-term engrafting, potential. Experimental Hematology 30(6):612-616.

McTaggart S, Al-Rubeai M. 2000. Effects of culture parameters on the production of retroviral vectors by a human packaging cell line. Biotechnology Progress 16(5):859-865.

Miller AD, Buttimore C. 1986. Redesign of retrovirus packaging cell-lines to avoid recombination leading to helper virus production. Molecular and Cellular Biology 6(8):2895-2902.

Miller AD, Garcia JV, Vonsuhr N, Lynch CM, Wilson C, Eiden MV. 1991. Construction and properties of retrovirus packaging cells based on gibbon ape leukemia-virus. Journal of Virology 65(5):2220-2224.

Miller DG, Adam MA, Miller AD. 1990. Gene-transfer by retrovirus vectors occurs only in cells that are actively replicating at the time of infection. Molecular and Cellular Biology 10(8):4239-4242.

Morgan JR, Ledoux JM, Snow RG, Tompkins RG, Yarmush ML. 1995. Retrovirus infection - Effect of time and target-cell number. Journal of Virology 69(11):6994-7000.

Moritz T, Keller DC, Williams DA. 1993. Human cord-blood cells as targets for gene-transfer - Potential use in genetic therapies of severe combined immunodeficiency disease. Journal of Experimental Medicine 178(2):529-536.

Moritz T, Patel VP, Williams DA. 1994. Bone-marrow extracellular-matrix molecules improve gene-transfer into human hematopoietic-cells via retroviral vectors. Journal of Clinical Investigation 93(4):1451-1457.

Morling FJ, Russell SJ. 1995. Enhanced transduction efficiency of retroviral vectors coprecipitated with calcium-phosphate. Gene Therapy 2(7):504-508.

Naka T, Sakoda T, Doi T, Tsujino T, Masuyama T, Kawashima S, Iwasaki T, Ohyanagi M. 2007. Ultrasound enhances retrovirus-mediated gene transfer. Preparative Biochemistry & Biotechnology 37(2):87-99.

Naldini L, Blomer U, Gallay P, Ory D, Mulligan R, Gage FH, Verma IM, Trono D. 1996. In vivo gene delivery and stable transduction of nondividing cells by a lentiviral vector. Science 272(5259):263-267.

O'Hara B, Johann SV, Klinger HP, Blair DG, Rubinson H, Dunn KJ, Sass P, Vitek SM, Robins T. 1990. Characterization of a human gene conferring sensitivity to infection by gibbon ape leukemia-virus. Cell Growth & Differentiation 1(3):119-127.

Ohta H, Sekulovic S, Bakovic S, Eaves CJ, Pineault N, Gasparetto M, Smith C, Sauvageau G, Humphries RK. 2007. Near-maximal expansions of hematopoietic stem cells in culture using NUP98-HOX fusions. Experimental Hematology 35(5):817-830.

Olah Z, Lehel C, Anderson WB, Eiden MV, Wilson CA. 1994. The cellular receptor for gibbon ape leukemia-virus is a novel high-affinity sodium-dependent phosphate transporter. Journal of Biological Chemistry 269(41):25426-25431.

Ory DS, Neugeboren BA, Mulligan RC. 1996. A stable human-derived packaging cell line for production of high titer retrovirus/vesicular stomatitis virus G pseudotypes. Proceedings of the National Academy of Sciences of the United States of America 93(21):11400-11406.

Palacios R, Steinmetz M. 1985. Il3-dependent mouse clones that express B-220 surface-antigen, contain Ig genes in germ-line configuration, and generate lymphocytes-B in vivo. Cell 41(3):727-734.

Palsson B, Andreadis S. 1997. The physico-chemical factors that govern retrovirus-mediated gene transfer. Experimental Hematology 25(2):94-102.

Pan D, Gunther R, Duan WM, Wendell S, Kaemmerer W, Kafri T, Verma IM, Whitley CB. 2002. Biodistribution and toxicity studies of VSVG-pseudotyped lentiviral vector after intravenous administration in mice with the observation of in vivo transduction of bone marrow. Molecular Therapy 6(1):19-29.

Paul RW, Morris D, Hess BW, Dunn J, Overell RW. 1993. Increased viral titer through concentration of viral harvests from retroviral packaging lines. Human Gene Therapy 4(5):609-615.

Pham L, Ye H, Cosset FL, Russell SJ, Peng KW. 2001. Concentration of viral vectors by co-precipitation with calcium phosphate. Journal of Gene Medicine 3(2):188-194.

Pizzato M, Marlow SA, Blair ED, Takeuchi Y. 1999. Initial binding of murine leukemia virus particles to cells does not require specific Env-receptor interaction. Journal of Virology 73(10):8599-8611.

Porter CD, Lukacs KV, Box G, Takeuchi Y, Collins MKL. 1998. Cationic liposomes enhance the rate of transduction by a recombinant retroviral vector in vitro and in vivo. Journal of Virology 72(6):4832-4840.

Prachar J, Hlubinova K, Kovarik A, Feldsamova A, Simkovic D. 1988. Concentration of retroviruses by low-speed centrifugation. Neoplasma 35(6):651-655.

Pui PWS, Trampler F, Sonderhoff SA, Groeschl M, Kilburn DG, Piret JM. 1995. Batch and semicontinuous aggregation and sedimentation of hybridoma cells by acoustic-resonance fields. Biotechnology Progress 11(2):146-152.

Ramsey WS, Hertl W, Nowlan ED, Binkowski NJ. 1984. Surface treatments and cell attachment. In Vitro-Journal of the Tissue Culture Association 20(10):802-808.

Reeves L, Cornetta K. 2000. Clinical retroviral vector production: step filtration using clinically approved filters improves titers. Gene Therapy 7(23):1993-1998.

Reeves L, Smucker P, Cornetta K. 2000. Packaging cell line characteristics and optimizing retroviral vector titer: The National Gene Vector Laboratory Experience. Human Gene Therapy 11(15):2093-2103.

Relander T, Brun ACM, Olsson K, Pedersen L, Richter J. 2002. Overexpression of gibbon ape leukemia virus (GALV) receptor (GLVR1) on human CD34(+) cells increases gene transfer mediated by GALV pseudotyped vectors. Molecular Therapy 6(3):400-406.

Roark DE, Geoghegan TE, Keller GH, Matter KV, Engle RL. 1976. Histone interactions in solution and susceptibility to denaturation. Biochemistry 15(14):3019-3025.

Roe TY, Reynolds TC, Yu G, Brown PO. 1993. Integration of murine leukemia-virus DNA depends on mitosis. Embo Journal 12(5):2099-2108.

Rosenbluh J, Hariton-Gazal E, Dagan A, Rottem S, Graessmann A, Loyter A. 2005. Translocation of histone proteins across lipid bilayers and mycoplasma membranes. Journal of Molecular Biology 345(2):387-400.

Ruiz-Carrillo A, Allfrey VG. 1973. Method for purification of histone fraction f3 by affinity chromatography. Archives of Biochemistry and Biophysics 154(1):185-191.

Sastry L, Xu Y, Cooper R, Pollok K, Cornetta K. 2004. Evaluation of plasmid DNA removal from lentiviral vectors by benzonase treatment. Human Gene Therapy 15(2):221-226.

Schagger H. 2006. Tricine-SDS-PAGE. Nature Protocols 1(1):16-22.

Schwamborn K, Albig W, Doenecke D. 1998. The histone H1 degrees contains multiple sequence elements for nuclear targeting. Experimental Cell Research 244(1):206-217.

Seamon JA, Jones KS, Miller C, Roth MJ. 2002. Inserting a nuclear targeting signal into a replication-competent Moloney murine leukemia virus affects viral export and is not sufficient for cell cycle-independent infection. Journal of Virology 76(16):8475-8484.

Segura MD, Kamen A, Garnier A. 2006. Downstream processing of oncoretroviral and lentiviral gene therapy vectors. Biotechnology Advances 24(3):321-337.

Segura MM, Kamen A, Lavoie MC, Garnier A. 2007. Exploiting heparin-binding properties of MoMLV-based retroviral vectors for affinity chromatography. J Chromatogr B Analyt Technol Biomed Life Sci 846(1-2):124-31.

Seitz B, Baktanian E, Gordon EM, Anderson WF, LaBree L, McDonnell PJ. 1998. Retroviral vector-mediated gene transfer into keratocytes: in vitro effects of polybrene and protamine sulfate. Graefes Archive for Clinical and Experimental Ophthalmology 236(8):602-612.

Sharma S, Miyanohara A, Friedmann T. 2000. Separable mechanisms of attachment and cell uptake during retrovirus infection. Journal of Virology 74(22):10790-10795.

Shechter D, Dormann HL, Allis CD, Hake SB. 2007. Extraction, purification and analysis of histones. Nature Protocols 2(6):1445-1457.

Singh D, Rigby PWJ. 1996. The use of histone as a facilitator to improve the efficiency of retroviral gene transfer. Nucleic Acids Research 24(15):3113-3114.

Sliva K, Schnierle BS. 2010. Selective gene silencing by viral delivery of short hairpin RNA. Virology Journal 7:n/a.

Song WZ, Zhang XM, Liu AQ, Lim CS, Yap PH, Hosseini HMM. 2006. Refractive index measurement of single living cells using on-chip Fabry-Perot cavity. Applied Physics Letters 89(20): 1-3.

Sperling R, Bustin M. 1975. Dynamic equilibrium in histone assembly - Self-assembly of single histones and histone pairs. Biochemistry 14(15):3322-3331.

Suzuki Y, Craigie R. 2007. The road to chromatin - nuclear entry of retroviruses. Nature Reviews Microbiology 5(3):187-196.

Szyda A, Paprocka M, Krawczenko A, Lenart K, Heimrath J, Grabarczyk P, Mackiewicz A, Dus D. 2006. Optimization of a retroviral vector for transduction of human CD34 positive cells. Acta Biochimica Polonica 53(4):815-823.

Tavoloni N, Rudenholz A. 1997. Variable transduction efficiency of murine leukemia retroviral vector on mammalian cells: Role of cellular glycosylation. Virology 229(1):49-56.

Tayi V. 2010. Quantitative analysis of retrovirus-mediated gene transfer into mammalian cells [Doctoral Thesis]. Vancouver: University of British Columbia.

Tayi VS, Bowen BD, Piret JM. 2010. Mathematical model of the rate-limiting steps for retrovirus-mediated gene transfer into mammalian cells. Biotechnology and Bioengineering 105(1):195-209.

Tenenbaum L, Hamdane M, Pouzet M, Avalosse B, Stathopoulos A, Jurysta F, Rosenbaum C, Hanemann CO, Levivier M, Velu T. 1999. Cellular contaminants of adeno-associated virus vector stocks can enhance transduction. Gene Therapy 6(6):1045-1053.

Themis M, Forbes SJ, Chan L, Cooper RG, Etheridge CJ, Miller AD, Hodgson HJF, Coutelle C. 1998. Enhanced in vitro and in vivo gene delivery using cationic agent complexed retrovirus vectors. Gene Therapy 5(9):1180-1186.

Thrasher AJ, Hacein-Bey-Abina S, Gaspar HB, Blanche S, Davies EG, Parsley K, Gilmour K, King D, Howe S, Sinclair J and others. 2005. Failure of SCID-X1 gene therapy in older patients. Blood 105(11):4255-4257.

Toyoshima K, Vogt PK. 1969. Enhancement and inhibition of avian sarcoma viruses by polycations and polyanions. Virology 38(3):414-426.

Trampler F, Sonderhoff SA, Pui PWS, Kilburn DG, Piret JM. 1994. Acoustic cell filter for high-density perfusion culture of hybridoma cells. Bio-Technology 12(3):281-284.

Trexler-Schmidt M, Sargis S, Chiu J, Sze-Khoo S, Mun M, Kao YH, Laird MW. 2010. Identification and prevention of antibody disulfide bond reduction during cell culture manufacturing. Biotechnology and Bioengineering 106(3):452-461.

Valentine RC, Allison AC. 1959. Virus particle adsorption .1. Theory of adsorption and experiments on the attachment of particles to non-biological surfaces. Biochimica Et Biophysica Acta 34(1):10-23.

vanHolde KE. 1989. Chromatin. Rich A, editor. New York: Springer-Verlag. 497 p.

Vauthier C, Schmidt C, Couvreur P. 1999. Measurement of the density of polymeric nanoparticulate drug carriers by isopycnic centrifugation. Journal of Nanoparticle Research 1(3):411-418.

Wagner A, Marc A, Engasser JM, Einsele A. 1992. The use of lactate-dehydrogenase (Ldh) release kinetics for the evaluation of death and growth of mammalian-cells in perfusion reactors. Biotechnology and Bioengineering 39(3):320-326.

Wagstaff KM, Glover DJ, Tremethick DJ, Jans DA. 2007. Histone-mediated transduction as an efficient means for gene delivery. Molecular Therapy 15(4):721-731.

Wang H, Kavanaugh MP, North RA, Kabat D. 1991. Cell-surface receptor for ecotropic murine retroviruses is a basic-amino-acid transporter. Nature 352(6337):729-731.

Warnock JN, Merten OW, Al-Rubeai M. 2006. Cell culture processes for the production of viral vectors for gene therapy purposes. Cytotechnology 50(1-3):141-162.

Watson K, Gooderham NJ, Davies DS, Edwards RJ. 1999. Nucleosomes bind to cell surface proteoglycans. Journal of Biological Chemistry 274(31):21707-21713.

Woodside SM, Bowen BD, Piret JM. 1997. Measurement of ultrasonic forces for particle-liquid separations. Aiche Journal 43(7):1727-1736.

Woodside SM, Piret JM, Groschl M, Benes E, Bowen BD. 1998. Acoustic force distribution in resonators for ultrasonic particle separation. Aiche Journal 44(9):1976-1984.

Yang YW, Hsieh YC. 2001. Protamine sulfate enhances the transduction efficiency of recombinant adeno-associated virus-mediated gene delivery. Pharmaceutical Research 18(7):922-927.

Yu H, Soong N, Anderson WF. 1995. Binding-kinetics of ecotropic (Moloney) murine leukemia retrovirus with NIH 3T3 cells. Journal of Virology 69(10):6557-6562.

Appendix

Appendix A. Evaluation of Acoustic Standing Wave Fields for Large-Scale Retroviral Transduction of Suspension Cells

A.1 Introduction

Acoustic standing wave fields have been used to manipulate fine particles based on differences in compressibility and density relative to the surrounding medium (Woodside et al. 1997). Particles of greater density and lower compressibility than the medium will be displaced to and accumulate within the pressure node planes of the wave fields. Such acoustic fields have been successfully applied to biological systems as a cell retention device in mammalian cell perfusion cultures (Gorenflo et al. 2003; Gorenflo et al. 2002). Recently, in experiments using a small-scale (~5 mL) acoustic device, they have also been reported to enhance the retroviral transduction of suspension as well as adherent cell lines, presumably through increased convection due to microstreaming (Lee and Peng 2005; Lee et al. 2005).

While promising, this small-scale approach would need to be adapted to the large number of cells (up to 4×10^7 cells/kg of body weight) required in clinical trials (Aiuti et al. 2009; Gaspar et al. 2004; Thrasher et al. 2005). In this work a larger-scale retroviral transduction device was designed to employ acoustic standing wave fields. This was done by adapting a BioSep 10L acoustic cell separator for use on a 100-mL stirred suspension system that was then tested with TF-1 cells and retroviral vectors pseudotyped with the gibbon ape leukemia virus (GALV) envelope (Gorenflo et al. 2005). As a decline in viable cell concentration, presumably due to cell lysis, was observed at higher power inputs and for prolonged exposure, the acoustic body was redesigned to improve heat dissipation from the piezoelectric transducer. This system enabled the acoustic

treatment of cells suspended in VCM without the occurrence of lysis. Finally, in order to investigate a potential interaction between cell lysate and the acoustic standing wave field, the lysate was mixed together with the target cells and retroviral vectors, and treated using the improved, non-cell-lysing, system. These efforts will provide valuable insight into the mechanism of action of acoustic standing wave fields on retroviral transduction.

A.2 Materials and methods

A.2.1 Cell lines and retroviral vectors

Human erythroleukemia TF-1 cells (CRL-2003, American Type Culture Collection (ATCC), Manassas, VA, USA) were cultured in Dulbecco's modified Eagle's medium (DMEM) (Invitrogen, Burlington, ON, Canada) supplemented with 10% FBS (Invitrogen) and 5 ng/mL human recombinant GM-CSF (Terry Fox Laboratory (TFL), Vancouver, BC, Canada).

Retroviral vectors with an enhanced green fluorescent protein (GFP) reporter gene under the control of MSCV long terminal repeats pseudotyped with a gibbon ape leukemia virus (GALV-GFP) envelope were produced from PG-13 packaging cells (Hennemann et al. 1999; Miller et al. 1991) cultured in DMEM with 10% FBS in 850 cm^2 roller bottles (Corning, Lowell, MA, USA) at 37^oC and 10% CO_2 in air. Up to 3 retroviral vector harvests were initiated after the cultures reached 90% confluence and were performed at 24 h intervals (Reeves et al. 2000). Virus-containing medium (VCM) was filtered with a 0.45 μm pore size Durapore PVDF membrane (Millipore, Billerica, MA, USA) and frozen at −80^oC.

A.2.2 Flow-through acoustic standing wave field device (BioSep 10L)

A BioSep 10L acoustic resonator (Applikon Biotechnology, Foster City, USA), typically used as a cell retention device in perfusion cultures, was modified as follows. The cell suspension was fed from the bottom (Figure A.1a) rather than at a downward angle from the side (Figure A.1b). This change in flow pattern was made in order to increase the residence time of the cells within the acoustic chamber. The modified BioSep 10L was then mounted on a 100-mL spinner flask (Bellco Biotechnology) (Figure A.2). The clarified medium outlet was connected to a 25-mL glass pipette that acted as a reservoir and was also used to monitor flow rates. The top of the pipette, in turn, was connected to a computer-operated peristaltic pump. Finally, the pump was connected back to the spinner flask to close the loop. In order to maintain a suitable pH, a mixture of 10% CO_2 in air was fed into the head-space of the spinner flask. The gas was vented in order to maintain isobaric conditions; and 0.22 μm filters were placed on the gas inlet and outlet as well as on both sides of the pump tubing to maintain aseptic conditions. Temperature control was maintained at 37^{o}C in the spinner flask by a water bath.

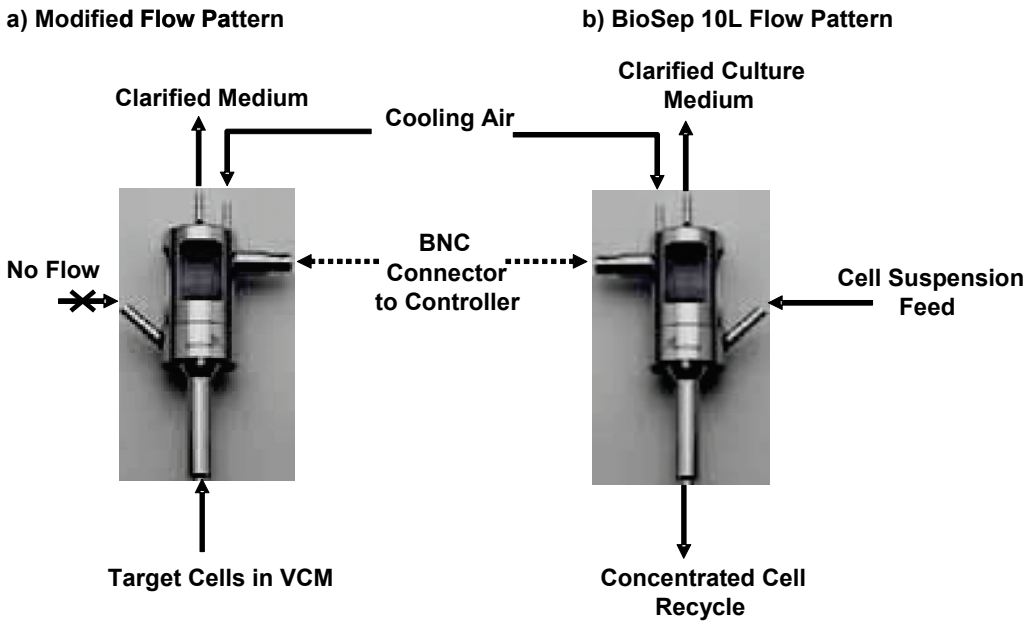

Figure A.1 Modified BioSep 10 L flow pattern.
a) The flow pattern was modified such that cells suspended in VCM were fed from the bottom of the BioSep 10L rather than at a downward angle from the side.
b) The recommended flow pattern for the BioSep 10L when used as a cell retention device in perfusion cultures. The cell suspension is fed from the side at a downward angle while the concentrated cell recycle exits from the bottom and the clarified medium from the top.

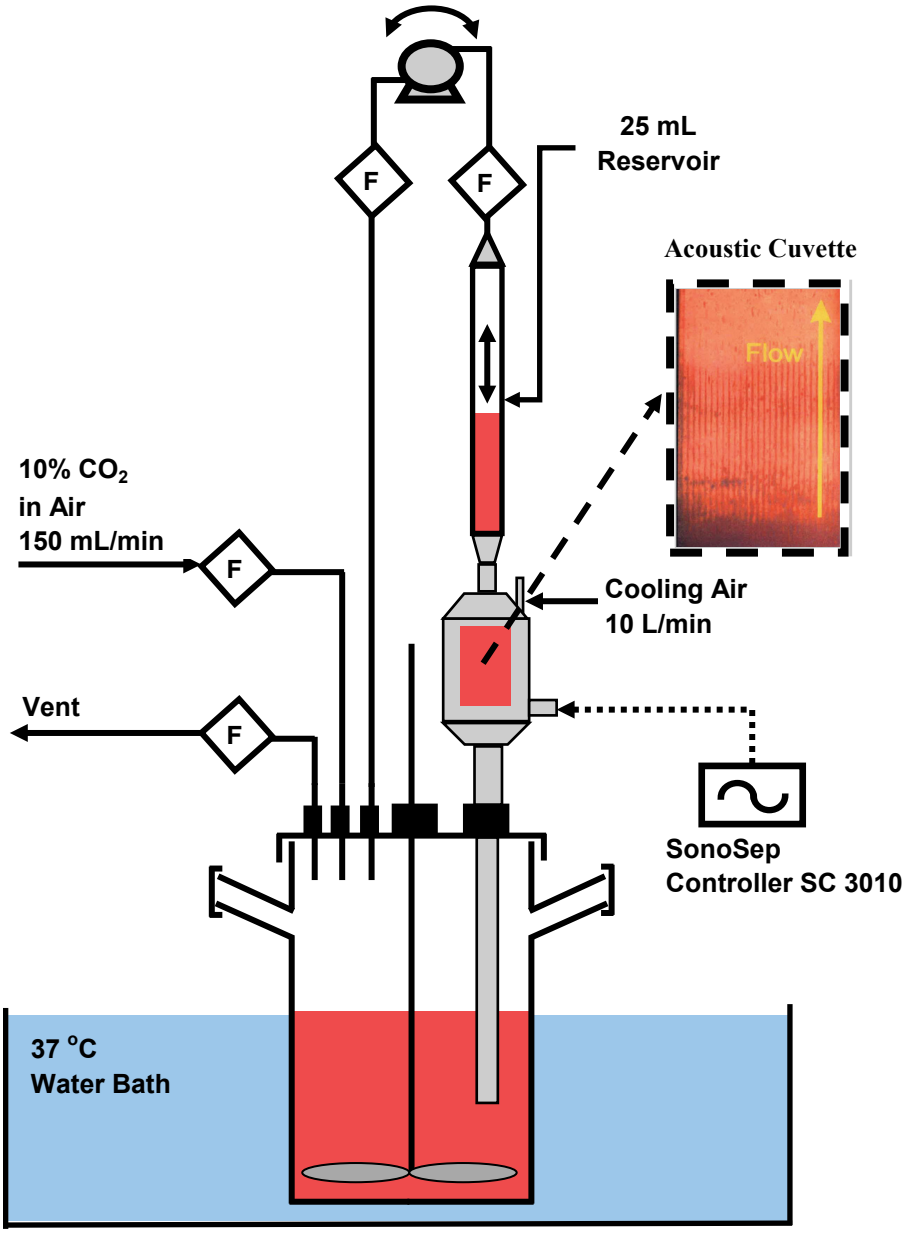

Figure A.2 Schematic diagram of the flow-through acoustic standing wave field system.
The system uses a modified BioSep 10L acoustic cell retention device mounted on a 100-mL spinner flask.

A suspension of TF-1 cells resuspended in a mixture of VCM diluted 1:2 with growth medium was added to the acoustic system and to a parallel control culture in an untreated T-75 flask (Sarstedt, Nümbrecht, Germany). In a limited number of experiments, the retroviral transduction achieved in an untreated stirred suspension was

also measured. Protamine sulfate (Sigma-Aldrich, St-Louis, MO, USA) was added to one run at 5 µg/mL using a 1 mg/mL stock solution prepared in PBS. The system was first primed to fill the acoustic chamber (Figure A.3). The piezoelectric transducer operating at a frequency of 1.95 MHz was then turned on and 25 mL of cell suspension were passed through the chamber. The acoustic resonator was then turned off and the contents of the reservoir and the acoustic chamber were back-flushed to the spinner flask. This process was repeated until the end of the transduction process. Periodically, samples were taken from the spinner flask as well as from the control cultures. The operating conditions are summarized in Table A.1.

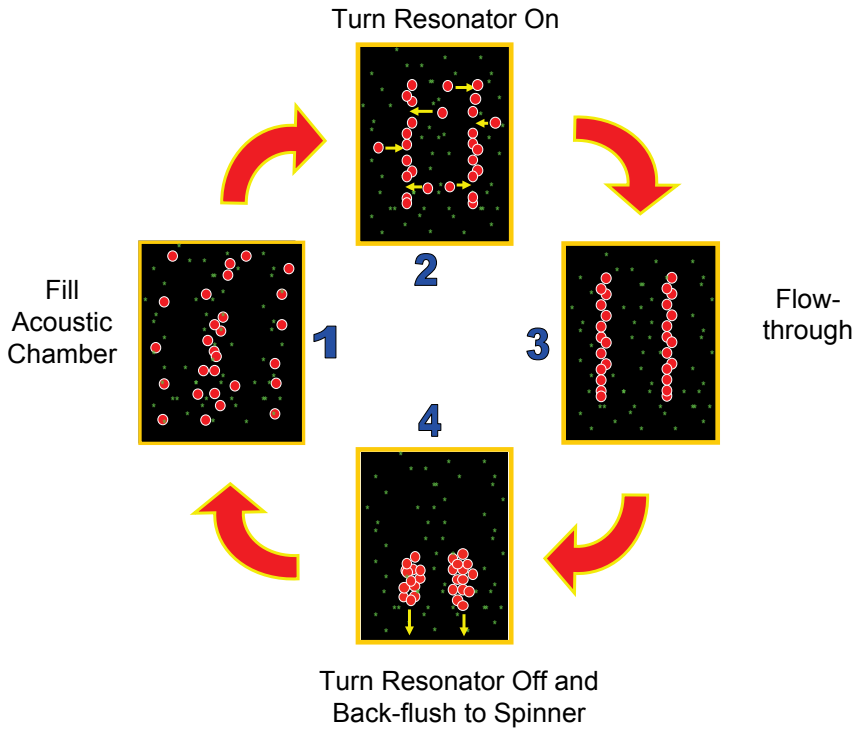

Figure A.3 Acoustic resonator operation cycle.

Table A.1 Acoustic flow-through system operating conditions using a 100-mL spinner flask design

Parameters	Step	Operating Range
Operating frequency	Flow-through	1.95 MHz
Power input	Flow-though	up to 5 W
Volume per cycle (Flow rate)	Prime	~18.5 mL (80 mL/min)
	Flow-through	~25 mL (7 mL/min)
	Back-flush	~50 mL (80 mL/min)
Cell suspension	Concentration	0.5 - 1.2 × 10^6/mL
	Volume	75 - 150 mL
Cooling air	Continuous	10 L/min
10% CO_2 in air	Continuous	120 - 150 mL/min

A.2.3 Transduction assay

3 mL samples of TF-1 cells in VCM were collected at specified times from the acoustically-treated spinner flask, the untreated spinner flask and the control T-flask. 0.6 mL of the cell sample was transferred to each of 2 wells of a non–tissue-culture-treated 6-well plate (Sarstedt). The cell suspension was diluted 1:5 with 2.4 mL of TF-1 growth medium. Cells were expanded in a 37ºC, 5% CO_2 balance air, humidified incubator for a total of 72 h from the start of the treatment. Transduction efficiency was measured using a FACS Calibur or FACS Scan (BD Biosciences, San Jose, CA, USA).

A.2.4 Cell viability and concentration

Cell viabilities and concentrations were measured using a Cedex automated cell counter (Innovatis, Bielefeld, Germany). Viable cell numbers were determined by the trypan blue exclusion method. The average of 20 images analyzed with the Std. Cell (v 5.00) algorithm was taken for each sample.

A.2.5 Cell lysate preparation

TF-1 cells in exponential growth were resuspended in DMEM at 4×10^6 lysed cells/mL and aliquoted into 5 mL fractions. The cells were frozen at -80^oC, thawed at 37^oC for 30 minutes and refrozen at -80^oC until use. These cell lysates were added to the target and VCM mixtures as required.

A.3 Results

A.3.1 Acoustic flow-through system (BioSep 10L)

Treatment of TF-1 cells suspended in VCM by the acoustic flow-through system at 5 W power input and 7 mL/min perfusion increased the transduction efficiency by 3- to 8-fold compared to T-flask control (Figure A.4). During the initial 2 - 4 h of treatment, the transduction rate increased relative to the control until a plateau was reached. In trial #1, the increase was sustained over the full 24 h of treatment, such that most of the retroviral vectors would have decayed. However, in each trial, cell recovery was low, ranging from 72% after 24 h in trial #1 to only 1% after only 6 h of treatment in trial #6. It was unclear whether the loss resulted from cells adsorbing to surfaces within the system or, since some cell debris was visible, if cell lysis had occurred. The addition of protamine sulfate (5 μg/mL) did not alter the response of the acoustic system.

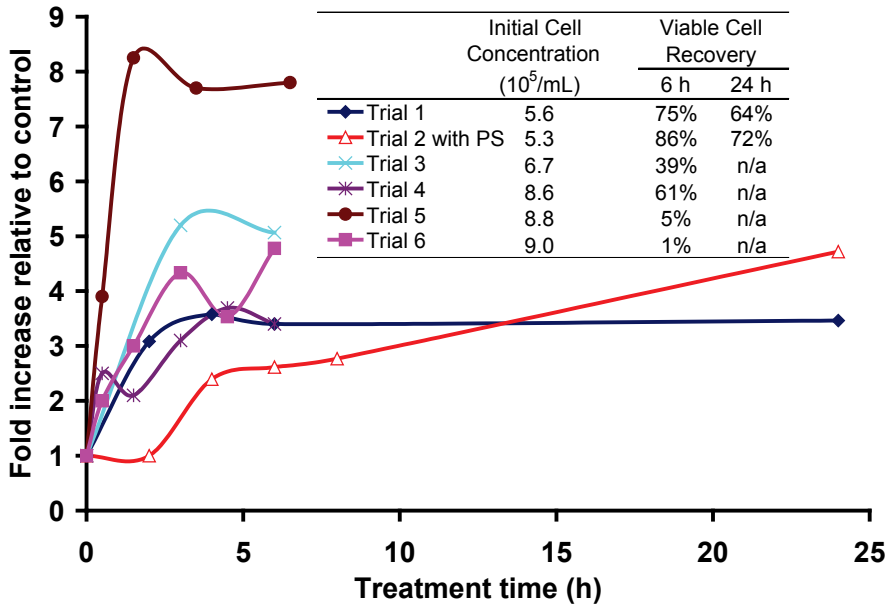

Figure A.4 Increase in the transduction efficiency of TF-1 cells with acoustic treatment at 5 W and 7 mL/min flow-through rate relative to the T-flask control.
A different batch of VCM was used for each trial. Protamine sulfate (PS, 5 µg/mL) was added to the TF-1 cell suspension in VCM for trial #2.

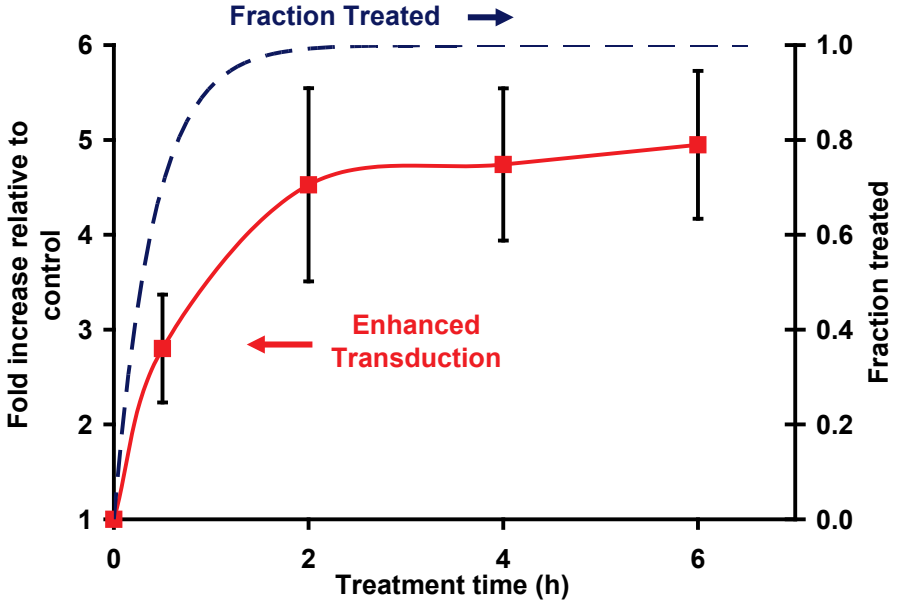

Figure A.5 Average increase in the transduction efficiency of TF-1 cells as a result of acoustic treatment at 5 W and 7 mL/min flow-through relative to the T-flask control.
The average increase was proportional to the fraction of the stirred suspension that was acoustically treated at least once assuming perfect mixing. (*n*=5, error bars: SEM)

As shown in Figure A.5, the increase in retroviral transduction was proportional to the fraction of the cell suspension treated at least once in the acoustic resonator. With this operating scheme and assuming perfect mixing, at least 2 h were required in order to treat over 99% of the 150 mL volume of target cells in VCM at least once. A reduction of the stirred suspension volume may therefore reduce the time required to obtain maximum enhancement and potentially lead to further increases in transduction.

A.3.2 Effect of volume and power input

In an attempt to further increase retroviral transduction by acoustic treatment, the stirred suspension volume was reduced 2-fold to 75 mL while maintaining the flow-through rate and volume per treatment cycle constant at 7 mL/min and 25 mL, respectively. Also, in order to further decrease the volume below 75 mL, the spinner flask was substituted for another 25-mL pipette, allowing for a 4-fold volume reduction down to 35 mL.

The 2-fold volume reduction yielded only a 2.0 - 2.7-fold increase in transduction efficiency using a 3 - 5 W power input range as shown in Figure A.6. This was below the 3- to 8-fold increase previously obtained when operating at 150 mL and 5 W. With the decreased volumes, higher cell losses and lower viabilities were observed (Figure A.7). The cell loss was a function of the power input, with >70% total cell loss occurring within 4.5 h at 5 W and within 24 h at 4 W (Figure A.8). However, at a power input of 3 W, the cell concentration increased by 1.5-fold and the viability remained high throughout the 24 h of acoustic treatment. Thus, cell losses were attributed to the operation of the acoustic resonator at higher power levels.

Operating at decreasing volumes had a detrimental effect on the total cell concentration (viable + nonviable cells) as well as on their viability. The combined drop in viability and cell concentration suggested that cells were damaged by the acoustic treatment, some to the point of lysis. Cell lysis was confirmed by a sharp increase in the lactate dehydrogenase concentration in the spent medium supernatant (data not shown). While larger cell culture volumes allowed for longer treatment times, the increased volume only diluted the negative effect of the acoustic treatment, thus partially masking it. It was hypothesized that overheating of the piezoelectric transducer due to the inefficient cooling design of the BioSep 10L housing for this transduction application may have resulted in running waves leading to cell losses due to lysis.

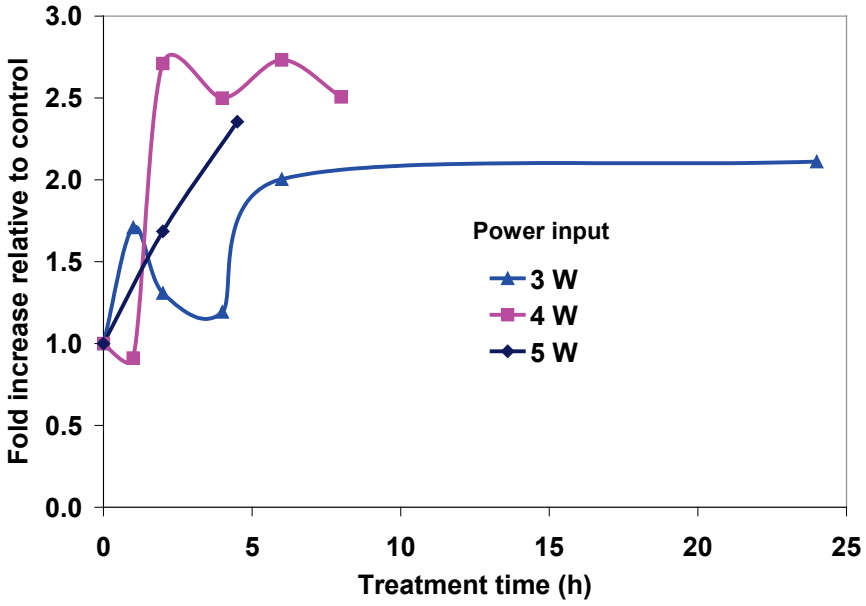

Figure A.6 Increase in transduction efficiency of TF-1 cells resuspended in VCM by acoustic treatment at power inputs of 3, 4 and 5 W for a constant 75-mL stirred suspension volume and a flow-through rate and a per cycle volume of 7 mL/min and 25 mL, respectively, relative to the T-flask control.

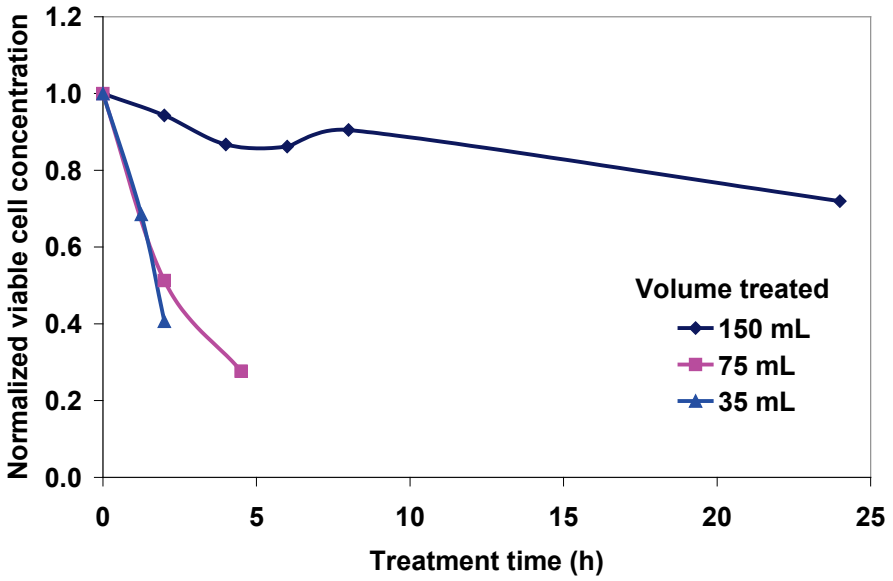

Figure A.7 Effect of volume treated on viable cell concentration normalized to the initial cell concentration measured by the Trypan blue exclusion assay of TF-1 cells resuspended in VCM. The 75 and 150 mL volumes were treated using an acoustic resonator mounted on a spinner flask while the 35 mL volume was treated using the 2 pipette design. The flow-through rate and per cycle volume were 7 mL/min and 25 mL respectively, while the power input was 5 W.

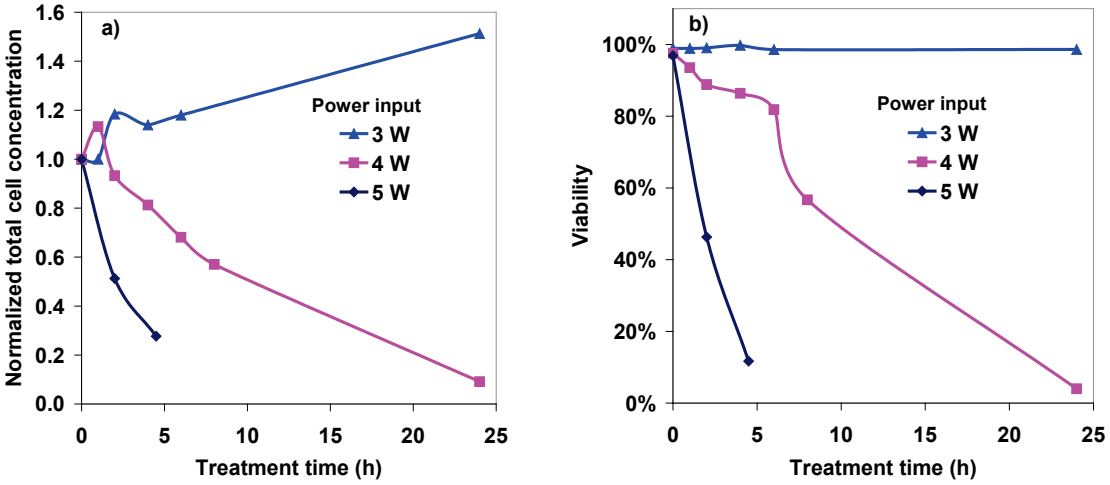

Figure A.8 Effect of the power input to the acoustic resonator on (a) the total cell concentration normalized to the initial concentration and (b) cell viability measured by the Trypan blue exclusion assay of TF-1 cells resuspended in 75 mL VCM treated at a constant flow-through rate of 7 mL/min and a per cycle volume of 25 mL.

A.3.3 Modified acoustic flow-through system (new body)

To address the potential overheating of the piezoelectric transducer, the acoustic resonator housing was further modified as described in Figures A.9-12 where the back was opened and the cooling air stream re-positioned perpendicular to the center of the transducer resulting in an improved air flow that enhanced heat dissipation. This modification reduced the maximum temperature from 42ºC, measured on the outside of the BioSep 10L housing covering the piezoelectric transducer and, therefore, likely an underestimate of the actual piezoelectric transducer temperature, to 29ºC measured on the transducer when operating with the modified housing. At the same time, a heat exchanger was also added to the upper pipette reservoir in order to reduce heat loss.

The performance of the modified design was first evaluated by measuring its impact on the viable cell concentration. As shown in Figure A.13, with enhanced heat dissipation, the viable cell concentration increased over a period of 36 h to a level approaching that of the untreated stirred suspension control. Having successfully resolved the cell loss issue previously experienced at 5 W with the BioSep 10L design, the effect of acoustic treatment on the retroviral transduction efficiency of TF-1 cells was next assessed using the modified design. Under these non-lysing conditions, it was found that the transduction efficiency was very similar to that of an untreated stirred suspension and the T-flask control (Figure A.14), i.e., that acoustic treatment no longer increased retroviral transduction. Based on these results, it was hypothesized that, under the cell lysing conditions of the BioSep 10L design, cell lysis products may have contributed to the observed increase in transduction.

Modified Acoustic Separator Body V 3.0 (similar to work order 927 from July 5, 2004)

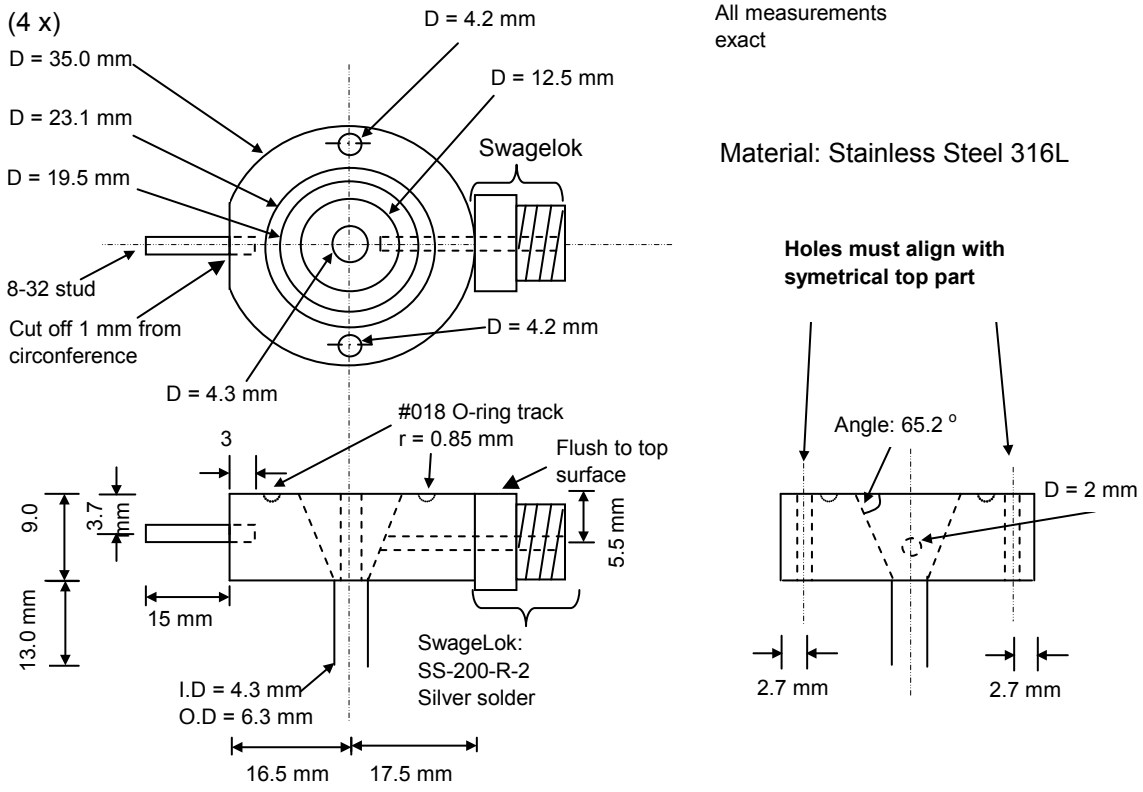

Figure A.9 New acoustic separator body v. 3.0 (open back design)

Needle Thermocouple Support Approximate measurements

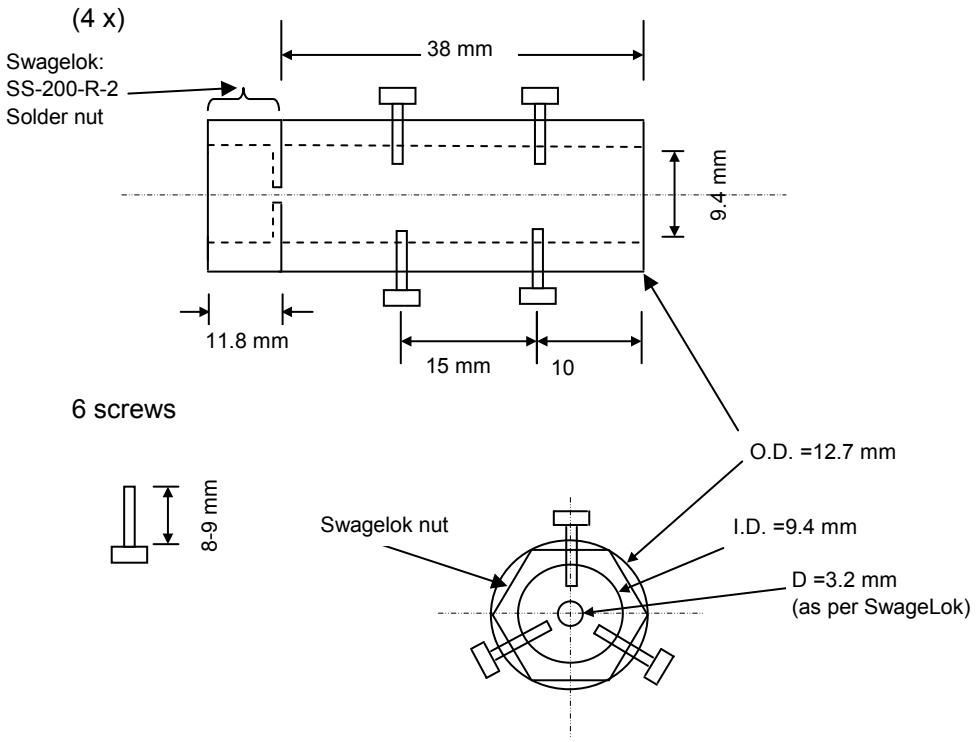

Material: Stainless Steel

Additional Parts Required

4x	90 mm long 8-32 stud links 2 symetrical pieces
4x	o-ring: 018-silicon
12x	nuts for #8-32 stud

Figure A.10 Thermocouple port used with new acoustic body (v. 3.0)

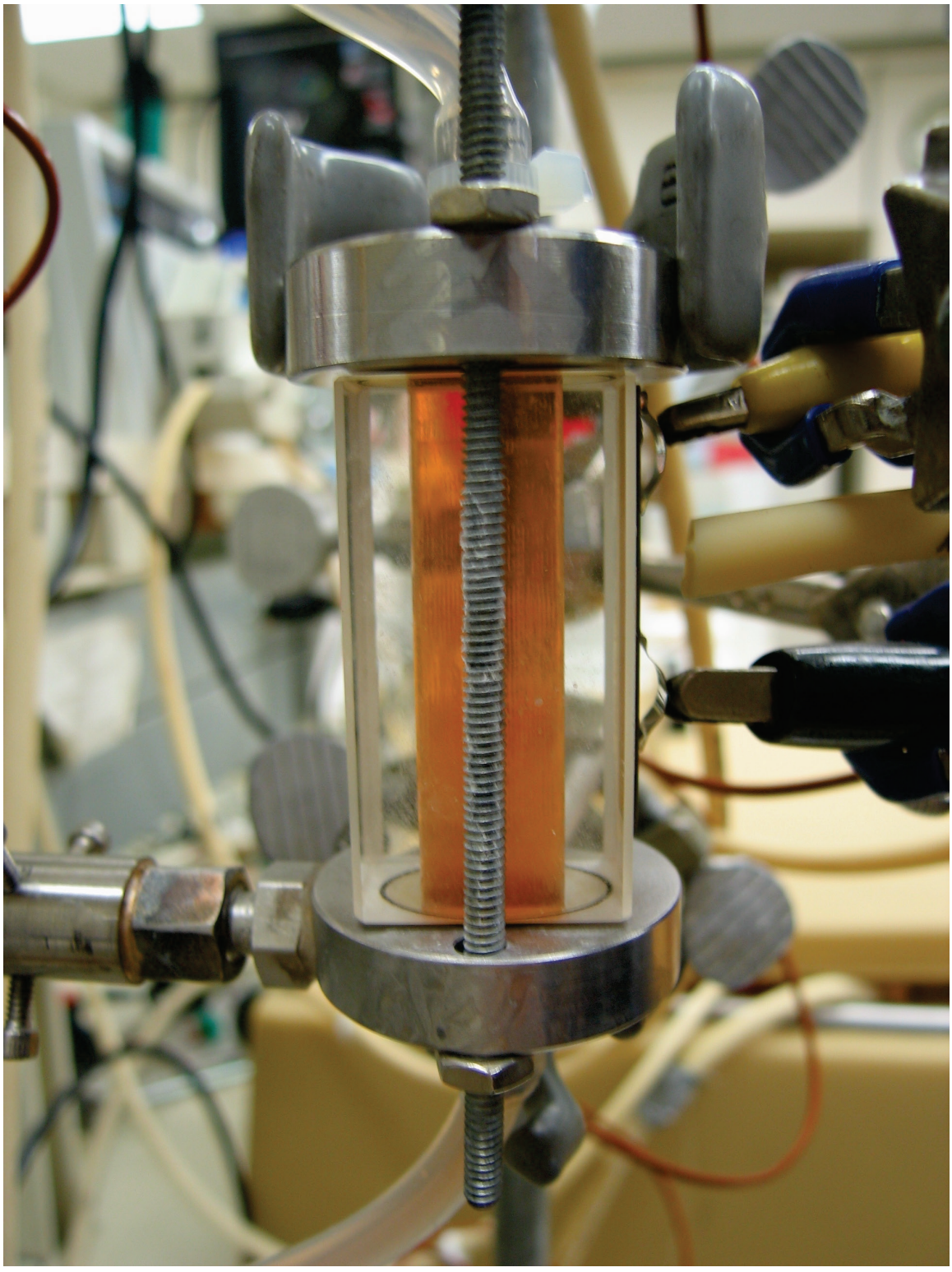

Figure A.11 New open back acoustic body design (side view) in operation

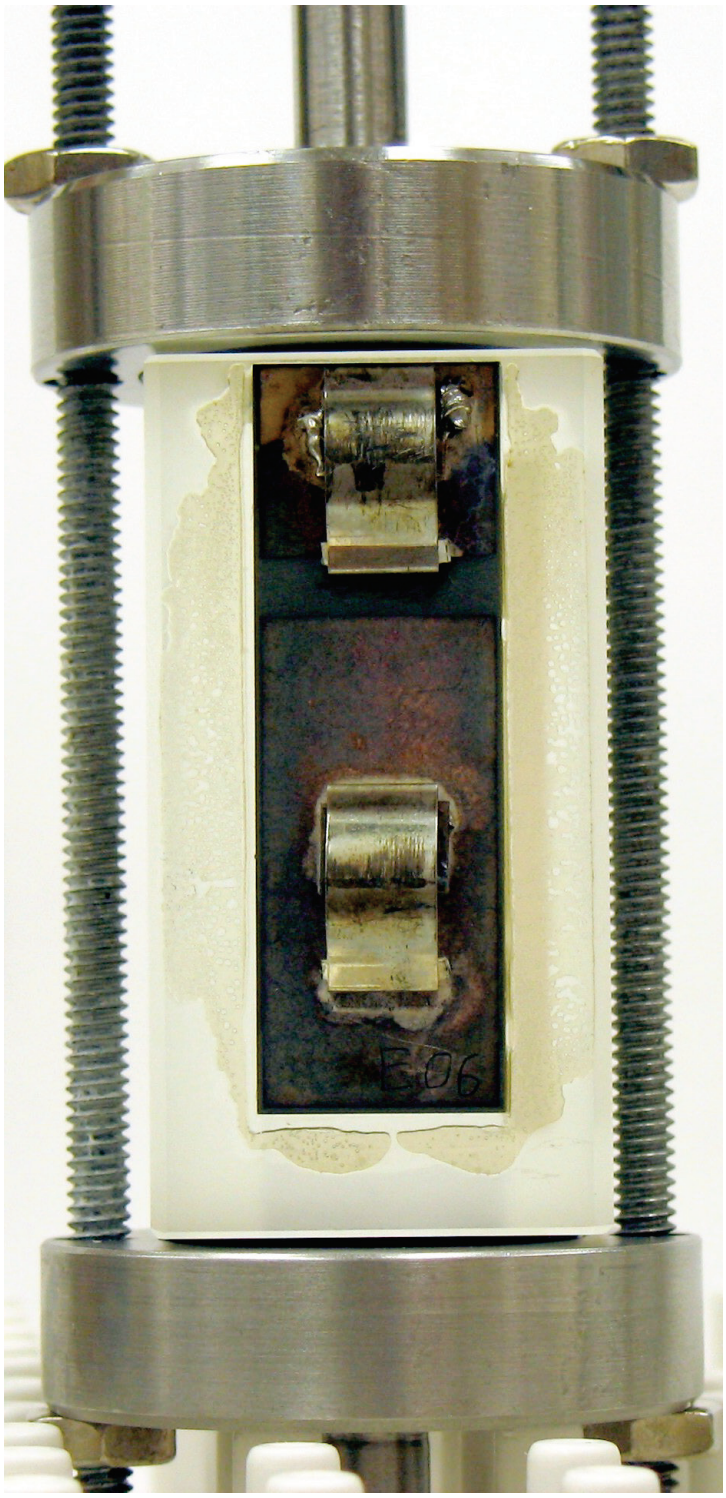

Figure A.12 New open back acoustic body design (rear view)

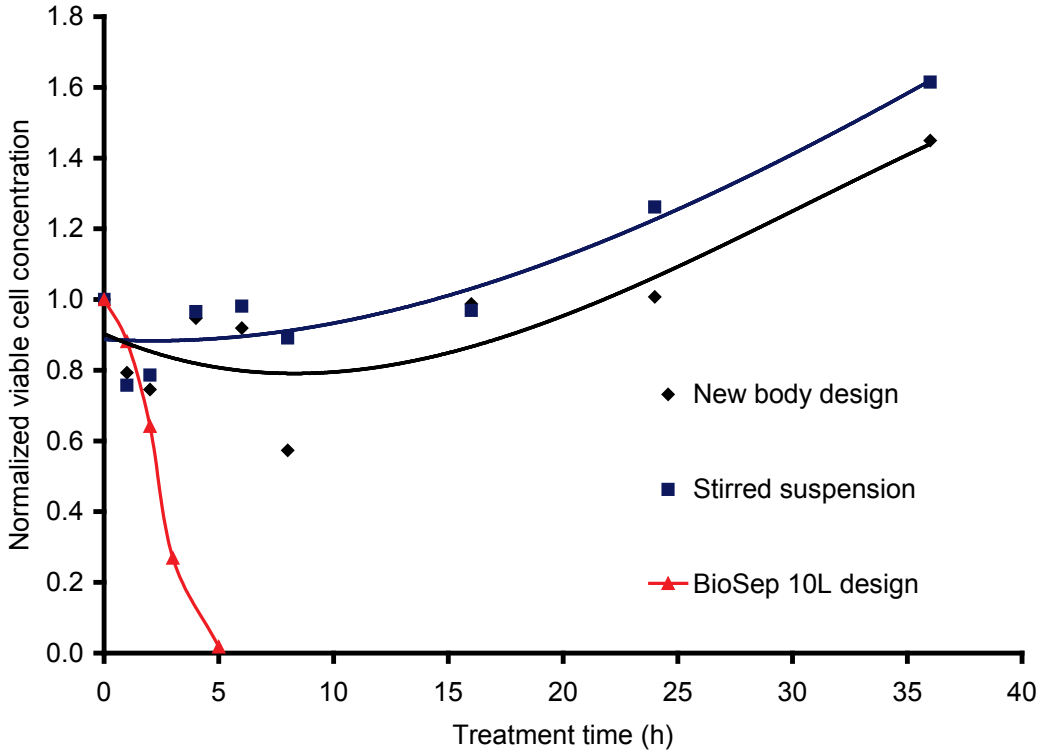

Figure A.13 Effect of new body acoustic flow-through design on TF-1 viable cell concentration normalized to the initial cell concentration relative to a stirred suspension control.
For comparison, previous BioSep 10L design results are also shown. All acoustic experiments were performed using a volume of 75 mL, a power input of 5 W and a flow-through rate and a per cycle volume of 7 mL/min and 25 mL, respectively.

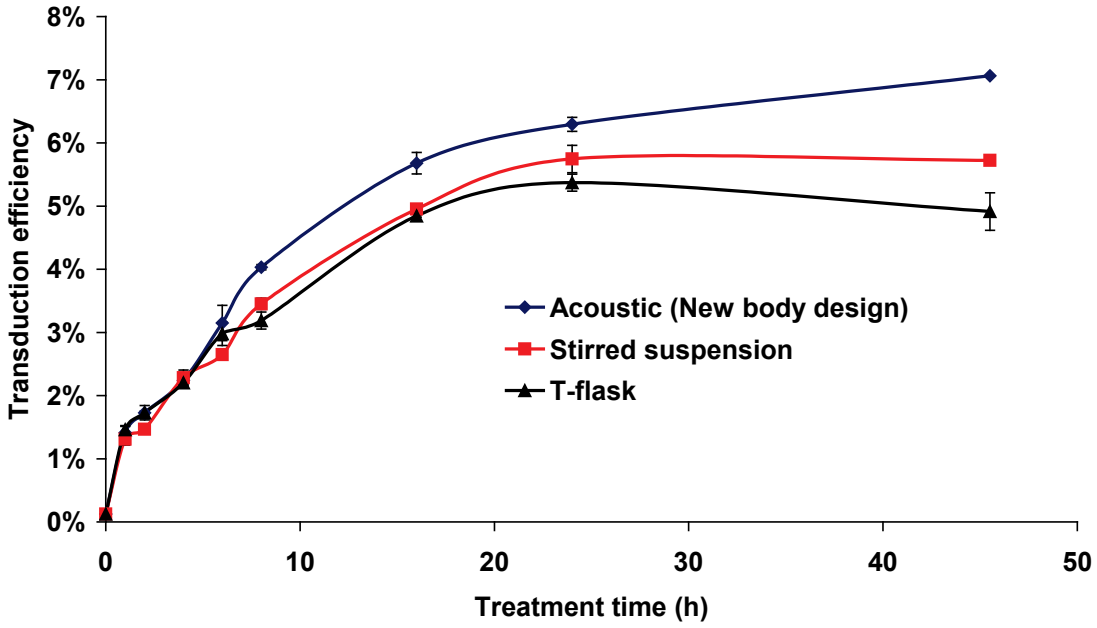

Figure A.14 Transduction efficiency of TF-1 cells resuspended in VCM treated with the new acoustic body design using a volume of 75 mL, a power input of 5 W and a flow-through rate and a per cycle volume of 7 mL/min and 25 mL, respectively, relative to T-flask and stirred suspension controls. The initial TF-1 cell concentration was 1.1×10^6 cells/mL.

A.3.4 Modified acoustic flow-through system with cell lysate

To determine if the products of cell lysis may have contributed to the increase in the retroviral transduction of TF-1 cells treated under relatively high power acoustic conditions, TF-1 cell lysate was mixed together with viable cells and VCM. The mixture was then split between the modified acoustic system as well as a stirred suspension and a static T-flask control. As a negative control, a T-flask without cell lysate was included. As shown in Figure A.15, the addition of lysate increased retroviral transduction in both the stirred suspension and the static T-flask by 5- and 6-fold, respectively, relative to the T-flask control without lysate. The acoustic treatment, under non-lysing conditions, doubled the transduction efficiency, achieving an increase of 12-fold relative to the T-

flask control without lysate. This suggests the presence of a synergistic interaction between cell lysate and the acoustic treatment. Viable cell concentrations after 24 h were similar for the acoustic system and the stirred suspension at, respectively, 1.36 and 1.41 times the initial cell concentration, confirming that the increase observed with the acoustic treatment was not due to the lysis of additional cells. Furthermore, cell concentrations and viabilities remained comparable between the acoustic system and the stirred suspension after 72 h of operation. Overall, these results demonstrate that, with acoustic standing wave fields, retroviral transduction was only enhanced in the presence of cell lysate. However, there was a synergistic interaction between the acoustic treatment and the products of cell lysate.

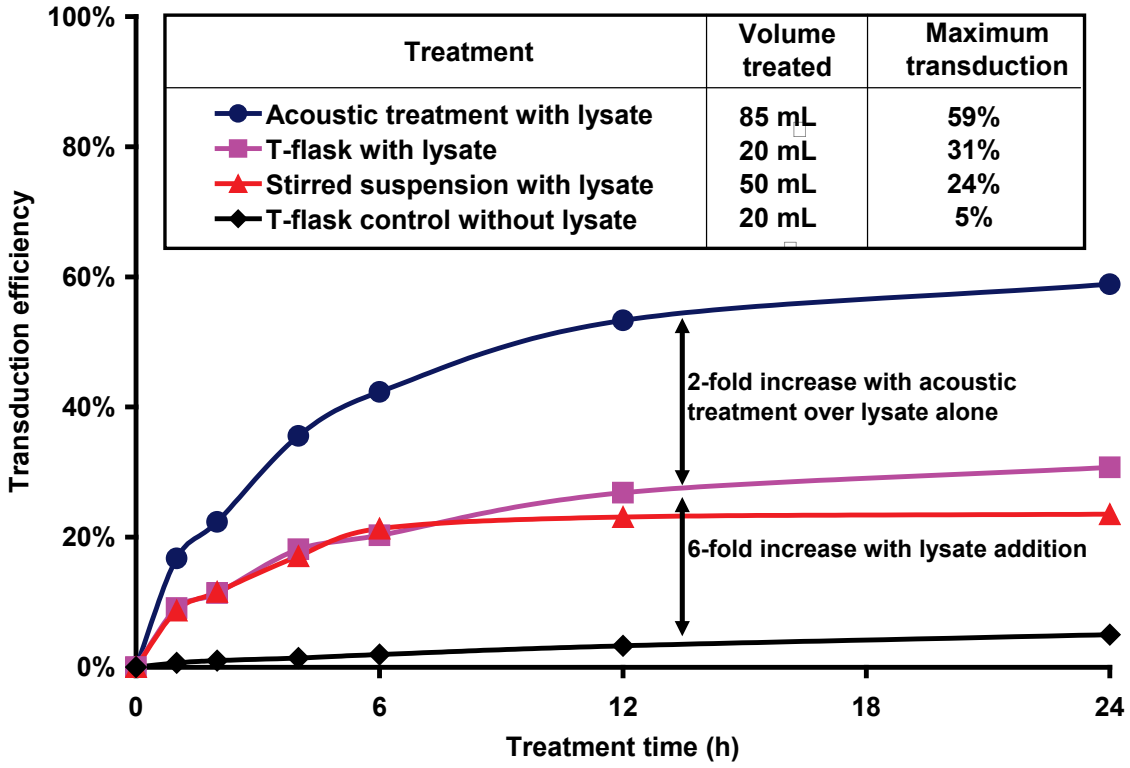

Figure A.15 Transduction efficiency of TF-1 cells at an initial concentration of 9×10^5 cells/mL mixed with VCM and TF-1 cell lysate at a lysed -to-viable cell ratio of 1.25 treated with: a) the new body acoustic flow-through system at a power input of 5 W, and a flow-through rate and per-cycle volume of 7 mL/min and 25 mL, respectively, b) in a stirred suspension and c) in a T-flask.
The results obtained for a T-flask control without cell lysate are also shown.

A.3 Discussion

The data presented in this appendix demonstrated that: 1) the retroviral transduction efficiency was only enhanced when the acoustic standing wave field was operated under conditions resulting in partial cell lysis; 2) enhanced heat dissipation from the piezoelectric transducer allowed the operation of the acoustic standing wave field without the occurrence of cell lysis; 3) in the absence of cell lysis, retroviral transduction was not enhanced by the acoustic standing wave field treatment alone; 4) the presence of cell lysate increased the retroviral transduction efficiency in static T-flask cultures as well as in stirred suspensions; and 5) there was a synergy between the presence of cell lysate and acoustic standing wave field treatment, leading to a 2-fold increase in retroviral transduction over that of lysate alone.

Previously, short term (< 20 min) treatment with acoustic standing wave fields was reported to increase transduction efficiency by 3-fold for both suspension and adherent cell lines (Lee and Peng 2005; Lee et al. 2005). The authors did not demonstrate a clear mechanism of action. While it could be observed that the target cells were readily displaced to the pressure nodes, it was hypothesize that improved convective mass transport due to microstreaming was responsible for the increase in retroviral transduction. This is inconsistent with previous results that have shown that increased convective mass transport alone (i.e. flow-through system) without the means to capture and maintain the retroviral vectors in close proximity to the target cells failed to increase retroviral transduction (Chuck and Palsson 1996a; Chuck and Palsson 1996b). Large mammalian cells with diameters of 10 - 20 μm are readily displaced and retained within the pressure nodes of a standing acoustic field thereby achieving separation efficiencies

above 90% (Gorenflo et al. 2003; Limaye et al. 1996; Pui et al. 1995). However, for smaller bacterial cells such as *E. coli* (~1 μm), the separation efficiency decreases to 70% and less (Limaye et al. 1996). As retroviral vectors have a diameter of ~100 nm (Tayi et al. 2010), 2 orders-of-magnitudes smaller than those of mammalian cells and likely similar densities, they will not be effectively displaced to and retained within the pressure nodes together with the target cells. Furthermore, the relationship between transduction performance and the acoustic standing wave field treatment time, whereby retroviral transduction efficiency peaked after 5 minutes and decreased for extended treatment times (up to 20 minutes) (Lee and Peng 2005), was inconsistent with the increase up to a plateau at extended treatment times reported for other convective methods such as centrifugation (Bahnson et al. 1995) and flow-through systems (Chuck and Palsson 1996a). Viability was also reported to decrease with acoustic treatment time in these earlier studies (Lee and Peng 2005). This suggests that the acoustic treatment negatively impacted and potentially lysed a fraction of the target cells. Decreased viability at high power input has been observed with standing wave fields (Pui et al. 1995). Thus, the 3-fold increase in transduction efficiency reported (Lee and Peng 2005; Lee et al. 2005) could easily be explained by the synergistic effect between cell lysate and acoustic standing wave fields observed in this work.

The data presented in this appendix could also explain the increase in retroviral transduction reported under an acoustic running wave regime (Naka et al. 2007). In this case, the running waves apparently lysed a fraction of the cells. It is therefore likely that at least part of the effect reported was due to the presence of the cell lysate rather than solely a consequence of the acoustic running waves.

The mechanism of action explaining the synergistic interaction observed between the lysate and the standing wave field has yet to be demonstrated. Components present within the cell lysate could potentially result in the aggregation of the retroviral vectors, leading to the formation of particles of larger diameter that can be displaced to the pressure nodes together with the target cells. For example, cationic polymers such as poly-L-lysines added to retroviral vectors were reported to form aggregates of 1 – 3 μm in diameter (Davis et al. 2004). Alternatively, debris aggregates present within the cell lysate may act as retroviral carriers as demonstrated in Chapter 3 with the PD80P fraction. Vector-loaded debris aggregates could then be displaced together with the target cells to the pressure nodes. Carrier systems have been developed where retroviral vectors were adsorbed onto heat killed bacteria (Darling et al. 2000) as well as paramagnetic particles using different ligands (Hughes et al. 2001). The aggregated f_3 histone reagent described in Chapter 5 could also serve a retroviral carrier. All these strategies could potentially be combined with the acoustic standing wave treatment to enable the large-scale application of these approaches as well as the potential achievement of higher transduction efficiency.

Appendix B. Supplementary Data

B.1 Chapter 3 raw data (transduction efficiency)

B.1.1 Density and size fractionation of cell lysate

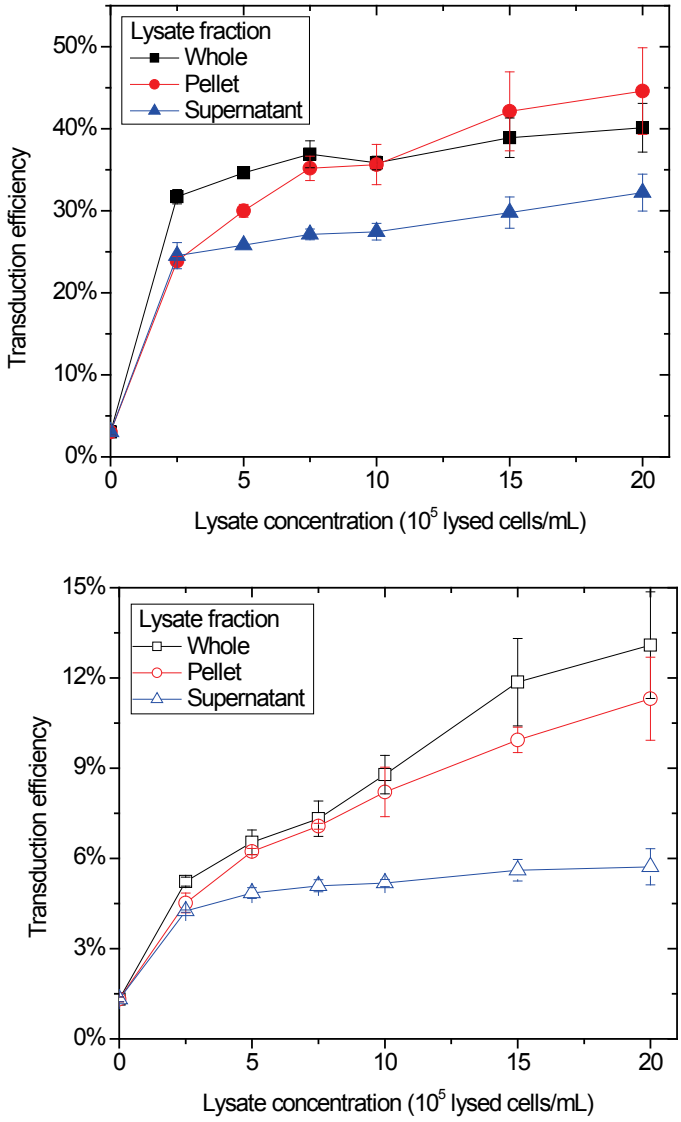

Figure B.1 The increase in transduction efficiency was dependent on the whole, pellet and supernatant lysate fraction concentration for both nBaF3 cells transduced with Eco-GFP vectors (top) and TF-1 cells by GALV-GFP vectors.
(*n*=3, error bars: SEM) (supplement to Figure 3.5)

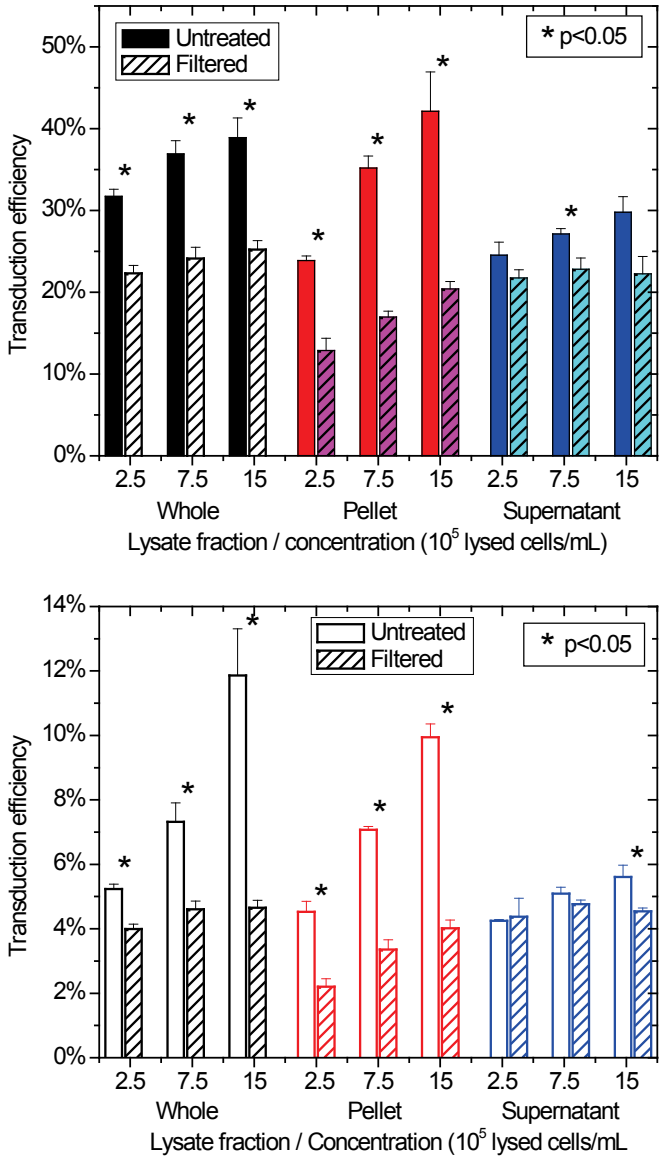

Figure B.2 Filtration at 0.2 µm of lysate fraction to remove debris aggregates significantly reduced the activity of the whole (black) and pellet (red) lysate fraction at all concentrations assayed but not that of the supernatant (blue) fraction assayed using nBaF3 targets cells with Eco-GFP vectors (top) and TF-1 target cells with GALV-GFP vectors (bottom).
(*n*=3, error bars: SEM) (supplement to Figure 3.6)

B.1.2 Enzymatic digestion of lysate

B.1.2.1 Phospholipase A_2

To investigate if the phospholipids such as phosphatidylserine were a significant contributor to the increase in transduction, whole lysate was digested using phospholipase A_2 (PL A_2). As PL A_2 is calcium dependent, EDTA was added to inhibit the activity of the residual phospholipase before the cell culture assay of the treated lysate activity. As shown in Figure B.3, the PL A_2 treatment of the lysate did not alter its activity. In the absence of EDTA, PL A_2 remained active causing partial cell lysis leading to an increase in transduction with both the control and the lysate. Based on these results, it is unlikely that phospholipids such as phosphatidylserine were responsible for the increase in transduction observed in the presence of whole cell lysate.

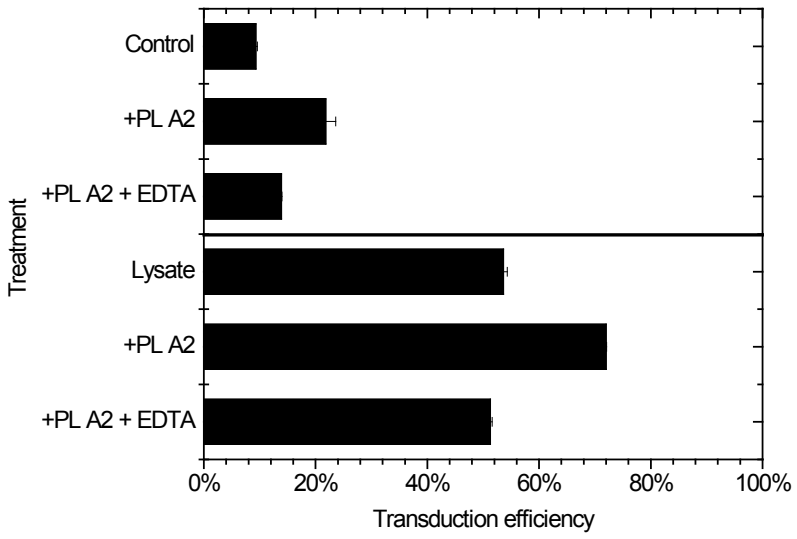

Figure B.3 Effect of phospholipase A_2 (PL A_2) treatment of TF-1 cell lysate (1.4×10^6 lysed cells/mL on the transduction efficiency of TF-1 target cells (5×10^5 cells/mL) resulting from a 6 h exposure to the VCM.

Lysate and control (DMEM) were pre-incubated with 2800 U/mL PL A_2 for 1 h at 37°C. Phospholipase activity was then inhibited by the addition of 10 mM EDTA to chelate Ca^{2+} prior to its addition to the mixture of target cells and VCM. Note: a different batch of VCM and concentration were used. (*n*=2, error bars: SEM)

B.1.2.2 DNase I

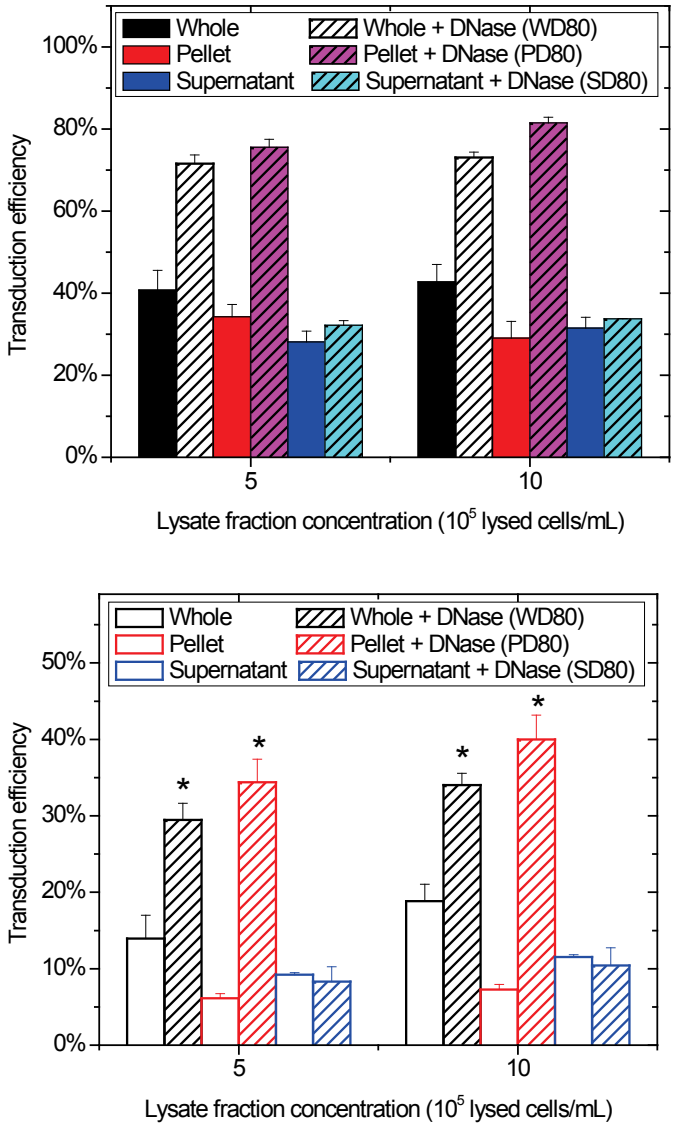

Figure B.4 The increase in transduction efficiency of DNase I treated whole (black), pellet (red) and supernatant (blue) lysate fractions was compared to that of the untreated lysate fractions using nBaF3 target cells with Eco-GFP vectors (top) and TF-1 target cells with GALV-GFP vectors (bottom).
(*n*=3, error bars: SEM) (supplement to Figure 3.8)

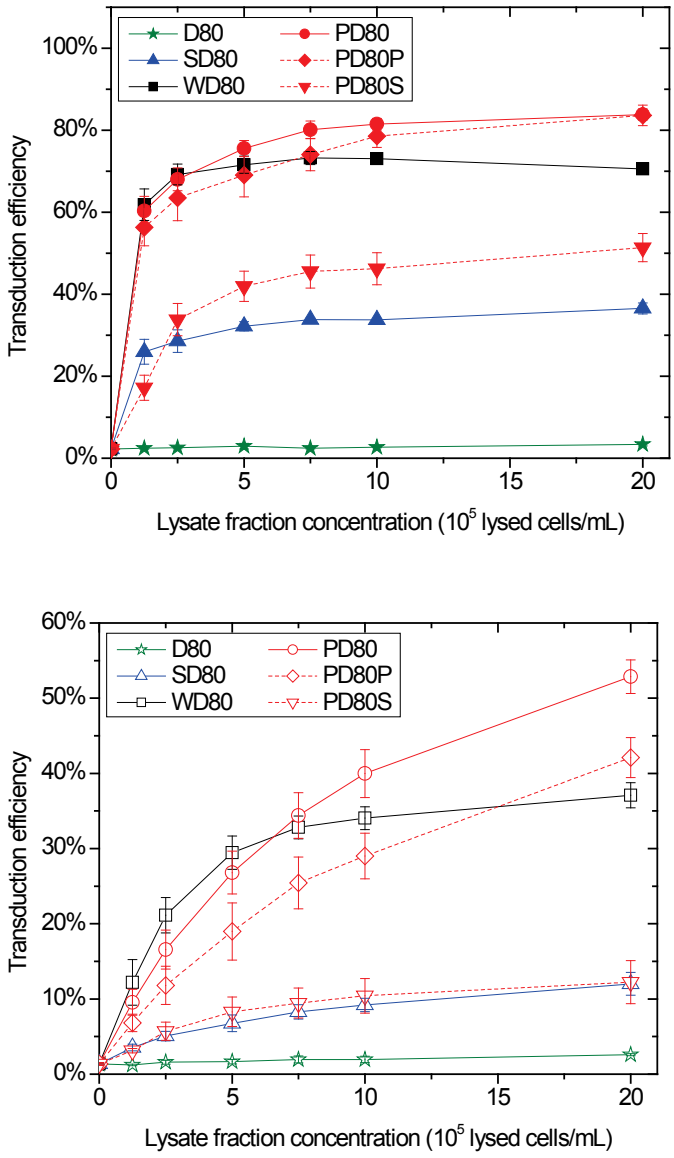

Figure B.5 Increase in transduction efficiency relative to the concentration of DNase I treated lysate fraction assayed on nBaF3 target cells with Eco-GFP vectors (top) and on TF-1 target cells with GALV-GFP vectors (bottom).
Lysate fractions included DNase-treated whole (WD80), supernatant (SD80), pellet (PD80), pellet fraction of PD80 (PD80P), supernatant fraction of PD80 (PD80S) and, as a control, DMEM with DNase I (D80). (*n*=3, error bars: SEM) (supplement to Figure 3.9)

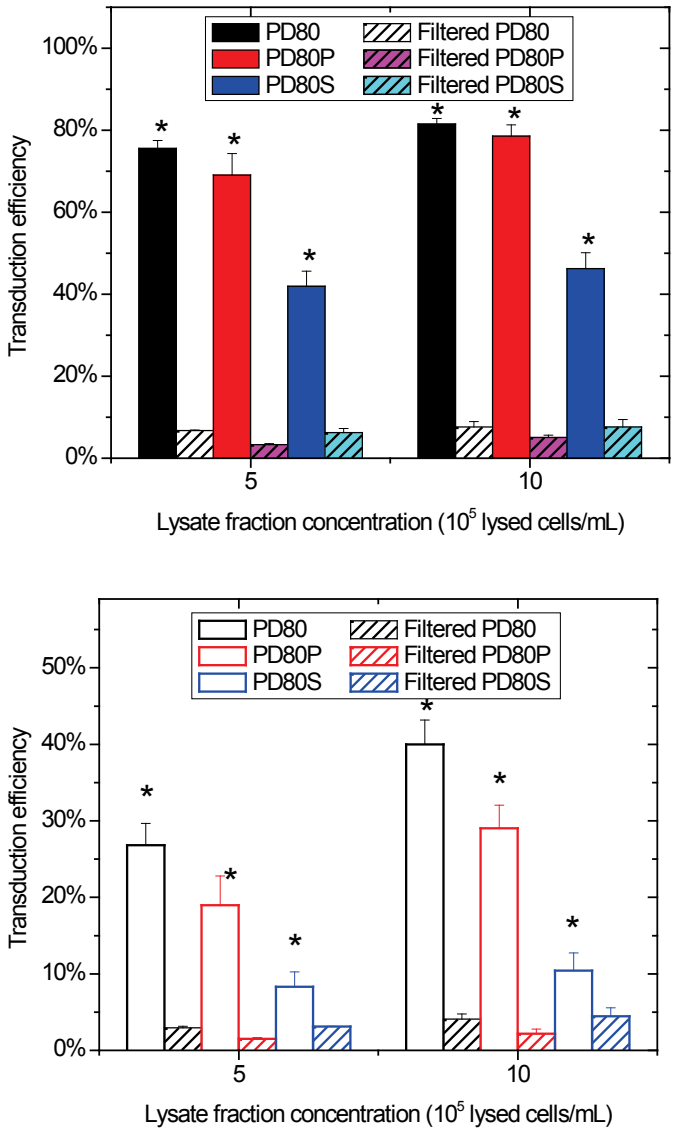

Figure B.6 Effect of filtration at 0.2 µm of the DNase I treated pellet (PD80, black), the pellet of PD80 (PD80P, red) and the supernatant of PD80 (PD80S, blue) on the transduction efficiency of nBaF3 target cells with Eco-GFP vectors (top) and TF-1 target cells with GALV-GFP vectors (bottom).
(*n*=3, error bars: SEM) (supplement to Figure 3.11)

B.1.2.3 Trypsin digestion of PD80P fraction

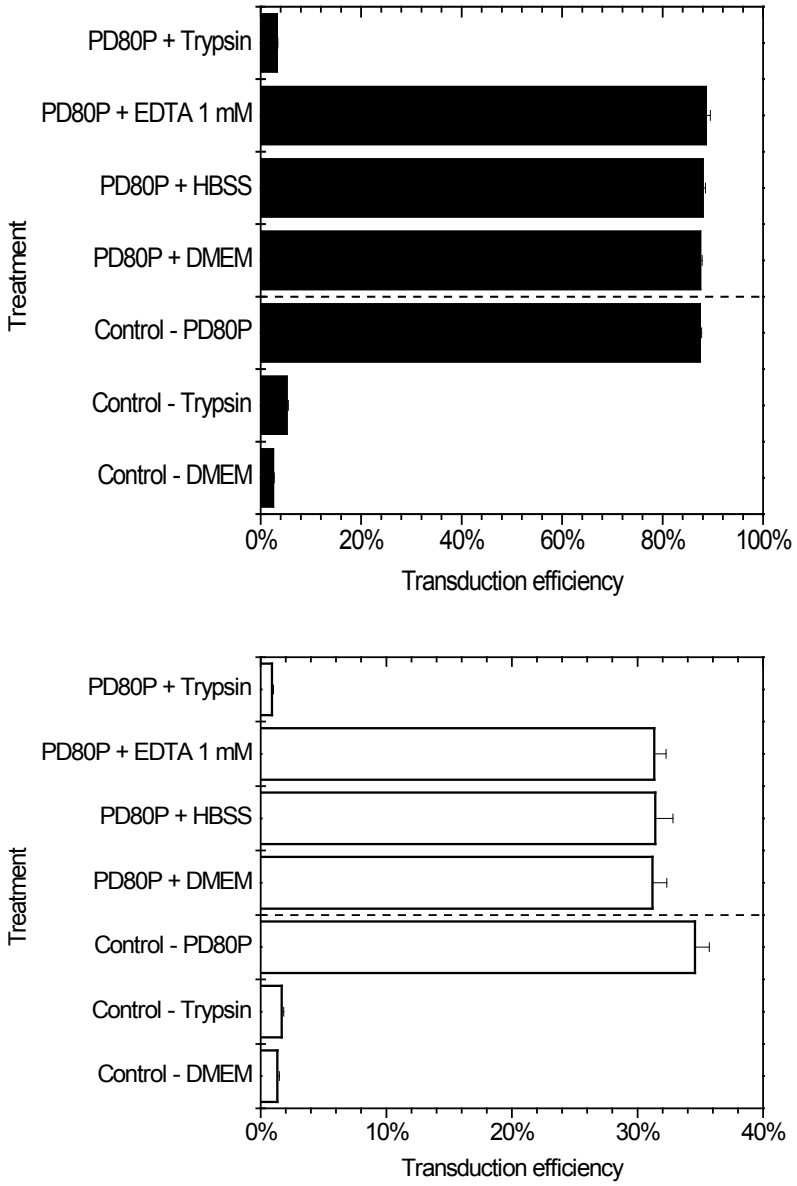

Figure B.7 Effect of treatment of the PD80P lysate fraction with trypsin (also containing EDTA in HBSS), HBSS with EDTA, and HBSS alone on the transduction efficiency of nBaF3 target cells with Eco-GFP vectors (top) and TF-1 target cells with GALV-GFP vectors.
Controls included residual trypsin in the absence of PD80P to evaluate the effect of carried over trypsin and PD80P with DMEM to evaluate potential loss of PD80P upon trypsin removal. (n=3, error bars: SEM) (supplement to Figure 3.14)

B.1.3 Nuclei and erythrocyte derived lysates

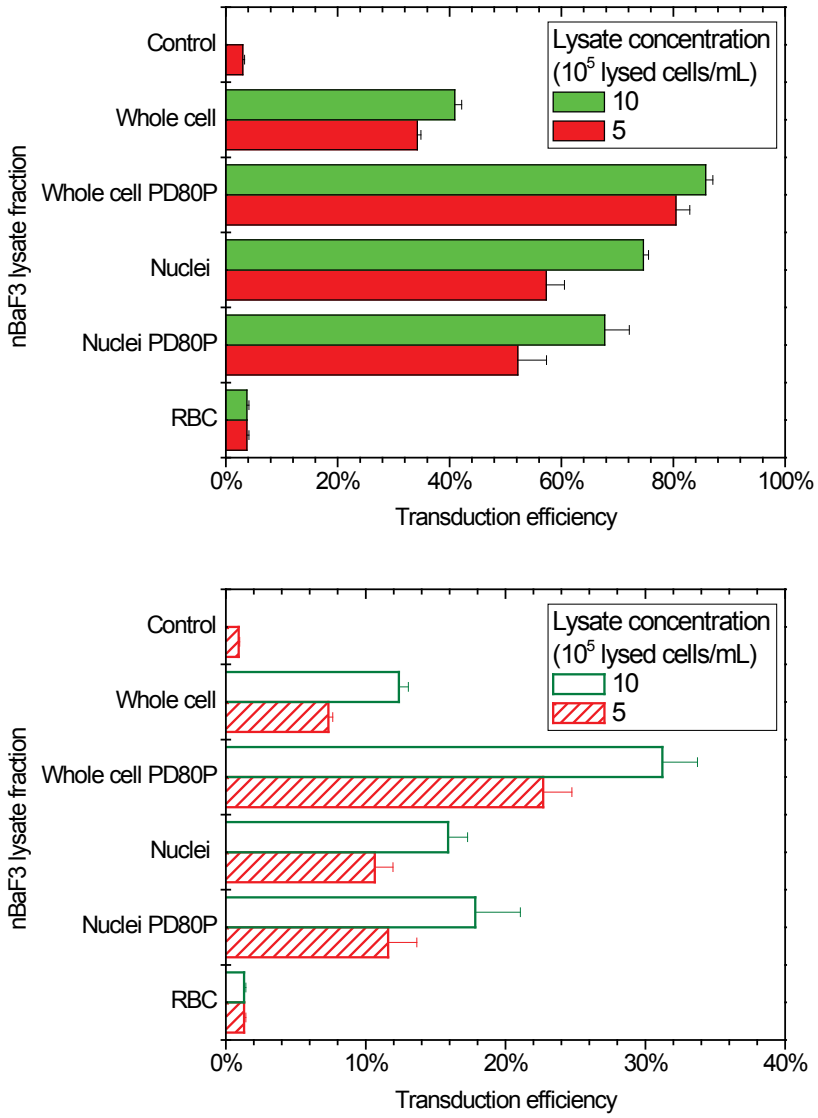

Figure B.8 Transduction efficiency obtained with nBaF3 whole cell and nuclei lysates, human erythrocyte (RBC) lysates and PD80P fractions derived from nBaF3 whole cell and nuclei assayed on nBaF3 target cells with Eco-GFP vectors (top) and on TF-1 target cells with GALV-GFP vectors (bottom).
(*n*=3, error bars: SEM) (supplement to Figure 3.15)

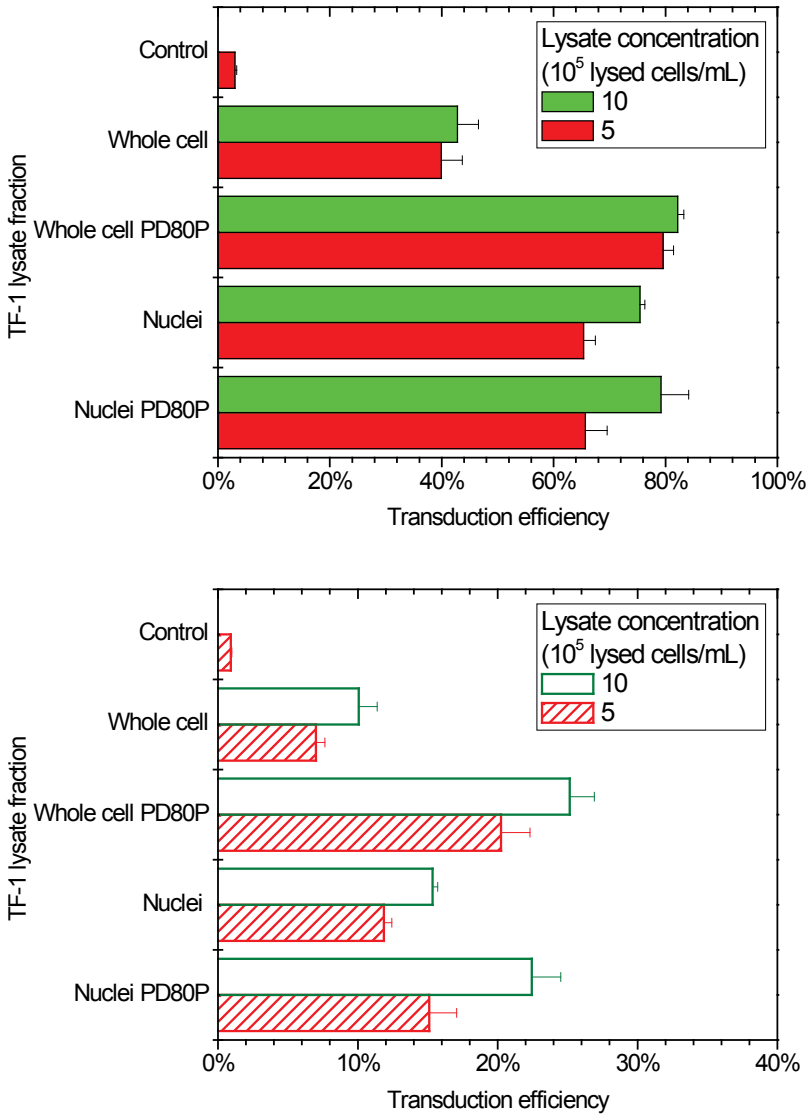

Figure B.9 Transduction efficiency obtained with TF-1 whole cell and nuclei lysates and PD80P fractions derived from TF-1 whole cell and nuclei assayed on nBaF3 target cells with Eco-GFP vectors (top) and on TF-1 target cells with GALV-GFP vectors (bottom).
(*n*=3, error bars: SEM) (supplement to Figure 3.16)

B.1.4 Mechanism

B.1.4.1 Sedimentation

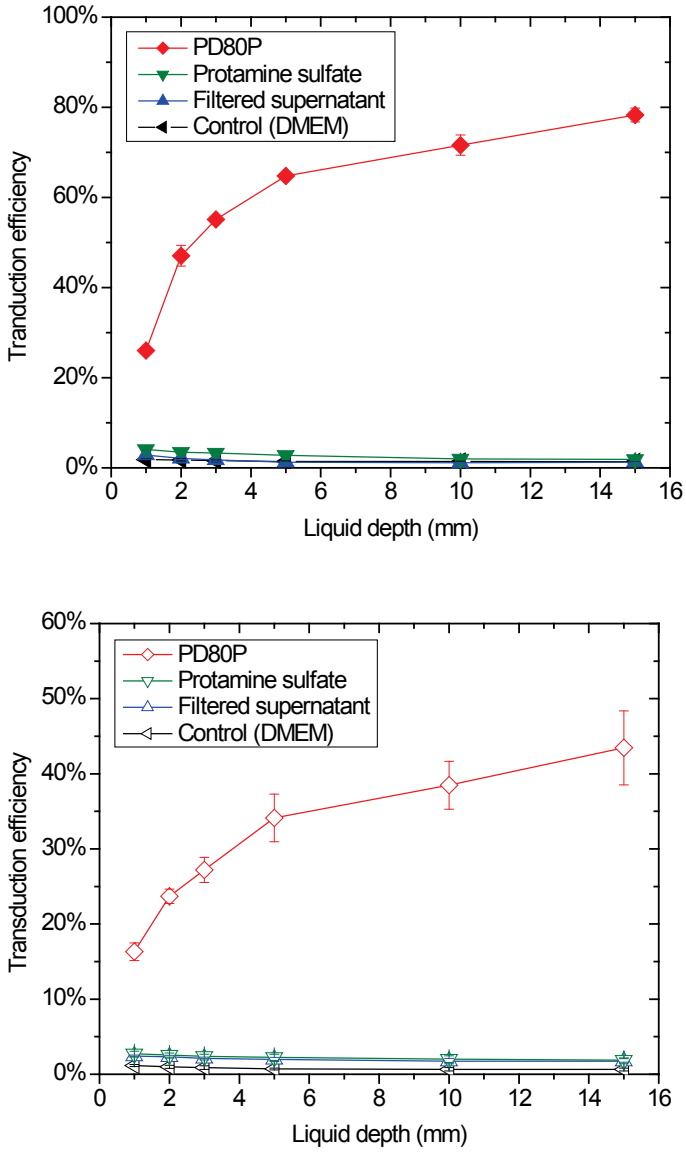

Figure B.10 Effect of liquid depth on the transduction efficiency with PD80P and filtered supernatant lysate fractions (5×10^5 lysed cells/mL), protamine sulfate (10 µg/mL) and, as a control, DMEM assayed on nBaF3 target cells (1.5×10^5 cells/cm^2) with Eco-GFP vectors (0.0625× concentration) (top) and on TF-1 target cells (1.5×10^5 cells/cm^2) with GALV vectors (0.125× concentration) (bottom).
(*n*=3, error bars: SEM) (supplement to Figure 3.17)

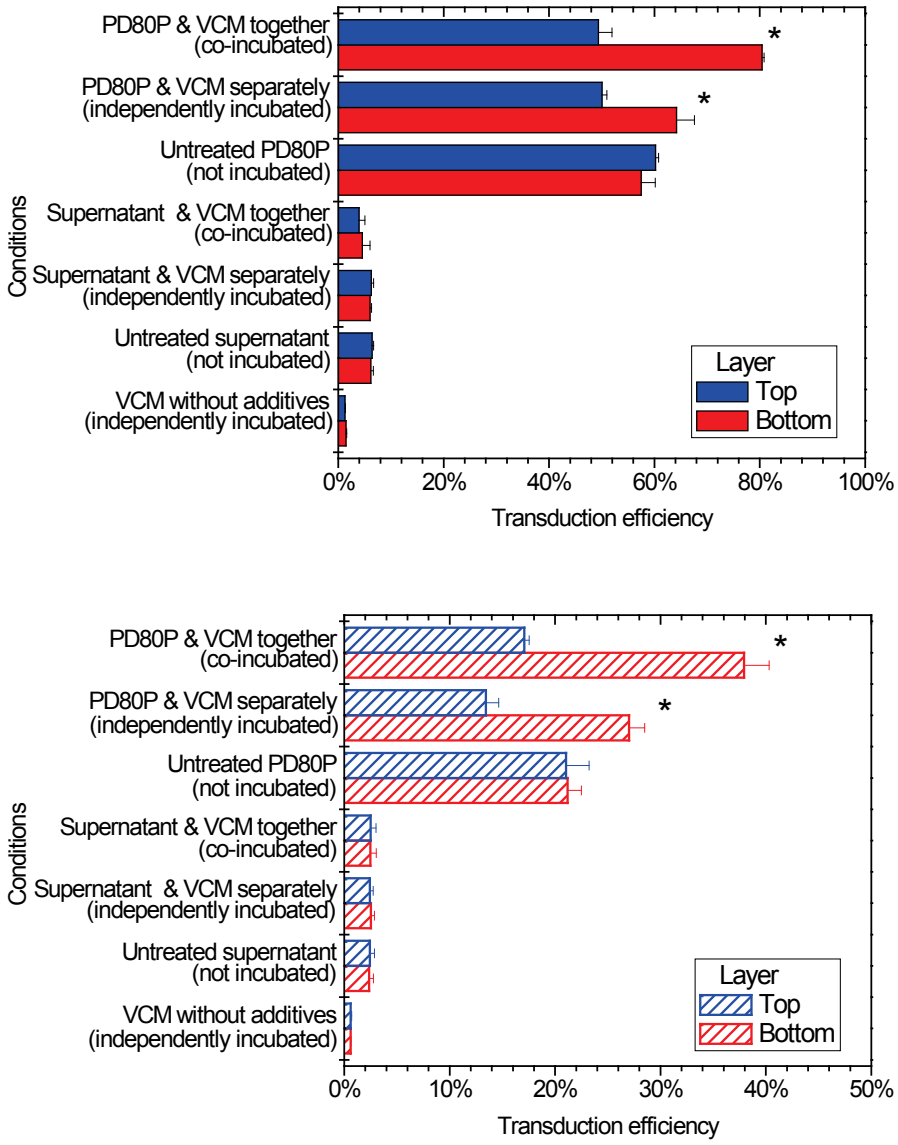

Figure B.11 Effect of pre-incubation of VCM with PD80P and supernatant together and separately at 1.8 cm liquid depth for 6 h at room temperature and equal separation of top and bottom layers prior to their addition to nBaF3 target cells (Eco-GFP vectors) (top) and to TF-1 target cells (GALV-GFP vectors) (bottom) on the transduction efficiency.
As control, untreated PD80P and supernatant were used in combination with incubated/separated VCM. (* significant difference between top and bottom fractions, $p<0.05$) (n=3, error bars: SEM) (supplement to Figure 3.18)

B.1.4.2 Cell surface adsorption

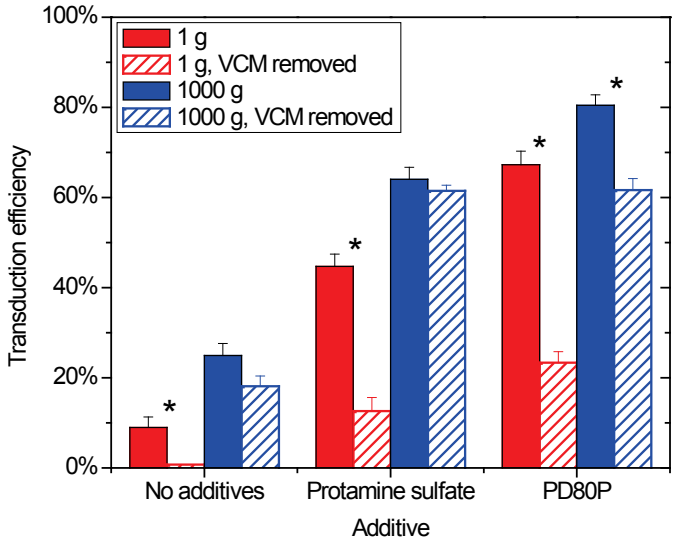

Figure B.12 Effect on centrifugation alone and in combination with protamine sulfate (10 µg/mL) and PD80P lysate fraction (5×10^5 lysed cells/mL) on the transduction efficiency of RAT-1 target cells with Eco-GFP vectors.
Target cells with VCM alone and in combination with additives were transduced under static conditions (1 g, red) and centrifugation at 1000 g (blue) for 1 h at 23°C. VCM was left in (full bars) or removed and replaced with growth medium (striped bars) before transferring the cells to an incubator at 37°C for an additional 23 h. (* significant difference between VCM removed and left in, $p<0.05$) (n=3, error bars: SEM) (supplement to Figure 3.19)

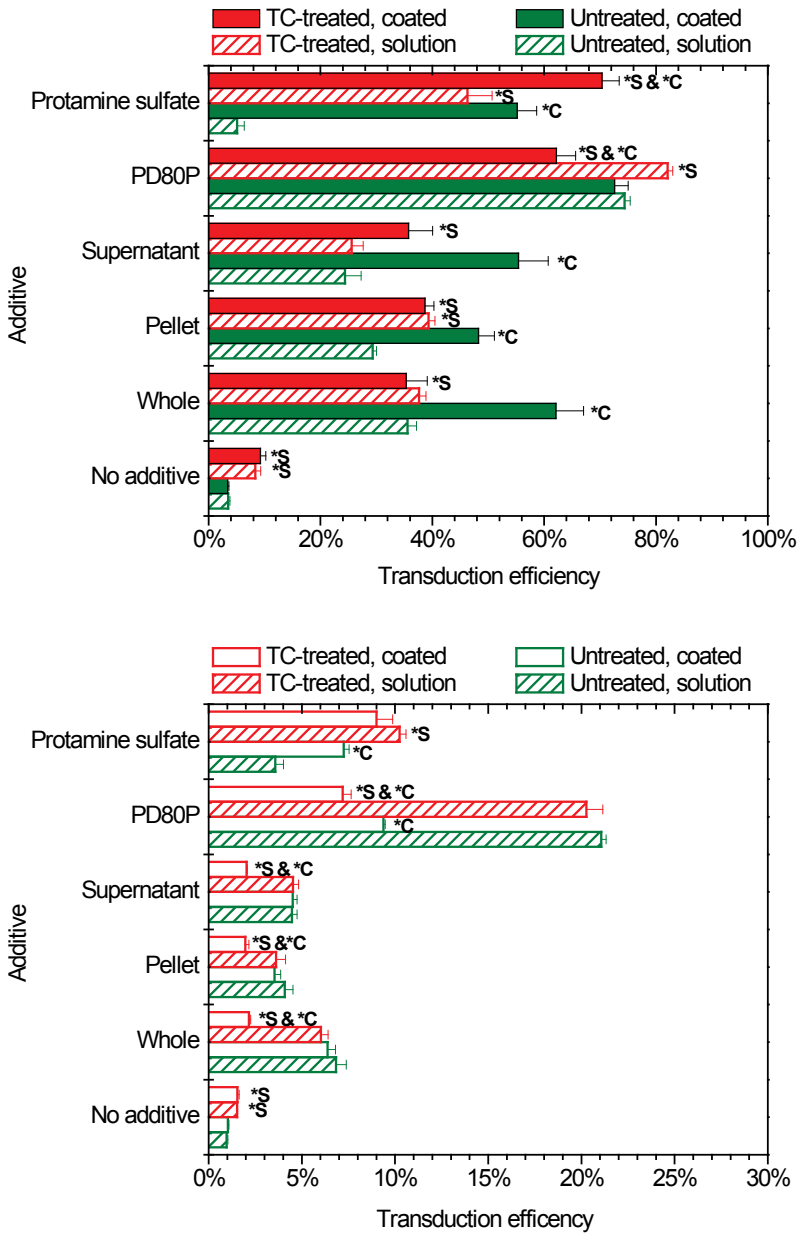

Figure B.13 Effect of cell culture vessel surface type and coating in the presence of whole, pellet, supernatant and PD80P lysate fractions as well as protamine sulfate and DMEM as a control on the transduction efficiency of nBaF3 target cells with Eco-GFP vectors (top) and of TF-1 target cells with GALV-GFP vectors (bottom).
Untreated (green) and tissue culture-treated surfaces were coated for 4 h with 5×10^5 lysed cells/mL, 10 µg/mL protamine sulfate in DMEM and DMEM as a control. Coating solutions were subsequently removed and surfaces were washed with DMEM. Target cells and VCM were added to coated wells, which were compared to uncoated wells where lysate fractions, protamine sulfate and DMEM were added in solution. (*S: significant surface effect, *C: significant coating effect, $p<0.05$) (n=3, error bars: SEM) (supplement to Figure 3.21)

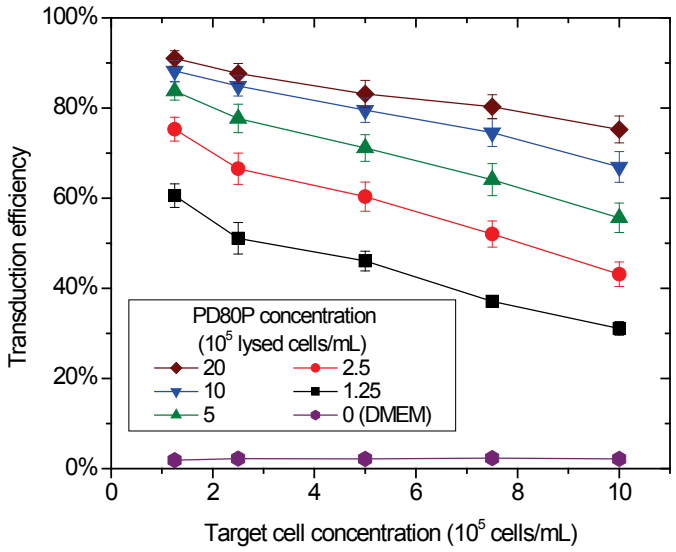

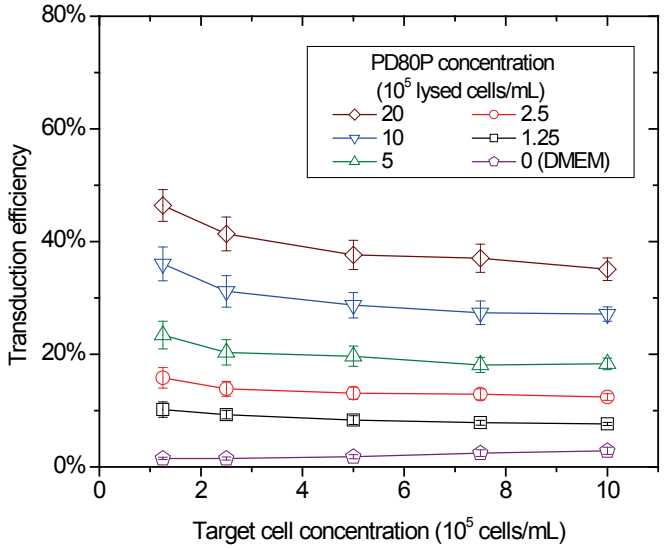

Figure B.14 Effect of initial target cell and PD80P lysate fraction concentration on the transduction efficiency of nBaF3 target cells with Eco-GFP vectors (top) and of TF-1 target cells with GALV-GFP vectors (bottom).
(*n*=3, error bars: SEM) (supplement to Figure 3.22)

B.2 Chapter 4 supplementary data

Table B.1 Viability of bulk mouse primary cell population following treatment.
Cells were transduced for 48 h with the Eco-GFP retroviral vector. Transduction was performed with VCM supplemented with 10 μg/mL rh histone H3.1, co-culture on irradiated Eco-GFP producing cells, with VCM alone (no additive) and, as a negative control, without VCM. (2 different batches of VCM were used, 2 different lots of histones H3.1 were used in trial 1 and trial 2&3)

VCM batch	Trial	Treatment			
		H3.1	Co-culture	VCM only	Negative Control
A	1	90.0%	94.0%	93.0%	93.0%
	2	92.1%	91.0%	90.8%	92.6%
B	3	99.6%	99.8%	97.8%	99.6%
	Average	**93.9%**	**94.9%**	**93.9%**	**95.1%**
	SEM	2.9%	2.6%	2.1%	2.3%

A.

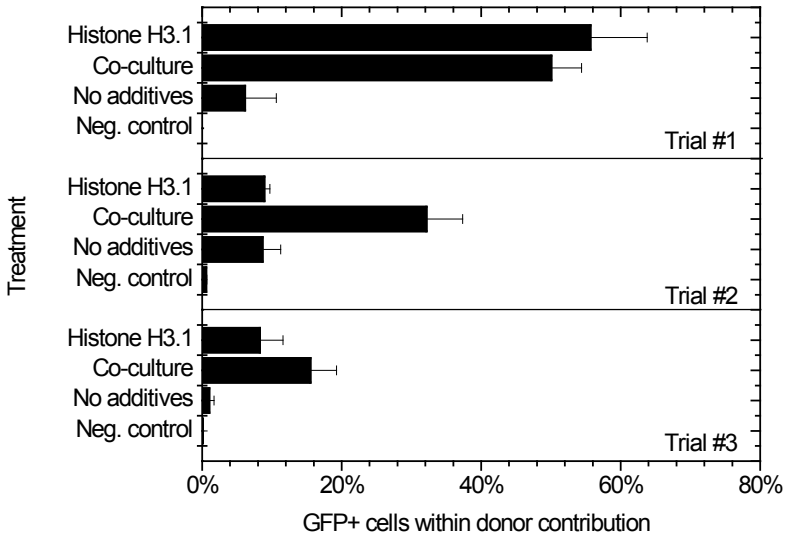

B.

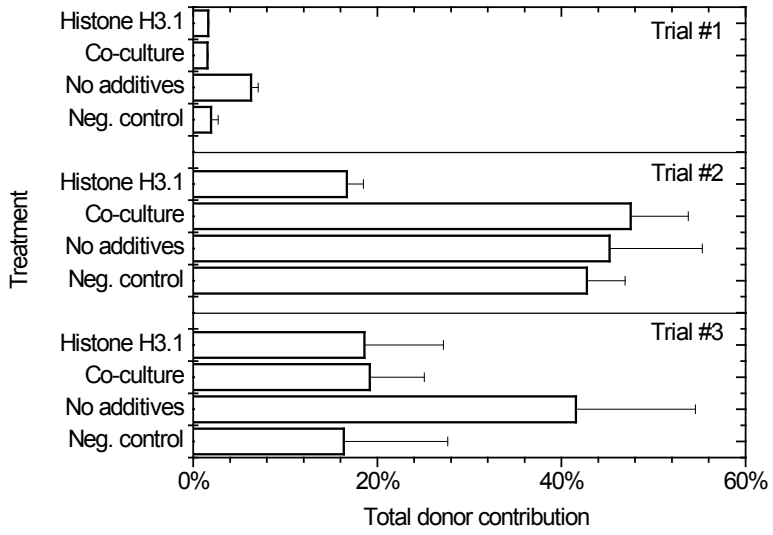

(continues on following page)

C.

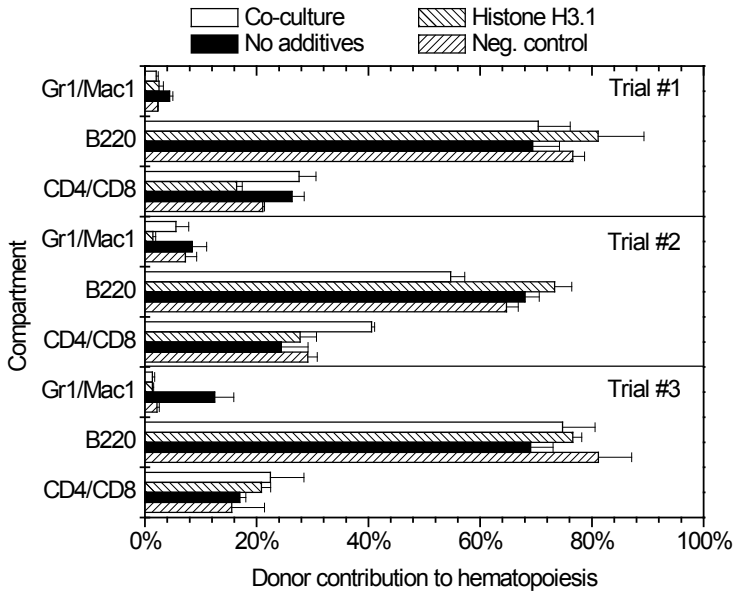

Figure B.15 Individual mouse reconstitution trial data.
A. Histone H3.1 treated cells persisted in the peripheral blood of recipient mice after 20 weeks post-transplant.
B. Total donor contribution of histone H3.1 treated cells to hematopoiesis after 20 weeks post-transplant were similar to that of the co-culture and negative control.
C. Histone H3.1 treated cells contributed to both lymphoid and myeloid lineages measured at 20 weeks post-transplant.
(trial #1 n=2, trial #2 n=4, trial #3 n=3).

A.

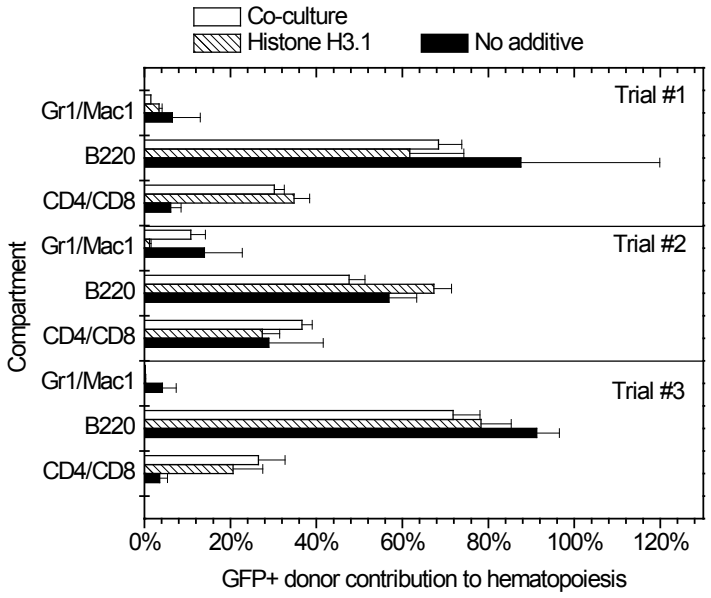

B.

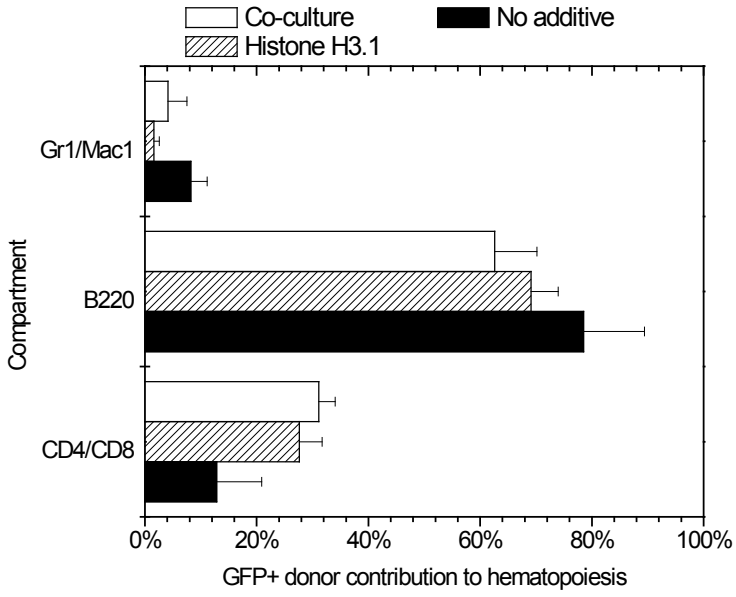

Figure B.16 (A) Contribution of GFP+ cells to myeloid and lymphoid lineages for each trial and (B) average of 3 trials.
(error bar: SEM) (bottom)

B.3 Chapter 5 raw data (transduction efficiency)

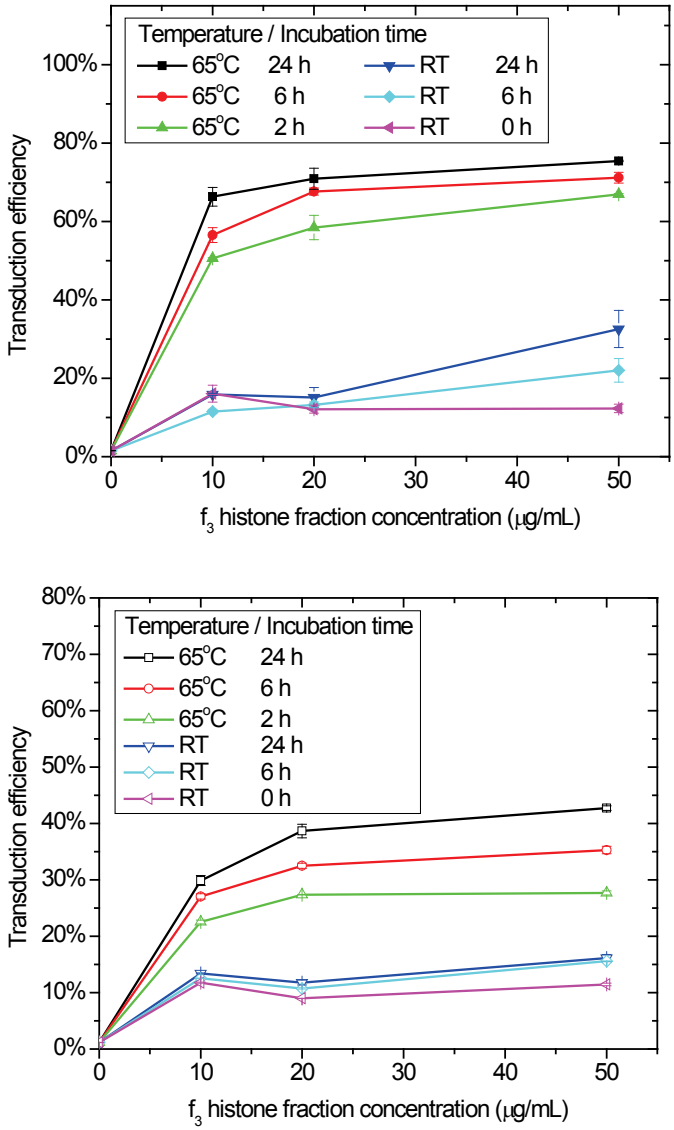

Figure B.17 Effect of f_3 histone fraction incubation temperature and time on the transduction efficiency of TF-1 and nBaF3 target cells.
nBaF3 target cells were transduced with Eco-GFP vectors (top) and TF-1 target cells with GALV-GFP (bottom). The histones were incubated at room temperature (~21°C) or at 65°C for up to 24 h prior to their addition to the target cell/retroviral vector mixture at 10, 20 and 50 μg/mL. (n=2 using same batch of histones) (supplement to Figure 5.2)

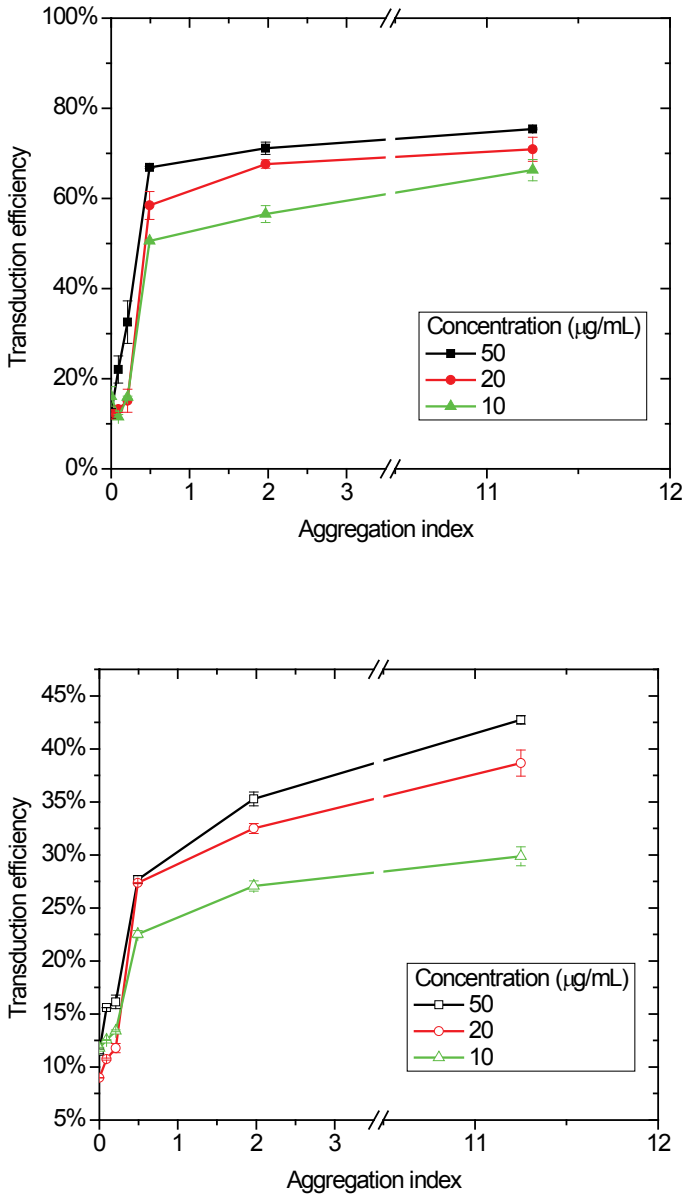

Figure B.18 Transduction efficiency relative to the aggregation index of the f_3 histone fractions of nBaF3 and TF1 target cells.
nBaF3 target cells were transduced with Eco-GFP vectors (top) and TF-1 target cells with GALV-GFP vectors (bottom). Histone aggregates were generated through incubation at 65°C or at room temperature (~21°C) for up to 24 h. (n=2 using same batch of histones) (supplement to Figure 5.3)

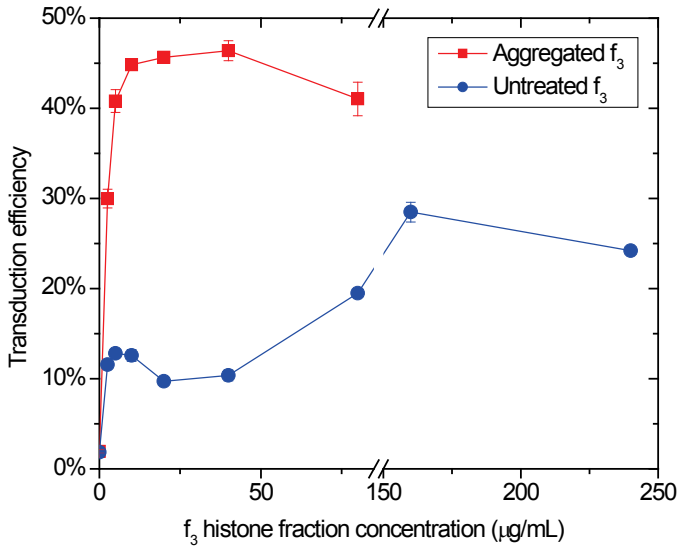

Figure B.19 Effect of the concentrations of the aggregated f_3 histone fraction and untreated f_3 histones on the transduction efficiency of TF-1 cells with GALV-GFP vectors.
The histones were aggregated by heat treatment at 65°C for 24 h. (n=3 for aggregated histones and n=6 for untreated histones except at 160 and 240 μg/mL where n=3, error bars: SEM) These data were used to generate Figure 5.5.

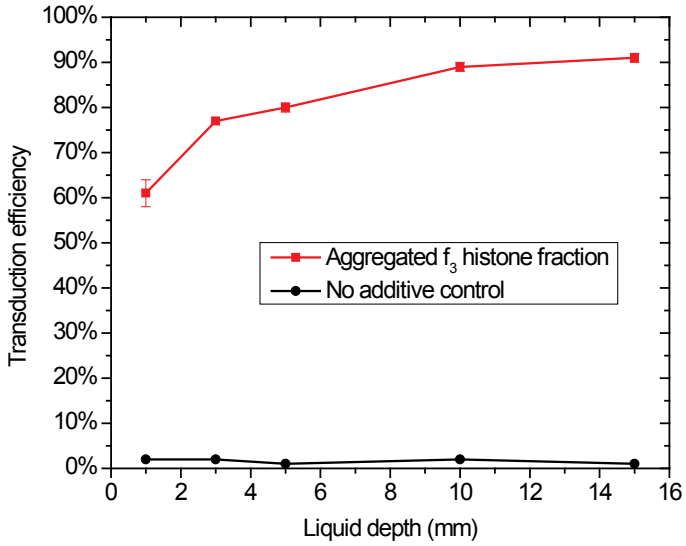

Figure B.20 Effect of the average liquid depth on the transduction efficiency of nBaF3 target cells with Eco-GFP vectors either in the presence of 20 μg/mL of aggregated f_3 histone fraction with no additives (control).
Vector concentration and target cell number (1.5×10^5 cells/cm^2) remained constant at all liquid depths. (n=2 using same batch of aggregated histones, error bars: SEM) (Supplement to Figure 5.10)

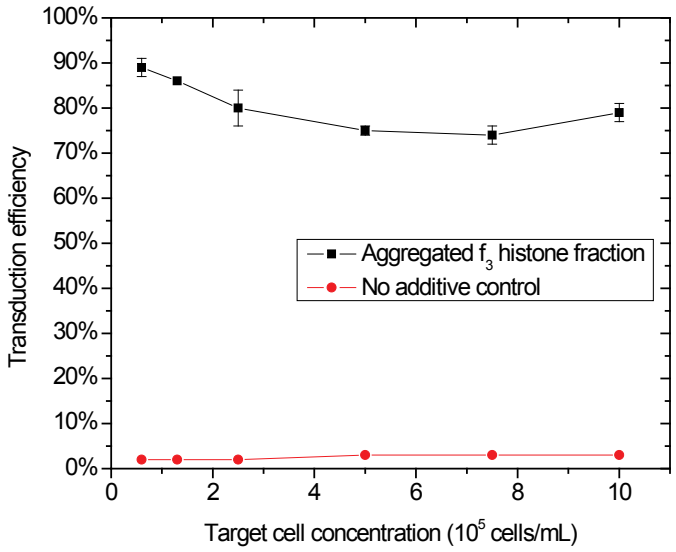

Figure B.21 Effect of the initial target cell concentration on the transduction efficiency of nBaF3 cells with aggregated f_3 histone fraction.
nBaF3 cell were transduced with Eco-GFP vectors either supplemented with 20 µg/mL of aggregated f_3 histone fraction or with no additives (control). (n=2 using the same batch of aggregated histones, error bars: SEM) (Supplement to Figure 5.11)

Table B.2 Viability of mouse primary bone marrow cells.
Viability was measured following a 48 h transduction with Eco-GFP VCM supplemented with 20 µg/mL of aggregated f_3, 10 µg/mL of rh histone H3.1, VCM alone (no additives) and, as a negative control, without VCM. (2 different batches A and B of VCM were used, trial 1 and 2 were performed concomitantly with the last 2 trials presented in the previous chapter.)

VCM batch	Trial	Treatment			
		Aggregated f_3	H3.1	No additives	Negative control
A	**1**	87.7%	92.1%	90.8%	92.6%
B	**2**	99.3%	99.6%	97.8%	99.6%

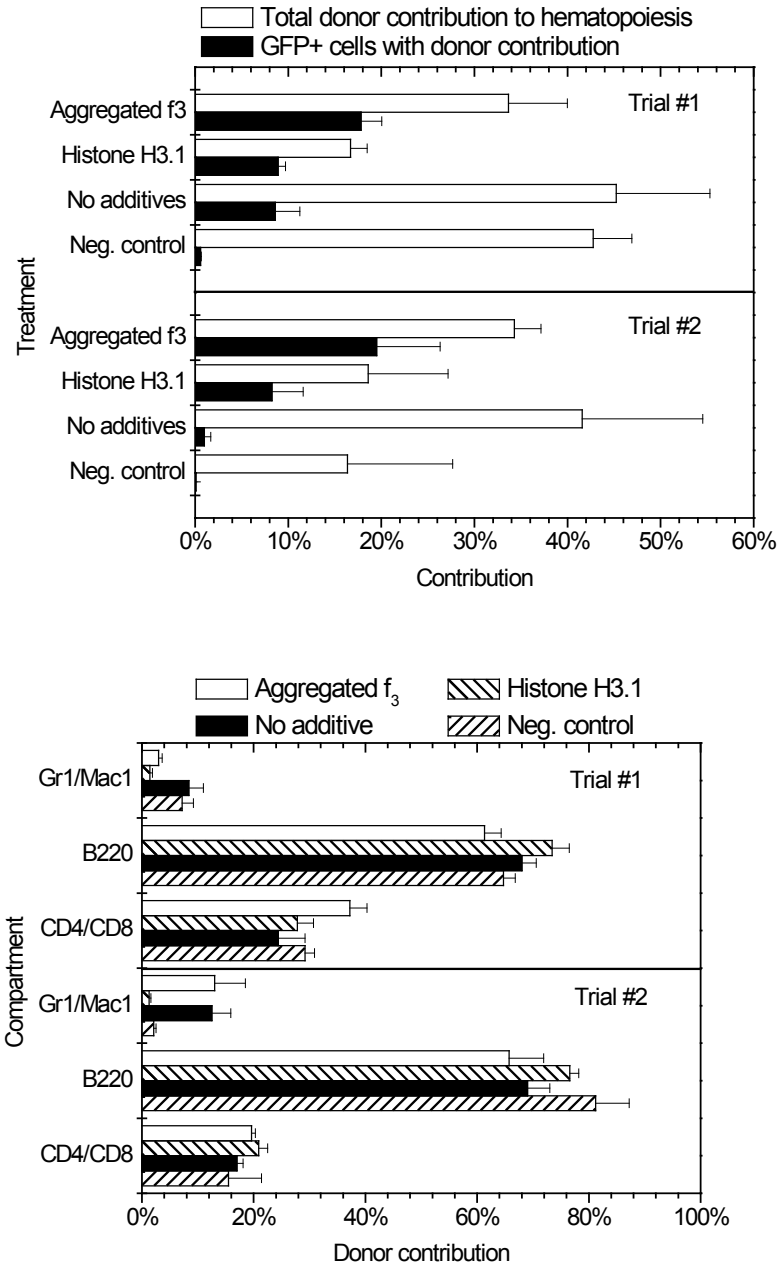

Figure B.22 Individual mouse reconstitution trial data at 20 weeks post-transplant.
(Top) Total donor contribution to hematopoiesis and GFP+ within donor contribution (top). (Bottom) Contribution to lymphoid and myeloid lineages. (trial #1 n=4, trial #2 n=3, error bars = SEM) (Supplement to Figure 5.12).

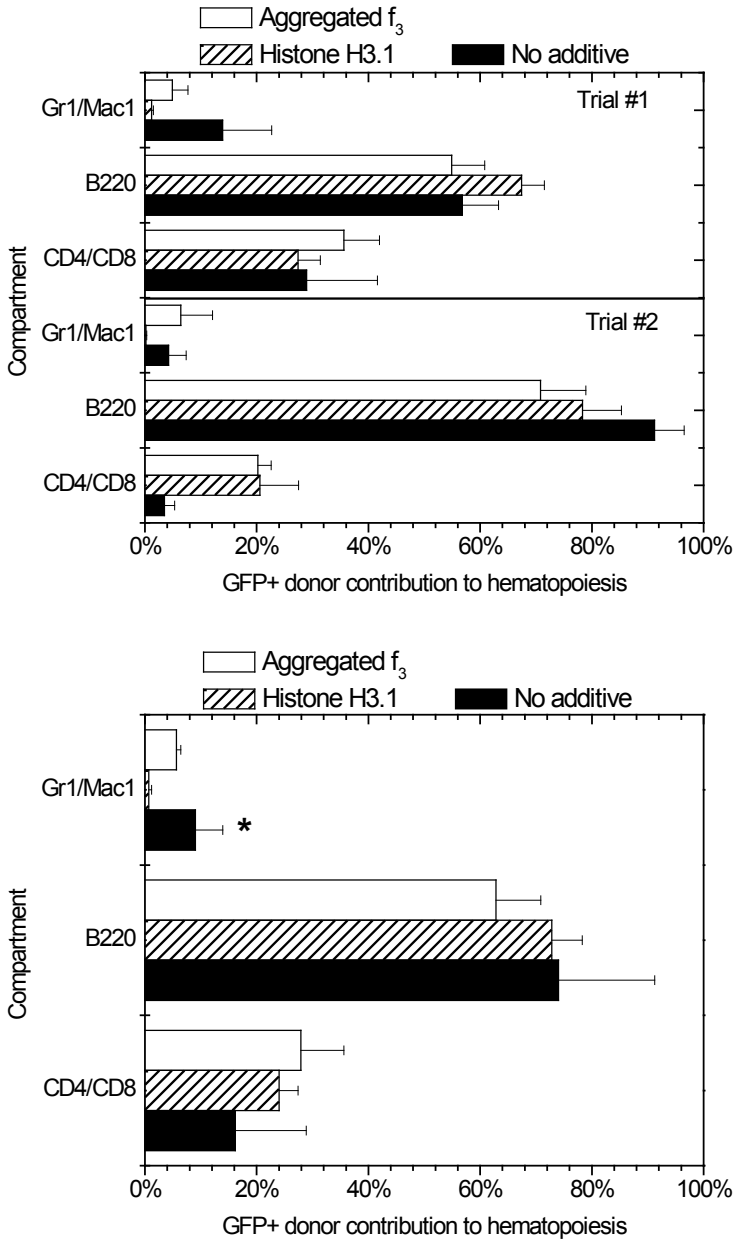

Figure B.23 Individual trial and average contribution of GFP+ cells to myloid and lymphoid lineages. (Top) Contribution of GFP+ cells to myeloid and lymphoid lineages for individual trials and (Bottom) average of the two trials. Average myeloid contribution was significantly greater with aggregated f_3 than with histone H3.1. (Error bar: SEM, * $p<0.05$) (Supplement to Figure 5.12).

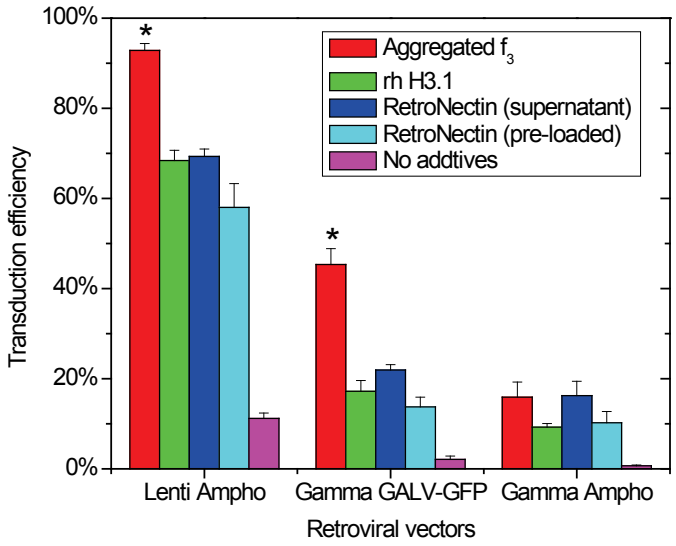

Figure B.24 Comparison of the effect of aggregated f_3 histone fraction, RetroNectin and rh H3.1 on the transduction efficiency of TF-1 cells with lenti- and gammaretroviral vectors.
TF-1 cells were transduced by amphotropic lentiviral vectors as well as GALV-GFP and amphotropic gammaretroviral vectors with 50 µg/mL of aggregated f_3 histone fraction, with 10 µg/mL of rh H3.1 histone, using surfaces coated with 5 µg/cm^2 RetroNectin pre-loaded with viral vectors or with viral supernatant, and, as a control, with no additives. The amphotropic lentiviral vectors were diluted 1:20, the GALV-GFP 1:8 and the amphotropic gammaretroviral vectors 1:4. (* $p<0.1$) (n=2, different batches of aggregated f_3 histones) ($p<0.05$) (Supplement to Figure 5.13)

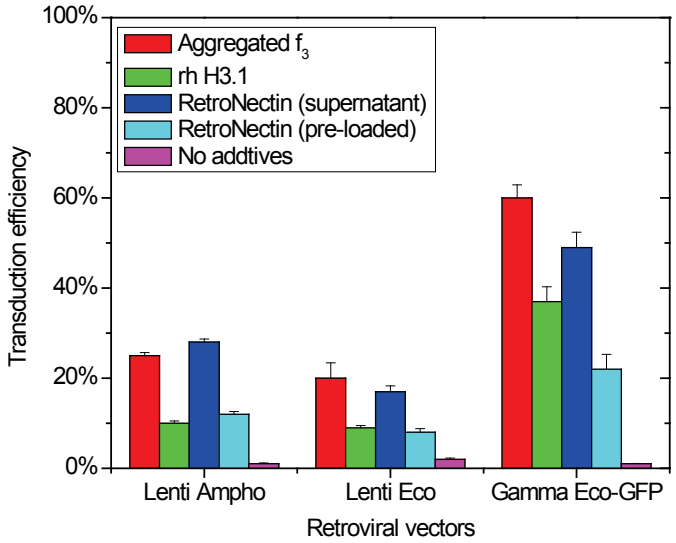

Figure B.25 Comparison of the effect of aggregated f_3 histone fraction, RetroNectin and rh H3.1 on the transduction efficiency of nBaF3 target cells with lenti- and gammaretroviral vectors.
nBaF3 cells were transduced by amphotropic and ecotropic lentiviral vectors as well as by Eco-GFP gammaretroviral vectors with 50 µg/mL of aggregated f_3 histone fraction, with 10 µg/mL rh H3.1 histone, using surfaces coated with 5 µg/cm^2 RetroNectin pre-loaded with viral vectors or with viral supernatant, and, as a control, with no additives. The amphotropic and ecotropic lentiviral vectors were diluted 1:20 and the Eco-GFP gammaretroviral vectors 1:16. (n=2, within same experiment) (Supplement to Figure 5.14)